THE COORDINATION CHEMISTRY OF XENON TRIOXIDE WITH OXYGEN BASES

By

KATHERINE M. MARCZENKO

A Thesis

Submitted to the School of Graduate Studies

In Partial Fulfillment of the Requirements

for the Degree

Masters of Science

McMaster University

MASTERS OF SCIENCE McMaster University
(Chemistry) Hamilton, ON

TITLE: THE COORDINATION CHEMISTRY OF XENON TRIOXIDE WITH OXYGEN BASES

AUTHOR: Katherine M. Marczenko, B. Sc. (University of Guelph)
SUPERVISOR: Professor Gary J. Schrobilgen
PAGES: 245

ABSTRACT

This thesis extends our fundamental knowledge in the area of high oxidation state chemistry of xenon trioxide, XeO_3. Oxygen coordination to the Xe(VI) atom of XeO_3 was observed in its adducts with triphenylphosphine oxide, $[(C_6H_5)_3PO]_2XeO_3$, dimethylsulfoxide, $[(CH_3)_2SO]_3(XeO_3)_2$, pyridine-N-oxide, $(C_5H_5NO)_3(XeO_3)_2$, and acetone, $[(CH_3)_2CO]_3XeO_3$. The crystalline adducts were characterized by low-temperature single-crystal X-ray diffraction and Raman spectroscopy. Unlike solid XeO_3, which detonates when mechanically or thermally shocked, the solid $[(C_6H_5)_3PO]_2XeO_3$, $[(CH_3)_2SO]_3(XeO_3)_2$, and $(C_5H_5NO)_3(XeO_3)_2$ adducts are insensitive to mechanical shock, but undergo deflagration when exposed to a flame. Both $[(C_6H_5)_3PO]_2XeO_3$ and $(C_5H_5NO)_3(XeO_3)_2$ are air-stable at room temperature. The xenon coordination sphere in $[(C_6H_5)_3PO]_2XeO_3$ is a distorted square pyramid and provides the first example of a five-coordinate Xe center in a XeO_3 adduct. The xenon coordination sphere of the remaining adducts are distorted octahedral comprised of three equivalent Xe---O secondary contacts that are approximately trans to the primary Xe–O bonds of XeO_3. Hirshfeld surfaces of XeO_3 and $(C_6H_5)_3PO$ in $[(C_6H_5)_3PO]_2XeO_3$ show the adduct is well-isolated in its crystal structure and provide a visual representation of the secondary Xe---O bonding in this adduct.

Crown ethers have been known for over 50 years, but no example of a complex between a noble-gas compound and a crown ether or another polydentate ligand had been reported. Xenon trioxide is shown to react with 15-crown-5 to form the kinetically stable

$(CH_2CH_2O)_5XeO_3$ adduct which, in marked contrast with solid XeO_3, does not detonate when mechanically shocked. The crystal structure shows that the five oxygen atoms of the crown ether are coordinated to the xenon atom of XeO_3. The gas-phase Wiberg bond valences and indices and empirical bond valences indicate the $Xe{-}{-}{-}O_{crown}$ bonds are predominantly electrostatic, σ-hole, bonds. Mappings of the electrostatic potential (EP) onto the Hirshfeld surfaces of XeO_3 and 15-crown-5 in $(CH_2CH_2O)_5XeO_3$ and a detailed examination of the molecular electrostatic potential surface (MEPS) of XeO_3 and $(CH_2CH_2O)_5$ reveal regions of negative EP on the oxygen atoms of $(CH_2CH_2O)_5$ and regions of high positive EP on the xenon atom that are also consistent with σ-hole bonding.

Reactions of crown ethers with HF acidified aqueous solutions of XeO_3 at room-temperature yielded adducts of 12-crown-4, $(CH_2CH_2O)_4XeO_3$, and 18-crown-6, $[(CH_2CH_2O)_6XeO_3{\cdot}2H_2O]_2{\cdot}HF$, whereas slow cooling of a solution of XeO_3 with 18-crown-6 in acetone yielded $(CH_2CH_2O)_6XeO_3{\cdot}2H_2O$. The adducts $(CH_2CH_2O)_4XeO_3$ and $(CH_2CH_2O)_6XeO_3{\cdot}2H_2O$ are shock-insensitive whereas the former adduct is air-stable at room temperature. The low-temperature, single-crystal X-ray structures show the Xe atom of XeO_3 coordinated to the oxygen atoms of the crown ether ring. Uncharacteristic xenon coordination numbers exceeding six (including the three primary bonds of XeO_3) were observed for all crown ether adducts. Raman spectroscopy frequency shifts are consistent with complex formation and provided evidence for the 2,2,1-cryptand adduct of XeO_3. Gas-phase Wiberg bond valences and indices and empirical solid-state bond valences confirmed the electrostatic nature of the $Xe{-}{-}{-}O$ bonding interactions. Comparisons between the XeO_3 and SbF_3 18-crown-6, 15-crown-5, and 12-crown-4 complexes are made.

Incorporation of xenon trioxide, XeO_3, into inorganic polyatomic salts under ambient conditions has been observed in several mixed xenate salts; $K[XeO_3XO_3]$ (X = Cl, Br), $K_2[XeO_3SeO_4]\cdot HF$, $K[(XeO_3)_nZO_3]$ (Z = I, N), and $M_2[(XeO_3)_\mathrm{n}CO_3]\cdot xH_2O$ (M = Na, K, Rb, Ba). Raman spectroscopy was used to identify the aforementioned compounds and $K[XeO_3ClO_3]$, $K[XeO_3BrO_3]$, $K_2[XeO_3SeO_4]\cdot HF$, and $Rb_2[(XeO_3)_2CO_3]\cdot 2H_2O$ were also characterized by low-temperature, single-crystal X-ray diffraction. The xenon atom of XeO_3 is seven coordinate in $K[XeO_3ClO_3]$ and six coordinate in all other compounds with Xe---O distances that are significantly less than the sum of the Xe and O van der Waals radii. These salts provide examples of XeO_3 coordinated to inorganic compounds and may provide insights into the inclusion of xenon oxides in minerals.

ACKNOWLEDGMENTS

I would like to thank my supervisor, Professor Gary J. Schrobilgen, for giving me the opportunity to conduct research in his lab and for always encouraging me in the acquisition of knowledge. His guidance and expertise were instrumental in my development as a chemist.

I would also like to thank Dr. Hélène P. A. Mercier for her many contributions to the operation of this research group. Her mentorship and friendship throughout my studies is greatly cherished.

I would like to thank current and previous Schrobilgen group members, James Goettel, John Debackere, and Mark Bortulus for their support and friendship. A special thank you to James Goettel, who trained me in the safe-handling of xenon trioxide, and offered many words of encouragement.

I would like to thank my committee member, Dr. David Emslie, for his time spent attending committee meetings, reading my Thesis, and for all the guidance he has provided throughout my time at McMaster. An extended thank you to Emslie group members; friendly faces whom never hesitated to lend and hand.

I would like to thank Dr. James Britten (X-ray facilities) for sharing his knowledge and passion for X-ray crystallography.

A special thanks to my parents, who have never discouraged me to pursue what I love and supported me financially throughout all of my studies. A heart-felt thanks to my partner, Alex, for participating in discussisions pertaining to my research and always offering kind words of love and support. Thank you.

PREFACE

The following Chapter has been submitted (Sept. 2018), in whole, to *Chem. Eur. J.* (Wiley-VCH).

Chapter 3: Xenon Trioxide Adducts of *O*-Donor Ligands; $[(CH_3)_2CO]_3XeO_3$, $[(CH_3)_2SO]_3(XeO_3)_2$, $(C_5H_5NO)_3(XeO_3)_2$, and $[(C_6H_5)_3PO]_2XeO_3$
Katherine M. Marczenko,[a] James T. Goettel,[a] Gary J. Schrobilgen, *Chem. Eur. J.*, Submitted Sept. **2018**.
[a] Experimental work was conducted equally by both the first author and Dr. J. Goettel.

The following Chapter is published, in whole, by Wiley-VCH.

Chapter 4: A Stable Crown Ether Complex with a Noble-Gas Compound
Katherine M. Marczenko, Hélène P. A. Mercier, Gary J. Schrobilgen, *Angew. Chem. Int. Ed. Eng.*, **2018**, *57*, 12448–12452.

All experimental and computational work was conducted by the first author. Mapping of the molecular electrostatic potentials was carried out by Dr. Hélène P. A. Mercier.

The following Chapters will be submitted (Nov. 2018) to *Inorg. Chem.* (*ACS* publications).

Chapter 5: Crown Ether and Cryptand Complexes of Xenon Trioxide
Katherine M. Marczenko, James T. Goettel, Gary J. Schrobilgen

All experimental synthesis and computational work was conducted by the first author. Dr. James T. Goettel assisted with crystallization techniques and low-temperature crystal mounting of $(CH_2CH_2O)_6XeO_3{\cdot}2H_2O$.

Chapter 6: Oxo-Anion Adducts of Xenon Trioxide
Katherine M. Marczenko, James T. Goettel, Ajit. S. Panesar, Gary J. Schrobilgen

The first author synthesized and characterized the $K[XeO_3XO_3]$ (X = Cl, Br), $K[(XeO_3)_nZO_3]$ (Z = I, N), and $K_2[XeO_3SeO_4]$ complexes with some assistance from Ajit S. Panesar (undergraduate student). Dr. James T. Goettel synthesized and characterized the $M_2[(XeO_3)_nCO_3]{\cdot}xH_2O$ (M = Na, K, Rb) salts.

LIST OF ABBREVIATIONS AND SYMBOLS

General

CCD	charge-coupled device
FT	Fourier transform
FEP	perfluoroethylene/perfluoropropylene copolymer
IR	infrared
Kel-F	chlorotrifluoroethylene polymer
PTFE	tetrafluoroethylene polymer
aHF	anhydrous HF
vdWr	Van der Waals Radii

X-ray Crystallography

$a, b, c, \alpha, \beta, \gamma$	unit cell parameters
V	unit cell volume
λ	wavelength
Z	molecules per unit cell
mol. wt.	molecular weight
ρ	density
μ	absorption coefficient
F	structure factor
R_1	conventional agreement index
wR_2	weighted agreement index

Raman Spectroscopy

$\Delta\nu$	frequency
cm^{-1}	wavenumber
ν	stretching mode
δ	bending mode
ρ_w	wagging mode
ρ_r	rocking mode
ρ_t	twisting mode
o.o.p.	out-of-plane
i.p.	in-plane
WF	width factor

Computational and Thermochemical

DFT	density functional theory
MEPS	molecular electrostatic potential surface
EP	electrostatic potential
NBO	natural bond orbital
NPA	natural population analysis
ΔH^o	standard enthalpy of reaction
ΔH_f^o	standard enthalpy of formation

TABLE OF CONTENTS

page

LIST OF FIGURES

LIST OF TABLES

CHAPTER 1

Introduction

1.1 Noble-gas Reactivity and the Binary Xenon Fluorides

The primary focus of this Thesis is on the chemistry of xenon(VI) trioxide, XeO_3. Noble-gases were thought to be chemically inert for many years because of the full octet of valence electrons. Several excellent review articles and historical accounts describe the discovery of noble-gas reactivity and experiments preceding the discovery.[1–14]

Isolation of fluorine was instrumental in the discovery of noble-gas reactivity. In 1886, Henri Moissan isolated elemental fluorine by the electrolysis of dry hydrogen fluoride and potassium bifluoride solutions.[15] He later attempted to demonstrate noble-gas reactivity with the reactions of argon and fluorine gases at room temperature and under the action of an induction spark, but without success. Several notable attempts were made by von Antropoff[16] and Yost and Kaye.[17] It was not until 1962 that the first noble-gas compound was synthesized. Neil Bartlett reacted deep red-brown PtF_6 vapor with xenon gas at room temperature.[18] The product that immediately formed was a yellow-orange solid, initially formulated as $[Xe][PtF_6]$ and later corrected to $[XeF][PtF_6]$ which gave $[XeF][Pt_2F_{11}]$ upon warming to ≤ 60 °C.[19,20] Within a decade of the discovery of noble-gas reactivity, over one-hundred noble-gas compounds were known.[21]

Over the past several years, noble-gas compounds, in particular XeF_2, have found synthetic applications in areas of small molecule syntheses and materials science. Since the first preparation of XeF_2[22,23] several effective preparations have been reported.[24–26] Up to 1 kg of XeF_2 can be prepared by UV irradiation of a gaseous xenon-fluorine mixture in a 1:2 molar ration with 1 mol% of HF in fluorine as a catalyst.[27] Xenon difluoride rapidly etches silicon and does not require external energy sources to initiate and maintain the etching process.[28] It has been used, for example, as a dry isotropic etchant for silicon, particularly in the fabrication of thermoelectric IR microsensors.[29] Gaseous XeF_2 is used for surface fluorination of polyethylene and polystyrene.[30] Elemental fluorine and XeF_2 have also been used to fluorinate single-wall carbon nanotubes at 200 ^{o}C.[31] Oxidative, aromatic, alkene, and radical fluorination are among several fluorination reactions that XeF_2 undertakes.[30–34] Xenon difluoride is a strong fluorinating and oxidizing agent which forms the more powerful fluorinating XeF^+ and $Xe_2F_3^+$ cations in the presence of strong fluoride ion acceptors.[35]

Xenon tetrafluoride, XeF_4, was first synthesized mere months after Bartlett's discovery of noble-gas reactivity at Argonne National Laboratory, IL, by the reaction of Xe and F_2 in a 1:5 molar ration at 400 ^{o}C (~2 to 3 atm).[36] Xenon tetrafluoride is a weaker fluoride ion donor than XeF_2[37] and requires stronger fluoride-ion acceptors to form the corresponding XeF_3^+ cation. Xenon tetrafluoride has been used as a decomposition agent of silicone rubber for the determination of trace metal impurities in the rubber.[38]

Xenon hexafluoride, XeF_6 is synthesized by the reaction of elemental xenon with 20 or greater equivalents of F_2 at ca. 300 ^{o}C and pressures above 50 atm (eq 1.1).[39] Although XeF_6 does not have any known applications, it is the precursor for all known Xe(VI) compounds (the hydrolysis of XeF_4 also forms XeO_3; see Sec. 1.2.2).[40] All known xenon oxide fluorides ($XeOF_4$, [41,42] XeO_2F_2, [43] XeO_3F_2, [44] XeO_2F_4[45]) are synthesized by reaction of XeF_6 and an oxide source (eq 1.1–1.5).

$$Xe + 3F_2 \longrightarrow XeF_6 \tag{1.1}$$

$$XeF_6 + H_2O \longrightarrow XeOF_4 + 2HF \tag{1.2}$$

$$XeF_6 + 2H_2O \longrightarrow XeO_2F_2 + 4HF \tag{1.3}$$

$$XeF_6 + XeO_4 \longrightarrow XeO_3F_2 + XeOF_4 \tag{1.4}$$

$$XeF_6 + XeO_3F_2 \longrightarrow XeO_2F_4 + XeOF_4 \tag{1.5}$$

1.2 Noble-gas Oxides

Xenon is the only group 18 element which forms stable binary oxides. Binary krypton oxides are suspected to form under high pressure,[46] however no experimental evidence of a binary krypton, or any other noble-gas oxide has been forthcoming.

Only three binary xenon oxides, XeO_2, XeO_3, and XeO_4, have been synthesized in macroscopic quantities. Xenon dioxide was the last of these three compounds to have been synthesized, lending to its designation as the “missing xenon oxide”.[47]

1.2.1 Xenon Dioxide

An early study reported the hydrolysis of XeF_4 and the formation of a transient yellow solid at 0 °C. The transient yellow product was never isolated or characterized.[48] Co-condensation of XeF_4 and H_2O at −80 °C yielded a pale-yellow product that was incorrectly formulated as $XeOF_2$ and was erroneously assumed to be the aforementioned transient yellow species.[49] The co-condensed product was later unambiguously assigned to a mixture of $XeOF_2$ and $XeOF_2{\cdot}n$HF.[50]

In 2011, macroscopic quantities of the aforementioned transient yellow solid were obtained and unambiguously shown to be XeO_2 by Raman spectroscopy.[47] The addition of crystalline XeF_4 to either water or 2.00 M $H_2SO_{4(aq)}$ at 0 °C with mixing for ca. 20 s produced bright yellow suspensions. The bright yellow solids were consistent with polymeric XeO_2 while the initial yellow-orange products were suspected to be a mixture of molecular XeO_2 and/or lower molecular weight polymorphs due to incomplete polymerization (eq 1.6).[47]

$$n\mathrm{XeF_4} + 2n\mathrm{H_2O} \longrightarrow [n\mathrm{XeO_2}\text{ and/or }{}^{n}/_{m}(\mathrm{XeO_2})_m] + 4n\mathrm{HF} \longrightarrow (\mathrm{XeO_2})_n + 4n\mathrm{HF}\ (n > m) \quad \text{(eq 1.6)}$$

The yellow product decomposes rapidly near ambient temperature but is kinetically stabilized at low-temperatures. As such, characterization was only possible by low-temperature Raman spectroscopy. Monomeric XeO_2 is predicted to have a square-planar AX_2E_2 (X = bond pair, E = valence electron lone pair) VSEPR[51] arrangement of bond pairs and lone pairs (Figure 1.1, Structure I). The insolubility of XeO_2 in aqueous media, as well as the Raman spectra of $Xe^{16}O_2$ and $Xe^{18}O_2$, support an extended (chain or network) XeO_2 structure with a local square-planar geometry around xenon (Figure 1.1, Structure II), which is consistent with the geometry predicted by the VSPER model of molecular geometry.[47]

Earth's atmosphere contains less than 10% of the aticpiated amount of xenon gas. It was hypothesized that xenon displaces silicon from quartz at high pressures and temperature. The vibrational spectra of $Xe^{16}O_2$ and $Xe^{18}O_2$ amend prior vibrational assignments of xenon doped SiO_2,[52] and is in accordance with speculation that at high temperatures and high pressures covalently bound xenon occurs in natural silicates deep in the Earth's crust, providing a plausible explanation for the Earth's missing xenon.

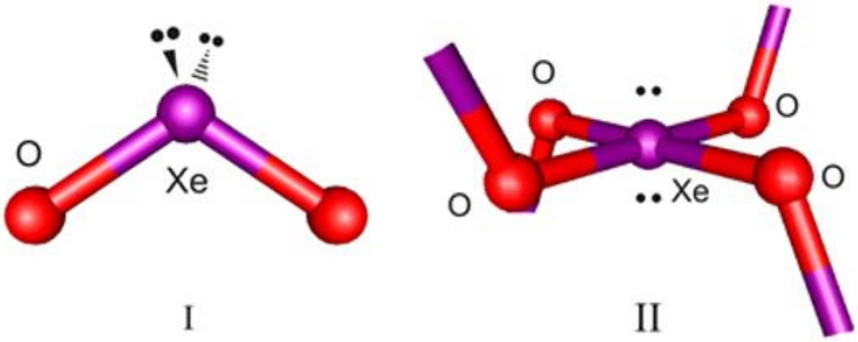

Figure 1.1. Monomeric (C_{2v}) and polymeric structures of XeO_2; reproduced with permission from ref. 47.

1.2.2 Xenon Trioxide

Xenon trioxide is the first xenon oxide to have been synthesized and structurally characterized. Pizter predicted that xenon oxides would be unstable and possibly explosive.[53] Bartlett and Rao inadequately synthesized XeO_3 in 1963 through the hydrolysis of XeF_4 (eq 1.7). The white solid detonated upon warming under vacuum, completely destroying the glass vessel. The event unfortunately led to the injury of one of Bartlett's eyes and hospitalization of both researchers. Bartlett and Rao[54] initially formulated the solid as $Xe(OH)_4$ or $XeO_2{\cdot}2H_2O$. Later that year, two independent research groups synthesized the compound and confirmed the solid was XeO_3 by vibrational spectroscopy[55] and single-crystal X-ray diffraction.[40]

A second study reported the synthesis of xenon trioxide by hydrolysis of XeF_6 (eq 1.8).[56] This synthetic route to XeO_3 is preferred over the hydrolysis of XeF_4 because it is more economic with respect to the XeO_3 yield, and the later is a redox disproportionation reaction that proceeds through the bright yellow XeO_2 intermediate, yielding a large molar excess (12mol) of HF with respect to XeO_3. Hydrogen fluoride can be removed through co-evaporation with H_2O or neutralization with MgO followed by centrifugation of precipitated MgF_2. Because small amounts of residual magnesium salts contaminate the solution, co-evaporation of HF and H_2O without neutralization is preferred.

$$6XeF_4 + 12H_2O \longrightarrow 2XeO_3 + 3O_2 + 4Xe + 24HF \qquad (1.7)$$

$$XeF_6 + 3H_2O \longrightarrow XeO_3 + 6HF \qquad (1.8)$$

The colorless XeO_3 solid readily absorbs water from humid air to form a concentrated aqueous solution.[57] The solid is not volatile at room temperature and extremely sensitive to both mechanical and thermal shock. The solid readily detonates with mild friction, when heated, when exposed to cellulose, and even when left undisturbed. Detonation of the solid results in liberation of Xe and O_2 gases and 406 kJ mol^{-1} of energy.[58] The highly explosive nature of this solid makes storing and handling of the compound extremely difficult, and has hindered research on XeO_3 in the solid state; however, its aqueous solution is stable indefinitely.

In 2016, Goettel and Schrobilgen reported the isolation and low-temperature X-ray crystal structures of two new phases of XeO_3, and a higher precision single-crystal X-ray structure of the original phase.[59] The solid-state structures (Figure 1.2) of XeO_3 show the trigonal pyramidal geometry of Xe (C_{3v})[60] with Xe---O bonding interactions between neighboring XeO_3 molecules.

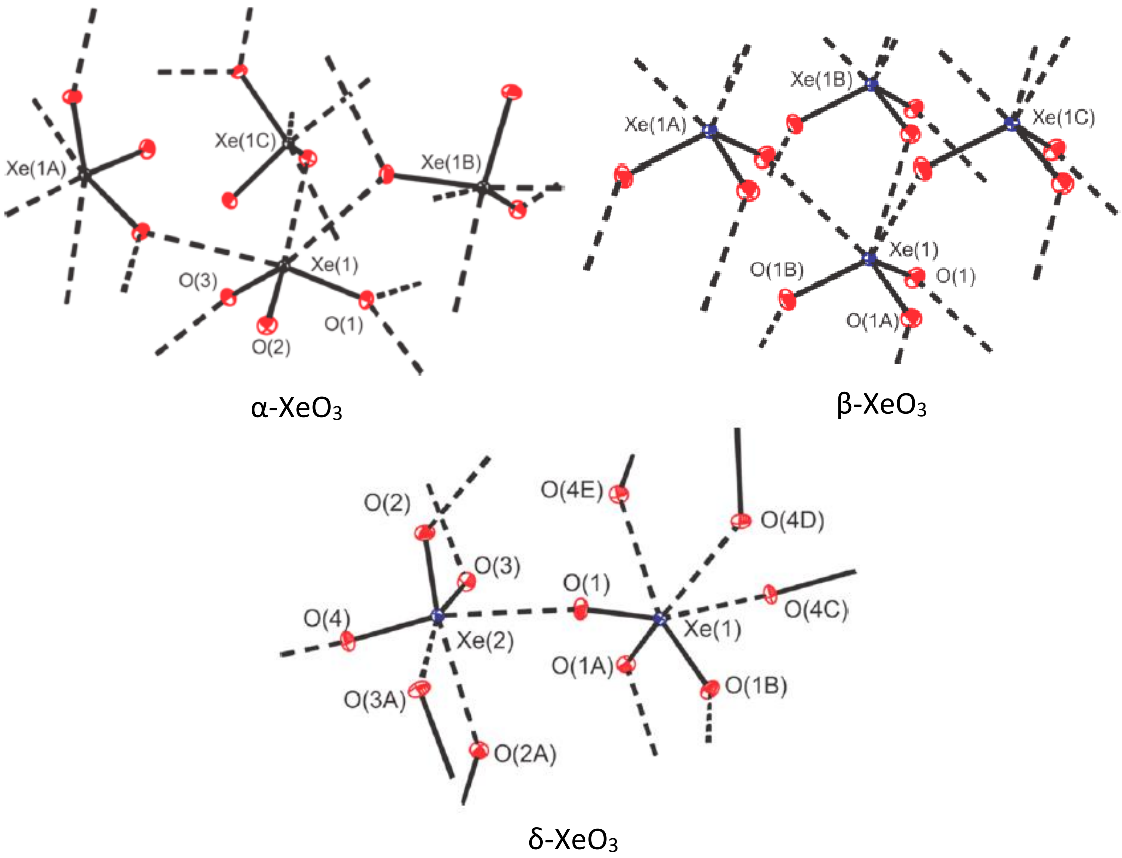

α-XeO_3

β-XeO_3

δ-XeO_3

Figure 1.2. The three solid state structures of XeO_3; reproduced with permission from ref. 59.

1.2.3 Xenon Tetroxide

Xenon is the only main-group element that exhibits the +8 oxidation state and oxygen is the only element that is able to stabilize xenon in this oxidation state. Xenon tetroxide, XeO_4, was first synthesized by Huston in 1963 by reaction of sodium perxenate (see Sec. 1. 2. 4) with concentrated sulfuric acid at room temperature (eq 1.9).[61]

$$Na_4XeO_6 + 2H_2SO_4 \longrightarrow XeO_4 + 2Na_2[SO_4] + 2H_2O \qquad (1.9)$$

Xenon tetroxide is a pale yellow solid which melts at −36.9 ± 0.2 °C to give a yellow liquid.[61] The liquid state of XeO_4 is thermodynamically unstable and will detonate with liberation of its elements and the release of 642 kJ mol^{-1} of energy.[57] Unlike XeO_3, XeO_4 does have an appreciable vapor pressure (ca. 25 mm Hg, 20 °C) and can be distilled under dynamic or static vacuum. Until recently, the crystal structure of XeO_4 was unknown and characterization was limited to mass spectrometry,[61] electron diffraction studies,[62] vibrational spectroscopy, and ^{129}Xe and ^{131}Xe solution NMR studies.[63] The crystal structure of XeO_4 (Figure 1.3) is isotypic with those of OsO_4 and RuO_4–II and contains four Xe−O bonds (1.747(2) Å) that are somewhat shorter than those of XeO_3 (1.7559(11)–1.7801(11) Å).[64]

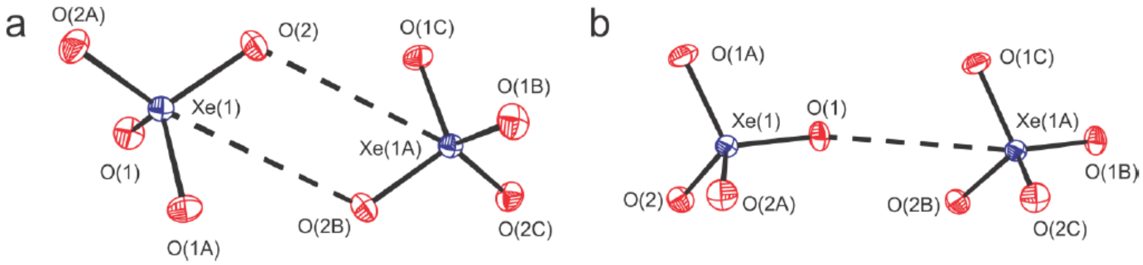

Figure 1.3. The X-ray crystal structure of XeO_4 showing (**a**) two contacts between two XeO_4 molecules and (**b**) the single shortest contact between two XeO_4 molecules; reproduced with permission from ref. 64.

1.2.4 Other Xenon Oxide Species

1.2.4.1 Perxenate Salts

Perxenate (XeO_6^{4-}) salts are the most stable xenon species known. The XeO_4^{6-} ion was obtained as its sodium salt by the hydrolysis of XeF_6 in aqueous NaOH (eq 1.10).[65,66]

A higher yeild synthesis employs the hydrolysis of XeF_6 followed by bascification and ozonation of the resulting aqueous XeO_3 solution (eq 1.11).[67]

$$2XeO_3 + 4OH^- \longrightarrow Xe + XeO_6^{4-} + O_2 + 2H_2O \qquad (1.10)$$

$$HXeO_4^- + O_3 + 4Na^+ + 3OH^- + (x - 2)H_2O \longrightarrow Na_4XeO_6{\cdot}xH_2O + O_2 \qquad (1.11)$$

Salts of the perxenate anion are typically yellow in color, stable under ambient conditions and can be heated to several hundred degrees celcius.[68] A large number of stable perxenate salts, including the lithium,[69] cesium,[69,70] barium,[71] lanthanum,[71] and americum salts,[72] have been reported. The hydrates, $Na_4XeO_6{\cdot}8H_2O$,[73,74] $Na_4XeO_6{\cdot}6H_2O$,[75,76] $K_4XeO_6{\cdot}9H_2O$,[77] $K_2Na_2XeO_6{\cdot}8H_2O$,[78] and $K_4XeO_6{\cdot}2XeO_3$[79] have been unambigiuously characterized by single-crystal X-ray diffraction. The perxenate anion has O_h symmetry with O–Xe–O bond angles which vary between 87 and 93° and Xe–O bond lengths of 1.875 Å.[74] The first solid-state ^{131}Xe NMR study was obtained for $Na_4XeO_6{\cdot}xH_2O$ (x = 0, 2). It was shown that upon hydration the XeO_6^{4-} anion distorts significantly from O_h symmetry.[67] Structural studies of perxenate salts by Raman,[80] infrared,[80] photoelectron,[81] and Mossbauer spectroscopy[82] have also been reported.

It was found that some perxenate salts can incorporate two molar equivalents of XeO_3 into their crystal lattices.[83] The proposed structures consists of perxenate anions with two Xe---O bridges to two molecules of XeO_3. The salts were sensitive to mechanical and thermal shock but could decompose without detonation if heated slowly.[84]

1.2.4.2 $(\eta^2{-}O_2)(Xe^{VIII}O_3)$

The UV photolysis of XeO_4 in noble-gas matrices at low-temperature afforded the Xe(VIII) peroxo-species $(\eta^2{-}O_2)(Xe^{VIII}O_3)$ and XeO_3.[85] The xenon(II) oxide, $Xe^{II}O$, has been postulated as an intermediate in some oxidation reactions of XeO_3.[70] Although it has not been synthesized in macroscopic amounts, it was obtained in an argon matrix by Hg-arc photolysis of $Ar/O_3/Xe$.[86] UV spectroscopy suggested the ground state of XeO is essentially a van der Waals molecule with a bond length considerably longer than that of the excited state value. Gas-phase quantum chemical calculations subsequently showed XeO to have an unbound 3π ground state.[87,88]

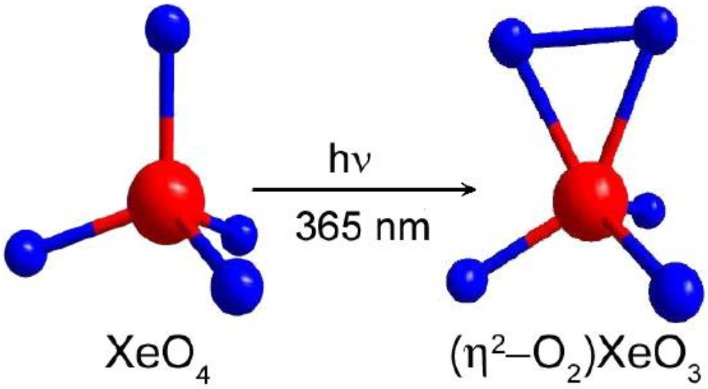

Figure 1.4. Energy minimized structure of $(\eta^2\text{–}O_2)(Xe^{VIII}O_3)$, which was formed in Ar and Ne matrices at −263 °C by the photolysis of XeO_4; reproduced with permission from ref. 85.

1.2.4.3 Xe(II) Oxide Cations

The first example of an isolated and structurally well-characterized Xe(II) oxide fluroide, $[FXeOXeF\text{---}XeF]^+$ (eq 1.12), led to the discovery of other xenon oxide cations.[89] The $[XeOXeOXe]^{2+}$ cation was subsequently synthesized as its $[\mu\text{–}F(ReO_2F_3)_2]_2$ salt (eq 1.13) which provded the first example of a xenon(II) oxide species and a noble-gas oxocation, as well as a rare example of a noble-gas dication (Figure 1.5). The $[XeOXeOXe]^{2+}$ cation interacts through fluorine bridges with two symmetry-equivalent

$[\mu\text{–F}(ReO_2F_3)_2]_2$ anions. The cation-anion F-bridge interaction was attributed to regions of high positive electrostatic potential on the terminal Xe atoms. The F-brdige contact is approximately trans to the Xe–O bonds and correspond to a highly directional sigma hole interaction.[90] The adduct-cation interactions in $[CH_3CN\text{---}XeOXe\text{---}NCCH_3][AsF_6]_2$ (eq 1.14) are also attributable to electrostatic σ-hole interactions.[91]

$$3XeF_2 + [H_3O][AsF_6] \longrightarrow [Xe_3OF_3][AsF_6] + 3HF \quad (1.11)$$

$$5XeF_2 + 4ReO_3F(FH)_2 \longrightarrow [XeOXeOXe][\mu\text{–F}(ReO_2F_3)_2]_2 + 2Xe + O_2 + 8HF \quad (1.12)$$

$$2[FXeOXe\text{---}FXeF][AsF_6] + 2CH_3CN$$

$$\longrightarrow [CH_3CN\text{---}XeOXe\text{---}NCCH_3][AsF_6] + XeF_2 + \tfrac{1}{2}O_2 + Xe \quad (1.13)$$

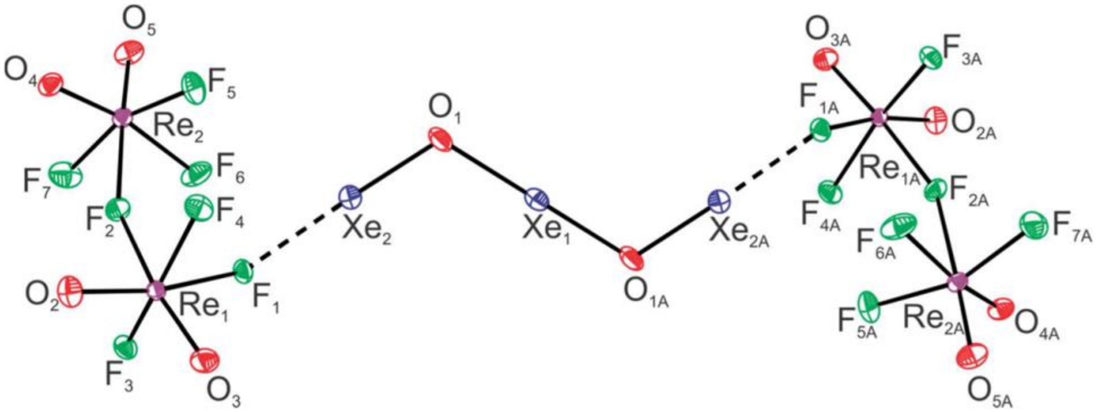

Figure 1.5. The single-crystal X-ray structure of $[XeOXeOXe][\mu\text{–F}(ReO_2F_3)_2]_2$; reproduced with permission from ref. 90.

1.3 Covalent and Noncovalent Interactions

1.3.1 Novel Xenon Element Bonds

Although the diversity of xenon-bonded compounds has significantly increased since the discovery of noble-gas reactivity, the majority of xenon compounds are still fluorine- and oxygen-bonded to xenon. The first Xe−N bonded compounds were synthesized by the reaction of XeF_2 with $HN(SO_2F)_2$ to form $FXeN(SO_2F)_2$ and $Xe[N(SO_2F)_2]_2$ (Figure 1.6).[92,93] The first Xe−C bonded compound, $[XeC_6F_5][C_6F_5BF_3]$, was synthesized by fluorine-pentafluorophenyl substitution of XeF_2.[94] Ligand transfer between $TMSC_6F_5$ and XeF_2 afforded $Xe(C_6F_5)_2$, the first homoleptic Xe−C bonded compound,[95] however, a Xe^{VI}–C bonded compound was not fully structurally characterized in the solid state until 2014 when Koppe *et al*. determined the crystal structure of $[C_6F_5XeF_2][BF_4]2HF$ (Figure 1.7).[96] Recently, Goettel and Schrobilgen synthesized $[N(CH_2CH_3)_4]_3{}^+[Br_3(XeO_3)_3]^{3-}$ and $[N(CH_3)_4]_4{}^+[Br_4(XeO_3)_4]_4$ (Figure 1.8), the first compounds to contain a Xe−Br bond.[97] Examples of Xe−Au,[98] Xe−Hg,[99] Xe−Xe[100] and Xe−Cl[101,102] bonded compounds are also known. Examples of Xe−S,[103] Xe−H,[103] Xe−Si,[104] and Xe−U[105] bonded compounds were observed in the gas-phase or low-temperature matrices, but not in macroscopic amounts. No evidence of a xenon-phosphorus bonded compound has been forthcoming.

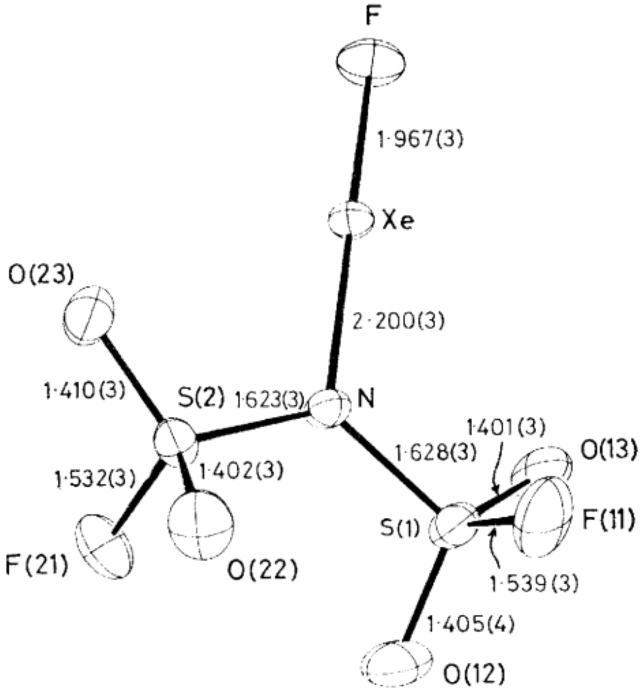

Figure 1.6. The X-ray crystal structure of FXeN(SO_2F_2); reproduced with permission from ref. 92.

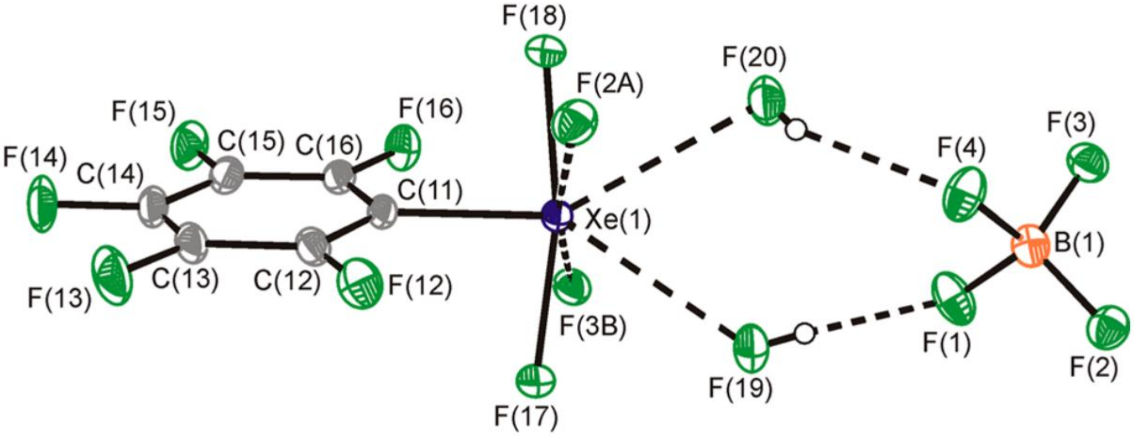

Figure 1.7. The X-ray crystal structure of $[C_6F_5XeF_2][BF_4]2HF$; reproduced with permission from ref. 96.

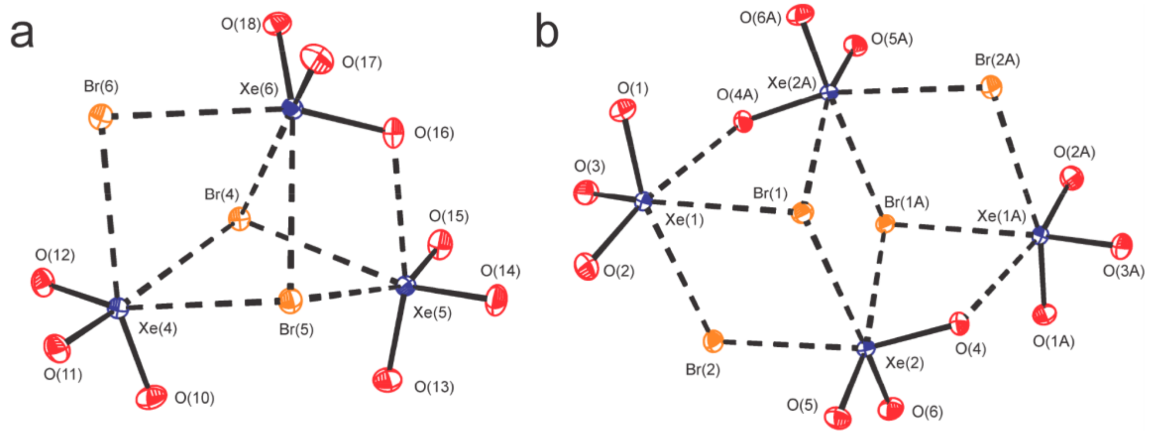

Figure 1.8. The X-ray crystal structures of the $[Br_3(XeO_3)_3]^{3-}$ and $[Br_4(XeO_3)_4]^{4-}$ anions in $[N(CH_2CH_3)_4]_3{}^{+}[Br_3(XeO_3)_3]^{3-}$ and $[N(CH_3)_4]_4{}^{+}[Br_4(XeO_3)_4]^{4-}$; reproduced with permission from ref. 101.

1.3.1 Noncovalent Interactions

The importance of noncovalent bonds is best demonstrated in dynamic biological processes. Not only are several types of noncovalent bonds critical to maintaining the three-dimensional structures of large molecules such as proteins, they also enable large molecules to bind specifically, but transiently, to one another.[106] Although the formation of a noncovalent bond releases only a small fraction of the energy released when a covalent bond is formed, multiple noncovalent bonds often result in highly stable interactions.[106] Noncovalent interactions are often classified as electrostatic, π-effects, van der Waals forces, or hydrophobic effects.[107–109]

An example of a noncovalent electrostatic interaction is a "σ-hole bond", which is synonomous with "halogen bonding". The pioneering work on σ-hole bonding interactions was reported by Guthrie[110] and continued many years later by Hassel,[111] who won the

1969 Nobel Prize in Chemistry for his discovery that halogens can act as electrophilic electron acceptors.[112] Present-day encounters with the concept of σ-hole bonding interactions range from crystal engineering and supramolecular chemistry,[113–117] to polymer science,[118] liquid crystals,[119,120] and conductive materials,[121,122] with groundwork applications in medicinal chemistry[114–117] and biological systems.[123–125]

The term "σ-hole bonding" is used to describe non-covalent, essentially electrostatic, interactions involving an electropositive atom, X, and an electron donor species, D. In a general definition,[108] the Lewis base (neutral or anionic) donates electron density to the Lewis acidic acceptor, which is covalently attached to atom Y. Hydrogen, pnictogen, chalcogen and halogen bonding are all types of σ-hole bonding interactions that are classified by the group of the element participating in bonding (with the exception of the group 1 element, hydrogen). In the case of hydrogen bonding, a hydrogen atom acts as the electron acceptor and forms a non-covalent interaction by accepting electron density from an electron rich site.[109]

Electron density is transferred from the covalent R−X bond resulting in interpenetration of the van der Waals volumes.[126,127] The X---D bonding interaction is rather strong and directional, occurring approximately trans to the polar-covalent R−X bond at an electropositive location on X termed the "σ-hole", with an approximately linear *trans*-R−X---D angle.[128]

Most examples of chalcogen bonds are noncovalent chalcogen-chalcogen interactions where the donor is also a chalcogen atom, similar to a halogen-halogen interaction.[129] Some have suggested the importance of such chalcogen-chalcogen interactions in protein folding.[130–132] Pnicogen-pnicogen interactions have bond strengths that are comparable to those of hydrogen bonding interactions and are important interactions in self-assembly processes in the field of supramolecular chemistry.[133]

Most noble-gas species exhibit so-called “hypervalent” bonding (bonding involving a main-group element with more than eight valence electrons).[134] Recent examples of a group 18 element, namely xenon, which engages in σ-hole bonding interactions have been published.[98,99,135,136]

1.4 Purpose and Scope of the Present Work

The overall goal of this research is to extend and deepen our knowledge of the fundamental chemistry of the noble-gas elements and high-oxidation-state compounds, namely Xe(VI). This includes extending the limits of our synthetic and characterization techniques to isolate extremely sensitive and unstable compounds. More specifically, a major focus of this research is to extend the chemistry of xenon trioxide (XeO_3) through exploration of its coordination chemistry using a variety of ligands and to structurally characterize the products.

The initial goal of this research was to explore the donor-acceptor properties of XeO_3. The strong oxidant properties of xenon fluorides, oxide fluorides, and oxides renders the syntheses of isolable organo-xenon compounds challenging. Examination of the Lewis acid strength of XeO_3 towards a variety of weak, strong, hard and/or soft organic Lewis bases led to the first examples of oxygen-base adducts of XeO_3, as well as the first examples of a complex between a noble-gas compound and a crown ether or other polydentate ligand. The Lewis acidity of XeO_3 towards soft sulfur and phosphorus donors was also examined and the products of these reactions were determined. The chemistry of XeO_3 with inorganic compounds was expanded through the syntheses and structural characterizations of several polyatomic anion–XeO_3 complexes, which also provide insights into the possible incorporation of xenon oxides into minerals.

The small number of compounds which contain XeO_3 has prevented a fuller understanding of Xe---L (L = N, O , F) interactions in the solid state. Computational studies and modelling of XeO_3 and its adducts using gas-phase structure optimizations, empirical and Wiberg bond valences, Wiberg bond indices, NPA charges, and Hirshfeld surface analyses have assisted with the characterization of secondary bonding (σ-hole) interactions in adducts with XeO_3, which may be extended to other XeO_3 adducts and xenon compounds in general.

Cumulatively, these research goals contribute to our understanding of secondary bonding interactions in Xe(VI) compounds. More specifically, this research demonstrates the importance of secondary bonding interactions and packing motifs for the kinetic stabilization of the extremely shock sensitive solid, XeO_3, in the solid state. The stabilization of XeO_3 in its adducts enables its safe handling and provides potential applications for clean oxidizers in organic transformations, such as epoxidations.

References

[1] G. J. Schrobilgen, M. D. Moran, "Noble Gas Compounds" in *Kirk-Othmer Encyclopedia of Chemical Technology*, 5th Ed., John Wiley & Sons, Inc., Hoboken, NJ, **2006**, Chapter 17, pp 323−343.

[2] G. J. Schrobilgen, "Noble Gas Chemistry" in *Encyclopedia of Physical Science and Technology*, 3rd ed., M.F. Hawthorne, Ed.; Academic Press: San Diego, 2002, Vol. 10, pp. 449−461.

[3] H. Selig, J. H. Holloway, In *Topics in Current Chemistry*; F. L. Bosche, Ed.; Springer-Verlag: Berlin, 1984; Vol. 124, pp 33−90.

[4] J. H. Holloway, *J. Fluorine Chem.* **1986**, *33*, 149.

[5] J. H. Holloway, E. G. Hope, *Adv. Inorg. Chem.* **1998**, *46*, 51.

[6] G. J. Schrobilgen, In *Synthetic Fluorine Chemistry*; G. A. Olah, G. K. S. Prakash, R. D. Chambers, Eds.; John Wiley & Sons, Inc.: New York, 1999, pp 31−42.

[7] M. Gerken, G. J. Schrobilgen, *Coord. Chem. Rev.* **2000**, *197*, 335.

[8] V. K. Brel, N. S. Pirkuliev, N. S. Zefirov, *Russ. Chem. Rev. (Engl. Transl.)* **2001**, *70*, 231.

[9] G. J. Schrobilgen, "Lewis Acid Properties of Noble Gas Cations", In *Synthetic Fluorine Chemistry*, R.D. Chambers, G.A. Olah and G.K.S. Prakash, eds., New York: Wiley and Sons, 1992, Chapter 1, pp. 1−30.

[10] B. Žemva, *Croat. Chem. Acta* **1988**, *61*, 163.

[11] B. Žemva, "The Chapter Noble-Gases: Inorganic Chemistry" in *Encyclopedia of Inorganic Chemistry*, John Wiley & Sons, Inc., New York, 1994, Vol. 5, pp 2660−2680.

[12] J. F. Lehmann, H. P. A. Mercier, G. J. Schrobilgen, *Coord. Chem. Rev.* **2002**, *233–234*, 1−39 and references therein.

[13] P. Laszlo, G. J. Schrobilgen, *Angew. Chem. Int. Ed. Engl.* **1988**, *27*, 479−489.

[14] P. Ball, "Not So Noble", In *Elegant Solutions: Ten Beautiful Experiments in Chemistry*, The Royal Society of Chemistry, Cambridge, UK, 2005, Chapter 7, pp. 139−150.

[15] H. Moissan, *Compt. Rend.* **1895**, *120* , 966.

[16] A. von Antropoff, H. Frauenhof, K. H. Krüger, *Naturwissenschaften* **1933**, *21*, 315.

[17] D. M. Yost, A. L. Kaye, *J. Am. Chem. Soc.* **1933**, *55*, 3890.

[18] N. Bartlett, *Proc. Chem. Soc.,* **1962,** 218.

[19] F. O. Sladky, P. A. Bulliner, N. Bartlett, *J. Chem. Soc. A* **1969**, 2179.

[20] L. Graham, O. Graudejus, N. K. Jha, N. Bartlett, *Coord. Chem. Rev.* **2000**, *197*, 321.

[21] G. J. Moody, *J. Chem. Educ.* **1974**, *51*, 628.

[22] R. Hoppe, W. Diihne, H. Mattauch, K. M. Rodder, *Angew. Chem.* **1962**, *74*, 903.

[23] C. L. Chernick, H. H. Claassen, P. R. Fields, H. H. Hyman, J. G. Ma1m, W. M. Manning, M. S. Matheson, L. A. Quarterman, F. Schreiner, H. H. SeIig, L. Sheft, S. Siegel, E. N. Sloth, L. Stein, M. Studier, J. L. Weeks, M. H. Zirin, *Science*, **1962**, *138*, 136.

[24] J. L. Weeks, C. L. Chernick, M. S. Matheson, *J. Amer. Chem. Soc.* **1962**, *84*, 4612.

[25] Hoppe, R.; Mattauch, H.; Rodder, K. M.; Diihne, W. *Z. Anorg. Chem.* **1963**, *324*, 214.

[26] D. F. Smith, *J. Chem. Phys*. **1963**, *38*, 270.

[27] K. Lutar, A. Šmalc, J. S1ivnik, *Vestn. Slovo Kem. Drus.***1979**, *26*, 435.

[28] H. F. Winters, J. W. Coburn, *Appl. Phys. Lett.* **1979**, 34, 70.

[29] D. Xu, B. Xiong, Y. Wang, M. Liu, T. Li, *J. Micromechanics and Microeng.* **2009**, 19, 12, 125003.

[30] S. H. Wheale, J. P. S. Badyal, *Polymer*, **2011**, *52*, 5250.

[31] J. T. Robinson, J. S. Burgess, C. E. Junkermeier, S. C. Badescu, F. K. P. Reinecke, M. K. Zalalutdniov, J. W. Baldwin, J. C. Culbertson, P. E. Sheehan, E. S. Snow, *Nano Lett.* **2010**, *10*, 3001.

[32] A. P. Lothian, C. A. Ramsden, M. M. Shaw, R. G. Smith, *Tetrahedron* **2011**, *67*, 2788.

[33] K. Sugamata, T. Sasamori, N. Tokitoh, *Chem. Asian J.* **2011**, *6*, 2301.

[34] R. C. Burns, I. D. MacLeod, T. A. O’Donnell, T. E. Peel, K. A. Philips, A. B. Waugh, *J. Inorg. Nucl. Chem.* **1977**, *39*, 1737.

[35] Melita Tramšek; Boris Žemva, "Synthesis, Properties and Chemistry of Xenon(II) Fluoride", **2006**, *Acta Chim. Slov*. *53*, 105.

[36] C. L. Chernick, J. G. Malm, *Inorg. Synth.* **1966**, *8*, 254.

[37] D. S. Brock, J. J. Casalis de Pury, H. P. A. Mercier, G. J. Schrobilgen, B. Silvi, *Inorg. Chem.* **2010**, *49*, 6673–6689.

[38] V. I. Rigin, N. K. Skvortsov, V. V. Rigin, *Analystica Chimica Acta*, **1997**, *340*, 1.

[39] J. G. Malm, C. L. Chernick, *Inorg. Synth.* **1966**, *8*, 258.

[40] D. H. Templeton, A. Zalkin, J. D. Forrester, S. M. Williamson, *J. Am. Chem. Soc.* **1963**, *85*, 817.

[41] H. Selig, "Fluorine Chemistry of the Noble-Gasses". In *Halogen Chemistry*; Gutmann, V., Ed.; Academic: London, UK, 1967; Vol. *1*, p. 403.

[42] H. Selig, *Inorg. Chem.* **1966**, *5*, 183.

[43] J. L. Huston, *J. Phys. Chem.* **1967**, *71*, 3339.

[44] J. L. Huston, *Inorg. Nucl. Chem. Letters* **1968**, *4*, 29.

[45] H. H. Claassen, J. L. Huston, *J. Chem. Phys.***1971**, *55*, 1505.

[46] P. Zaleski-Ejgierd, P. M. Lata, *Scientific Reports,* **2016**, 6, 18938.

[47] D. S. Brock, G. J. Schrobilgen, *J. Am. Chem. Soc.* **2011**, *133,* 6265.

[48] S. M. Williamson, C. W. Koch, In *Noble-Gas Compounds*; Hyman, H. H. Ed.; University of Chicago Press: Chicago, IL, 1963; pp 149−151.

[49] J. S. Ogden, J. J. Turner, *Chem. Comm.* **1966**, *19*, 693.

[50] D. S. Brock, V. Bilir, H. P. A. Mercier, G. J. Schrobilgen, *J. Am. Chem. Soc.* **2007**, *129*, 3598.

[51] R. J. Gillespie, I. Hargittai, *The VSEPR Model of Molecular Geometry*; Allyn and Bacon: Boston, MA. 1991.

[52] C. Sanloup, B. C. Schmidt, E. M. Chamorro Perez, A. Jambon, E. Gregoryanz, M. Mohamed Mezouar, *Science*, **2005**, *310*, 1174.

[53] K. S. Pitzer, Bonding in xenon fluorides and halogen fluorides. *Science*, **1963**, *139*, 414.

[54] N. Bartlett, P. R. Rao, Xenon hydroxide: an experimental hazard. *Science*, **1963**, *139*, 506.

[55] D. F. Smith, Xenon trioxide. *J. Am. Chem. Soc*. **1963**, *85*, 816.

[56] D. F. Smith, *J. Am. Chem. Soc.* **1963**, *85*, 816.

[57] S. R. Gunn, *J. Am. Chem. Soc*. **1965**, *87*, 2290.

[58] S. R. Gunn, *In Noble-Gas Compounds* Hyman, H. H., Ed.; University of Chicago Press: Chicago, IL, 1963; pp 149−151.

[59] J. T. Goettel, G. J. Schrobilgen, *Inorg. Chem.* **2016**, *55*, 12975.

[60] H. Selig, H. H. Claassen, C. L. Chernick, J. G. Malm, J. L. Huston, *Science* **1964**, *143*, 1322.

[61] J. L. Huston, M. H. Studier, E. N. Sloth, *Science*, **1964**, *143*, 1161.

[62] G. Gunderson, K. Hedberg, J. L. Huston, *J. Chem. Phys.* **1970**, *52*, 812.

[63] M. Gerken, G. J. Schrobilgen *Inorg. Chem.* **2002**, 4*1*, 198.

[64] J. T. Goettel, Ph. D. Thesis, McMaster University, Hamilton, ON, Canada, 2017.

[65] J. G. Malm, B. D. Holt, R. W. Bane, In *Noble-Gas Compounds*; Hyman, H. H., Ed.; University of Chicago Press: Chicago, IL, 1963; p 167.

[66] E. H. Appelman, S. M. Williamson, *Inorg. Synth.* **1968**, *11*, 210.

[67] M. A. Forgeron, R. E. Wasylishen, M. Gerken, G. J. Schrobilgen, *Inorg. Chem.* **2007**, *46*, 3585.

[68] N. N. Aleinikov, V. K. Isupov, I. S. Kirin, B. L. Korsunskii, F. I. Dubovitskii, *Chem. Russ. Bull.* **1974**, *23*, 250.

[69] V. K. Isupov, I. S. Kirin, N. N. Alejnikov, B. L. Korsunskij, *Zh. Neorg. Khim.* **1977**, *22*, 1297.

[70] E. H. Appelman, J. G. Malm, *J. Am. Chem. Soc.* **1964**, *86*, 2141.

[71] L. D. Shustov, N. S. Tolmacheva, S. Nabiev, E. K. Il'in, V. D. Klimov, V. P. Ushakov, *Zh. Neorg. Khim.* **1989**, *34*, 1673.

[72] Y. Marcus, D. Cohen, *Inorg. Chem.* **1966**, *5*, 1740.

[73] E. H. Appelman, G. D. Downey, H. H. Claassen, *Inorg. Chem.* **1971**, *10*, 1817.

[74] J. A. Ibers, W. C. Hamilton, D. R. MacKenzie, *Inorg. Chem.* **1964**, *3*, 1412.

[75] A. Zalkin, J. D. Forrester, D. H. Templeton, S. M. Williamson, C. W. Koch, *Science* **1963**, *142*, 501.

[76] A. Zalkin, J. D. Forrester, D. H. Templeton, *Inorg. Chem.* **1964**, *3*, 1417.

[77] A. Zalkin, J. D. Forrester, D. H. Templeton, S. M. Williamson, C. W. Koch, *J. Am. Chem. Soc.* **1964**, *86*, 3569.

[78] S. N. Britvin, S. A. Kashtanov, M. G. Krzhizhanovskaya, A. A. Gurinov, O. V. Glumov, S. Strekopytov, Y. L. Kretser, A. N. Zaitsev, N. V. Chukanov, S. V. Krivovichev, *Angew. Chem. Int. Ed.* **2015**, *54*, 14340.

[79] S. N. Britvin, S. A. Kashtanov, S. V. Krivovichev, N. V. Chukanov, *J. Am. Chem. Soc.* **2016**, *138*, 13838.

[80] J. L. Peterson, H. H. Claassen, E. H. Appelman, *Inorg. Chem.* **1970**, *9*, 619.

[81] C. K. Jørgensen, H. Berthou, *Chem. Phys. Lett.* **1975**, *36*, 432.

[82] H. D. Waard, S. Bukshpan, G. J. Schrobilgen, J. H. Holloway, D. Martin, *J Chem. Phys.* **1979**, *70*, 3247.

[83] B. Jaselskis, *Rec. Chem. Prog.* **1970**, *31*, 103.

[84] T. M. Spittler, B. Jaselskis, *J. Am. Chem. Soc.* **1966**, *88*, 2942.

[85] T. Vent-Schmidt, J. T. Goettel, G. J. Schrobilgen, S. Riedel, *Chem. Eur. J.* **2015**, *21*, 11244.

[86] B. S. Ault, L. Andrews, *Chem. Phys. Lett.* **1976**, *43*, 350.

[87] T. H. Dunning, P. J. Hay, *J. Chem. Phys.* **1977**, *66*, 3767.

[88] M. Yamanishi, K. Hirao, K. Yamashita, *J. Chem. Phys.* **1998**, *108*, 1514.

[89] M. Gerken, M. D. Moran, H. P. A. Mercier, B. E. Pointner, G. J. Schrobilgen, B. E. Hoge, K. O. Christe, J. A. Boatz, *J. Am. Chem. Soc.* **2009**, *131*, 13474.

[90] M. V. Ivanova, H. P. A. Mercier, G. J. Schrobilgen, *J. Am. Soc. Chem.* **2015**, *137*, 13398.

[91] J. R. DeBackere, M. B. Bortolus, G. J. Schrobilgen, *Angew. Chem. Int. Ed.* **2016**, *55*, 11917.

[92] D. D. DesMarteau, R. D. LeBlond, S. F. Hossain, D. Nothe, *J. Am. Chem. Soc.* **1981**, *103*, 7734.

[93] J. F. Sawyer, G. J. Schrobilgen, S. J. Sutherland, *Inorg. Chem.* **1982**, *21*, 4064.

[94] H-J. Frohn, S. Jakobs, G. Henkel, *Angew. Chem. Int. Ed.* **1989**, *28*, 1506.

[95] N. Maggiarosa, D. Naumann, W. Tyrra, *Angew. Chem. Int. Ed.* **2000**, *39*, 4588.

[96] K. Koppe, J. Haner, H. P. A. Mercier, H-J. Frohn, G. J. Schrobilgen, *Inorg. Chem.* **2014**, *53*, 11640.

[97] J. T. Goettel, V. G. Haensch, G. J. Schrobilgen, *J. Am. Chem. Soc.* **2017**, *139*, 8725.

[98] S. Seidel, K. Seppelt, *Science* **2000**, *290*, 117.

[99] I. C. Hwang, S. Seidel, K. Seppelt, *Angew. Chem. Int. Ed.* **2003**, *42*, 4392.

[100] P. Chaudhary, J. T. Goettel, H. P. A. Mercier, S. Sowlati-Hashjin, P. Hazendonk, M. Gerken, *Chem. Eur. J.* **2015**, *21*, 6247.

[101] H. J. Frohn, T. Schroer, G. Henkel, *Angew. Chem. Int. Ed.* **1999**, *38*, 2554.

[102] S. Seidel, K. Seppelt, *Angew. Chem. Int. Ed.* **2001**, *40*, 4225.

[103] M. Pettersson, J. Lundell, L. Khriachtchev, E. Isoniemi, M. Räsänen, *J. Am. Chem. Soc.* **1998**, *120*, 7979.

[104] R. Cipollini, F. Grandinetti, *J. Chem. Soc., Chem. Commun.* **1995**, ***7***, 773.

[105] J. Li, B. E. Bursten, B. Liang, L. Andrews, *Science*, **2002**, *295*, 2242.

[106] L. J. Prins, D. N. Reinhoudt, P. Timmerman, *Angew. Chemie. Int. Ed. Eng.* **2001**, *40*, 2382.

[107] P. Politzer, J. S. Murray, T. Clark, *Top. Curr. Chem.* **2015**, *358*, 19.

[108] A. Bauza, T. J. Mooibroek, A. Frontera, *ChemPhysChem* **2015**, *16*, 2496.

[109] P. Politzer, J. S. Murray, T. Clark, *Phys. Chem. Chem. Phys.* **2013**, *15*, 11178.

[110] F. J. Guthrie, *J. Chem. Soc*. **1863**, *16*, 239.

[111] O. Hassel, J. Hvoslef, *Acta Chem. Scand*. **1954**, *8*, 873.

[112] O. Hassel, *Science*, **1970**, *170*, 497.

[113] P. Metrangolo, H. Neukirch, T. Pilati, G. Resnati, *Acc. Chem. Res*. **2005**, *38*, 386.

[114] M. Fourmigue, P. Auban-Senzier, *Inorg. Chem*. **2008**, *47*, 9979.

[115] C. Bissantz, B. Kuhn, M. Stahl, *J. Med. Chem.* **2010**, *53*, 5061.

[116] Y. Lu, T. Shi, Y. Wang, H. Yang, X. Yan, X. Luo, H. JiangW. Zhu, *J. Med. Chem.* **2009**, *52*, 2854.

[117] E. Parisini, P. Metrangolo, T. Pilati, G. Resnati, G. Terraneo, *Chem. Soc. Rev*. **2011**, *40*, 2267.

[118] P. Metrangolo, G. Resnati, T. Pilati, R. Liantonio, F. Meyer, *J. Polym. Sci., Part A: Polym. Chem.* **2007**, *45*, 1.

[119] D. W. Bruce, P. Metrangolo, F. Meyer, C. Prasang, G. Resnati, G. Terraneo, A. C. Whitwood, *New J. Chem.* **2008**, *32*, 477.

[120] D. W. Bruce, P. Metrangolo, F. Meyer, T. Pilati, C. Prasang, G. Resnati, G. Terraneo, S. G. Wainwright, A. C. Whitwood, *Chem. Eur. J.* **2010**, *16*, 9511.

[121] Fourmigue, M.; Batail, P. *Chem. Rev.*, **2004**, *104*, 5379.

[122] M. Brezgunova, K. S. Shin, P. Auban-Senzier, O. Jeannin, M. Fourmigue, *Chem. Commun.* **2010**, *46*, 3926.

[123] P. Auffinger, F. A. Hays, E. Westhof, P. S. Ho, *Proc. Natl. Acad. Sci.* U.S.A., **2004**, *101*, 16789.

[124] A. R. Voth, F. A. Hays, P. S. Ho *Proc. Natl. Acad. Sci.* U.S.A., **2007**, *104*, 6188.

[125] A. R. Voth, P. Khuu, K. Oishi, P. S. Ho *Nat. Chem.* **2009**, *1*, 74.

[126] K. E. Riley, J. S. Murray, J. Fanfrlík, J. Řezáč, R. J. Solá, M. C. Concha, F. M. Ramos, P. Politzer, *J. Mol. Model.* **2011**, *17*, 3309.

[127] J. S. Murray, P. Lane, T. Clark, K. E. Riley, P. Politzer, *J. Mol. Model.* **2012**, *18*, 541.

[128] P. Scilabra, G. Terraneo, G. Resnati, *J. Fluorine Chem.* **2017**, *203*, 62.

[129] W. Z. Wang, B. M. Ji, Y. Zhang, *J. Phys. Chem. A* **2009**, *113*, 8132.

[130] E. A. Meyer, R. K. Castellano, F. Diederich, *Angew. Chem. Int. Ed.*, **2003**, *42*, 1210.

[131] T. P. Tauer, M. E. Derrick, C. D. Sherrill, *J. Phys. Chem. A* **2005**, *109*, 191.

[132] C. A. Morgado, J. P. McNamara, I. H. Hillier, N. A. Burton, M. A. Vincent, *J. Chem. Theory Comput*. **2007**, *3*, 1656.

[133] M. M. Watt, M. S. Collins, D. W. Johnson *Acc. Chem. Res*. **2013**, *36*, 955.

[134] J. I. Musher *Angew. Chem. Int. Ed. Engl.* **1969**, *8*, 54.

[135] J. T. Goettel, K. Matsumoto, H. P. A. Mercier, G. J. Schrobilgen *Angew. Chem. Int. Ed.* **2016**, *55*, 13780; *Angew. Chem.* **2016**, *128*, 13984.

[136] J. T. Goettel, H. P. A. Mercier, G. J. Schrobilgen *J. Fluorine Chem*. **2018**, *211*, 60.

CHAPTER 2

Experimental

2.1 Standard Techniques

2.1.1 Dry Box and Vacuum Line Techniques

The compounds prepared and used in this work were extremely moisture- and temperature-sensitive. Volatile compounds were handled under rigorously anhydrous conditions on glass and metal vacuum line systems. Non-volatile materials were handled in an inert atmosphere (N_2 gas) dry box (Vacuum Atmospheres Model DLX, oxygen and moisture (<0.1 ppm) equipped with a glass cyrowell for low temperature work. Low temperature preparative work inside the drybox was accomplished using a metal Dewar filled with 4.5 mm copper-plated spheres (air rifle BBs) that were previously cooled in ca. –140 ^{o}C in the glass cyrowell of the dry box.

Preparative work involving volatile corrosive fluorides that attack glass, e.g., HF, was carried out on metal vacuum lines constructed primarily from 316 stainless steel and nickel fitted with 316 stainless steel valves (Autoclave Engineers, Inc., Figure 2.1). Pressures were measured at ambient temperatures using MKS Model PDR-5B pressure transducers having wetted surfaces constructed of Inconel. The pressure transducer possessed a range of 0–1150 Torr, which was accurate to ±0.5 Torr.

Preparative work involving volatile materials that do not attack glass was carried out on Pyrex glass vacuum lines equipped with grease-free 6mm J. Young glass stopcocks

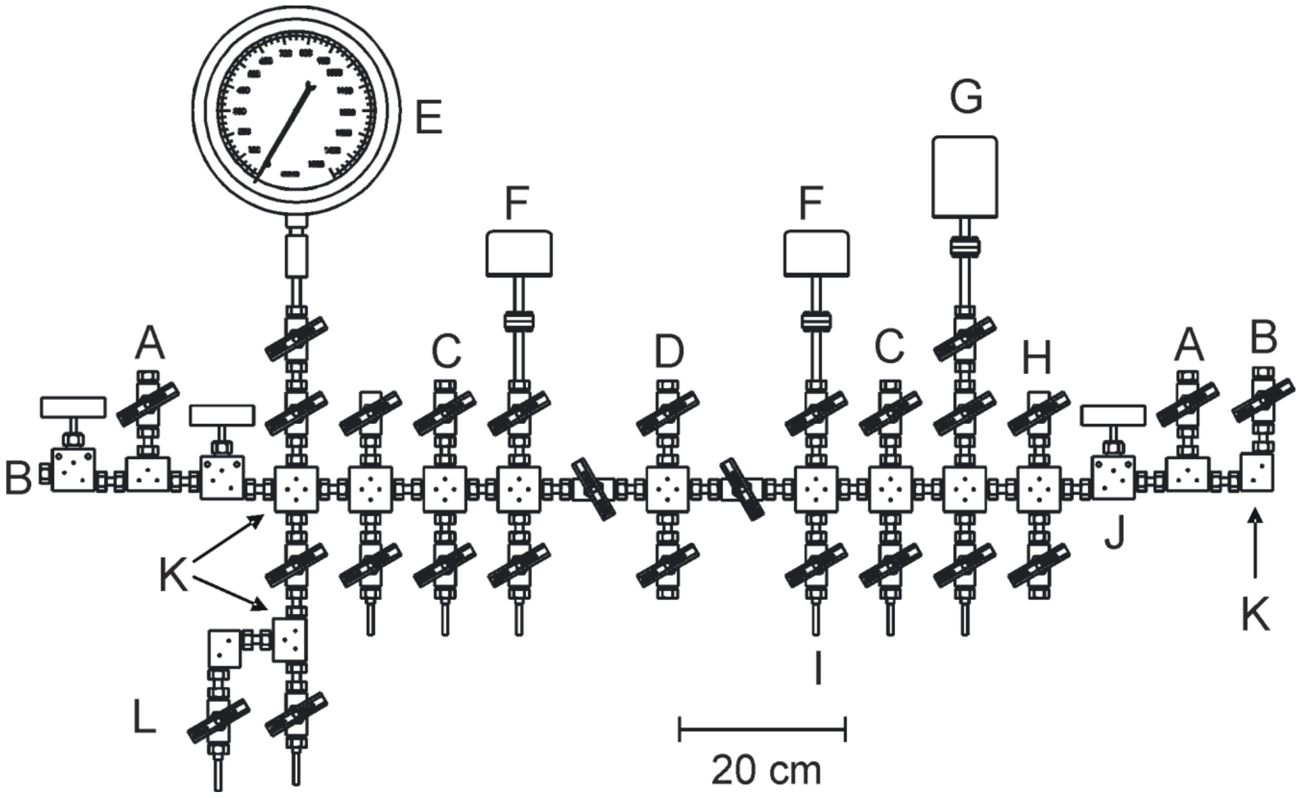

Figure 2.1. The metal vacuum line used for the manipulation of corrosive materials. (A) Outlet to liquid nitrogen and soda lime traps followed by a two-stage direct-drive rotary vacuum pump (Edwards E2M8) – roughing vacuum. (B) Outlet to soda lime and liquid nitrogen traps followed by a two-stage direct-drive rotary vacuum pump (Edwards E2M8) – high vacuum. (C) Dry N_2 inlets. (D) F_2 inlet. (E) Bourdon pressure gauge (0–1500 Torr). (F) MKS Model PDR-5B pressure transducers (0–1000 Torr). (G) MKS Model PDR-5B pressure transducer (0–10 Torr). (H) Ultra-high purity argon inlet. (I) ¼-in. o.d. ($^1/_8$-in. i.d.) nickel reaction vessel port. (J) High-pressure stainless steel valve (Autoclave Engineers). (K) 316 stainless steel X-, T-, and L-connections employing $^3/_8$-in. o.d. ($^1/_8$-in. i.d.) threaded nickel tubing. (L) Submanifold. From ref. 1.

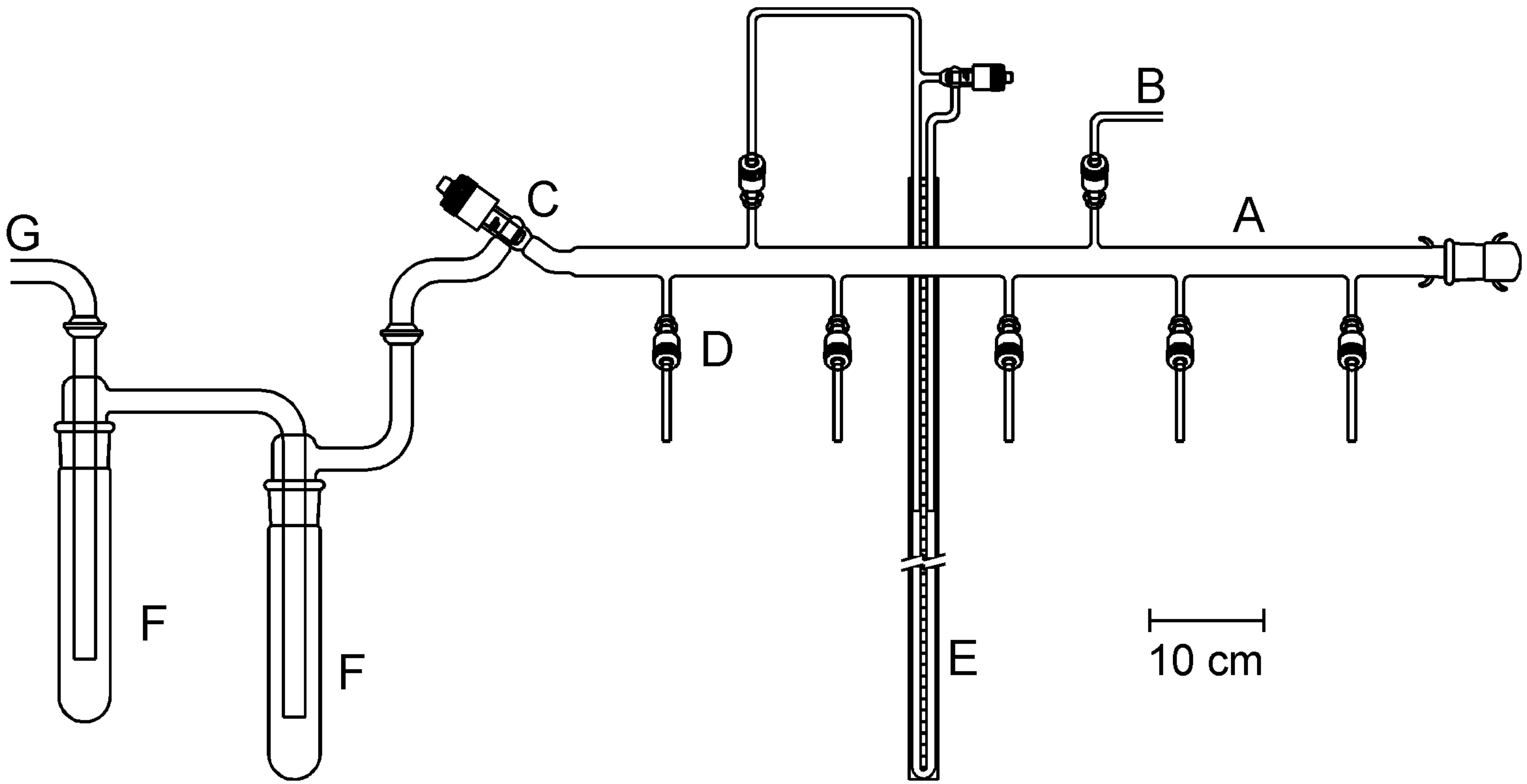

Figure 2.2. Glass vacuum line used for the manipulation of non-corrosive volatile materials. (A) Main vacuum manifold. (B) Dry N_2 inlet. (C) 15-mm greaseless glass J. Young stopcock with PTFE barrel. (D) 6-mm greaseless J. Young stopcock with PTFE barrel. (E) Mercury manometer. (F) Liquid N_2 cold trap. (G) Outlet to vacuum pump. Reproduced with permission from ref. 1.

outfitted with PTFE barrels (Figure 2.2). Pressures inside the glass manifold were monitored using a mercury manometer.

Vacuum on the glass vacuum lines (ca. 10^{-3}–10^{-4} torr) was accomplished using Edwards two-stage internal vane E2M8 direct-drive vacuum pumps. Vacuum was maintained on the metal line using two E2M8 vacuum pumps. The first vacuum pump provided the high vacuum (ca. 10^{-4} torr) source for the manifold and was fitted with a glass liquid nitrogen trap. The second, a roughing pump, was used for the removal of volatile fluoride and oxide fluoride compounds. The rough pump drew reactive, volatile fluorine compounds through a fluoride/fluorine trap consisting of a stainless steel tube (ca. 60 cm, 15 cm dia.) packed with soda lime absorbent (Fisher Scientific, 4–8 mesh), followed by a glass liquid nitrogen trap to remove CO_2 and water formed by the reaction of fluoride materials with soda lime, and other volatile materials that were unreactive towards soda lime.

2.1.2 Preparative Apparatus and Sample Vessels

All synthetic work was carried out in reactors constructed from lengths of ¼–in o.d. FEP tubing which were heat sealed at one end and heat-flared (45^{o} SAE) at the other. The tubing was connected to Kel-F valves, encased in aluminum housings, using brass flare fittings. All vessels were connected to vacuum lines using ¼–in. stainless steel Swagelok Ultratorr unions. Before use, reaction vessels were rigorously dried by pumping for ca. 12 h under dynamic vacuum on a glass manifold, followed by passivation with ca. 1000 Torr of F_2 for ca. 12 h on the metal vacuum line. Once passivated, vessels were evacuated under dynamic vacuum to remove all volatile impurities and back-filled with dry N_2 (ca. 1000

Torr) prior to use. Similarly, connections made to a metal vacuum line were dried under dynamic vacuum and passivated with F_2 gas overnight. Connections made to a glass vacuum line were dried under dynamic vacuum overnight. All connections to vacuum lines were made using thick-walled ¼–in. FEP tubing in conjunction with either a ¼–in. PTFE Swagelok connector outfitted with PTFE compression fittings (front and back ferrels) or a ¼–in. stainless steel Swagelok Ultra-Torr connectors outfitted with stainless steel compression fittings and Viton rubber O-rings.

2.2 Preparation and Purification of Starting Materials

2.2.1 Sources and Purification of Gases; N_2, Ar, F_2, and Xe

Technical grade nitrogen gas (Praxair, 9.998%), high purity argon gas (VitalAire), also employed for the back pressuring of reaction vessels, technical grade fluorine gas (Air Products) and ultra-high purity Xe (Air Products, 99.995%) were used without further purification. House nitrogen boil-off was used for the low temperature Raman spectroscopy device and low temperature crystal-mounting apparatus. The nitrogen boil-off for the low temperature crystal-mounting apparatus passed through a column consisting of Drierite® followed by 4 Å molecular sieves.

2.2.2 Purification of Solvents; Anhydrous HF, SO_2ClF, CH_3CN, and Acetone

HF. Anhydrous hydrogen fluoride, HF (Harshaw Chemical Co.), was purified by addition of ca. 5 atm of fluorine gas to a commercial HF sample contained in a nickel can approximately one month prior to use, converting residual water to HF and O_2 gas. The HF was then distilled into a Kel-F storage vessel equipped with a Kel-F valve for storage at room temperature. Transfer of HF was accomplished by vacuum distillation from the Kel-

F storage container through connections constructed from FEP on a metal vacuum line (Figure 2.3).

SO_2ClF. Sulfuryl chloride fluoride (Allied Chemical Co., Baker and Adams Division, >90%, ca. 100 g crude material) was purified by fractional distillation through two FEP U-tube traps cooled to –78 ^{o}C and –90 ^{o}C respectively, effectively removing the impurity SO_2F_2. The remaining SO_2ClF was then condensed into an FEP U-tube containing ca. 80 g of SbF_5 at –78 ^{o}C and slowly warmed up to room temperature with vigorous mixing to remove the impurity SO_2. The purified SO_2ClF was condensed into an FEP U-tube containing KF and cooled to –78 ^{o}C. Again, the mixture was slowly warmed to room-temperature with vigorous mixing and allowed to stand for ca. 2 h at room temperature to remove any residue HF. The sample was again cooled to –78 ^{o}C ad condensed into a 1.25–in. FEP reaction vessel containing XeF_2 (1.7 g) for 24 h to ensure all impurities with reducing properties were removed. Finally, the liquid was distilled by dynamic pumping at –78 ^{o}C into a Pyrex glass vessel, outfitted with a 6-mm J. Young all glass stopcock, over a bed of KF for storage at room-temperature. Transfers were performed using a glass vacuum line by vacuum distillation of SO_2ClF through a sub-manifold comprised of a Y-shaped glass connection to the reaction vessel (Figure 2.4).

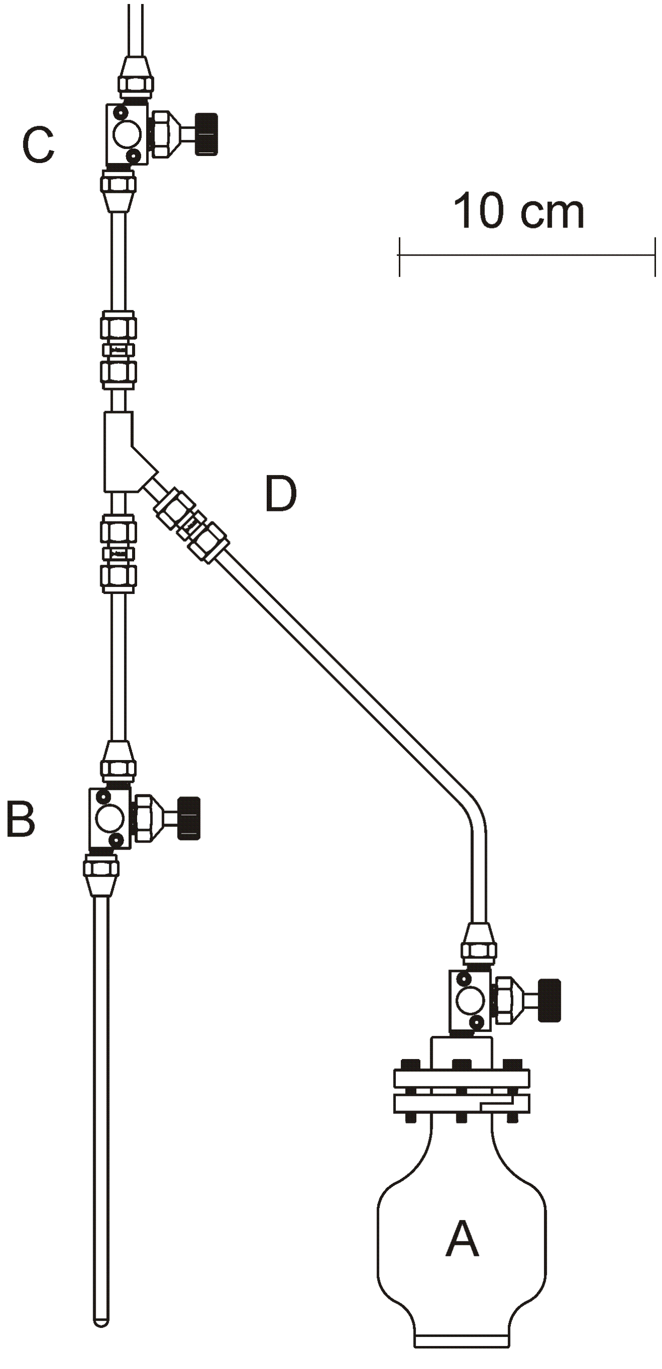

Figure 2.3. Hydrogen fluoride distillation apparatus. (A) Kel-F storage vessel containing HF. (B) FEP reaction vessel fitted with a Kel-F valve. (C) Kel-F valve connected to vacuum manifold. (D) Kel-F Y-connection with ¼-in. PTFE Swagelok unions. Reproduced with permission from ref. 1.

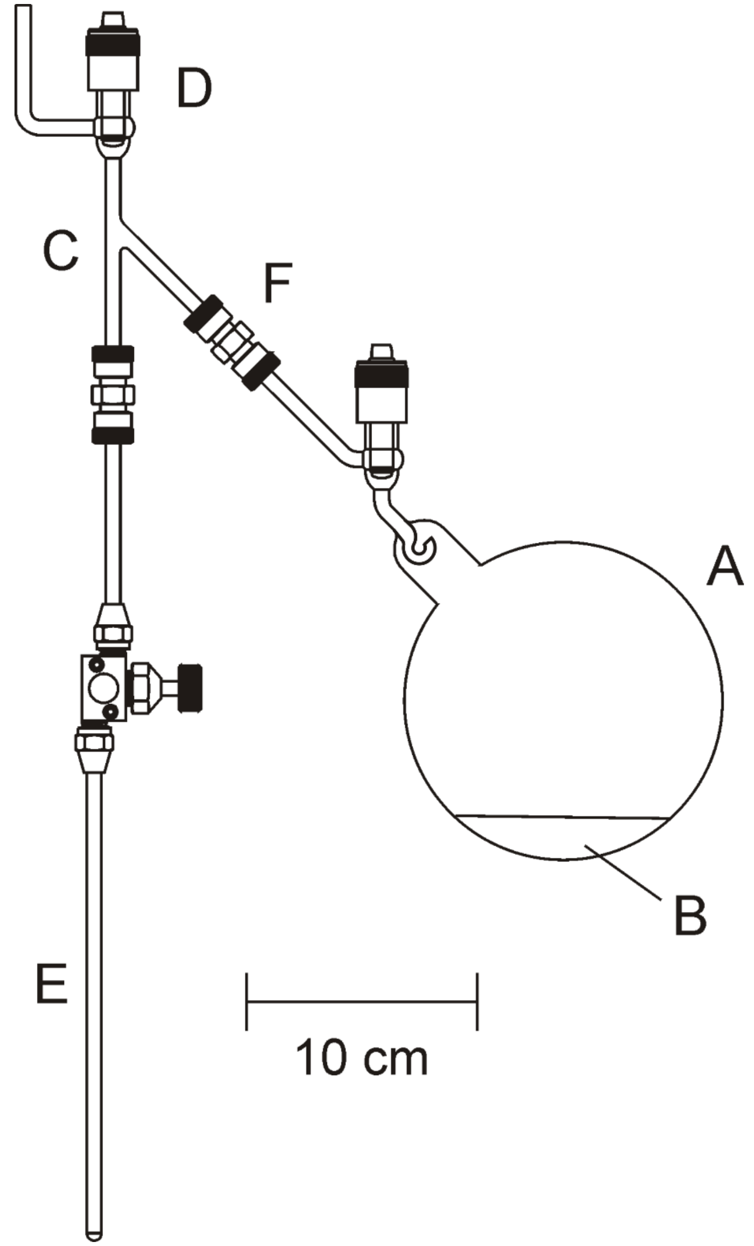

Figure 2.4. Apparatus used for the vacuum transfer of SO_2ClF solvent. (A) 250-mL glass vessel equipped with a grease-free 6-mm J. Young PTFE/glass stopcock outfitted with PTFE barrel. (B) Bed of dry, powdered KF. (C) Glass Y-connector. (D) 6-mm J. Young PTFE/glass valve. (E) FEP reaction vessel fitted with a Kel-F valve. (F) Stainless steel Swagelok Ultratorr Union. Reproduced with permission from ref. 1.

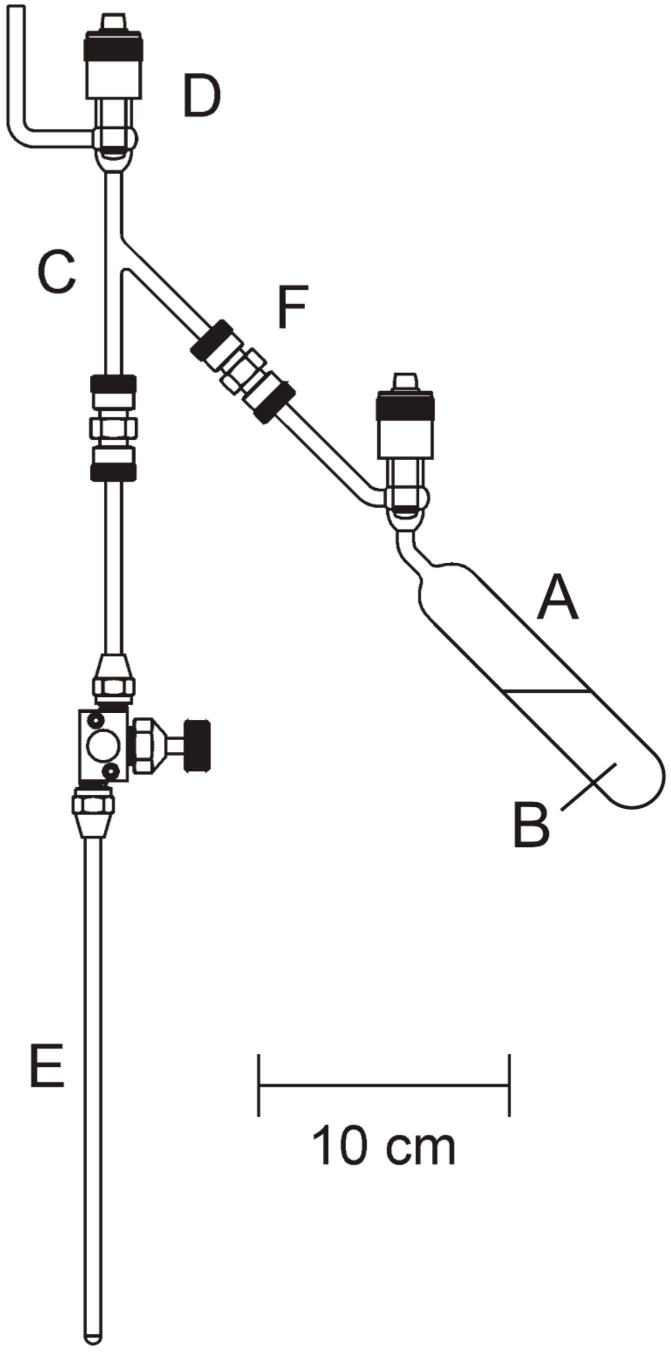

Figure 2.5. Apparatus used for the vacuum transfer of CH_3CN solvent. (A) 200-mL glass vessel equipped with a grease-free 6-mm J. Young PTFE/glass stopcock outfitted with PTFE barrel. (B) CH_3CN. (C) Glass Y-connector. (D) 6-mm J. Young PTFE/glass valve. (E) FEP reaction vessel fitted with a Kel-F valve. (F) Stainless steel Swagelok Ultratorr Union. Reproduced with permission from ref. 1.

CH_3CN. Acetonitrile (Caledon, HPLC Grade) was purified according to the literature method[2] and was stored over molecular sieves in a glass vessel outfitted with a grease-free 6-mm J. Young glass/PTFE stopcock. Acetonitrile was transferred under vacuum using a glass vacuum line and a glass Y-piece into a smaller glass dispensing vessel outfitted with a grease-free 6-mm J. Young glass/PTFE stopcock. For individual reaction vessels, acetonitrile was then dispensed under vacuum using a glass vacuum line and a glass Y-piece. (Figure 2.5).

Acetone. Acetone was purified by double vacuum distillation onto $MgSO_4$ at 0 °C and was thoroughly degassed using a freeze-pump-thaw sequence. Purified acetone was stored over $MgSO_4$ in a glass vessel outfitted with a grease-free 6-mm J. Young glass/PTFE stopcock. Acetone was transferred under vacuum using a glass vacuum line and a glass Y-piece.

2.2.3 Preparation and Purification of XeF_2, XeF_4 and XeF_6

Xenon difluoride[3] and XeF_4[4] were prepared according to the literature methods and stored in a Kel-F tube inside a dry box until needed. Xenon hexafluoride was prepared by the reaction of Xe and F_2 similar to the method described by Malm and Chernick.[5] Small amounts of XeF_4 impurity, identified by two weak bands at 502 and 543 cm^{-1} in the Raman spectrum, did not interfere with the chemistry described herein.

2.2.4 Synthesis of XeO_3

Method 1. In a typical preparation, XeF_6 (1–2 g) was transferred under static vacuum into a ½-in. o.d. FEP U-tube fitted with Swagelok Stainless steel valves. Using a flow of dry nitrogen gas, XeF_6 vapor was swept into a 100 mL FEP bottle containing water (ca. 20 mL) while stirring with a Teflon coated stir-bar (Figure 2.6). The resulting solutions of XeO_3

and dilute $HF_{(aq)}$ ($XeO_3 \cdot 6HF$) were transferred to trays constructed from FEP using pipettes drawn from FEP. Solid XeO_3 was obtained by allowing evaporation of the solvent in the fume hood. Solid XeO_3 can only be reliably obtained if the relative humidity is below 30% at 20 °C. Concentrations of XeO_3 were determined by mass measurements.

Method 2. In a typical reaction, XeF_6 (28.0 mg, 0.115 mmol) was transferred under static vacuum at −196 °C into a 1/4 –in. FEP reactor. Freon-114 (ca. 0.5 ml) was vacuum distilled onto XeF_6 at −196 °C; the reactor was warmed to room temperature, whereupon XeF_6 dissolved to form a bright yellow solution. Acetonitrile (ca. 0.5 mL) was vacuum distilled into and frozen in the top portion of the reaction vessel at −196 °C. The reactor was allowed to warm to −40 °C and the contents were carefully mixed by allowing the XeF_6 to diffuse into the upper CH_3CN layer. Three equivalents of H_2O (6.22 mg, 0.345 mmol) were added to the reaction vessel at 0 °C by use of a microsyringe. The reaction mixture was slowly warmed to 20 °C and thoroughly mixed. A fine white powder ($O_3Xe(NCCH_3)_2$) was obtained upon removal of volatiles under dynamic vacuum at −40 to −30 °C. Acetonitrile (ca. 0.5 mL) was vacuum distilled into the top portion of the reactor at −78 °C *(Caution! To avoid detonation, never rapidly cool the reactor significantly below −78 °C)*. The reactor was warmed to −40 °C whereupon the solid dissolved to form a clear, colorless solution.

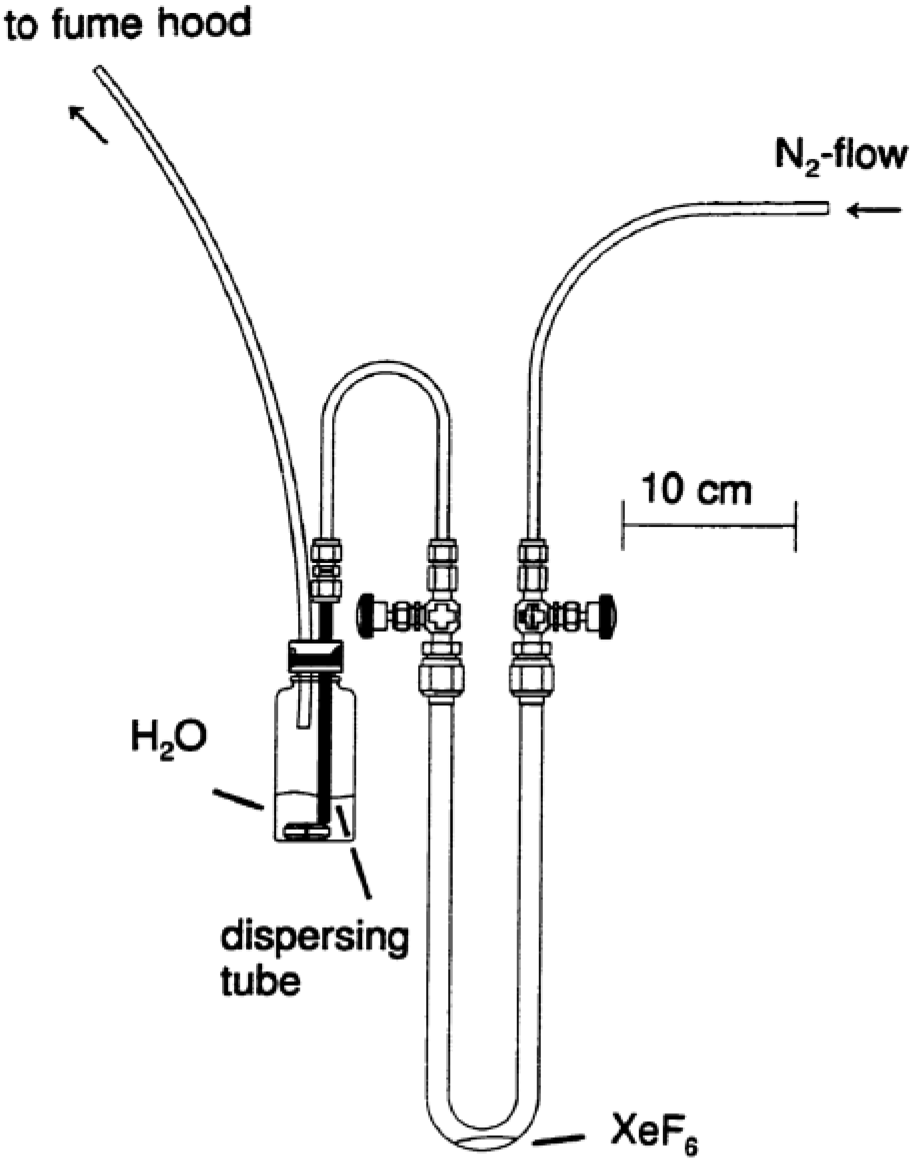

Figure 2.6. Apparatus for the synthesis of aqueous XeO_3 solutions. An FEP trap containing XeF_6 and a Teflon capped FEP bottle containing water and a Teflon coated stir bar. Reproduced with permission from ref. 21.

2.2.5 Preparation of HF-Free XeO_3 under Atmospheric Conditions

An aqueous solution of XeO_3 was synthesized by hydrolysis of XeF_6 as previously described.[6] An aliquot (ca. 10 mg, 0.056 mmol XeO_3) of the resulting aqueous solution, $XeO_3{\cdot}6HF$, was transferred into a 3 × 3 cm FEP (hexafluoropropylene, tetrafluoroethylene copolymer) fluoroplastic tray by use of a pipette fabricated from FEP tubing. Water and HF were removed from XeO_3 by evaporation overnight in a fume hood to give solid XeO_3. The sample was transferred to a plastic (HDPE) desiccator and dried over 4 Å molecular sieves for 2−3 h to ensure that all surface water had been removed from $XeO_{3(s)}$.

2.3 Raman Spectroscopy

All Raman spectra were recorded on a Bruker RFS 100 Fourier transform Raman spectrometer employing a quartz beam splitter and a liquid-nitrogen cooled Ge diode detector. The 1064-nm line of a Nd-YAG laser was used for excitation with a laser spot of <0.1 mm at the sample and configured such that only the 180°-backscattered radiation was detected. The scanner velocity was 5kHz and the wavelength range was 5894 to 10394 cm^{-1} relative to the laser line at 9394 cm^{-1}, resulting in a spectral range of 3501 to –999 cm^{-1}. Fourier transformations were processed using a Blackman Harris 4-tem apodization and a zero-filling factor of 2. Typical acquisitions used 1.0 cm^{-1} resolution, 100–500 mW power, and involved 512 scans for strongly scattering sample and 1024 – 2048 scans for weakly scattering samples. Low temperature spectra were acquired using a Bruke I0121 low temperature accessory which provided a temperature of –78 °C for samples containing XeO_3 and a temperature range of –150 to –160 °C for all other samples, with an estimated error of ±1 °C.

2.4 Quantum-Chemical Calculations

All calculations were performed using Gaussian 09[7] software packages. Geometries were fully optimized using density functional theory methods and the Def2-TZVP and/or Def2-TZVPD basis sets. Basis sets were obtained online from the EMSL Basis Set Exchange (https://bse.pnl.gov/bse/portal).[8] Fundamental vibrational frequencies were calculated along with Raman intensities, and Natural Bond Orbital (NBO) analyses were obtained for the optimized local minima. The program GaussView[9] was used to visualize the vibrational displacements that form the basis of the vibrational mode descriptions presented. Natural bond orbital analyses were carried out by use of the NBO program (version 6.0)[10] implemented in Gaussian 09. The MEPs diagrams were drawn with Jmol.[11] The CrystalExplorer 3.1[12] program was used for Hirshfeld surface analyses and the computational program Tonto,[13] as implemented in CrystalExplorer, was used for wavefunction calculations and for mapping of the electrostatic potential surface (B88LYP/321-G) onto the Hirshfeld surface.

2.5 X-ray Crystallography

2.5.1 Crystal Growth

Crystallization of samples at room-temperature was accomplished by slow evaporation of the solvent in a fume-hood. For all samples that were grown at low temperatures, slow-cooling of acetone bathes was accomplished by addition of either dry-ice or liquid nitrogen in small quantities.

2.5.2 Low-temperature Crystal Mounting

Samples which were thermally unstable and/or moisture sensitive were mounted at low temperatures using the apparatus depicted in Figure 2.9 and 2.10. The reaction vessels containing the samples were first cut open below the Kel-F valve under the flow of cold nitrogen gas of the trough, which maintaining the sample at –78 C. The sample was then rapidly dumped into the aluminum trough, precooled (–100 ±5 ^{o}C) by the flow of dry nitrogen gas through a 5-L dewar filled with liquid N_2 (Figure 2.7).

A trough constructed of ¾-in. FEP tubing was utilized for samples which contained solvent or were prone to detonation. Reaction vessels containing the samples were placed in the trough and cut open below the Kel-F valve under the flow of cold nitrogen. The temperature inside the trough was measured using a copper-constantan thermocouple positioned in the sample region of the trough. Crystals were then selected using a stereo-zoom microscope and mounted on glass fibers (0.05 to 0.1mm o.d.), nylon loops, or dual-thickness polymer loops (MicroMount;^{TM} MiTeGen, 200–500 μm) using perfluorinated polyether oil (Ausimont Inc., Fombblin Z15 or Z25) which served as an adhesive upon freezing at low temperature. The glass fibres were previously mounted with epoxy cement to a copper pin fitted to a magnetic base and affixed to the end of a magnetic wand (Hampton Research). The magnetic wand could be fastened to an adjustable support stage such that samples could be inspected under the stereo-zoom microscope once affixed to the glass fibre. The mounted crystal and magnetic pin were quickly (ca. 5 s) transferred from the crystal mounting apparatus to the magnetic mount of the goniometer by means of cryotongs (Hampton Research) which were precooled in liquid N_2 prior to use. The crystals

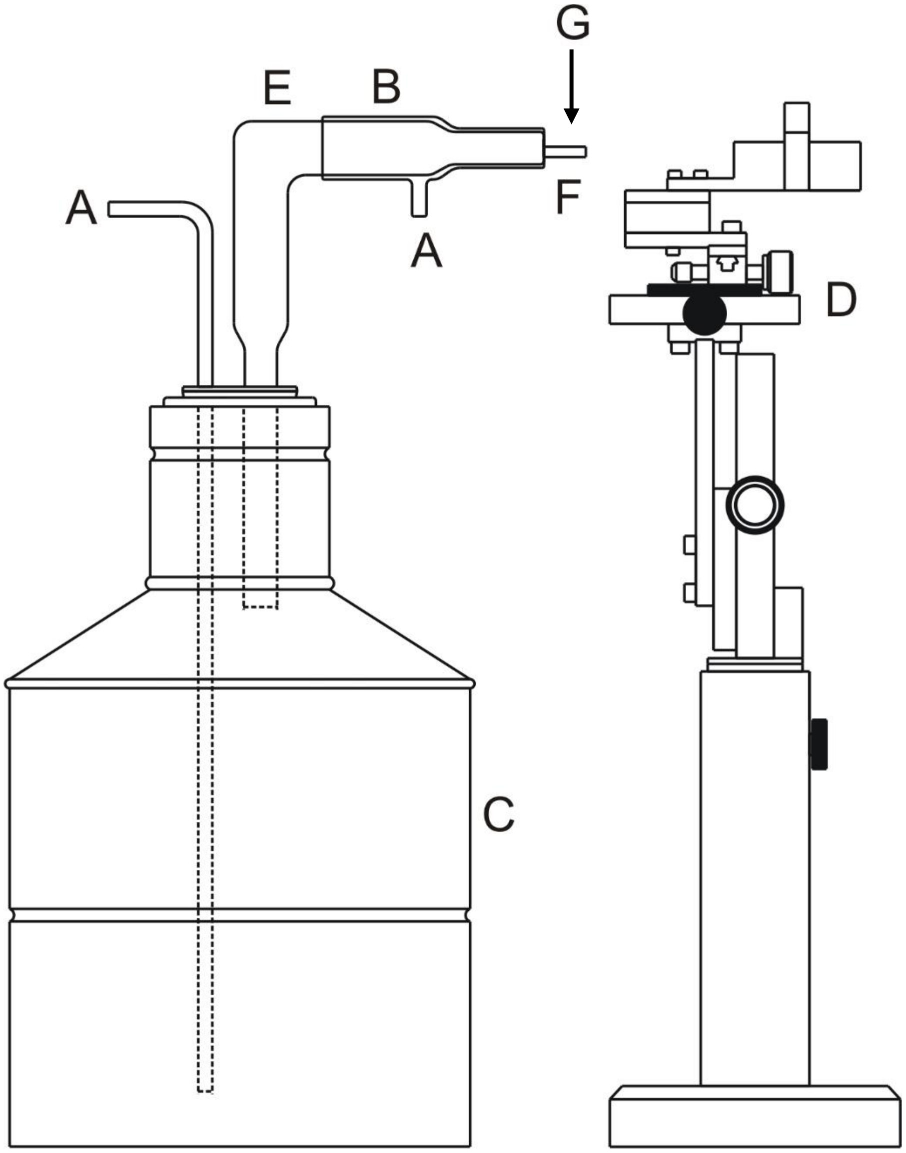

Figure 2.7. Low-temperature crystal mounting apparatus. (A) Nitrogen inlet. (B) Glass sleeve for ambient nitrogen flow. (C) Liquid N_2 dewar. (D) Adjustable support stage. (E) Silvered dewar (glass). (F) Aluminum trough. (G) Stereo-zoom microscope. Reproduced with permission from ref. 1.

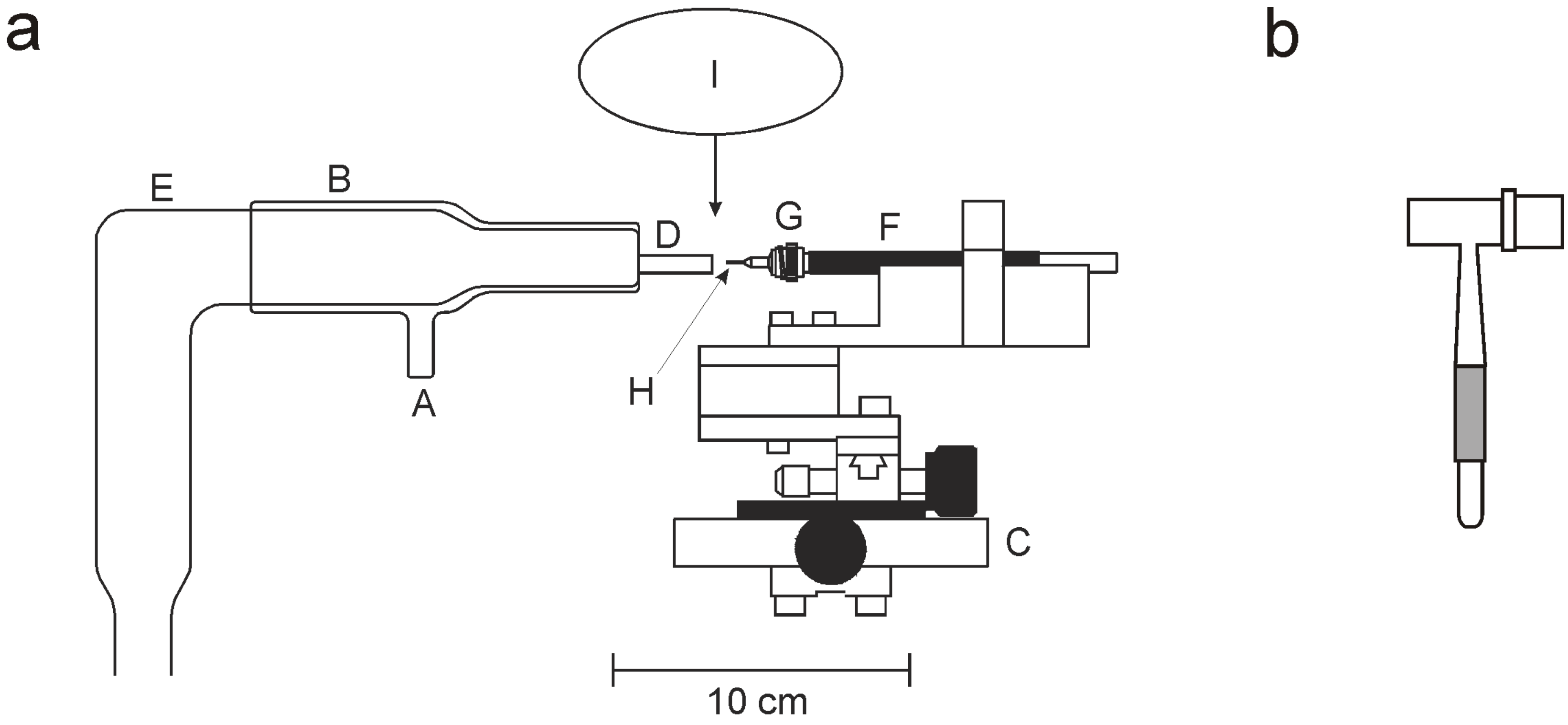

.Figure 2.8 (a) Enlarged view of the crystal mounting apparatus; (A) Ambient nitrogen gas flow inlet. (B) Glass sleeve for ambient nitrogen gas flow. (C) Adjustable support stage. (D) Aluminum trough. (E) Silvered glass jacketed dewar. (F) Magnetic-tipped wand affixed to (G) the magnetic-based copper pin-fibre assembly. (H) Glass fibre. (I) Stereo-zoom microscope. (b) A set of cryotongs employed in the transfer of the copper pin-fibre assembly with adhered crystal from the support stage to the goniometer head. Reproduced with permission from ref. 1.

were maintained at low temperature on the goniometer head by a cold N_2 gas flow provided by a Oxford Cryosystems low temperature cryostream accessory.

2.5.3 Data Collections

The crystallographic data acquired during the course of this Thesis were collected on a Bruker SMART APEX II diffractometer equipped with an APEX II 4K CCD (charge-coupled device) area detector and a triple-axis gonoiometer controlled by the APEX II Graphical User Interface (GUI) software.[14] A Bruker Triumph curve crystal monochromator was used with a Mo Kα (λ = 0.71073 A) X-ray source. The crystal-to-detector distance was 4.954 cm. Data collections were carried out in 512 x 512 pixel mode using 2 x 2 pixel binning. Diffraction data collection was typically done at –173 ^{o}C and consisted of φ- and ω- scans at a fixed $\chi = 54.74^{o}$ with 0.5^{o} frames. Processing of the raw data was done by use of the APEX III GUI software which applied Lorentz and polarization corrections to three-dimensionally integrated diffraction spots.[15]

2.5.4 Solution and Refinement of Structures

The program SADABS[16] was used for the scaling of diffraction data, the application of a decay correction, and an empirical absorption correction based on the intensity ratios of redundant reflections. The XPREP[17] program was used to confirm the unit cell dimensions and the crystal lattices. Cell Now[18] was used periodically to find unit cells for non-merohedrally twinned or multiple crystals. In these cases, the program TWINABS[19] was used to scale and process the reflection data. The final refinements were obtained by introducing anisotropic parameters for all the atoms except hydrogen, an extinction parameter, and the recommended weight factor. The maximum electron densities in the final difference Fourier maps were located around the heavy atoms. All calculations were performed using the SHELXTL[20] package and/or Olex2[21] software for the structure determination, refinement, and molecular graphics. Structure solutions were obtained by intrinsic phasing and direct methods. The PLATON[19] program could not suggest additional or alternative symmetries.

References

[1] N. Leblond, Ph. D. Thesis, McMaster University, Hamilton, ON, Canada, 1998.

[2] J. M. Winfield, *J. Fluorine Chem.* **1984**, *25*, 91.

[3] H. P. A. Mercier, J. C. P. Sanders, G. J. Schrobilgen, S. S. Tsai, *Inorg. Chem.* **1993**, *32*, 386.

[4] C. L. Chernick, J. G. Malm, *Inorg. Synth.* **1966**, *8*, 254.

[5] J. G. Malm, C. L. Chernick, *Inorg. Synth.* **1966**, *8*, 258.

[6] J. T. Goettel, G. J. Schrobilgen, *Inorg. Chem.* **2016**, *55*, 12975.

[7] M. J. Frisch, G. W. Trucks, H. B. Schlegel, G. E. Scuseria, M. A. Robb, J. R. Cheeseman, G. Scalmani, V. Barone, B. Mennucci, G. A. Petersson, H. Nakatsuji, M. Caricato, X. Li, H. P. Hratchian, A. F. Izmaylov, J. Bloino, G. Zheng, J. L. Sonnenberg, M. Hada, M. Ehara, K. Toyota, R. Fukuda, J. Hasegawa, M. Ishida, T. Nakajima, Y. Honda, O. Kitao, H. Nakai, T. Vreven, J. A. Montgomery, J. E. Peralta, F. Ogliaro, M.. Bearpark, J. J. Heyd, E. Brothers, K. N. Kudin, V. N. Staroverov, R. Kobayashi, J. Normand, K. Raghavachari, A. Rendell, J. C. Burant, S. S. Iyengar, J. Tomasi, M. Cossi, N. Rega, N. J. Millam, M. Klene, J. E. Knox, J. B. Cross, V. Bakken, C. Adamo, J. Jaramillo, R. Gomperts, R. E. Stratmann, O. Yazyev, A. J. Austin, R. Cammi, C. Pomelli, J. W. Ochterski, R. L. Martin, K. Morokuma, V. G. Zakrzewski, G. A. Voth, P. Salvador, J. J. Dannenberg, S. Dapprich, A. Daniels, D. Farkas, J. Foresman, J. V. Ortiz, J. Cioslowski, D. J. Fox, Gaussian 09, Revision D.01; Gaussian, Inc: Wallingford, CT, **2009**.

[8] Basis sets were obtained from the Extensible Computational Chemistry Environment Basis Set Database, version 2/25/04, as developed and distributed by

the Molecular Science Computing Facility, Environmental and Molecular Science Laboratory, which is part of the Pacific Northwest Laboratory, P.O. Box 999, Richland, WA 99352.

[9] GaussView, version 3.0; Gaussian Inc.: Pittsburgh, PA, **2003.**

[10] NBO 6.0. E. D. Glendening, J. K. Badenhoop, A. E. Reed, J. E. Carpenter, J. A. Bohmann, C. M. Morales, C. R. Landis, F. Weinhold, Theoretical Chemistry Institute, University of Wisconsin, Madison, **2013**.

[11] Jmol, an open–source Java viewer for chemical structures in 3D (http://www.jmol.org/).

[12] S. K. Wolff, D. J. Grimwood, J. J. McKinnon, M. J. Turner, D. Jayatilaka, M. A. Spackman, *CrystalExplorer* (Version 3.1), University of Western Australia, **2012**.

[13] Tonto: A Fortran Based Object-Oriented System for Quantum Chemistry and Crystallography, D. Jayatilaka and D. J. Grimwood, Computational Science - ICCS **2003**, *4*, 142.

[14] APEX2, release v2014.9–0; Bruker AXS Inc.: Madison, WI, **1995.**

[15] G. M. Sheldrick, SADABS (Siemens Area Detector Absorption Corrections), version 2.03; Siemens Analytical X-ray Instruments, Inc.: Madison, WI, **1999**.

[16] G. M. Sheldrick, SHELXTL–Plus, release 5.1; Siemens Analytical X-ray Instruments, Inc.: Madison, WI, **1998**.

[17] G. M., Sheldrick, *CELL NOW*, program for unit cell determination: Göttingen, Germany, **2003**.

[18] G. M. Sheldrick, *TWINABS*: Program for the empirical absorption corrections for twins, Bruker–AXS, Madison, WI, **2003**.

[19] G. M. Sheldrick, *SHELXTL*, release 6.14; Siemens Analytical X-ray Instruments, Inc.: Madison, WI, 2000–2003.

[20] O. V. Dolomanov, L. J. Bourhis, R. J. Gildea, J. A. K. Howard, H. Puschmann, *J. Appl. Crystallogr.* **2009**, *42*, 339.

[21] A. L. Spek, *J. Appl. Crystallogr.* **2003**, *36*, 7.

[22] M. Gerken, Ph. D. Thesis, McMaster University, Hamilton, Canada, 2000

CHAPTER 3

Xenon Trioxide Adducts of *O*-Donor Ligands; $[(CH_3)_2CO]_3XeO_3$, $[(CH_3)_2SO]_3(XeO_3)_2$, $(C_5H_5NO)_3(XeO_3)_2$, and $[(C_6H_5)_3PO]_2XeO_3$

K. M. Marczenko,[a] J. T. Goettel,[a] G. J. Schrobilgen, *Chem. Eur. J.* Submitted Sept. 2018.
[a] Both authors contributed equally to the work.

Abstract: *Oxygen coordination to the Xe(VI) atom of XeO_3 was observed in its adducts with triphenylphosphine oxide, $[(C_6H_5)_3PO]_2XeO_3$, dimethylsulfoxide, $[(CH_3)_2SO]_3(XeO_3)_2$, pyridine-N-oxide, $(C_5H_5NO)_3(XeO_3)_2$, and acetone, $[(CH_3)_2CO]_3XeO_3$. The crystalline adducts were characterized by low-temperature single-crystal X-ray diffraction and Raman spectroscopy. Unlike solid XeO_3, which detonates when mechanically or thermally shocked, the solid $[(C_6H_5)_3PO]_2XeO_3$, $[(CH_3)_2SO]_3(XeO_3)_2$, and $(C_5H_5NO)_3(XeO_3)_2$ adducts are insensitive to mechanical shock, but undergo deflagration when exposed to a flame. Both $[(C_6H_5)_3PO]_2XeO_3$ and $(C_5H_5NO)_3(XeO_3)_2$ are air-stable at room temperature. The xenon coordination sphere in $[(C_6H_5)_3PO]_2XeO_3$ is a distorted square pyramid and provides the first example of a five-coordinate Xe center in a XeO_3 adduct. The xenon coordination sphere of the remaining adducts are distorted octahedral comprised of three equivalent Xe---O secondary contacts that are approximately trans to the primary Xe–O bonds of XeO_3. Hirshfeld surfaces of XeO_3 and $(C_6H_5)_3PO$ in $[(C_6H_5)_3PO]_2XeO_3$ show the adduct is well-isolated in its crystal structure and provide a visual representation of the secondary Xe---O bonding in this adduct.*

3.1 Introduction

Xenon trioxide is a strong oxidant that rapidly oxidizes primary and secondary alcohols to CO_2 and H_2O.[1,2,3] The solid readily detonates when subjected to mild mechanical or thermal shock, decomposing to Xe and O_2 gases with the liberation of 402 ±8 kJ mol^{-1} of energy.[4] In the solid state, XeO_3 molecules have three short Xe---O contacts between the Lewis basic oxygen atoms of neighboring XeO_3 molecules and the Lewis acidic Xe^{VI} atom.[5]

The xenon–ligand bonds in XeO_3 adducts are best described as predominantly electrostatic, (weakly covalent) interactions between the highly electrophilic regions of the Xe atom, a σ-hole, and the nucleophilic region of the electronegative ligand atom.[6] The electrostatic potential of the xenon atom at and in the vicinity of the C_{3v}-axis is positive and only slightly lower in energy than the three σ-holes that occur opposite to the polar-covalent Xe–O double bonds.[6,7] Secondary bonding interactions occur approximately trans to the three primary Xe–O bonds, as observed for the *N*-coordinated pyridine and pyridinium salt adducts[8] and nitrile adducts[9] of XeO_3. The σ-bonding interactions between the electrophilic xenon atom and the five nucleophilic oxygen atoms of the crown ether ligand of $(CH_2CH_2O)_5XeO_3$ result in a xenon coordination number of 8, the highest coordination number thus far observed for Xe^{VI} in XeO_3.[6] Prior to this study, there were no examples in which the number of secondary bonds with the xenon atom of XeO_3 was less than three.

The 15-crown-5 adduct of XeO_3, $(CH_2CH_2O)_5XeO_3$,[6] is thus far the only structurally documented example of XeO_3 coordinated to an oxygen base. Early studies involving the interaction of XeO_3 with *t*-butyl alcohol suggested the formation of a solvate and the reaction of XeO_3 with *t*-butoxide gave a shock-insensitive precipitate.[1] It was speculated that the product is an ester-like XeO_3-alcohol intermediate with Xe---O bonding interactions, however no spectroscopic or structural characterizations of these compounds have been forthcoming.

The choices of compatible oxygen-base ligands and solvents for adduct formation with XeO_3 are limited by the strong oxidant properties of XeO_3. Although tertiaryarylphosphines, such as triphenylphosphine ($P(C_6H_5)_3$), are air- and moisture insensitive ligands which coordinate to metal ions and Lewis acids,[10] they readily undergo oxidation to their phosphine oxides. Adducts between $P(C_6H_5)_3$ and relatively strong oxidizers such as SO_3 have been reported.[11] Similarly, dimethylsulfoxide (DMSO)[12] and acetone[13] are oxidatively resistant solvents that coordinate to transition metal ions and other Lewis acids.

The present study provides further insights into the Lewis acid behavior of XeO_3 through the synthesis and structural characterization of XeO_3 coordination complexes with several E–O bonded ligands (E = C, S, N, P). The complexes have been characterized in the solid-state by low-temperature, single-crystal X-ray diffraction, Raman spectroscopy, and quantum-chemical calculations which were used to aid in the assignment of vibrational frequencies and assess the relative strengths of the Xe---O adduct bonds.

3.2 Results and Discussion

3.2.1 Syntheses

Solid XeO_3 detonates on contact with liquid DMSO and acetylacetone (acac) but readily dissolves in acetone without detonation. Xenon trioxide is very soluble and stable in acetone for several months at room temperature and has proven to be a useful solvent for XeO_3.[6] When acetone solutions of XeO_3 wre allowed to evaporate at room temperature, solid, unsolvated XeO_3 was obtained. Slow cooling of these solutions from 20 to −78 °C resulted in the formation of clear, colorless, block-shaped crystals of $[(CH_3)_2CO]_3XeO_3$ (**1**) (eq 1), which were stored at −78 °C to prevent loss of acetone due to adduct dissociation.

$$3(CH_3)_2CO + XeO_3 \xrightarrow{-78\ ^\circ C} [(CH_3)_2CO]_3XeO_3 \qquad (1)$$

An aqueous solution containing a 1:6 molar ratio of XeO_3:HF was mixed with DMSO at room temperature. Slow evaporation of the mixture yielded large, plate-shaped crystals of $[(CH_3)_2SO]_3(XeO_3)_2$ (**2**) (eq 2). The crystalline product was significantly less shock-sensitive than solid XeO_3, but slowly decomposed to $(CH_3)_2SO_2$, Xe, and O_2 at room temperature (eq 3) over a period of several days.

$$3(CH_3)_2SO + 2XeO_3 \xrightarrow{RT} [(CH_3)_2SO]_3(XeO_3)_2 \qquad (2)$$

$$[(CH_3)_2SO]_3(XeO_3)_2 \xrightarrow{RT} 3(CH_3)_2SO_2 + 2Xe + {}^{3}/_{2}O_2 \qquad (3)$$

Slow addition of an acetone solution of C_5H_5NO to solid XeO_3 resulted in detonation. Stable solutions of C_5H_5NO and XeO_3 in a 3:2 molar ratio were obtained by dissolution of the ligand in an aqueous solution of XeO_3 (*vide supra*). Evaporation of the solution yielded a large, rod-shaped crystal of $(C_5H_5NO)_3(XeO_3)_2$ (**3**) (eq 3). The crystal was insensitive to mechanical shock and was cut into smaller fragments without incident for an X-ray crystal structure determination. The adduct underwent rapid deflagration when brought into contact with a flame.

$$3(C_5H_5)NO + 2XeO_3 \xrightarrow{RT} (C_5H_5NO)_3(XeO_3)_2 \qquad (4)$$

The reaction between XeO_3 and $(C_6H_5)_3P$ in CH_3CN afforded a fine precipitate of $[(C_6H_5)_3PO]_nXeO_3{\cdot}(CH_3CN)_x$. Attempts to grow crystals of the solvate suitable for an X-ray structure determination were unsuccessful, however layering of a CH_3CN solution of $P(C_6H_5)_3$ onto an aqueous solution of XeO_3 at room temperature resulted in the formation of clear, colorless, block-shaped crystals of $[(C_6H_5)_3PO]_2XeO_3$ (**4**) that were stable at room temperature (eq 5). The reaction between XeO_3 and $P(C_6H_5)_3$ in acetone at –78 °C also yielded (**4**) as large block-shaped crystals.

$$2(C_6H_5)_3P + 2XeO_3 \longrightarrow [(C_6H_5)_3PO]_2XeO_3 + Xe\uparrow + \tfrac{1}{2}\,O_2\uparrow \qquad (5)$$

Reaction mixtures containing 1,2-bis(diphenylphosphino)ethane and XeO_3 in CH_3CN or acetone resulted in decomposition products which did not contain XeO_3. In contrast, when the reaction was carried out at 0 °C by layering a CH_3CN solution of 1,2-bis(diphenylphosphino)ethane onto an aqueous solution of XeO_3, a crystalline precipitate formed (eq 6) which was stable at room temperature and consisted of small, block-shaped crystals of $[(C_6H_5)_2POCH_2]_2XeO_3{\cdot}CH_3CN$ (Figure S1).

$$2[(C_6H_5)_2PCH_2]_2 + 2XeO_3 + CH_3CN \xrightarrow{0\ ^{\circ}C} [(C_6H_5)_2POCH_2]_2XeO_3{\cdot}CH_3CN + Xe\uparrow + \tfrac{1}{2}\,O_2\uparrow \qquad (6)$$

The extreme shock sensitivity of solid XeO_3 is largely attributable to the extended ---O_3Xe---$O_{(XeO3)}$ networks that occur in all three solid phases of XeO_3[5] and provide a means to efficiently propagate the detonation shock wave throughout the crystal lattice. Although the shock-sensitivity of (**1**) could not be explicitly tested due to adduct dissociation and loss of acetone upon warming to room temperature, at no point during the synthesis, Raman spectral acquisition, crystal isolation, and X-ray structure determination did the crystalline adduct detonate. Crystalline samples of (**2**), (**3**), and (**4**) were shock-insensitive but underwent rapid deflagration when exposed to a flame. As in the cases of the stable XeO_3 *N*-base adducts, $(C_6H_5N)_3XeO_3$,[8] $[C_5H_5NH]_4[HF_2]_2[F]_2(XeO_3)_2$,[8] and *O*-base adduct, $(CH_2CH_2O)_5XeO_3$,[6] the crystal structures of (**1**), (**2**), (**3**), and (**4**) lack extended ---O_3Xe---$O_{(XeO3)}$ networks (*vide infra*). The structural units of these adducts are well isolated which diminishes their shock sensitivities. Rapid oxidation of "soft" Lewis acids is observed when the Lewis acid center is phosphorus at room temperature, whereas slower oxidation occurs (ca. 12 h) at low temperatures (–78 °C) or when the Lewis acid center is sulfur (over several days at room temperature).

3.2.2 X-ray Crystallography

A summary of crystal data and refinement results is provided in Table 3.1. The single-crystal X-ray structures of $[(CH_3)_2CO]_3XeO_3$ (**1**), $[(CH_3)_2SO]_3(XeO_3)_2$ (**2**), $(C_5H_5NO)_2(XeO_3)_2$ (**3**) and $[(C_6H_5)_3PO]_2XeO_3$ (**4**) are shown in Figures 3.1–3.4, respectively. The preliminary crystal structure of $[(C_6H_5)_2POCH_2]_2XeO_3{\cdot}CH_3CN$ is provided in Figure 3.16. Important bond lengths and angles are provided in Table 3.2, and more extensive lists of geometric parameters are given in Tables 3.5–3.8.

The primary Xe–O bond lengths (1.762(1)–1.779(1) Å) and O–Xe–O bond angles (100.20(5)–103.2(2)°) lie within the bond length and bond angle ranges of the three solid phases of XeO_3 (1.7558(11)–1.7801(11) Å and 100.51(5)−105.09(6)°).[5] The *trans*–O−Xe---O contact angles of the adducts described in this study lie within the range 152.46(5)−172.80(4)° and are comparable to those of σ-hole bonded group 14–17 adducts (155−180°).[7] The empirical bond valence method of I. D. Brown[14] was used to determine the contributions of individual Xe---O contacts to the total bond valence of xenon in compounds (**1**), (**2**), (**3**), and (**4**) (Table 3.10). Inclusion of all Xe---O contacts provides bond valence values that are very close to the ideal value of 6 for $\mathrm{Xe^{VI}}$. The Xe---O bond valences, which span 0.089–0.205 v. u., are consistent with very weak covalent bonding between O and Xe, in accordance with their experimental bond lengths (Table 3.2).

Table 3.1. Summary of X-ray Crystal Data and Refinement Results for $[(CH_3)_2CO]_3XeO_3$ (**1**), $[(CH_3)_2SO]_3(XeO_3)_2$ (**2**), $(C_5H_5NO)_3(XeO_3)_2$ (**3**) and $[(C_6H_5)_3PO]_2XeO_3$ (**4**), (**4′**) and $[(C_6H_5)_2POCH_2]_2XeO_3{\cdot}CH_3CN$ (**5**).

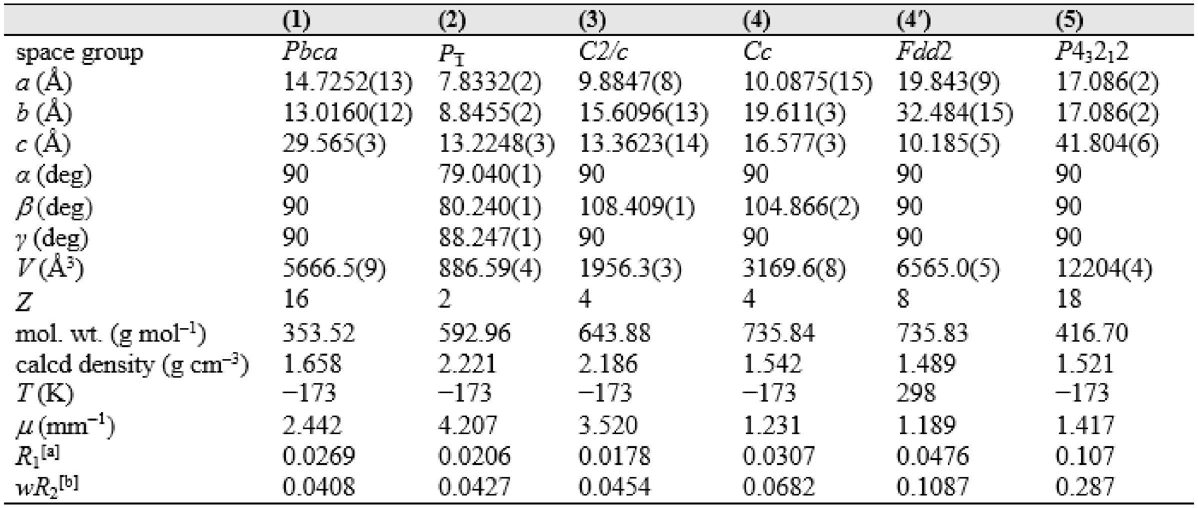

	(1)	**(2)**	**(3)**	**(4)**	**(4′)**	**(5)**
space group	*Pbca*	$P\bar{1}$	*C2/c*	*Cc*	*Fdd2*	$P4_32_12$
a (Å)	14.7252(13)	7.8332(2)	9.8847(8)	10.0875(15)	19.843(9)	17.086(2)
b (Å)	13.0160(12)	8.8455(2)	15.6096(13)	19.611(3)	32.484(15)	17.086(2)
c (Å)	29.565(3)	13.2248(3)	13.3623(14)	16.577(3)	10.185(5)	41.804(6)
α (deg)	90	79.040(1)	90	90	90	90
β (deg)	90	80.240(1)	108.409(1)	104.866(2)	90	90
γ (deg)	90	88.247(1)	90	90	90	90
V (Å^3)	5666.5(9)	886.59(4)	1956.3(3)	3169.6(8)	6565.0(5)	12204(4)
Z	16	2	4	4	8	18
mol. wt. (g mol^{-1})	353.52	592.96	643.88	735.84	735.83	416.70
calcd density (g cm^{-3})	1.658	2.221	2.186	1.542	1.489	1.521
T (K)	−173	−173	−173	−173	298	−173
μ (mm^{-1})	2.442	4.207	3.520	1.231	1.189	1.417
R_1[a]	0.0269	0.0206	0.0178	0.0307	0.0476	0.107
wR_2[b]	0.0408	0.0427	0.0454	0.0682	0.1087	0.287

Table 3.2. Selected Bond Lengths (Å) and Bond Angles (deg) for $[(CH_3)_2CO]_3XeO_3$ (**1**), $[(CH_3)_2SO]_3(XeO_3)_2$ (**2**), $(C_5H_5NO)_3(XeO_3)_2$ (**3**), and $[(C_6H_5)_3PO]_2XeO_3$ (**4**).

	(1)		**(2)**		**(3)**	**(4)**
Xe−O	1.764(1)	1.762(1)	1.763(1)	1.765(1)	1.768(1)	1.763(4)
	1.768(1)	1.765(1)	1.767(1)	1.771(1)	1.773(1)	1.770(4)
	1.768(1)	1.767(1)	1.771(1)	1.772(1)	1.779(1)	1.774(4)
Xe---O	2.738(2)	2.740(2)	2.693(1)	2.683(1)	2.586(2)	2.591(4)
	2.745(2)	2.777(2)	2.726(1)	2.703(1)	2.604(1)	2.605(3)
	2.768(2)	2.778(2)	2.871(1)	2.770(1)	2.896(1)	
O–Xe–O	101.70(9)	101.49(9)	101.96(7)	101.27(7)	100.20(5)	100.8(2)
	101.80(9)	101.86(9)	102.31(7)	101.92(7)	100.65(5)	102.2(2)
	102.37(9)	102.11(9)	102.29(7)	102.25(6)	102.26(5)	103.2(2)
O---Xe---O	76.49(6)	79.90(6)	75.92(4)	74.55(4)	69.01(3)	81.21(9)
	76.58(6)	81.03(6)	67.65(4)	69.43(4)	87.04(3)	
	85.23(6)	83.66(6)	71.71(4)	75.35(4)	87.32(3)	
Xe---O---Xe			91.58(4)	93.34(4)	110.99(4)	
			96.08(4)		132.84(4)	
trans-O---Xe−O	161.16(8)	161.47(8)	152.46(5)	157.08(5)	153.49(4)	159.6(1)
	163.94(8)	166.72(8)	161.32(5)	159.63(5)	167.96(4)	162.2(1)
	164.84(8)	166.89(8)	161.80(5)	161.77(5)	172.80(4)	
cis-O---Xe−O	83.31(7)	83.49(8)	87.96(5)	92.59(5)	82.71(4)	84.0(1)
	89.48(7)	87.98(8)	96.31(5)	87.18(5)	86.56(4)	89.8(1)
	92.70(7)	88.69(8)	88.97(5)	92.96(5)	101.16(4)	

3.2.2.1 $[(CH_3)_2CO]_3XeO_3$ (1).

The structural unit of (**1**) consists of two crystallographically unique $[(CH_3)_2CO]_3XeO_3$ units (Figure 3.1) in which the XeO_3 molecules are each coordinated to three acetone molecules through Xe---O bonds (2.738(2)–2.778(2) Å). The C–O bond lengths (1.210(3)–1.223(4) Å) show little variation and are slightly elongated with respect to those of solid acetone (1.208(3), 1.209(3) Å).[15] The ability of acetone to form a 3:1 adduct contrasts with RCN (R = CH_3, CH_2CH_3) which forms $RCNXeO_3$ and $(RCN)_2XeO_3$ but not $(RCN)_3XeO_3$.[9] These observations are in accordance with the higher Lewis basicity of acetone (76.03 ±0.21 kJ mol^{-1}) relative to those of acetonitrile (60.39 ±0.46 kJ mol^{-1}) and propionitrile (60.95 ±0.21 kJ mol^{-1}) as measured on the BF_3 affinity scale in CH_2Cl_2 solvent.[16]

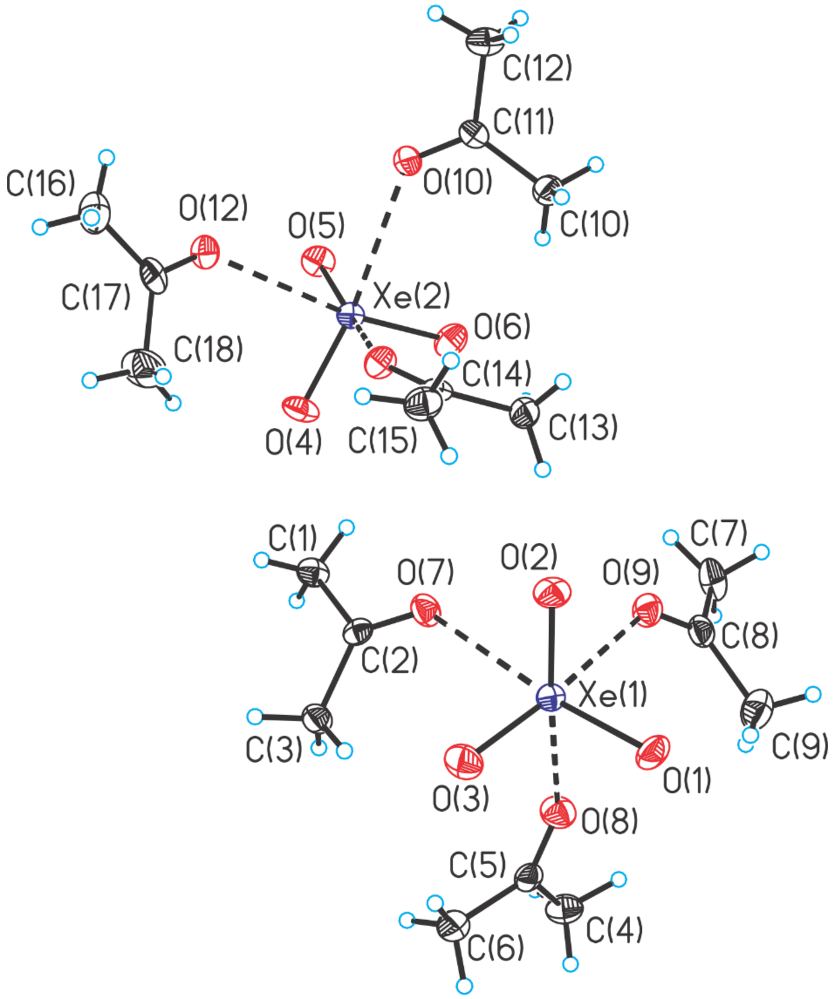

Figure 3.1. The structural unit in the crystal structure of $[(CH_3)CO]_3XeO_3$ (**1**); thermal ellipsoids are shown at the 50% probability level.

3.2.2.2 $[(CH_3)_2SO]_3(XeO_3)_2$ (2).

The structural unit of (**2**) consists of three DMSO ligands that oxygen-bridge two XeO_3 molecules (Figure 3.2). The oxygen atoms of the XeO_3 molecules are nearly eclipsed. The methyl groups of two DMSO ligands are orientated towards $Xe_{(2)}O_3$, and the methyl groups of the third DMSO ligand are directed towards $Xe_{(1)}O_3$. The structure provides an instance where two non-bonded Xe(VI) atoms are in close proximity. The Xe···Xe distance (3.9974(3) Å) is similar to the Xe···Xe distances in the *C*2/c and *P*2_1/c phases of solid XeF_6 (*C*2/c, 3.974(1); *P*2_1/c, 3.925(1) Å)[17] which are somewhat less than the sum of the Xe van der Waals radii (4.32 Å[18] or 4.12 Å[19]). In contrast, the Xe···Xe distances in all three phases of solid XeO_3 exceed 4.0 Å.[5] The Xe---O bond lengths (2.6825(12)–2.8709(12) Å) are very similar to those of solid XeO_3 (2.678(2)–2.8387(12) Å).[5] The structural units are well separated and the sulfur atoms of the DMSO ligands have no significant contacts. The S–O bonds (1.524(1)–1.538(1) Å) are somewhat longer than those of solid DMSO (1.513(5) Å)[20] but are significantly shorter than those of protonated DMSO in $[(CH_3)_2SOH]_4[Ge_3F_{16}]$ (1.587(3), 1.593(3) Å),[21] and similar to those of the hemi-protonated $[((CH_3)_2SO)_2H]^+$ cation (1.531(4), 1.536(4) Å).[21]

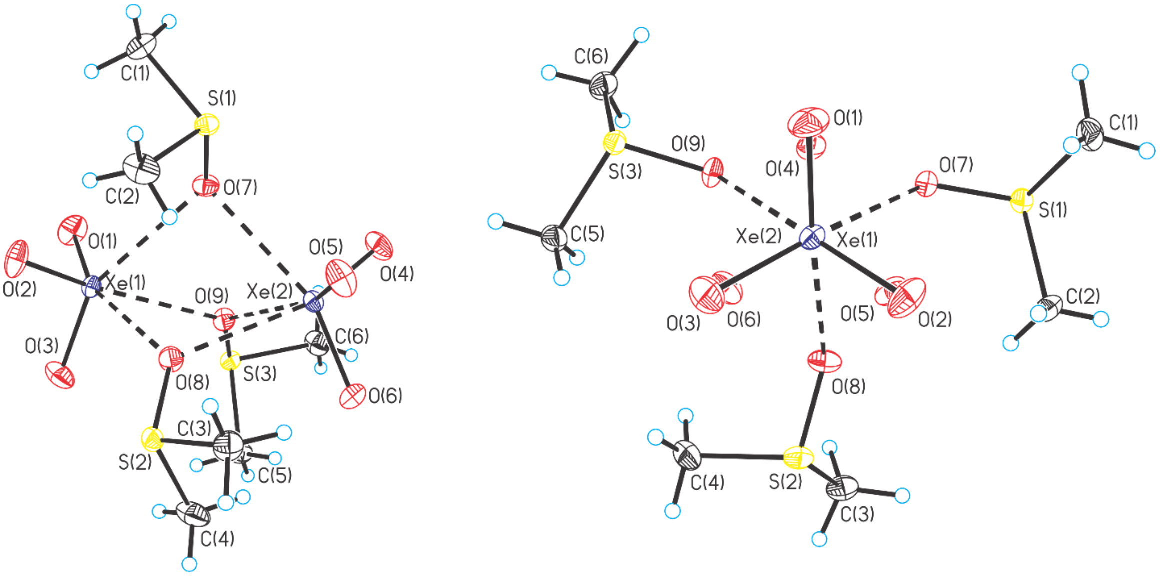

Figure 3.2. The structural unit in the crystal structure of $[(CH_3)_2SO]_3(XeO_3)_2$ (**2**) as viewed perpendicular (left) and along (right) the Xe···Xe axis; thermal ellipsoids are shown at the 50% probability level.

3.2.2.3 $(C_5H_5NO)_3(XeO_3)_2$ (3).

The structural unit of $[C_5H_5NO]_3(XeO_3)_2$ consists of two XeO_3 molecules which are O-bridged by a C_5H_5NO ligand and are each O-coordinated to a terminal C_5H_5NO ligand (Figure 3.3). The structural units are arranged in chains that are parallel to the *c*-axis of the unit cell. The terminal C_5H_5NO ligands and XeO_3 molecules are related by a C_2-axis which passes through O(4) and C(3) of the central bridging C_5H_5NO ligand. The later lies on a pseudo-mirror plane and is bonded through two relatively short Xe---O bonds (2 × 2.604(1) Å) to adjacent XeO_3 molecules. The XeO_3 molecules are coordinated through one shorter (2.586(1) Å) and one longer (2.896(1) Å) Xe---O bond with their terminal C_5H_5NO ligands. This arrangement may be described as five-membered oxygen-bridged units linked by weak Xe---O bonding interactions to form infinite chains parallel to the *c*-axis. The N–O bonds (1.336(1), 1.345(2) Å) are slightly longer than those of (C_5DH_4NO, 1.318(3); $C_5H_2D_3NO$, 1.319(6); C_5D_5NO, 1.308(3) Å).[23] Elongation of the N–O bond has been previously observed in C_5H_5NO adducts with Lewis acid centers such as the boron-azine cations ($C_5H_5NOBC_4H_4NC_2H_6$, 1.383(2) Å).[24]

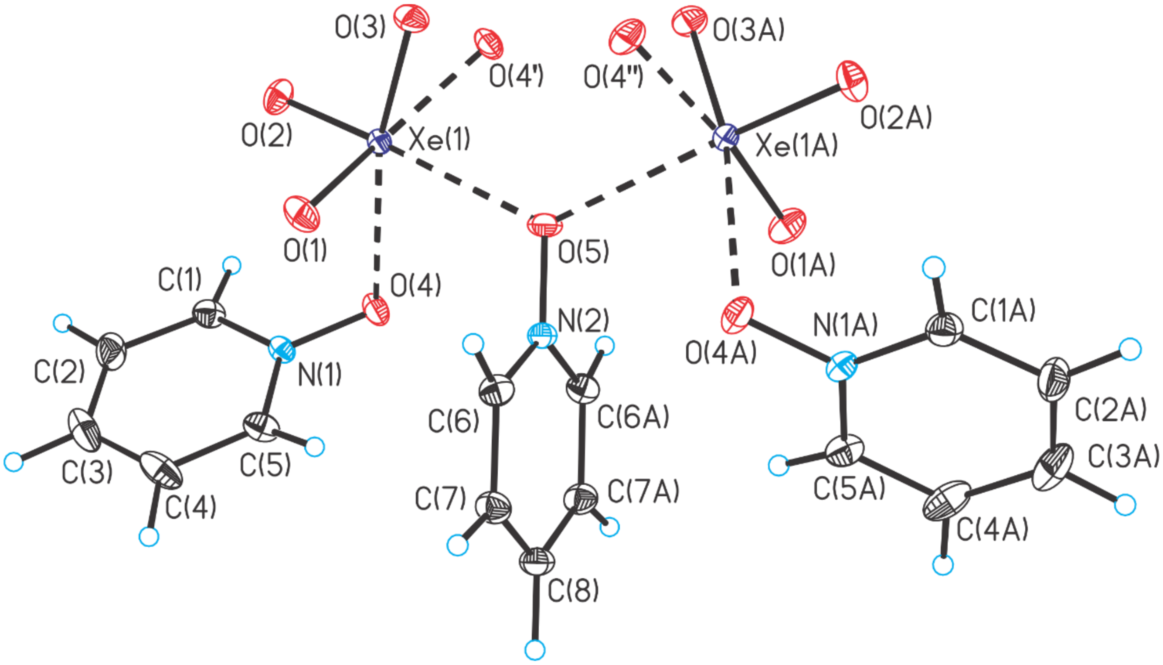

Figure 3.3. The crystal structure of $(C_6H_5NO)_3(XeO_3)_2$ (**3**); thermal ellipsoids are shown at the 50% probability level.

3.2.2.4 $[(C_6H_5)_3PO]_2XeO_3$

The room-temperature structure of $[(C_6H_5)_3PO]_2XeO_3$ belongs to the orthorhombic space group *Fdd*2 ($Z = 8$) and consists of two symmetry-equivalent $(C_6H_5)_3PO$ molecules which are coordinated to a disordered XeO_3 molecule. Upon cooling to −173 °C, a phase transition occurs to give an ordered phase of $[(C_6H_5)_3PO]_2XeO_3$ which belongs to the orthorhombic *Cc* space group ($Z = 4$). Other than two Xe---O ligand bonds, there are no significant secondary contacts to the Xe atom of XeO_3 (Figure 3.4). Coordination of less than three ligands to XeO_3 has not been previously encountered and is likely a consequence of the steric bulk of $(C_6H_5)_3PO$ ligands, which prevents additional Xe---O bonding interactions with neighboring XeO_3 molecules. The resulting Xe coordination sphere may be described as a distorted square pyramid. The lower coordination number results in Xe---O bonds (2.605(3) and 2.591(3) Å) that are significantly shorter than those of solid XeO_3 (2.678(2)–2.8387(12) Å). One $(C_6H_5)_3PO$ ligand has *cis*–O---Xe–O bond angles (89.8(1), 89.1(2)°) that are very close to 90°, whereas the remaining O---Xe–O angles are smaller (84.0(1)°) and larger (95.0(1)°). The small O---Xe---O bridge bond angle (81.2(1)°), which results from contacts with ligands, may be the result of the greater repulsion between the Xe---O and Xe–O double-bond domains. The O(2), O(3), O(4) and O(5) atoms are coplanar within ±0.07 Å and Xe lies 0.28 Å out of this plane. The shorter average Xe–O bond lengths of (**4**) result in a higher Xe^{VI} bond valence (5.601 v.u.) than the Xe–O bonds of $(C_6H_5NO)_3(XeO_3)_2$ (5.536 v.u.). This permits a Xe^{VI} bond valence of 5.999 to be achieved for (**4**) despite only two Xe---O bonding interactions.

The P–O bonds (1.504(3), 1.508(3) Å) of the $(C_6H_5)_3PO$ ligands are elongated relative to that of solid $(C_6H_5)_3PO$ (1.484(1) Å) whereas the P–C bonds (1.804(6)–1.809(6) Å) are not significantly different from those of solid $(C_6H_5)_3PO$ (1.798(2)–1.804(2) Å).[25] The P–O bond of the cationic aza-borine adduct of $(C_6H_5)_3PO$ ($(C_6H_5)_3POBC_4H_4NC_2H_6$, 1.5563(13) Å)[24] is significantly longer than those of the XeO_3 adduct.

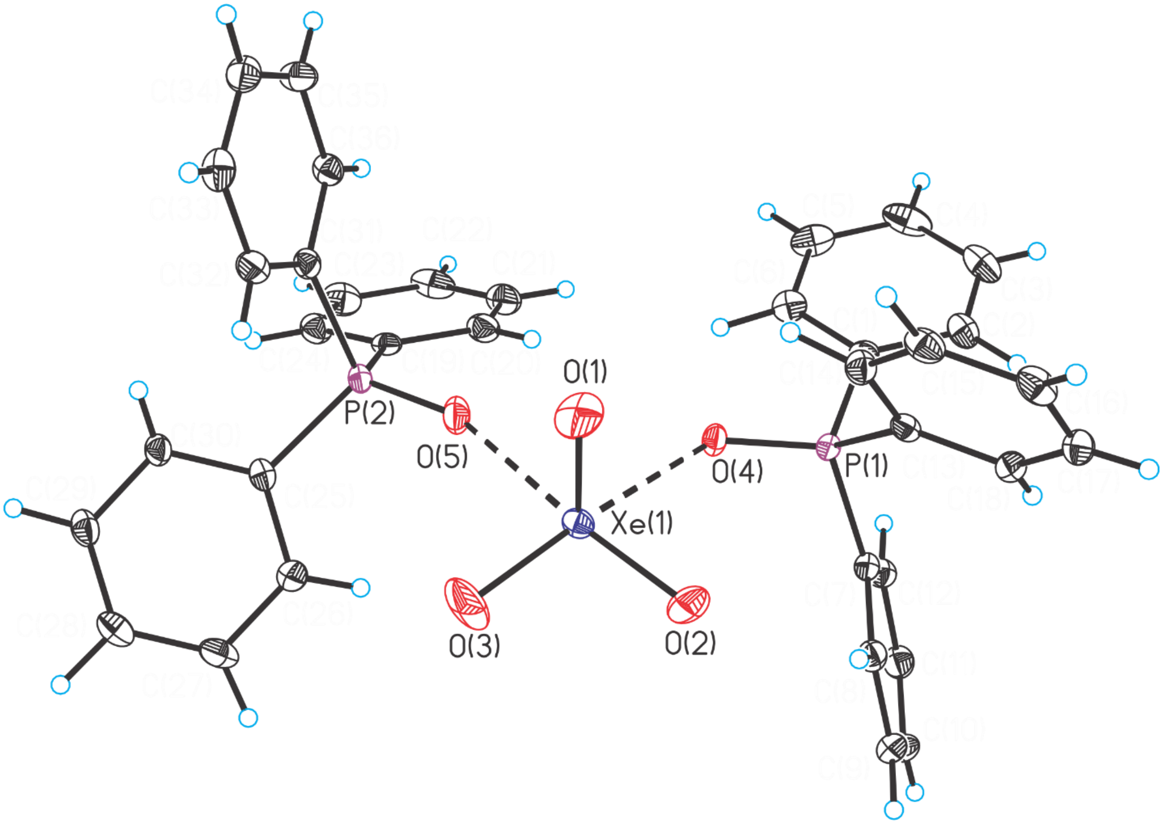

Figure 3.4. The structural unit in the crystal structure of $[(C_6H_5)_3PO]_2XeO_3$; thermal ellipsoids are shown at the 50% probability level.

Hirshfeld surfaces (see Chapter 4 − Supporting Information; Hirshfeld Surface Anaysis) mapped with the d_{norm} function provide an unbiased means to identify close contacts in complex crystal structures.[26] Hirshfeld surfaces of XeO_3 and $(C_6H_5)_3PO$ in (**4**) mapped with the d_{norm} functions and are depicted in Figures 3.5 and 3.17, respectively. Contacts shorter than the sums of the xenon and oxygen van der Waals radii appear as circular red regions on the light blue surface. The two large, intense red areas on the Hirshfeld surface of (**4**) (Figure 3.2) indicate that the adduct has only two Xe---O secondary bonds. Additional smaller, light red areas on the surface arise from O---C(H) hydrogen bonding between neighboring $[(C_6H_5)_3PO]_2XeO_3$ molecules in the crystal lattice.

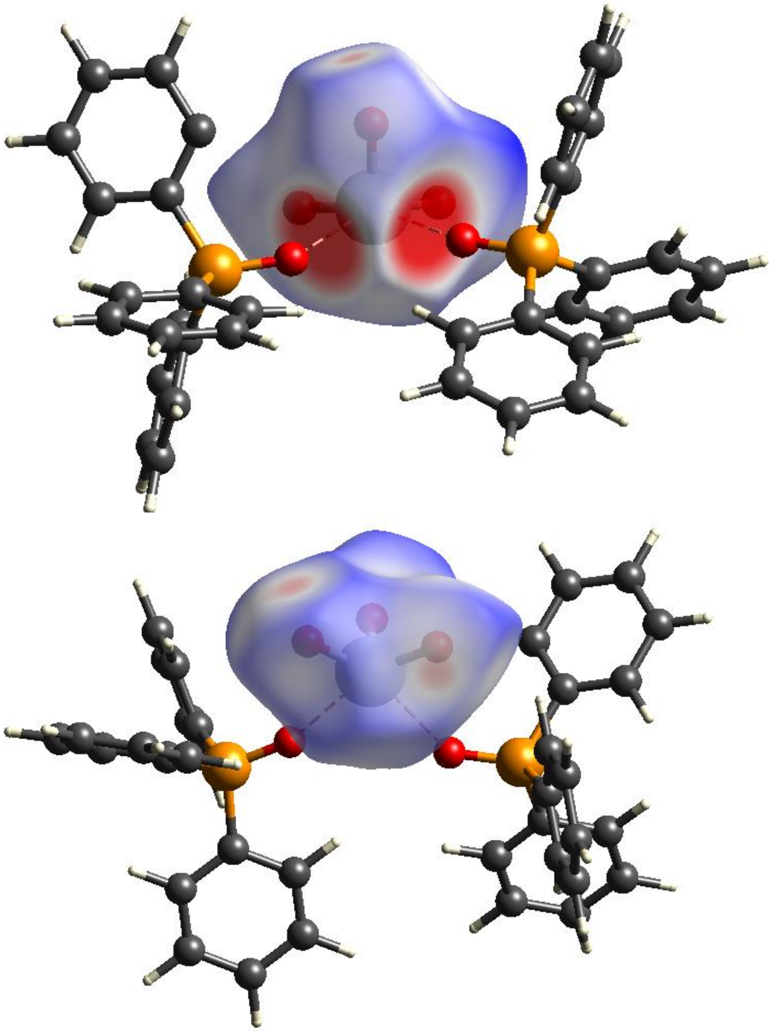

Figure 3.5. The Hirshfeld surface of XeO_3 in $[(C_6H_5)_3PO]_2XeO_3$. Two views of the surface are provided which highlight the five-coordinate Xe atom of XeO_3 and its secondary bonding interactions with the $(C_6H_5)_3PO$ ligand.

3.2.3 Raman Spectroscopy

Complete lists of vibrational frequencies and their assignments are provided for $[(CH_3)_2CO]_3XeO_3$ (**1**), $[(CH_3)_2SO]_3(XeO_3)_2$ (**2**), $(C_5H_5NO)_3(XeO_3)_2$ (**3**), $(Ph_3PO)_2XeO_3$ (**4**) and $[(C_6H_5)_2POCH_2]_2XeO_3{\cdot}NCCH_3$ (**5**) in Tables 3.10–3.14, respectively, and their Raman spectra are depicted in Figures 3.6–3.10. Raman spectral assignments were aided by comparison with the published assignments of XeO_3 and its adducts,[5,6,8,9] and with the calculated vibrational frequencies and intensities of the energy-minimized gas-phase geometries of (**1**)–(**4**) (Figure 3.11; see Quantum-Chemical Calculations). Vibrational assignments for the ligands were made by comparison with the published assignments of $(CH_3)CO$,[27] $(CH_3)_2SO$,[28] C_5H_5NO,[29] $(C_6H_5)_3PO$.[30] The Raman spectra of (**2**)–(**5**) were recorded in air at 20 °C, which also confirmed the room-temperature stabilities of solid compounds as well as their insensitivities to atmospheric moisture. Although (**2**) slowly decomposes at room temperature by oxidation of the ligand to $(CH_3)SO_2$ (eq 3), it was possible to record its Raman spectrum at room temperature without appreciable decomposition. The Raman spectrum of (**1**) was recorded at –78 °C in a sealed FEP sample tube to prevent adduct dissociation.

As previously shown for other XeO_3 adducts,[5,6,8,9] coordination of XeO_3 to a Lewis base results in a shift of the most intense band, $\nu_{sym}(A_1)$, to lower frequency (778 (**1**); 769 (**2**); 761 (**3**); 776 (**4**) 772 (**5**) cm^{-1}) relative to that of $XeO_{3(aq)}$. The asymmetric XeO_3 stretching ($\nu_{as}(E)$, 804, 830, 835 (**1**); 819, 826, and 833 (**2**); 803, 810, and 819 (**3**); 831 (**4**) 788, 826 (**5**) cm^{-1}) and bending modes ($\delta_{umb}(A_1)$, (343 (**1**); 342, 350 (**2**); 342 (**3**)**;** 345 (**4**) 303 (**5**) cm^{-1}), $\delta_{as}(E)$, (314 (**1**); 307, 311 (**2**); 311 (**3**); 253, 289, and 307 (**4**) 269 (**5**) cm^{-1})) are shifted relative to $XeO_{3(aq)}$.

Calculations predict significant coupling of the symmetric and asymmetric stretches of both XeO_3 molecules in (**2**) and (**3**). The bands assigned to the asymmetric stretches result from in-phase and out-of-phase coupling. Although the calculations predict two vibrational bands associated with the symmetric XeO_3 stretches, only one band was assigned to this mode. Significant coupling does not occur in the adducts (**1**) and (**4**).

The complexation shifts for the ν(PO) stretching modes of $(C_6H_5)_3PO$ Lewis acid-base adducts were previously shown to be approximately proportional to the strength of the Lewis acid.[31] The bands assigned to the ν(PO) of $[(C_6H_5)_3PO]_2XeO_3$ (1155 cm^{-1}) are shifted 30 cm^{-1} to lower frequency relative to free $(C_6H_5)_3PO$ (1185 cm^{-1}), but are shifted less than that of $((C_6H_5)_3PO)_2SbCl_3$ (50 cm^{-1}),[32] suggesting that XeO_3 is a weaker Lewis acid than $SbCl_3$. The complexation shifts for the P–O stretching modes of $((C_6H_5)_3PO)_3BiCl_3$ (25 cm^{-1}) and $((C_6H_5)_3PO)_2BiBr_3$ (39 cm^{-1})[32] (determined by Raman spectroscopy), suggest the Lewis acid strength of XeO_3 is similar to that of $BiCl_3$ but less than that of $BiBr_3$.

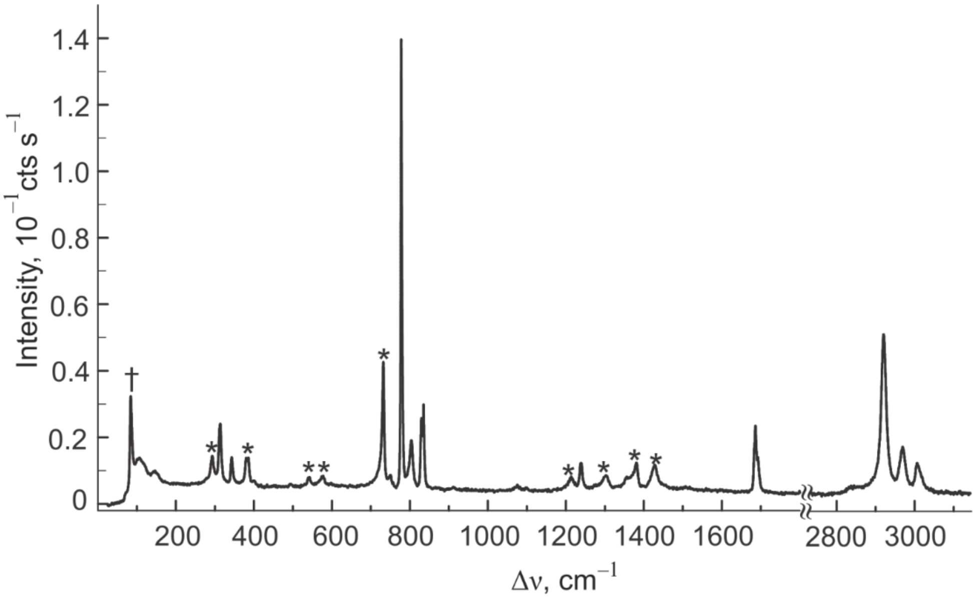

Figure 3.6. The Raman spectrum of $[(CH_3)_2CO]_3XeO_3$ recorded at −78 °C using 1064-nm excitation. Symbols denote FEP sample tube lines (*) and an instrumental artifact (†).

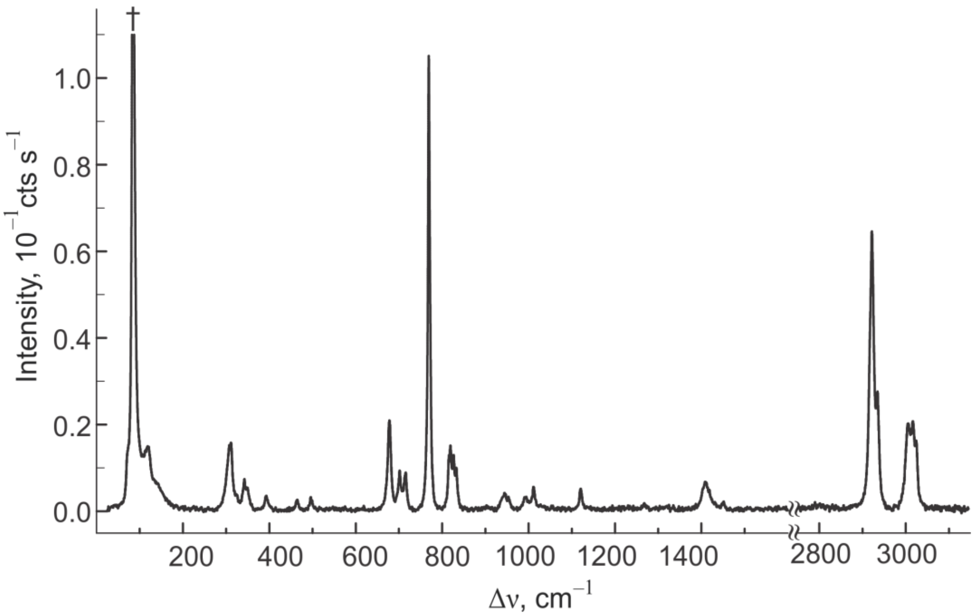

Figure 3.7 The Raman spectrum of $[(CH_3)_2SO]_3(XeO_3)_2$, recorded at 20 °C using 1064-nm excitation. Symbol (†) denotes an instrumental artifact.

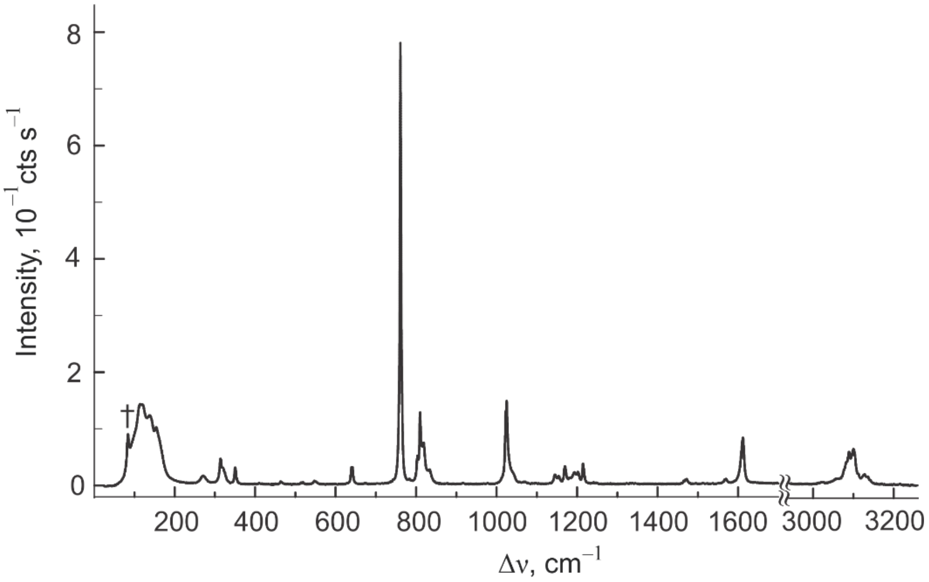

Figure 3.8 The Raman spectrum of $(C_5H_5NO)_3(XeO_3)_2$, recorded at 20 °C using 1064-nm excitation. Symbol (†) denotes an instrumental artifact.

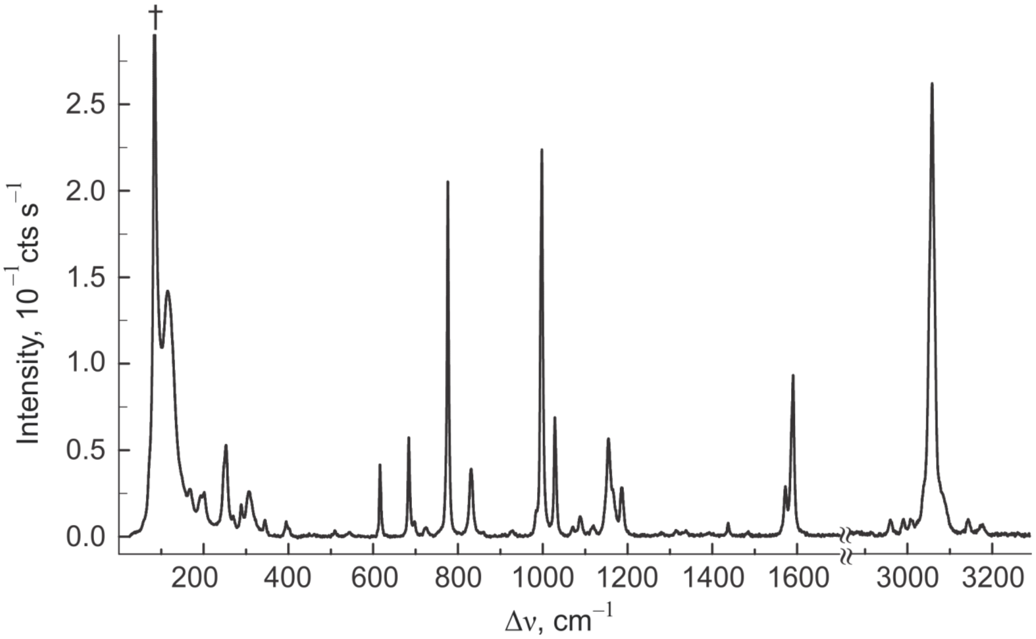

Figure 3.9. The Raman spectrum of $[(C_6H_5)_3PO]_2XeO_3$, recorded at 20 °C using 1064-nm excitation. Symbol (†) denotes an instrumental artifact.

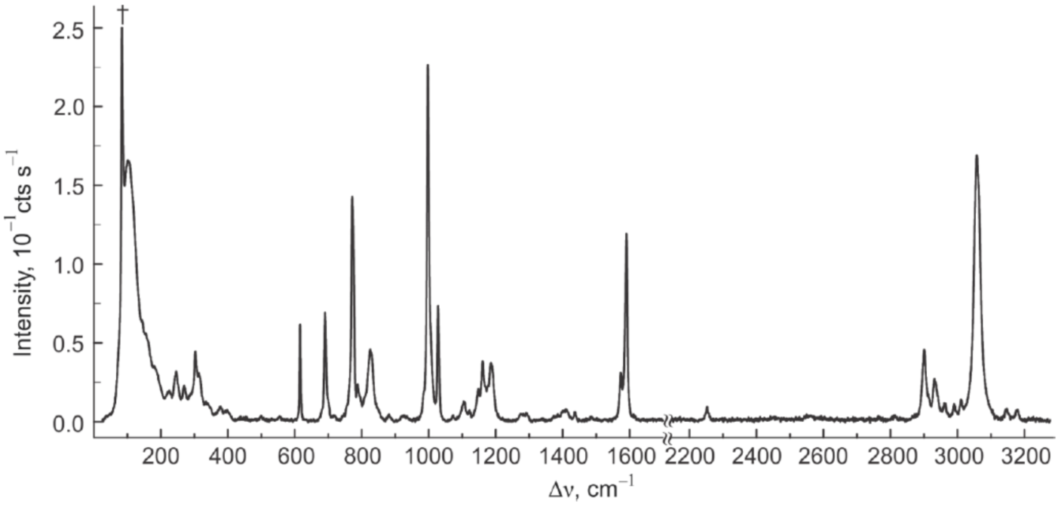

Figure 3.10. The Raman spectrum of $[(C_6H_5)_2POCH_2]_2XeO_3{\cdot}NCCH_3$ recorded at 20 °C using 1064-nm excitation. The symbol (†) denotes an instrumental artifact.

3.2.4 Quantum-Chemical Calculations

The energy-minimized geometries, with all frequencies real, were calculated for $[(CH_3)_2CO]_3XeO_3$ (**1**) (B3LYP, C_1 symmetry, Figure 3.11a), $[(CH_3)_2SO]_3(XeO_3)_2$ (**2**)

(B3LYP, C_1 symmetry; APFD, C_1 symmetry, Figure 3.11b), $(C_5H_5NO)_3(XeO_3)_2$ (**3**) (B3LYP, C_1 symmetry; APFD, C_2 symmetry, Figure 3.11c) and $(Ph_3PO)_2XeO_3$ (**4**) (B3LYP, C_1 symmetry, Figure 3.11d) using the Def2-TZVP basis set. Selected calculated bond lengths and bond angles for (**1**)–(**4**) are provided in Tables 3.5–3.8. Overall, the calculated geometric parameters are in good agreement with those obtained from the crystal structures.

As previously shown for $(CH_2CH_2O)_5XeO_3$,[8] the calcualted Xe–O and Xe---O distances more closely resemble the experimental values when calculated at the APFD/Def2-TZVP level of theory because the B3LYP level overestimates bond lengths. The geometries of (**1**) and (**4**) were optimized using the B3LYP/Def2-TZVP level due to convergence failures at the APFD level. The Xe–O and Xe---O bond distances of (**1**) and (**4**) are slightly elongated relative to their experimental distances (Xe–O: (**1**) exptl, 1.762(1)–1.767(1), calcd, 1.784–1.786 Å; (**4**) exptl, 1.763–1.772, calcd, 1.783–1.785 Å; Xe---O: (**1**) exptl. 2.738(1)–2.780(1), calcd, 2.864–2.866 Å; (**4**) exptl, 2.591(1)–2.605(1), calcd, 2.723–2.731 Å).

The gas-phase optimized (APFD) structure of (**2**) reproduces the eclipsed conformation of the XeO_3 molecules in the crystal structure. The calculated Xe···Xe distance (3.968 Å) is slightly shorter than the experimental distance (3.997(1) Å). The calculated Xe–O (1.762–1.780 Å) and Xe---O (2.675–2.825 Å) bond lengths are in excellent agreement with their respective experimental values (Xe–O, 1.763–1.772; Xe---O, 2.682(1)–2.871(1)).

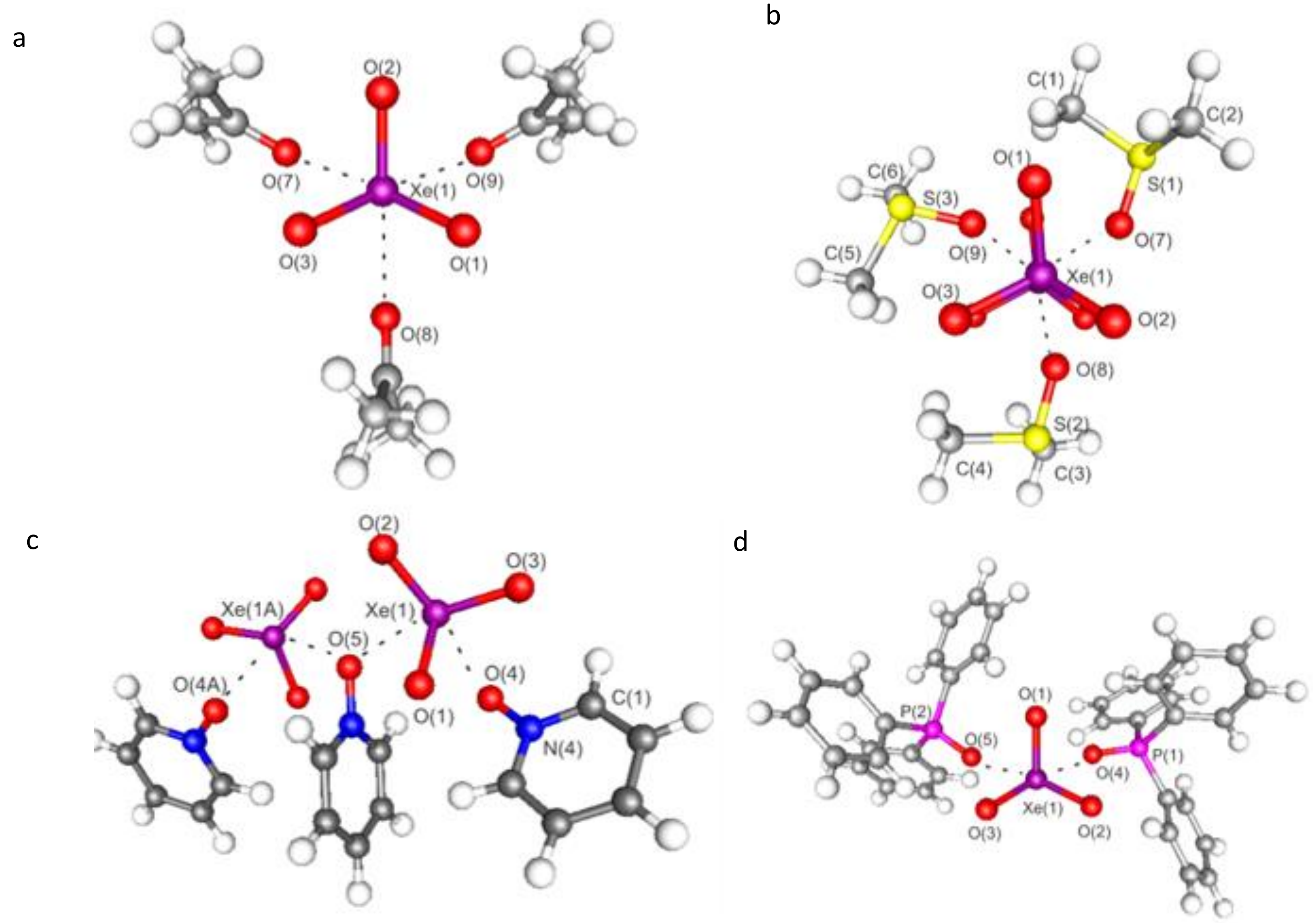

Figure 3.11. Gas-phase optimized geometries of (a) $[(CH_3)_2CO]_3XeO_3$, (b) $[(CH_3)_2SO]_3(XeO_3)_2$, (c) $(C_5H_5NO)_3(XeO_3)_2$, and (d) $[(C_6H_5)_3PO]_2XeO_3$.

The isolated repeat units in (**3**) was optimized at the B3LYP and APFD level (**3′**) with only two Xe---O contacts. The crystal structure geometry significantly distorted at the B3LYP level of theory (C_1 symmetry) but was maintained at the APFD level (C_2-symmetry). The absence of the third Xe---O contact between neighboring chains resulted in shorter Xe–O bonds (exptl, 1.770– 1.781; calcd, 1.763–1.772 Å), but had no significant effect on the Xe---O bond lengths (exptl, 2.591(2)–2.606(1); calcd, 2.616–2.680 Å).

The Natural Population Analysis (NPA) atomic charges, Wiberg bond indices, and Wiberg valences were calculated for compounds (**1**)–(**4**) (Table 3.3; Tables 3.14–3.18). The results are consistent with enhancement of the polar covalent Xe–O bonds in all compounds. The NPA charges of the Xe atom and O_{XeO3} atoms are significantly more positive and more negative, respectively, than those of XeO_3. Apart from (**3**), the Wiberg valences of Xe also decrease upon coordination. The Wiberg bond indices of the primary Xe–O bonds decrease upon coordination of XeO_3 to a Lewis base. The small Wiberg bond indices (0.023−0.076) of the Xe---O adduct bonds are consistent with very weak covalent bonding. The changes in atomic charges and bond indices that accompany coordination are consistent with enhanced polar-covalent character of the primary Xe–O bonds of XeO_3 and predominantly electrostatic Xe---O bonds in (**1**)–(**4**), as observed for the σ-hole bonded *N*-base adducts[8,9] and *O*-base adduct[6] of XeO_3.

Table 3.3. Natural Population Analysis (NPA) Charges and Wiberg Valences for the Xe atom and O_{XeO_3} atoms, and the Wiberg Xe–O Bond Indices for XeO_3 and Compounds (**1**)–(**4**).

		B3LYP					**APFD**			
		XeO_3	**(1)**	**(2)**		**(4)**	**XeO_3**	**(2)**		**(3)**
Atomic Charges	Xe	2.688	2.854	2.854	2.861	2.866	2.640	2.924	2.933	2.844
	O	–0.896	–0.962	–0.978	–0.964	–0.964	–0.880	–0.955	–0.966	–0.989
		–0.896	–0.968	–0.971	–0.957	–0.968	–0.880	–1.012	–1.034	–0.955
		–0.896	–0.973	–0.961	–0.974	–0.959	–0.880	–0.997	–0.991	–0.979
Wiberg Valences	Xe	[3.390]	[3.351]	[3.356]	[3.356]	[3.354]	[3.386]	[3.348]	[3.346]	[3.402]
	O	[1.550]	[1.470]	[1.458]	[1.476]	[1.466]	[1.551]	[1.500]	[1.489]	[1.439]
		[1.550]	[1.464]	[1.467]	[1.485]	[1.475]	[1.551]	[1.432]	[1.403]	[1.507]
		[1.550]	[1.458]	[1.480]	[1.463]	[1.486]	[1.551]	[1.449]	[1.459]	[1.473]
Bond Indices	Xe–O	1.130	1.091	1.088	1.079	1.077	1.129	1.117	1.107	1.050
		1.130	1.083	1.095	1.072	1.090	1.129	1.048	1.021	1.109
		1.130	1.076	1.075	1.092	1.101	1.129	1.064	1.076	1.078
	Xe---O		0.027	0.023	0.028	0.033		0.029	0.041	0.076
			0.027	0.024	0.030	0.033		0.032	0.042	0.049
			0.027	0.027	0.025			0.029	0.026	

The predicted average binding energies of $[(CH_3)_2CO]_3XeO_3$, $[(CH_3)_2SO]_3(XeO_3)_2$, $(C_5H_5NO)_3(XeO_3)_2$ and $[(C_6H_5)_3PO]_2XeO_3$ are provided in Table 3.4. The binding energies of $[(CH_3)_2CO]_3XeO_3$ and $[(C_6H_5)_3PO]_2XeO_3$ are similar, despite the fact that $[(C_6H_5)_3PO]_2XeO_3$ has only two Xe---O bonding interactions and $[(CH_3)_2CO]_3XeO_3$ has three, but agrees with the two shorter and stronger Xe---O bonds in $[(C_6H_5)_3PO]_2XeO_3$ versus the three weaker bonds in the acetone adduct. The $(C_5H_5NO)_3(XeO_3)_2$ and $[(CH_3)_2SO]_3(XeO_3)_2$ adducts have binding energies that are approximately 1.5–2 times as large as the other two adducts, since it has four and six Xe---O bonding interactions in the gas phase, respectively. The formation of (**2**) and (**3**) is spontaneous and exothermic and room temperature. The thermodynamic parameters for (**1**) are consistent with experimental observation and indicate that the system is in equilibrium with adduct dissociation occurring at higher temperatures.

Table 3.4. Calculated binding energies[a] for $[(CH_3)_2CO]_3XeO_3$ (**1**), $[(CH_3)_2SO]_3(XeO_3)_2$ (**2**), $(C_5H_5NO)_3(XeO_3)_2$ (**3**) and $[(C_6H_5)_3PO]_2XeO_3$ (**4**).

	(**1**)[b]	(**1**)[c]	(**2**)[b]	(**3**)[b]	(**4**)[b]
Binding energy (kJ mol^{-1})	–92.2		–178.2	–141.9	–93.8
ΔH_{rxn}	–82.1	–88.5	–220.0	–186.5	
ΔG_{rxn}	32.8	–14.0	–38.5	–17.9	

[a] B3LYP/Def2-TZVP. [b] 298 K. [c] 195 K.

3.3 Conclusion

Examples of XeO_3 oxygen-base adducts were synthesized and structurally characterized. The $[(C_6H_5)_3PO]_2XeO_3$ adduct contains well-isolated, distorted square pyramidal XeO_3 units and provides the only example presently known for a XeO_3 adduct which has only two secondary bonding interactions. The $[(CH_3)_2CO]_3XeO_3$, $[(CH_3)_2SO]_3(XeO_3)_2$, and $(C_5H_5NO)_3(XeO_3)_2$ adducts each display different packing motifs which are well-isolated structural units, dimers, and chains, respectively. The triphenylphosphine oxide and pyridine-*N*-oxide adducts are air-stable at room temperature and are insensitive to mechanical shock. The mean shifts of the ν(PO) vibrational modes for $[(C_6H_5)_3PO]_2XeO_3$ indicate that XeO_3 is a weaker Lewis acid than $SbCl_3$ but is comparable to the Lewis acid strength of $BiCl_3$ and $BiBr_3$. Calculations show enhancement of the Xe–O primary bonds upon coordination and predominantly electrostatic Xe---O bonding interactions between the nucleophilic O atoms of the oxygen bases and the electrophilic σ-holes of the xenon atoms.

Acknowledgements

We thank the Natural Sciences and Engineering Research Council of Canada (NSERC) for support in the form of a Discovery Grant (G.J.S.) and an Alexander Graham Bell CGS-award (J.T.G). We thank Dr. Hélène P. A. Mercier for her valued comments relating to the manuscript and for her assistance with the vibrational assignments. We are also grateful for the computational resources provided by SHARCNet (Shared Hierarchical Academic Research Computing Network, www.sharcnet.ca) and compute Canada.

Experimental Section

Caution! *Solid XeO_3 detonates when subjected to mild thermal or mechanical shock. Great care must be taken during the syntheses and handling of XeO_3 and its adducts. For these reasons, the quantity of XeO_3 used in each synthesis was limited to 5–15 mg. Reaction vessels used in this study were fabricated from FEP (hexafluoropropylene, tetrafluoroethylene copolymer) fluoroplastic, which is inert to attack by HF, strong oxidants and fluorinating agents, and generally does not shatter to produce sharp shards when a detonation occurs at the reagent scales described in this study. Appropriate protective equipment (face shield, leather gloves, ear protection) must be used.*

Apparatus and Materials

All volatile, air-sensitive, corrosive fluorides were handled on metal vacuum lines constructed of nickel, 316 stainless steel, and FEP fluoroplastic. Anhydrous HF (Harshaw Chemicals Co.) was purified as previously described.[33]

Xenon hexafluoride was prepared by the reaction of Xe (99.995%, Air Products and Chemicals, Inc.) and F_2 (98+%, Air Products and Chemicals, Inc.) similar to the method described by Malm and Chernick.[34] Small amounts of XeF_4 impurity, identified by two strong peaks at 502 and 543 cm^{-1} in the Raman spectrum, also formed XeO_3 when hydrolyzed[35] and therefore did not interfere with the synthesis of XeO_3.

Aqueous solution of XeO_3 was synthesized by hydrolysis of XeF_6 as previously described.[5] An aliquot (ca. 10 mg, 0.056 mmol XeO_3) of the resulting aqueous solution, $XeO_3{\cdot}6HF_{(aq)}$, was transferred into a 3 × 3 cm FEP (hexafluoropropylene, tetrafluoroethylene copolymer) fluoroplastic tray by use of a pipette fabricated from FEP tubing. Water and HF were removed from XeO_3 by evaporation overnight in a fume hood to give solid XeO_3. The sample was transferred to a plastic (HDPE) desiccator and dried over 4 Å molecular sieves for 2−3 h to ensure that all surface water had been removed from $XeO_{3(s)}$.

$[(CH_3)_2CO]_3XeO_3$ (1). In a typical reaction, acetone (ca. 0.2 mL) was pipetted onto dry XeO_3 (ca. 6 mg, 0.03 mmol) in an FEP tray. Acetone was carefully pipetted onto solid XeO_3 which rapidly dissolved to give a clear, colorless solution which was then pipetted into a ¼-in FEP reactor. Clear, colorless, block-shaped crystals grew upon slow cooling from 20 to −78 °C. The solvent was removed under dynamic vacuum at −78 to −60 °C and the reactor was backfilled at −78 °C with N_2 as soon as the solvent removal was complete. The sample was stored at −78 °C to prevent adduct dissociation and loss of acetone.

$[(CH_3)_2SO]_3(XeO_3)_2$ (2). A stoichiometric excess of $(CH_3)_2SO$ (ca. 0.2 mL, 2.8 mmol) was mixed with an aliquot (ca. 0.2 mL, 0.056 mmol of XeO_3) of aqueous $XeO_3{\cdot}6HF$ obtained by hydrolysis of XeF_6 at room temperature. Slow evaporation of the mixture at room temperature inside a fume hood yielded large, colorless, plate-shaped crystals of $[(CH_3)_2SO]_3(XeO_3)_2$. The crystalline material had a wax-like appearance and was shock insensitive, but slowly decomposed to $(CH_3)_2SO_2$, Xe, and O_2 at room temperature over a period of several days.

$(C_5H_5NO)_3(XeO_3)_2$ (3). An aqueous solution of C_5H_5NO (ca. 7 mg, 0.07 mmol) was mixed with an aqueous solution of XeO_3 (ca. 12 mg, 0.067 mmol) in an FEP tray. Evaporation of the solution yielded a single, large, rod-shaped crystal of $(C_5H_5NO)_3(XeO_3)_2$. The crystal was insensitive to mechanical shock and was easily cut into smaller pieces for crystal mounting. Crystalline $(C_5H_5NO)_3(XeO_3)_2$ underwent rapid deflagration when brought into contact with a flame.

$[(C_5H_5)_3PO]_2XeO_3$ (4). A CH_3CN solution of triphenylphosphine (12 mg, 0.067 mmol) was layered onto an aqueous solution of XeO_3 (10 mg, 0.056 mmol) at 0 °C in a ¼-in FEP reaction vessel. The reaction mixture was left to stand undisturbed overnight. Clear, colorless, block-shaped crystals of $[(C_6H_5)_3PO]_2XeO_3$ grew which were separated from the mother liquor by use of an FEP pipette. The crystals were stable at room temperature.

$[(C_6H_5)_3PO]_nXeO_3{\cdot}xCH_3CN$. Triphenylphosphine (8.5 mg, 0.032 mmol) was dissolved in a CH_3CN solution of XeO_3 (5 mg, 0.03 mmol) at −10 °C. Slow cooling afforded a fine precipitate of $[(C_6H_5)_3PO]_nXeO_3{\cdot}xCH_3CN$. Attempts to grow crystals suitable for an X-ray structure determination were unsuccessful.

$[(C_6H_5)_2POCH_2]_2XeO_3{\cdot}NCCH_3$. A concentrated solution of DPPE (1,2-bis(diphenylphosphino)-ethane) in CH_3CN (6 mg, 0.02 mmol) was layered onto an aqueous solution of XeO_3 (3 mg, 0.02 mmol) at 0 °C in a ¼-in. FEP reaction vessel. The reaction mixture was left undisturbed for 4 h. A crystalline precipitate formed which consisted of small block-shaped crystals of $[(C_6H_5)_2POCH_2]_2XeO_3{\cdot}CH_3CN$ which were stable at room temperature for several days.

X-ray Crystallography. *(a) Crystal Mounting.* Single-crystals of $[(CH_3)_2SO]_3(XeO_3)_2$, $(C_5H_5NO]_3(XeO_3)_2$ and $[(C_6H_5)_3PO]_2XeO_3$ were submerged in perfluoropolyether oil (Fomblin Z-25) in the open atmosphere and were selected at room temperature and mounted at the tip of a dual-thickness polymer loop (MiTeGen, Ithaca, NY; MicroMount;™ 100–500 μm) using Halocarbon 25-5S grease (Halocarbon Products Corporation, River Edge, NJ). Single-crystals of $[(CH_3)_2CO]_3XeO_3$ were mounted on an X-ray diffractometer at low-temperatures using a previously described procedure.[36] Samples which contained isolated dry crystals were mounted by carefully pouring the crystals into a ¾-in. FEP cold trough held at −80 ±5 °C. While still inside the cold trough, the crystal was affixed to a nylon cryoloop (MiTeGen MicroMounts ™) that had been dipped in an inert perfluorinated polyether.

(b) Collection and Reduction of X-ray Data. Crystals were centered on a Bruker SMART APEX II diffractometer equipped with an APEX II 4K CCD (charge-coupled device) area detector and a triple-axis goniometer that was controlled by the APEX II Graphical User Interface (GUI) software.[37] A Bruker Triumph curved crystal monochromator was used with a Mo Kα (λ = 0.71073 Å) radiation source for all compounds. Diffraction data collection at −173 °C consisted of ω- and ϕ-scans collected at 0.5° intervals. The crystal-to-detector distance was 4.960 cm (compounds (**1**) and (**3**)) or 4.954 cm (compounds (**2**) and (**4**)) and data collection was carried out in a 512 x 512 pixel mode using 2 x 2 pixel

binning. The raw data was processed by use of the APEX III GUI software.[37] The SADABS[38] program was used for scaling the diffraction data.

(c) Solution and Refinement of the Structure. The XPREP program[39] was used to confirm unit cell dimensions and the crystal lattice. All calculations were carried out using the SHELXTL-plus[39] and the Olex2[40] packages for structure determination, solution refinement, and molecular graphics. Space group choices were confirmed using Platon.[41] The final refinements were obtained by introducing anisotropic thermal parameters and the recommended weightings for all of the atoms except the hydrogen atoms. The H atoms were placed at locations derived from a difference map. The H atoms were included as riding contributions with isotropic displacement parameters that were 1.2 times those of the attached carbon atoms. The maximum electron density in the final difference Fourier map was located near the xenon atom.

Raman Spectroscopy. The Raman spectra were recorded on a Bruker RFS 100 FT-Raman spectrometer using 1064-nm excitation, 300 mW laser power, and ±0.5 cm^{-1} resolution as previously described.[36]

Computational Details. Density-functional theory (DFT) was employed to study the electronic structures of XeO_3, $[(CH_3)_2CO]_3XeO_3$, $[(CH_3)_2SO]_3(XeO_3)_2$, $(C_5H_5NO]_3(XeO_3)_2$ and $[(C_6H_5)_3PO]_2XeO_3$, and the ligands. All basis sets were obtained online from the EMSL Basis Set Exchange (https://bse.pnl.gov/bse/portal).[42] Quantum-chemical calculations were carried out using the program Gaussian 09[43] for geometry optimizations and to create wavefunction files. The GaussView[44] program was used to visualize the vibrational displacements that form the basis for the vibrational mode descriptions given in Table S1. The CrystalExplorer 3.1[45] program was used for Hirshfeld surface analyses. Natural bond orbital analyses were performed using APFD densities with the NBO program (version 6.0).[46]

References

[1] B. Jaselskis, J. P. Warriner, *Anal. Chem.* **1966**, *38*, 563–564.

[2] S. A. Shackelford, G. U. Yuen, *Inorg. Nucl. Chem. Lett.* **1973**, *9*, 605–609.

[3] L. A. Khamidullina, S. V. Lotnik, V. P. Kazakov, *Kinet. Catal.* **2008**, *49*, 27–33.

[4] S. R. Gunn in *Noble-Gas Compounds* (Ed.: H. H. Hyman), University of Chicago Press, Chicago, IL, **1963**, pp. 149–151.

[5] J. T. Goettel, G. J. Schrobilgen, *Inorg. Chem.* **2016**, *55*, 12975–12981.

[6] K. M. Marczenko, H. P. A. Mercier, G. J. Schrobilgen, *Angew. Chem. Int. Ed. Engl.* **2018**, *57*, 12448–12452.

[7] P. Scilabra, G. Terraneo, G. Resnati, *J. Fluorine Chem.* **2017**, *203*, 62, and references therein.

[8] J. T. Goettel, H. P. A. Mercier, G. J. Schrobilgen, *J. Fluorine Chem.* **2018**, *211*, 60–69.

[9] J. T. Goettel, K. Matsumoto, H. P. A. Mercier, G. J. Schrobilgen, *Angew. Chem. Int. Ed. Engl.* **2016**, *55*, 13780–13783.

[10] I. J. Galpin, G. W. Kenner, A. Marston, *Bioorg. Chem.* **1979**, *8*, 323–332.

[11] I. J. Galpin, G. W. Kenner, A. Marston, O. S. Mills, *J. Chem. Soc., Chem. Commun.* **1981**, *15*, 789–790.

[12] W. L. Driessen, W. L. Groeneveld, *Recueil des Travaux Chimiques des Pays-Bas*, **1969**, *88*, 977–988.

[13] M. Calligaris, *Coord. Chem. Rev.* **2004**, *248*, 351–375.

[14] I. D. Brown, *The Chemical Bond in Inorganic Chemistry*, IUCr Monographs in Crystallography, 12, Oxford University Press, Oxford, UK, **2002**.

[15] D. R. Allan, S. J. Clark, R. M. Ibberson, S. Parson, C. R. Pulham, L. Sawyer, *Chem Commun.* **1999**, *8*¸751.

[16] C. Laurence, J. F. Gal in *Lewis Basicity and Affinity Scales: Data and Measurement*. John Wiley & Sons, West Sussex, UK, **2009**, pp. 85–109.

[17] S. Hoyer, T. Emmler, K. Seppelt, *J. Fluorine Chem.* **2006**, *127*, 1415–1422.

[18] A. Bondi, *J. Phys. Chem.* **1964**, *68*, 441–451.

[19] S. Alvarez, *Dalton Trans.* **2013**, *42*, 8617–8636.

[20] R. Thomas, C. B. Shoemaker, K. Eriks, *Acta Crystallogr.* **1966**, *21*, 12–20.

[21] M. Hopfinger, K. Lux, A. Kornath, *ChemPlusChem* **2012**, *77*, 476–481.

[22] V. Vasylyeva, T. Kedziorski, N. Metzler–Nolte, C. Schauerte, K. Merz, *Cryst. Growth Des.* **2010**, *10*, 4224–4226.

[23] A. J. Marwitz, J. T. Jenkins, L. N. Zakharov, S. Y. Liu, *Organomet.* **2011** *30*, 52–54.

[24] A. L. Spek, *Acta Crystallogr. C* **1987**, *43*, 1233–1235.

[25] M. A. Spackman, D. Jayatilaka, *CrystEngComm,* **2009**, *11*, 19–32.

[26] M. Ito, N. Hata, *Bull. Chem. Soc. Jpn.* **1955**, *28*, 353–355.

[27] W. N. Martens, R. L. Frost, J. Kristof, J. T. Kloprogge, *J. Raman. Spec.* **2002**, *33*, 84 91.

[28] M. T. Forel, M. Tranquille, *Spectrochim. Acta* **1970**, *26*, 1023.

[29] W. D. Horrocks, F. A. Cotton, *Spectrochim. Acta* **1961**, *17*, 134–147.

[30] N. N. Aleinikov, B. L. Korsunskii, F. I. Dubovitskii, *Bull. Acad. Sci. USSR, Div. Chem. Sci.* **1974**, *23*, 254−256.

[31] M. J. Frazer, W. Gerrard, R. Twaits, *J. Inorg. Nucl. Chem.* **1963**, *25*, 637–640.

[32] S. Milicćev, D. Hadẑi, *Inorg. Chimica Acta.* **1977**, *21*, 201–207.

[33] A. A. A. Emara, G. J. Schrobilgen, *Inorg. Chem.* **1992**, *31*, 1323–1332.

[34] J. G. Malm, C. L. Chernick, *Inorg. Synth.* **1966**, *8*, 258–260.

[35] J. L. Huston, *Inorg. Chem.* **1982**, *21*, 685–688.

[36] M. Gerken, D. A. Dixon, G. J. Schrobilgen, *Inorg. Chem.* **2000**, *39*, 4244–4255.

[37] APEX2, release v2014.9-0; Bruker AXS Inc.: Madison, WI, **1995**.

[38] G. M. Sheldrick, SADABS (Siemens Area Detector Absorption Corrections), version 2.03; Siemens Analytical X-ray Instruments, Inc.: Madison, WI, **1999**.

[39] G. M. Sheldrick, SHELXTL-Plus, release 5.1; Siemens Analytical X-ray Instruments, Inc.: Madison, WI, **1998**.

[40] O. V. Dolomanov, L. J. Bourhis, R. J. Gildea, J. A. K. Howard, J. Puschmann, *J. Appl. Crystallogr*. **2009**, *42*, 339–341.

[41] A. L. Spek, *J. Appl. Crystallogr*. **2003**, *36*, 7–13.

[42] Basis sets were obtained from the Extensible Computational Chemistry Environment Basis set Database, version 2/25/04, as developed and distributed by the Molecular Science Computing Facility, Environmental and Molecular Science Laboratory, which is part of the Pacific Northwest Laboratory, P.O. Box 999, Richland, WA, 99352.

[43] M. J. Frisch, G. W. Trucks, H. B. Schlegel, G. E. Scuseria, M. A. Robb, J. R. Cheeseman, G. Scalmani, V. Barone, B. Mennucci, G. A. Petersson, H. Nakatsuji, M. Caricato, X. Li, H. P. Hratchian, A. F. Izmaylov, J. Bloino, G. Zheng, J. L. Sonnenberg, M. Hada, M. Ehara, K. Toyota, R. Fukuda, J. Hasegawa, M. Ishida, T. Nakajima, Y. Honda, O. Kitao, H. Nakai, T. Vreven, J. A. Montgomery, J. E. Peralta, F. Ogliaro, M.. Bearpark, J. J. Heyd, E. Brothers, K. N. Kudin, V. N. Staroverov, R. Kobayashi, J. Normand, K. Raghavachari, A. Rendell, J. C. Burant, S. S. Iyengar, J. Tomasi, M. Cossi, N. Rega, N. J. Millam, M. Klene, J. E. Knox, J. B. Cross, V. Bakken, C. Adamo, J. Jaramillo, R. Gomperts, R. E. Stratmann, O. Yazyev, A. J. Austin, R. Cammi, C. Pomelli, J. W. Ochterski, R. L. Martin, K. Morokuma, V. G. Zakrzewski, G. A. Voth, P. Salvador, J. J. Dannenberg, S. Dapprich, A. Daniels, D. Farkas, J. Foresman, J. V. Ortiz, J. Cioslowski, D. J. Fox, Gaussian 09, Revision D.01; Gaussian, Inc: Wallingford, CT, **2009**.

[44] GaussView, version 3.0; Gaussian Inc.: Pittsburgh, PA, **2003**.

[45] Crystal Explorer (Version 3.1) S. K. Wolff, D. J. Grimwood, J. J. McKinnon, M. J. Turner, D. Jayatilaka, M. A. Spackman, University of Western Australia, **2012**.

[46] NBO 6.0. Glendening, E. D.; Badenhoop, J. K.; Reed, A. E.; Carpenter, J. E.; Bohmann, J. A.; Morales, C. M.; Landis, C. R.; Weinhold, F. Theoretical Chemistry Institute, University of Wisconsin, Madison, **2013**.

3.4 Supporting Information

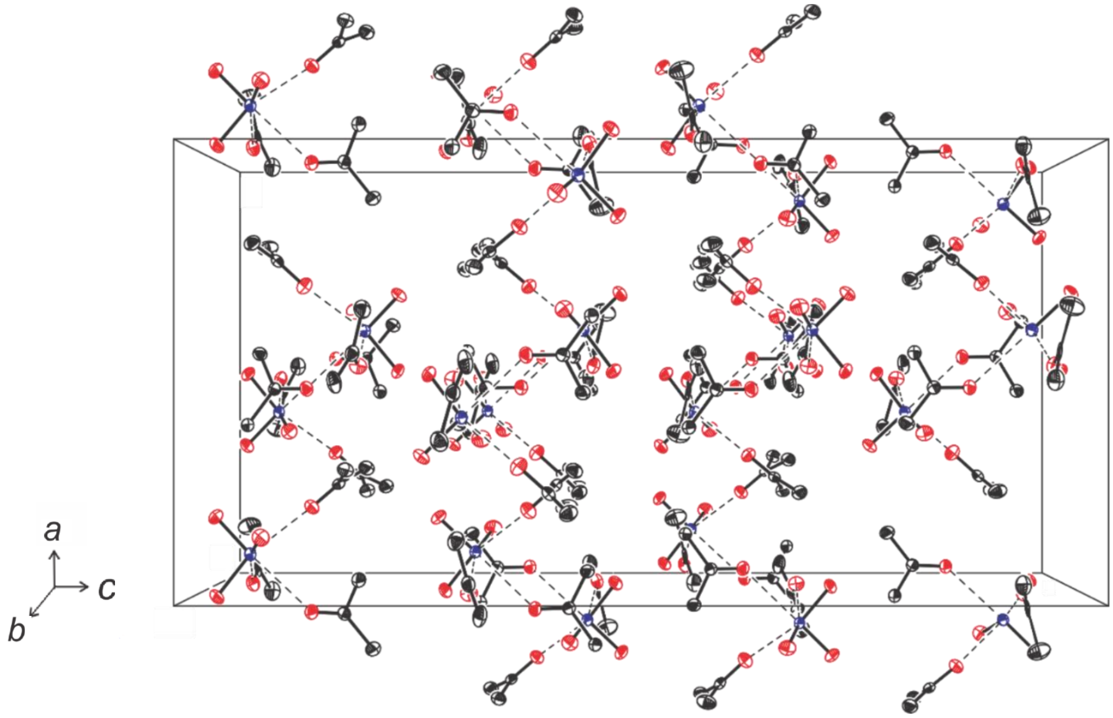

Figure 3.12. The packing diagram for $[(CH_3)CO]_3XeO_3$; thermal ellipsoids are shown at the 50% probability level and hydrogen atoms have been omitted for clarity.

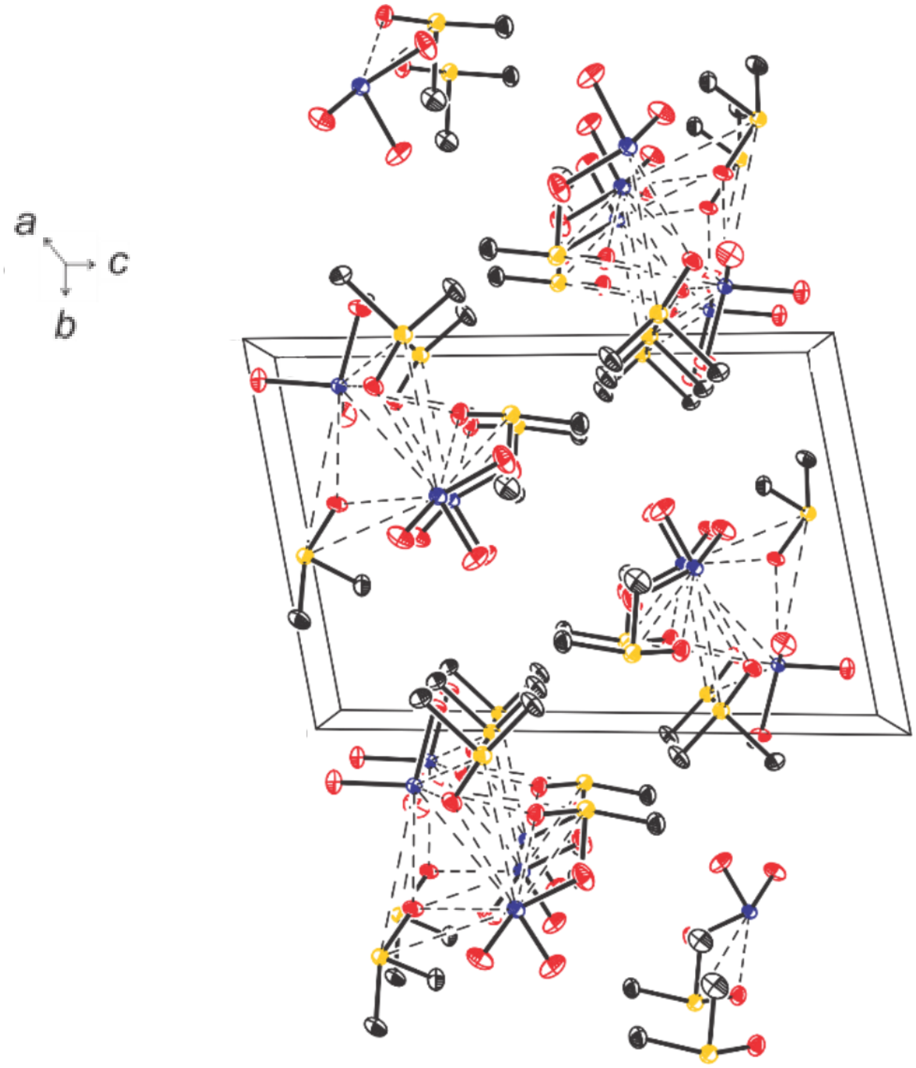

Figure 3.13. The packing diagram for $[(CH_3)SO]_3(XeO_3)_2$; thermal ellipsoids are shown at the 50% probability level and hydrogen atoms have been omitted for clarity.

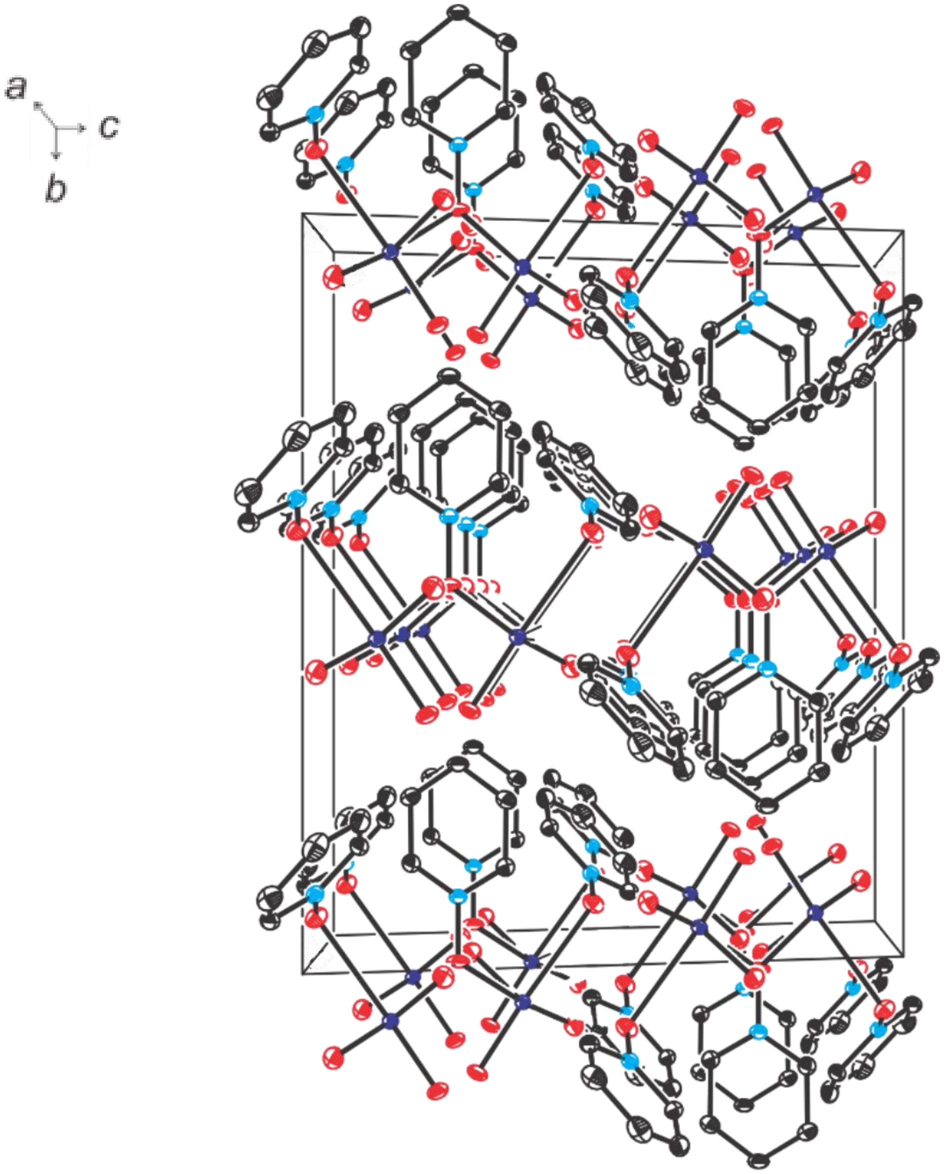

Figure 3.14. The packing diagram for $(C_5H_5NO)_3(XeO_3)_2$; thermal ellipsoids are shown at the 50% probability level and hydrogen atoms have been omitted for clarity.

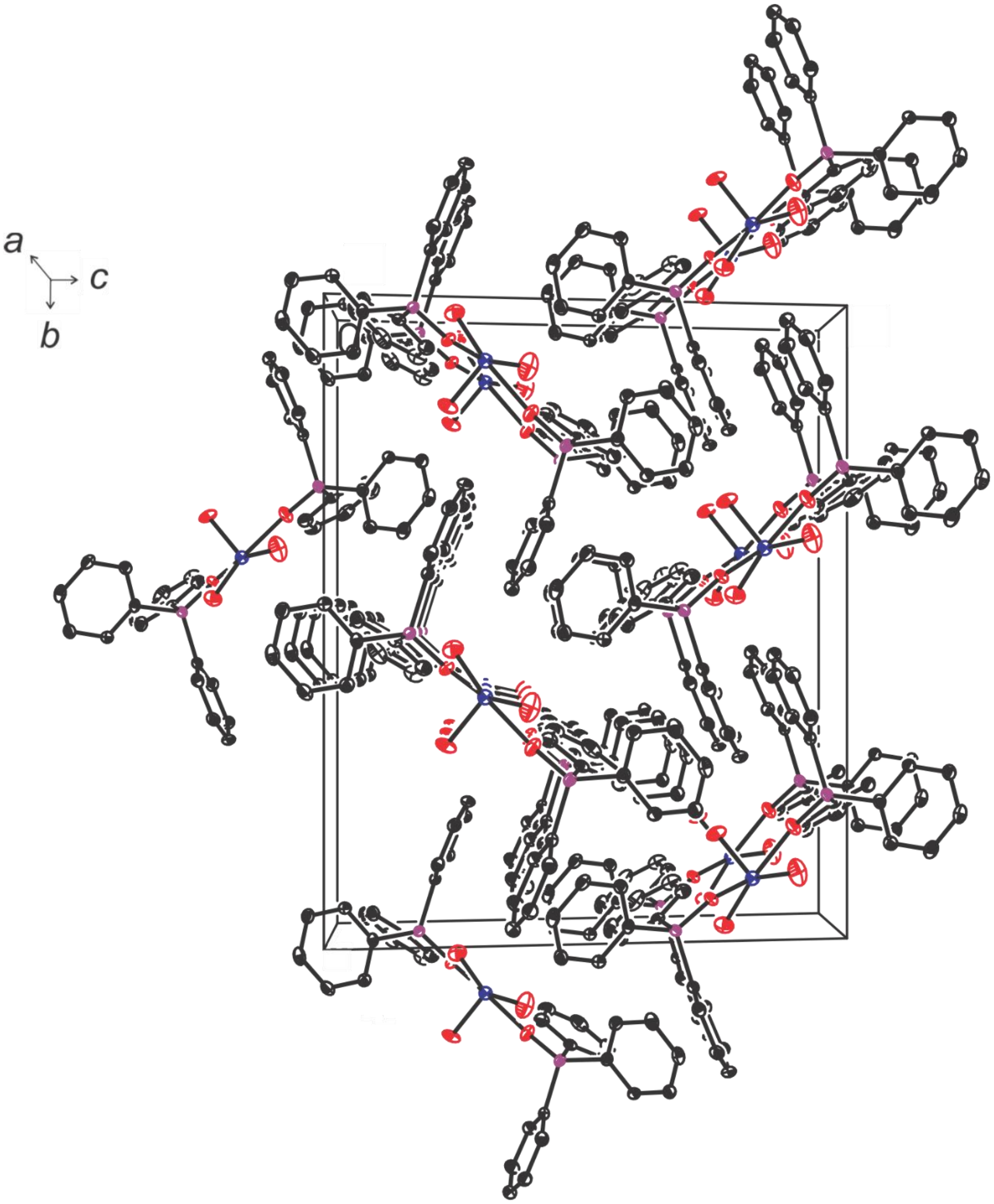

Figure 3.15. The packing diagram for $[(C_6H_5)_3PO]_2XeO_3$; thermal ellipsoids are shown at the 50% probability level and hydrogen atoms have been omitted for clarity.

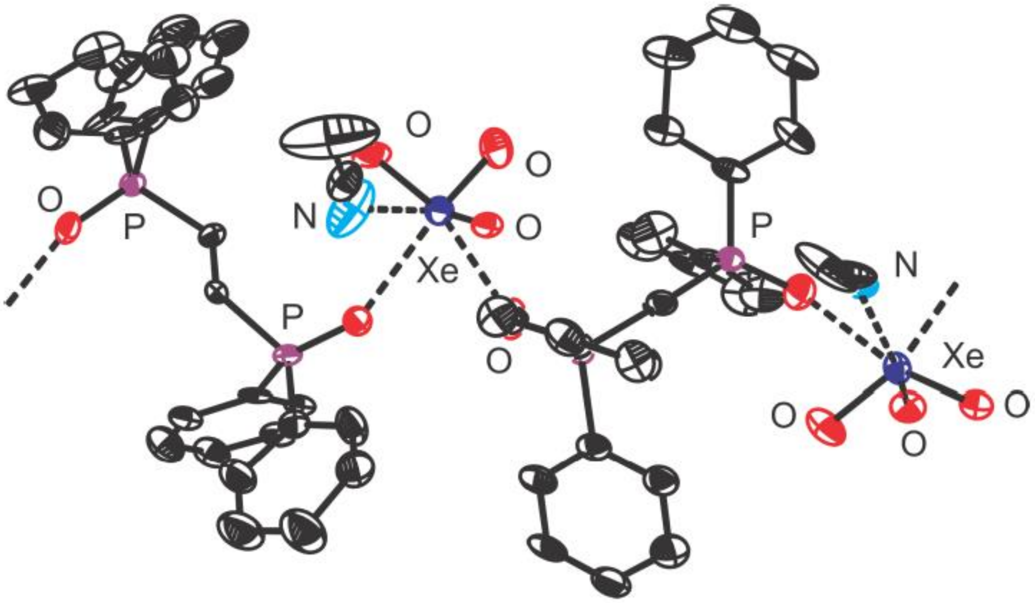

Figure 3.16. The preliminary X-ray crystal structure of $[(C_6H_5)_2POCH_2]_2XeO_3{\cdot}CH_3CN$ (**5**); the hydrogen atoms have been omitted for clarity and thermal ellipsoids are shown at the 50% probability levels.

Table 3.5. Experimental and calculated[a] (C_1 symmetry) geometrical parameters for $[(CH_3)_2CO]_3XeO_3$.

Bond Lengths (Å)				
exptl				calcd
Xe1–O1	1.768(2)	Xe2–O4	1.765(2)	1.786
Xe1–O2	1.768(2)	Xe2–O5	1.767(2)	1.784
Xe1–O3	1.764(2)	Xe2–O6	1.762(2)	1.785
Xe1–O7	2.768(2)	Xe2–O10	2.778(2)	2.866
Xe1–O8	2.745(2)	Xe2–O11	2.740(2)	2.864
Xe1–O9	2.738(2)	Xe2–O12	2.777(2)	2.865
O7–C2	1.211(4)	O10–C11	1.217(4)	1.216
C1–C2	1.506(4)	C10–C11	1.488(4)	1.507
C2–C3	1.488(4)	C11–C12	1.499(4)	1.509
C4–C5	1.484(5)	C13–C14	1.493(5)	1.507
C5–C6	1.487(5)	C14–C15	1.491(5)	1.509
O8–C5	1.223(4)	O11–C14	1.210(3)	1.216
C7–C8	1.492(5)	C16–C17	1.485(5)	1.509
C8–C9	1.493(4)	C17–C18	1.484(5)	1.507
O9–C8	1.223(3)	O12–C17	1.221(3)	1.216

Bond Angles (º)				
exptl				calcd
O2–Xe1–O1	101.70(9)	O4–Xe2–O5	101.86(9)	103.11
O1–Xe1–O3	101.80(9)	O4–Xe2–O6	101.59(9)	102.89
O2–Xe1–O3	102.37(9)	O5–Xe2–O6	102.11(9)	103.29
O1–Xe1–O8	85.95(8)	O4–Xe2–O12	88.85(8)	85.94
O2–Xe1–O8	161.16(8)	O6–Xe2–O12	166.72(8)	166.70
O3–Xe1–O8	92.70(7)	O6–Xe2–O10	88.69(8)	83.79
O1–Xe1–O7	164.84(8)	O5–Xe2–O11	161.47(8)	166.71
O3–Xe1–O7	90.91(7)	O6–Xe2–O11	91.05(8)	85.94
O2–Xe1–O9	86.22(7)	O4–Xe2–O11	87.98(8)	83.99
O1–Xe1–O9	89.48(7)	O5–Xe2–O12	83.49(8)	85.61
O3–Xe1–O9	163.94(8)	O4–Xe2–O10	166.89(8)	166.99
O8–Xe1–O9	76.58(6)	O10–Xe2–O11	83.66(6)	87.06
Xe1–O9–C8	135.7(2)	Xe2–O11–C14	142.5(2)	128.92
O7–C2–C3	122.5(3)	O10–C11–C10	121.8(3)	122.02
O7–C2–C1	120.7(3)	O10–C11–C12	121.6(3)	120.60
O8–C5–C4	120.8(3)	O11–C14–C13	122.0(3)	120.60
O8–C5–C6	121.1(3)	O11–C14–C15	121.3(3)	122.01
O9–C8–C7	120.7(3)	O12–C17–C18	121.3(3)	120.60
O9–C8–C9	122.0(3)	O12–C17–C16	121.3(3)	122.03
C1–C2–C3	116.7(3)	C10–C11–C12	116.6(3)	117.36
C4–C5–C6	118.1(3)	C13–C14–C15	116.8(3)	117.38
C7–C8–C9	117.4(3)	C16–C17–C18	117.6(3)	117.36

[a] B3LYP/Def2-TZVP.

Table 3.6. Experimental and calculated[a] (C_1 symmetry) geometrical parameters for $[(CH_3)_2SO]_3(XeO_3)_2$.

Bond Lengths (Å)			Bond Angles (°)		
	exptl	calcd[a]		exptl	calcd[a]
Xe1–O1	1.763(1)	1.770	O1−Xe1−O2	101.96(7)	102.96
Xe1–O2	1.767(1)	1.760	O1−Xe1−O3	102.31(7)	103.56
Xe1–O3	1.771(1)	1.774	O2−Xe1−O3	102.29(7)	103.63
Xe2–O4	1.765(1)	1.768	O4−Xe2−O5	102.25(6)	103.62
Xe2–O5	1.771(1)	1.762	O4−Xe2−O6	101.92(7)	103.04
Xe2–O6	1.772(1)	1.780	O5−Xe2−O6	101.27(7)	101.93
Xe1–O7	2.871(1)	2.805	O4−Xe2−O7	94.20(5)	91.20
Xe1–O8	2.726(1)	2.752	O5−Xe2−O7	87.18(5)	102.86
Xe1–O9	2.693(1)	2.721	O1−Xe1−O7	96.31(5)	89.17
Xe2–O7	2.703(1)	2.825	O3−Xe1−O7	152.46(5)	149.47
Xe2–O8	2.770(1)	2.694	O1−Xe1−O8	161.32(5)	157.70
Xe2–O9	2.683(1)	2.675	O2−Xe1−O8	88.96(5)	91.41
S1–O7	1.529(1)	1.511	O3−Xe1−O8	89.89(5)	89.21
S1–C1	1.782(2)	1.789	O1−Xe1−O9	90.26(5)	84.21
S1–C2	1.788(2)	1.791	O2−Xe1−O9	161.80(5)	166.04
S2–O8	1.524(1)	1.511	O3−Xe1−O9	87.96(5)	85.99
S2–C3	1.786(2)	1.788	O8−Xe1−O9	75.92(4)	78.46
S2–C4	1.779(2)	1.789	O4−Xe2−O9	92.96(5)	91.20
S3–O9	1.538(1)	1.512	O5−Xe2−O7	87.18(5)	87.45
S3–C5	1.785(2)	1.787	O6−Xe2−O7	159.63(5)	147.48
S3–C6	1.782(2)	1.790	O4−Xe2−O8	161.77(5)	160.41
			O6−Xe2−O8	92.59(5)	90.04
			O5−Xe2−O9	157.08(5)	168.24
			O7−Xe2−O9	74.56(4)	71.87
			O6−Xe2−O9	92.09(5)	87.45
			Xe1−O8−S2	130.34(7)	128.55
			Xe2−O7−S1	117.52(6)	122.53
			Xe1−O9−Xe2	96.08(4)	94.66
			Xe1−O9−S3	124.15(6)	125.89
			Xe2−O9−S3	135.49(7)	128.83
			O7−S1−C1	105.05(8)	106.38
			O7−S1−C2	105.35(8)	105.32
			O8−S2−C3	104.82(8)	105.52
			O8−S2−C4	105.19(9)	105.42
			O9−S3−C5	105.24(8)	106.16
			O9−S3−C6	104.39(8)	105.41
			C1−S1−C2	98.7(1)	98.39
			C3−S2−C4	99.2(1)	98.47
			C5−S3−C6	99.36(9)	98.44

[a] APFD/Def2-TZVP.

Table 3.7. Experimental and calculated[a] (C_2 symmetry) geometrical parameters for $[(C_5H_5NO]_3(XeO_3)_2$.

Bond Lengths (Å)			**Bond Angles (º)**		
	exptl	calcd[a]		exptl	calcd[a]
Xe1–O1	1.768(1)	1.772	O1–Xe1–O2	100.65(5)	102.54
Xe1–O2	1.779(1)	1.763	O1–Xe1–O3	102.26(5)	103.10
Xe1–O3	1.773(1)	1.770	O2–Xe1–O3	100.20(5)	104.24
Xe1–O4	2.586(1)	2.616	O1–Xe1–O4	86.08(4)	80.88
Xe1–O5	2.604(1)	2.680	O2–Xe1–O4	87.22(4)	85.25
Xe1–O4’	2.896(1)		O1–Xe1–O5	82.71(4)	80.87
O4–N1	1.335(2)	1.292	O2–Xe1–O5	172.80(4)	159.50
N1–C1	1.353(2)	1.350	O3–Xe1–O4	167.96(4)	168.40
N1–C5	1.354(2)	1.350	O3–Xe1–O5	85.19(4)	85.25
C1–C2	1.380(2)	1.377	O1–Xe1–O4’	153.49(4)	
C2–C3	1.392(2)	1.387	O2–Xe1–O4’	101.16(4)	
C3–C4	1.385(3)	1.387	O3–Xe1–O4’	87.22(4)	
C4–C5	1.377(2)	1.376	Xe1–O4–N1	107.00(8)	104.15
C6–C7	1.382(2)	1.377	O4–N1–C1	119.7(1)	119.76
C1–H1	0.94(2)	1.079	O4–N1–C5	118.9(1)	119.90
C2–H2	0.95(2)	1.082	N1–C1–C2	119.9(1)	120.67
C3–H3	0.98(3)	1.083	N1–C5–C4	120.1(1)	120.71
C4–H4	1.00(2)	1.082	C1–N1–C5	121.4(1)	120.29
C5–H5	0.89(2)	1.078	C1–C2–C3	119.6(2)	119.96
C6–H6	0.85(2)	1.078	C2–C3–C4	119.2(2)	118.41
C7–H7	0.94(2)	1.082	C3–C4–C5	119.7(2)	119.94

[a] APFD/Def2-TZVP.

Table 3.8. Experimental and calculated[a] (C_1 symmetry) geometrical parameters for $[(C_6H_5)_3PO]_2XeO_3$ at –173 °C.

	Bond Lengths (Å)			**Bond Angles (°)**	
	exptl	calcd[a]		exptl	calcd[a]
Xe1–O1	1.763(4)	1.786	O1–Xe1–O2	102.2(2)	103.96
Xe1–O3	1.770(3)	1.785	O1–Xe1–O3	103.2(2)	104.10
Xe1–O2	1.774(4)	1.785	O2–Xe1–O3	100.8(2)	101.94
Xe1–O4	2.605(3)	2.731	O1–Xe1–O4	95.0(1)	89.44
Xe1–O5	2.591(4)	2.723	O2–Xe1–O4	84.0(1)	84.32
P1–O4	1.507(3)	1.498	O3–Xe1–O4	159.6(1)	162.99
P1–C1	1.805(4)	1.821	O1–Xe1–O5	89.1(2)	84.32
P1–C7	1.811(4)	1.821	O2–Xe1–O5	162.2(1)	162.31
P1–C13	1.812(4)	1.821	O3–Xe1–O5	89.8(1)	84.32
P2–O5	1.505(3)	1.497	O4–Xe1–O5	81.2(1)	84.27
P2–C19	1.804(4)	1.821	Xe1–O4–P1	134.9(2)	142.57
P2–C25	1.812(3)	1.814	Xe1–O5–P2	157.9(2)	148.07
P2–C31	1.808(4)	1.821	O4–P1–C1	109.1(2)	110.24
C5–C4	1.389(7)	1.398	O4–P1–C7	113.2(2)	112.88
C5–C6	1.383(7)	1.389	O4–P1–C13	112.2(2)	112.44
C5–H5	0.97(8)	1.083	O5–P2–C19	109.9(2)	112.82
C9–H9	0.99(7)	1.083	O5–P2–C25	111.3(2)	110.44
C25–C30	1.406(6)	1.398	O5–P2–C31	112.7(2)	112.82
C29–C30	1.399(5)	1.389	C7–P1–C13	106.8(2)	106.27

[a] B3LYP/Def2-TZVP.

Table 3.9. Bond valences[a] for $[(CH_3)_2CO]_3XeO_3$, $[(CH_3)_2SO]_3(XeO_3)_2$, $(C_5H_5NO)_2(XeO_3)_2$, and $[(C_6H_5)_3PO]_2XeO_3$.

	$[(CH_3)_2CO]_3XeO_3$		$[(CH_3)_2SO]_3(XeO_3)_2$		$(C_5H_5NO)_2(XeO_3)_2$	$[(C_6H_5)_3PO]_2XeO_3$
Xe–O	1.892	1.903	1.897	1.887	1.872	1.898
	1.872	1.887	1.877	1.857	1.847	1.862
	1.872	1.877	1.857	1.852	1.817	1.842
Xe---O	0.136	0.135	0.154	0.158	0.205	0.202
	0.133	0.122	0.128	0.150	0.195	0.195
	0.125	0.122	0.095	0.125	0.089	
Total	6.032	6.047	6.008	6.028	6.026	5.999

[a] Values are in valence units (v.u.) as defined in reference [14].

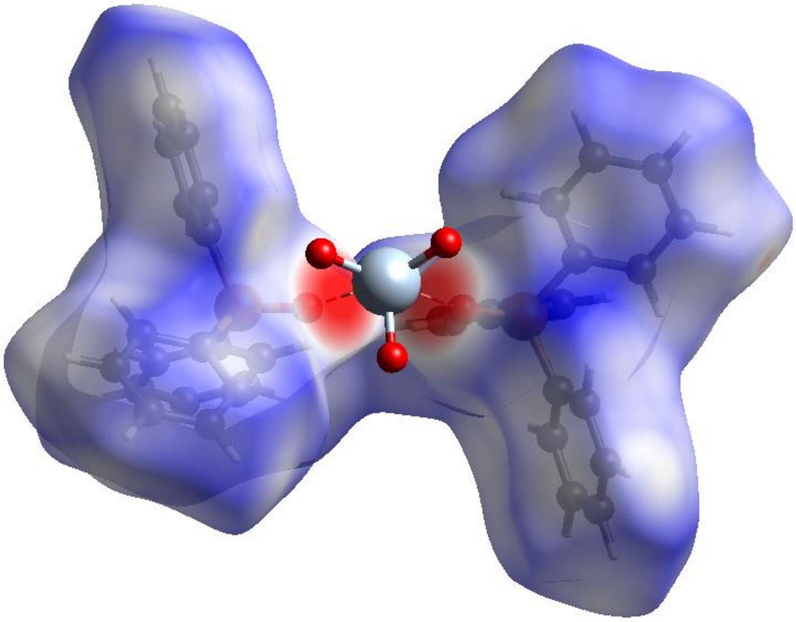

Figure 3.17. The Hirshfeld surface of the triphenylphosphine ligand in $[(C_6H_5)_3PO)_2XeO_3$ mapped with the d_{norm} function.

Table 3.10. Raman and calculated vibrational frequencies (cm^{-1}); and assignments for $[(CH_3)_2CO]_3(XeO_3)_2$ (**1**), XeO_3, and $(CH_3)_2CO$.

exptl	calcd		exptl		calcd	vibrational
$XeO_{3(aq)}$[a]	**XeO_3 (C_{3v})[b]**	**$[(CH_3)_2CO]_3XeO_3$[b]**	**$[(CH_3)_2CO]_3XeO_3$[c]**	**$(CH_3)_2CO$[a]**	**$(CH_3)_2CO$[b]**	**assignments[d]**
		3145(91)[10] 3145(33)[6] 3145(27)[4] 3144(44)[4] 3144(40)[1] 3144(38)[1] 3097(79)[13] 3097(119)[13] 3097(48)[24] 3085(102)[7] 9085(73)[11] 9085(29)[<1] 3037(651)[3] 3037(55)[15] 3037(69)[14] 3031(60)[<1] 3031(62)[<1] 3031(7)[<1]	3010(<1) 3006(5) 2969(7) 2920(34) 2695(1)	3643(2) 3005(10) 2968(7) 2922(100) 2847(2) 2701(3) 2695(<1) 2284(2)	3143(73)[7] 3142(55)[12] 3089(96)[18] 3081(14)[<1] 3036(273)[6] 3026(2)[1]	ν(CH), combination bands, and overtones
		1766(41)[2] 1757(20)[479] 1757(19)[510]	1692, sh 1686(15)	1705(12)	1789(9)[184]	ν(CO)
		1493(7)[22] 1492(8)[19] 1492(2)[5] 1473(13)[3] 1473(16)[7] 1473(7)[1] 1462(9)[7] 1461(5)[18] 1461(6)[13] 1459(11)[14] 1459(12)[35] 1458(8)[39]	1428(5)	1432(7)	1487(<1)[21] 1470(15)[25] 1465(15)[4] 1460(2)[1]	$\delta_{as}(CH_3)$
		1394(2)[87] 1393(1)[3] 1393(2)[3] 1388(<1)[56] 1388(1)[38] 1388(1)[26]	1356(1)	1371(<1) 1360(1)	1388(1)[56] 1387(2)[19]	$\delta_s(CH_3)$

Table 3.10. continued…

exptl	calcd		exptl		calcd	vibrational
$XeO_{3(aq)}$[a]	XeO_3 (C_{3v})[b]	$[(CH_3)_2CO]_3XeO_3$[b]	$[(CH_3)_2CO]_3XeO_3$[c]	$(CH_3)_2CO$[a]	$(CH_3)_2CO$[b]	assignments[d]
		1247(15)[186] 1246(13)[17] 1246(16)[5]	1239(6) 1214(2) 1210(1)	1225(4)	1235(2)[75]	δ(CC)
		1119(<1)[7] 1119(<1)[5] 1118(<1)[1]			1120(<1)[2]	$\rho_t(CH_2)$
		1088(5)[1] 1088(3)[<1] 1088(3)[<1]	1075(1)	1068(3)	1085(3)[<1]	$\rho_r(CH_2)$
		926(3)[10] 926(2)[6] 926(4)[4]	911(1)			$\rho_r(CH_2)$
		885(2)[2] 884(1)[<1] 884(1)[1]		834(1)	887(2)[10] 885(1)[<1]	$\rho_\omega(CH)$
857(8) 819(26) 809(63)	855(92)[11]	828(14)[138] 824(14)[146]	835(19) 830(7) 804(9)			$\nu_{as}(XeO_3)$
		790(38)[1] 790(1)[1] 790(4)[1]		792(21)	783(14)[2]	ν(CC)
764(100) 754, sh	788(4)[53]	779(125)[14]	778(100)			$\nu_s(XeO_3)$
		546(1)[39] 545(2)[5] 545(2)[3]	557(1) 542(1)	533(4)	537(2)[14]	$\delta(CCO)_{ip}$
		495(<1)[2] 495(1)[1] 495(<1)[<1]	495(1)	499(<1) 490(1)	491(1)[1]	$\delta(CCCO)_{oop}$

Table 3.10. continued…

exptl	calcd		exptl		calcd	vibrational assignments[d]
$XeO_{3(aq)}$[a]	XeO_3 (C_{3v})[b]	$[(CH_3)_2CO]_3XeO_3$[b]	$[(CH_3)_2CO]_3XeO_3$[c]	$(CH_3)_2CO$[a]	$(CH_3)_2CO$[b]	
		392(<1)[1] 392(<1)[12] 391(<1)[11]			380(1)[2]	$\delta(CCC)_{ip}$
351(1) 323(3)	308(33)[3]	335(2)[40]	343(6)			$\delta_{umb}(XeO_3)$
311(42) 297(11)	271(9)[5]	308(4)[30] 304(3)[27]	314(13)			$\delta_{as}(XeO_3)$
146(5) 110(10) 99(16)		151(1)[9] 150(1)[9] 144(<1)[<1] 139(<1)[4] 137(<1)[6] 128(<1)[9] 120(<1)[4] 112(<1)[8] 108(<1)[8] 97(1)[1] 92(1)[4] 91(1)[2] 76(3)[1] 71(1)[<1] 68(1)[<1] 63(<1)[<1] 57(1)[2] 35(<1)[1] 31(1)[3] 27(1)[<1] 26(1)[3] 25(<1)[<1] 17(2)[2] 16(2)[3]	171(<1) 149(<1) 143(1) 107(1) 100(1)	275(<1) 162(<1) 116(<1) 107(1) 107(1)	132(<1)[<1] 43(<1)[<1]	deformation modes / lattice modes

[a] The spectrum was recorded in a ¼-in. diameter FEP sample tube at −140 °C. Values in parentheses are relative Raman intensities. Abbreviations denote shoulder (sh) and broad (br). [b] The B3LYP/Def2–TZVP level of theory was used. Values in parentheses and square brackets are calculated Raman intensities (Å amu^{-1}) and infrared intensities (km mol^{-1}), respectively. [c] The spectrum was recorded in a ¼-in. FEP diameter sample tube at −78 °C. Weak bands were observed at 757(1), 434(1), 418(1) cm^{-1} which could not be assigned. [d] Symbols denote stretch (ν), bend (δ), rock (ρ_r), twist (ρ_t), wag (ρ_ω), umbrella (umb), symmetric (s), and asymmetric (as)

Table 3.11. Raman and calculated vibrational frequencies (cm^{-1}); and assignments for $[(CH_3)_2SO]_3(XeO_3)_2$ (**2**), $XeO_{3(aq)}$, and $(CH_3)_2SO$.

exptl	calcd				exptl		calcd		vibrational
$XeO_{3(aq)}$[a]	XeO_3		$[(CH_3)_2SO]_3(XeO_3)_2$		$[(CH_3)_2SO]_3(XeO_3)_2$[d]	$(CH_3)_2SO$[a]	$(CH_3)_2SO$		assignments[e]
	APFD[b]	*B3LYP*[c]	*B3LYP*[b]	*APFD*[c]			*B3LYP*[b]	*APFD*[c]	
			3153(26)[3]	3180(13)[5]					ν(CH), combination bands, and overtones
			3152(45)[2]	3175(35)[2]					
			3152(53)[2]	3174(50)[2]					
			3151(25)[1]	3172(41)[1]		3026(<1)			
			3151(17)[1]	3170(31)[2]		3001(21)			
			3151(27)[2]	3168(62)[3]		2995(9)			
			3141(93)[1]	3166(86)[1]	3024(1)	2988(76)	3141(98)[4]	3159(103)[2]	
			3141(130)[2]	3163(48)[1]	3016(19)	2957(1)	3140(43)[2]	3159(40)[1]	
			3141(136)[2]	3132(66)[<1]	3006(5)	2919(46)	3134(101)[13]	3137(100)[9]	
			3138(16)[<1]	3131(81)[1]	2935(4)	2908(73)	3130(11)[<1]	3133(9)[<1]	
			3138(16)[<1]	3159(29)[1]	2922(61)	2881(9)	3039(278)[8]	3054(274)[7]	
			3138(15)[<1]	3156(26)[1]		2828(2)	3037(<1)[5]	3034(1)[3]	
			3045(556)[7]	3059(401)[19]		2808(1)			
			3045(184)[21]	3056(31)[6]		2408(2)			
			3045(107)[24]	3054(250)[11]		2368(2)			
			3041(44)[2]	3053(10)[<1]					
			3041(31)[3]	3052(272)[26]					
			3041(35)[4]	3049(43)[3]					
			1481(3)[23]	1487(9)[17]					$\delta_{as}(CH_3)$
			1481(3)[16]	1470(4)[20]					
			1481(2)[22]	1467(<1)[43]					
			1465(4)[2]	1453(14)[8]					
			1465(9)[1]	1452(5)[1]			1475(2)[18]	1464(3)[19]	
			1465(12)[<1]	1448(4)[2]	1452(2)	1448(26)	1457(16)[<1]	1443(13)[6]	
			1458(11)[13]	1445(18)[14]	1418(1)	1423(20)	1455(15)[5]	1443(13)[<1]	
			1457(17)[2]	1445(9)[1]			1442(1)[9]	1428(3)[10]	
			1457(13)[1]	1439(1)[7]					
			1444(5)[7]	1430(9)[7]					
			1444(7)[7]	1429(12)[11]					
			1444(8)[9]	1425(3)[6]					

Table 3.11. continued…

exptl	calcd				exptl		exptl		vibrational
$XeO_{3(aq)}$ [a]	XeO_3		$[(CH_3)_2SO]_3(XeO_3)_2$		$[(CH_3)_2SO]_3(XeO_3)_2$[d]	$(CH_3)_2SO$[a]	$(CH_3)_2SO$		assignments[e]
	APFD[b]	*B3LYP*[c]	*B3LYP*[b]	*APFD*[c]			*B3LYP*[b]	*APFD*[c]	
			1352(8)[4] 1352(3)[27] 1352(1)[21] 1330(<1)[1] 1330(<1)[3] 1330(<1)[3]	1341(4)[41] 1339(3)[23] 1336(1)[6] 1317(<1)[6] 1315(<1)[3] 1313(<1)[1]	1409(7) 1401, sh	1411(3)	1337(2)[10] 1316(<1)[1]	1311(2)[19] 1286(<1)[3]	$\delta_s(CH_3)$
			1052(7)[3] 1052(3)[6] 1051(1)[27]	1076(31)[54] 1062(8)[539] 1058(15)[293]	1127(<1) 1121(5)		1024(2)[16]	993(2)[11]	$\rho_r(CH_2)$
			1043(19)[1] 1034(9)[361] 1034(9)[359]	1050(3)[33] 1040(2)[18] 1038(<1)[2]	1011(5) 1008(<1) 1000(<1)	1037(1) 1021(38)	1115(10)[137]	1141(10)[140]	ν(SO)
			968(9)[1] 967(9)[119] 967(9)[108]	973(3)[29] 968(4)[9] 966(4)[17]	994(2) 991(1)	963(12)	957(4)[8]	907(3)[8]	ν(SO) $\rho_r(CH_2)$
			953(2)[6] 953(2)[5] 953(2)[4] 915(<1)[4] 915(<1)[3] 915(<1)[4]	938(2)[11] 934(2)[13] 933(1)[11] 903(1)[7] 899(1)[6] 894(1)[7]	953(1) 944(4) 944(4)	942(3) 904(3)	925(3)[8] 890(<1)[2]	891(1)[15] 873(2)[<1]	$\rho_r(CH_2)$
857(8) 819(26) 809(63)	901(11)[98]	855(92)[11]	831(18)[157] 829(17)[206] 823(18)[22] 820(17)[72]	884(20)[155] 879(23)[71] 859(18)[220] 852(17)[35]	833(2) 826(3) 819(14)				$\nu_{as}(Xe_1O_3)$ $\nu_{as}(Xe_1O_3) + \nu_{as}(Xe_2O_3)$ $\nu_{as}(Xe_1O_3) - \nu_{as}(Xe_2O_3)$ $\nu_{as}(Xe_2O_3)$
764(100) 754, sh	836(51)[4]	788(4)[53]	779(113)[15] 776(72)[27]	822(86)[24] 812(61)[30]	769(100)				$\nu_s(Xe_1O_3)$ $\nu_{as}(Xe_2O_3)$
			687(10)[16] 687(16)[9] 686(15)[1]	717(10)[6] 712(9)[6] 711(10)[9]	716(6) 702(8) 678(20) 505(<1)	705(55) 673(100)	661(14)[19]	647(12)[14]	$\nu_{as}(SC_2)$

Table 3.11. continued…

exptl	calcd				expt1		calcd		vibrational
$XeO_{3(aq)}$[a]	XeO_3		$[(CH_3)_2SO]_3(XeO_3)_2$		$[(CH_3)_2SO]_3(XeO_3)_2$[d]	$(CH_3)_2SO$[a]	$(CH_3)_2SO$		assignments[e]
	APFD[b]	*B3LYP*[c]	*B3LYP*[b]	*APFD*[c]			*B3LYP*[b]	*APFD*[c]	
			390(<1)[23] 388(3)[1] 387(3)[4]	406(2)[16] 396(2)[10] 390(3)[3]	467(<1) 465(3) 460(<1) 414(1) 402(<1) 393(4) 387(<1)	388(19)	375(2)[7]	370(1)[6]	$\rho_r(CSO)$ $\rho_r(CSC)$
			339(4)[13]	351(1)[139]	359(<1) 350(<1) 347(1)	336(27) 323(2)	322(3)[9]	322(3)[9]	$\delta(OCS)$
351(1) 323(3)	322(3)[34]	308(33)[3]	342(3)[2] 340(3)[11] 334(3)[48] 333(2)[95]	359(3)[6] 354(5)[2] 348(4)[15] 347(2)[7]	342(6)				$\delta_{umb}(Xe_1O_3) + \delta_{umb}(Xe_2O_3)$ $\delta_{umb}(Xe_1O_3) - \delta_{umb}(Xe_2O_3)$
311(42) 297(11)	284(4)[10]	271(9)[5]	300(5)[18] 298(5)[25] 294(3)[2] 292(3)[7]	321(4)[35] 314(4)[25] 311(4)[11] 306(2)[5]	311(15)				$\delta_{as}(XeO_3)$ $\delta_{as}(Xe_2O_2)$ $\delta_{as}(Xe_2O_2) + \delta_{as}(Xe_1O_2)$ $\delta_{as}(Xe_2O_2) - \delta_{as}(Xe_1O_2)$ $\delta_{as}(Xe_1O_2)$

Table 3.11. continued…

exptl	calcd				explt		calcd		vibrational
$XeO_{3(aq)}$[a]	XeO_3		$[(CH_3)_2SO]_3(XeO_3)_2$		$[(CH_3)_2SO]_3(XeO_3)_2$[d]	$(CH_3)_2SO$[a]	$(CH_3)_2SO$		assignments[e]
	APFD[b]	*B3LYP*[c]	*B3LYP*[b]	*APFD*[c]			*B3LYP*[b]	*APFD*[c]	
			287(1)[3]	298(3)[2]	307(<1)	312(13)	284(3)[<1]	289(2)[<1]	δ(CSC)
			286(3)[2]	284(1)[1]					
			286(2)[<1]	281(1)[1]					
			249(<1)[<1]	260(1)[<1]			229(<1)[1]	238(<1)[1]	$\rho_t(CH_3)$
			248(<1)[<1]	256(1)[<1]					
			247(<1)[1]	244(<1)[1]					
			210(<1)[<1]	226(<1)[2]					
			209(<1)[<1]	220(<1)[<1]					
			209(<1)[<1]	212(<1)[7]					
146(5) 110(10) 99(16)			168(<1)[48]	202(1)[22]	84(150)	119(14) 99(1)	183(<1)[<1]	181(<1)[<1]	deformation modes / lattice modes
			153(2)[24]	185(<1)[26]					
			148(2)[8]	172(2)[15]					
			140(2)[5]	152(<1)[2]					
			135(2)[1]	146(<1)[1]					
			116(<1)[<1]	140(1)[1]					
			106(<1)[3]	127(1)[1]					
			104(<1)[<1]	122(1)[2]					
			98(<1)[2]	118(<1)[1]					
			95(<1)[1]	115(1)[3]					
			86(<1)[2]	100(<1)[4]					
			82(<1)[4]	97(<1)[4]					
			74(<1)[6]	9(<1)[6]					
			69(<1)[<1]	81(<1)[1]					
			62(<1)[2]	77(<1)[2]					
			60(1)[1]	75(<1)[1]					
			55(<1)[<1]	67(<1)[<1]					
			51(<1)[1]	64(1)[<1]					
			49(<1)[4]	58(<1)[2]					
			47(<1)[1]	54(<1)[1]					
			45(<1)[<1]	49(1)[2]					
			43(<1)[<1]	46(<1)[1]					
			24(<1)[2]	42(<1)[1]					
			24(<1)[2]	35(<1)[4]					

[a] The spectrum was recorded in a ¼-in. diameter FEP sample tube at −140 °C. Values in parentheses are relative Raman intensities. Abbreviations denote shoulder (sh) and broad (br). [b] The B3LYP/Def2–TZVP level of theory was used. [c] The APFD/Def2–TZVP level of theory was used. Values in parentheses and square brackets are calculated Raman intensities (Å amu^{-1}) and infrared intensities (km mol^{-1}), respectively. [d] The spectrum was recorded in an aluminum sample holder at 22 °C. Values in parentheses are relative Raman intensities. [e] Symbols denote stretch (ν), bend (δ), rock (ρ_r), twist (ρ_t), wag (ρ_ω), umbrella (umb), symmetric (s), and asymmetric (as).

Table 3.12. Raman and calculated vibrational frequencies (cm^{-1}); and assignments for $(C_5H_5NO)_3(XeO_3)_2$ (**3**), $XeO_{3(aq)}$, and C_5H_5NO.

exptl	**calcd**				**exptl**		**calcd**		**vibrational**
$XeO_{3(aq)}$[a]	**XeO_3 (C_{3v})**		**$(C_5H_5NO)_3(XeO_3)_2$**		**$(C_5H_5NO)_3(XeO_3)_2$**[d]	**C_5H_5NO**[d]	**C_5H_5NO**		**assignments**[e]
	B3LYP[b]	*APFD*[c]	*B3LYP*[b]	*APFD*[c]			*APFD*[c]	*B3LYP*[b]	
			3246(83)[1] 3456(76)[1] 3240(58)[9] 3237(63)[10] 3229(93)[13] 3215(287)[22] 3215(242)[2] 3215(216)[2] 3210(7)[20] 3205(111)[4] 3205(108)[4] 3204(130)[21] 3196(60)[<1] 3196(58)[<1] 3195(59)[4]	3289(65)[1] 3288(7)[13] 3277(246)[<1] 3276(7)[21] 3273(61)[5] 3273(29)[5] 3227(80)[1] 3227(341)[1] 3227(184)[<1] 3221(64)[1] 3218(129)[2] 3218(42)[2] 3206(38)[<1] 3206(79)[1] 3203(55)[1]	3136(<1) 3128(1) 3100(8) 3100(8) 3089(2) 3026(<1) 2937(<1) 2481(1)	3108(14) 3082(49) 3058(16) 3001(2) 2914(1) 2454(4) 2376(1)	3254(159)[<1] 3253(29)[1] 3225(145)[2] 3206(79)[5] 3200(71)[<1]	3243(159)[<1] 3242(31)[<1] 3214(148)[3] 3196(80)[6] 3190(73)[<1]	ν(CH), combination bands, and overtones
			1662(65)[21] 1660(130)[14] 1660(42)[68] 1601(1)[1] 1600(1)[1] 1599(1)[2]	1680(35)[6] 1680(57)[24] 1678(40)[5] 1623(1)[<1] 1622(2)[<1] 1622(1)[<1]	1612(11)	1615(7) 1604(47)	1678(25)[50] 1600(<1)[5]	1658(27)[37] 1583(<1)[5]	A_1, ring vib
			1519(6)[28] 1516(8)[2] 1516(1)[40] 1514(3)[101] 1507(4)[40] 1507(1)[224]	1522(4)[62] 1519(<1)[16] 1519(5)[3] 1518(2)[77] 1518(<1)[95] 1517(<1)[102]	1570(1) 1567(<1) 1472(2) 1470(<1) 1465(<1)	1551(6) 1468(6) 1458(4)	1519(2)[5] 1513(9)[161]	1512(2)[4] 1499(7)[110]	B_2, ring vib
			1282(6)[13] 1278(2)[560]	1309(4)[242] 1306(13)[1]		1252(2)	1375(7)[166]	1362(1)[<1]	ν(NO)

Table 3.12. continued…

exptl	calcd				exptl		calcd		vibrational assignments[e]
$XeO_{3(aq)}$[a]	XeO_3 (C_{3v})		$(C_5H_5NO)_3(XeO_3)_2$		$(C_5H_5NO)_3(XeO_3)_2$[d]	C_5H_5NO[d]	C_5H_5NO		
	B3LYP[b]	*APFD*[c]	*B3LYP*[b]	*APFD*[c]			*APFD*[c]	*B3LYP*[b]	
			1383(2)[<1] 1372(1)[<1] 1371(2)[<1] 1270(8)[335] 1268(3)[30] 1267(3)[7] 1266(1)[25] 1215(2)[42] 1204(9)[40] 1203(11)[49] 1180(6)[<1] 1178(8)[<1] 1177(8)[<1] 1111(3)[3] 1104(3)[6] 1104(3)[5] 1072(4)[<1] 1069(3)[<1] 1069(3)[<1]	1366(<1)[1] 1363(<1)[<1] 1363(<1)[<1] 1316(13)[253] 1313(1)[70] 1305(<1)[12] 1305(15)[8] 1215(6)[11] 1211(12)[15] 1211(1)[26] 1182(1)[<1] 1182(10)[<1] 1181(5)[<1] 1117(<1)[6] 1115(2)[4] 1114(<1)[2] 1078(1)[<1] 1077(<1)[<1] 1077(3)[<1]	1215(5) 1202(3) 1194(3) 1183(<1) 1170(3) 1154(1) 1145(2)	1323(4) 1229(9) 1173(11) 1168(11) 1147(43)	1356(1)[<1] 1282(1)[3] 1202(3)[25] 1177(7)[1] 110(2)[5] 1068(8)[<1]	1333(8)[190] 1254(1)[2] 1196(3)[29] 1173(7)[1] 1094(2)[4] 1062(12)[<1]	A_1, δ(CH) B_2, δ(CH) δ(CH) B_2, ν(ring vib.)
			1042(194)[3] 1041(25)[63] 1041(38)[53]	1047(14)[3] 1042(12)[36] 1042(162)[22]	1069(<1) 1067(<1)	1068(4)	1030(29)[35]	1033(29)[41]	B_2, δ(CH)
			999(<1)[1] 994(1)[1] 993(1)[1] 990(1)[1] 979(<1)[1] 979(<1)[<1] 953(<1)[10] 936(1)[5] 936(<1)[7] 869(<1)[<1] 860(67)[4] 858(7)[89] 856(11)[85] 854(1)[1] 854(1)[<1]	1011(<1)[<1] 995(<1)[<1] 995(<1)[<1] 980(1)[<1] 972(<1)[2] 972(<1)[<1] 938(1)[3] 928(<1)[2] 928(<1)[<1] 884(29)[129] 883(43)[205] 863(20)[9] 848(1)[9] 841(1)[21] 841(3)[4]	1025(19) 919(<1) 915(<1) 833(<1)	1044(16) 1017(100) 979(4) 959(4) 841(36) 829(40)	980(<1)[<1] 969(<1)[<1] 908(<1)[11] 855(31)[10] 839(<1)[<1]	977(<1)[<1] 967(<1)[<1] 906(<1)[10] 861(27)[12] 838(<1)[<1]	A_1, ν(ring vib.) A_1, α(ring vib.) B_1, γ(CH) B_2, γ(CH)

Table 3.12. continued…

exptl	calcd				exptl		calcd		vibrational
$XeO_{3(aq)}$[a]	XeO_3 (C_{3v})		$(C_5H_5NO)_3(XeO_3)_2$		$(C_5H_5NO)_3(XeO_3)_2$[d]	C_5H_5NO[d]	C_5H_5NO		assignments[e]
	B3LYP[b]	*APFD*[c]	*B3LYP*[b]	*APFD*[c]			*APFD*[c]	*B3LYP*[b]	
857(8) 819(26) 809(63)	855(92)[11]	901(11)[98]	829[203](20) 827[183](27) 813[83](34) 805[284](16)	861(28)[147] 858(11)[140] 857(41)[35] 856(<1)[18]	819(10) 810(17) 803(7)				$\nu_{as}(XeO_3)$
764(100)	788(4)[53]	836(51)[4]	789[50](<1) 788[37](<1)	816(200)[<1] 816(16)[18]	761(100)				$\nu_s(XeO_3)$
			788(<1)[40] 771(14)[43] 765(478)[2] 698(<1)[40] 695(1)[39] 694(1)[31] 655(9)[<1] 655(9)[<1] 655(7)[<1] 566(4)[25] 561(6)[17] 561(5)[24] 531(<1)[4] 529(<1)[4] 525(<1)[4] 496(3)[14] 483(3)[12] 483(3)[11] 425(<1)[<1] 425(<1)[<1] 425(<1)[<1]	797(1)[39] 791(<1)[54] 791(2)[21] 693(1)[76] 692(<1)[53] 692(1)[23] 630(4)[<1] 621(13)[<1] 621(2)[<1] 562(1)[7] 558(3)[5] 558(1)[13] 550(2)[<1] 537(1)[4] 537(1)[<1] 486(1)[5] 486(1)[14] 483(<1)[11] 423(1)[1] 423(<1)[<1] 423(<1)[<1]	642(4) 639(4) 551(<1) 547(1) 519(1) 514(<1) 464(1)	683(4) 637(35) 544(21) 468(12) 463(10) 417(2)	784(<1)[49] 695(<1)[36] 612(6)[36] 547(6)[5] 527(<1)[9] 484(1)[7] 427(<1)[<1]	780(<1)[51] 693(<1)[34] 651(6)[<1] 555(7)[6] 524(<1)[8] 483(1)[6] 428(<1)[<1]	B_1, ϕ(ring vib.) B_1, γ(CH) B_2, α(ring vib.) A_1, α(ring vib.) B_2, β(NO)
351(1) 323(3)	308(33)[3]	322(3)[34]	348(3)[22] 341(2)[70]	352(<1)[41] 351(3)[20]	350(4)				$\delta_{umb}(XeO_3)$

Table 3.12. continued…

exptl	calcd				exptl		calcd		vibrational
$XeO_{3(aq)}$[a]	XeO_3 (C_{3v})		$(C_5H_5NO)_3(XeO_3)_2$		$(C_5H_5NO)_3(XeO_3)_2$[d]	C_5H_5NO[d]	C_5H_5NO		assignments[e]
	B3LYP[b]	*APFD*[c]	*B3LYP*[b]	*APFD*[c]			*APFD*[c]	*B3LYP*[b]	
			310(6)[31]	335(8)[125]					
311(42) 297(11)	271(9)[5]	284(4)[10]	305(4)[12] 304(3)[37] 295(2)[9] 266(1)[29]	323(2)[1] 322(2)[42] 305(4)[28] 304(3)[<1]	314(6) 271(2)				$\delta_{as}(XeO_3)$
146(5) 110(10) 99(16)			259(<1)[19] 245(1)[21] 180(5)[1] 155(1)[55] 144(2)[11] 134(2)[7] 127(10)[31] 123(9)[21] 113(5)[4] 105(5)[1] 94(5)[<1] 81(1)[6] 70(2)[7] 65(3)[5] 62(1)[6] 50(3)[1] 47(2)[1] 40(2)[1] 35(3)[<1] 29(2)[<1] 27(2)[<1] 25(6)[<1] 17(6)[<1] 12(3)[3] 11(2)[3] 10(1)[3]	292(2)[25] 291(1)[61] 191(16)[12] 166(1)[20] 165(4)[15] 165(6)[6] 160(3)[1] 138(1)[<1] 122(4)[3] 110(3)[<1] 103(1)[2] 101(6)[<1] 89(5)[<1] 87(1)[2] 74(<1)[1] 71(4)[<1] 65(1)[<1] 63(4)[5] 59(3)[7] 38(2)[<1] 36(1)[2] 35(<1)[2] 32(4)[<1] 25(2)[<1] 16(1)[1] 12(<1)[<1]	154(13) 137(16) 119(<1) 114(18) 84(4)	244(1)	210(<1)[3]	210(<1)[4]	deformation modes / lattice modes

[a] The spectrum was recorded in a ¼-in. diameter FEP sample tube at −140 °C. Values in parentheses are relative Raman intensities. Abbreviations denote shoulder (sh) and broad (br). [b] The B3LYP/Def2–TZVP level of theory was used. [c] The APFD/Def2–TZVP level of theory was used. Values in parentheses and square brackets are calculated Raman intensities (Å amu^{-1}) and infrared intensities (km mol^{-1}), respectively. [d] The spectrum was recorded in an aluminum sample holder at 22 °C. Values in parentheses are relative Raman intensities. [e] Symbols denote stretch (ν), bend (δ), umbrella (umb), symmetric (s), asymmetric (as), out-of-plane deformation (γ), in-plane deformation (β), in-plan ring deformation (α), and non-planar ring de-formation (ϕ).

Table 3.13. Raman and calculated vibrational frequencies (cm^{-1}); and assignments for $[(C_6H_5)_3PO]_2XeO_3$ (**4**), $[(C_6H_5)_2POCH_2]_2XeO_3{\cdot}NCCH_3$ (**5**), $XeO_{3(aq)}$, and $(C_6H_5)_3PO$.

exptl	calcd		exptl		calcd	vibrational
$XeO_{3(aq)}$[a]	XeO_3 *B3LYP*[b]	$[(C_6H_5)_3PO]_2XeO_3$ *B3LYP*[b]	$[(C_6H_5)_3PO]_2XeO_3$ [c]	$[(C_6H_5)_2POCH_2]_2XeO_3{\cdot}NCCH_3$	$(C_6H_5)_3PO$ *B3LYP*[b]	assignments[d]
		3204(205)[19]				ν(CH), combination bands, and overtones
		3204(268)[15]				
		3201(233)[12]				
		3199(328)[13]				
		3197(311)[19]				
		3196(325)[21]				
		3195(137)[10]				
		3195(46)[15]			3047(588)[14]	
		3194(198)[9]			3046(147)[25]	
		3194(171)[9]			3045(346)[20]	
		3192(110)[14]	3178(3)		3044(33)[9]	
		3190(19)[9]	3175(<1)	3180(4)	3040(90)[2]	
		3188(75)[9]	3172(1)	3147(4)	3038(13)[17]	
		3187(49)[11]	3143(4)	3058(75)	3036(82)[4]	
		3186(73)[14]	3058(127)	3011(6)	3031(54)[4]	
		3186(81)[15]	3026(<1)	29905)	3031(57)[14]	
		3182(76)[2]	3012(<1)	2961(5)	3026(127)[16]	
		3182(64)[1]	3007(2)	2932(12)	3023(136)[2]	
		3179(123)[6]	2991(3)	2901(20)	3022(120)[4]	
		3179(111)[9]	2960(4)		3016(55)[<1]	
		3177(103)[4]			3015(32)[<1]	
		3176(104)[4]			3014(17)[1]	
		3175(135)[18]				
		3172(144)[17]				
		3169(41)[<1]				
		3169(43)[<1]				
		3168(39)[<1]				
		3168(38)[<1]				
		3168(30)[2]				
		3168(51)[9]				

Table 3.13. continued…

exptl	calcd		exptl		calcd	
$XeO_{3(aq)}$[a]	XeO_3 *B3LYP*[b]	$[(C_6H_5)_3PO]_2XeO_3$ *B3LYP*[b]	$[(C_6H_5)_3PO]_2XeO_3$ [c]	$[(C_6H_5)_2POCH_2]_2XeO_3{\cdot}NCCH_3$	$(C_6H_5)_3PO$ *B3LYP*[b]	Vibrational Assignments[d]
		1634(22)[4] 1634(47)[1] 1634(31)[<1] 1634(28)[8] 1634(18)[3] 1633(39)[1] 1618(7)[<1] 1617(4)[1] 1617(9)[1] 1616(11)[<1] 1616(9)[1] 1616(8)[1]	1591(45) 1572(7)	1590(53) 1573(14)	1627(43)[2] 1625(38)[1] 1625(53)[1] 1618(11)[1] 1617(8)[<1] 1614(10)[<1]	ν(Ring)$_{ip}$ + δ(CH)
		1527(<1)[3] 1527(<1)[5] 1524(<1)[3] 1524(1)[2] 1522(<1)[3] 1521(1)[3]			1536(<1)[5] 1535(<1)[5] 1531(<1)[5]	
		1474(<1)[9] 1474(1)[61] 1472(2)[8] 1472(1)[14] 1471(2)[13] 1471(1)[13]	1489(<1) 1485(1) 1437(4)	1435(3) 1410(4)	1485(1)[25] 1482(1)[9] 1481(1)[14]	δ(CH)
		1370(2)[2] 1370(2)[2] 1366(1)[3] 1364(1)[3] 1359(2)[1] 1358(2)[2]			1384(2)[6] 1382(2)[5] 1371(<1)[4]	
		1319(<1)[2] 1319(<1)[2] 1318(1)[2] 1317(1)[3] 1316(<1)[3] 1315(<1)[3]	1338(1) 1318(<1) 1314(2)	1291(3)	1324(1)[2] 1321(<1)[1] 1314(<1)[1]	ν(Ring)$_{ip}$ + δ(CH)

Table 3.13. continued…

exptl	calcd		exptl		calcd	
$XeO_{3(aq)}$[a]	XeO_3 *B3LYP*[b]	$[(C_6H_5)_3PO]_2XeO_3$ *B3LYP*[b]	$[(C_6H_5)_3PO]_2XeO_3$ [c]	$[(C_6H_5)_2POCH_2]_2XeO_3{\cdot}NCCH_3$	$(C_6H_5)_3PO$ *B3LYP*[b]	vibrational assignments[d]
		1219(3)[3] 1219(5)[5] 1216(4)[4] 1214(5)[2] 1211(6)[8] 1210(4)[3]	1280(1)		1231(3)[2] 1228(3)[9] 1220(4)[9] 1202(5)[<1] 1202(4)[<1] 1201(1)[<1]	
		1195(150)[98]	1186(10)	1186(16) 1161(17)		δ(CH)
		1188(5)[1] 1188(2)[1] 1188(2)[1] 1187(3)[2] 1187(2)[<1] 1187(5)[3]				
		1182(27)[576]	1155(27)	1148(9)		ν(PO)
		1132(6)[80] 1131(6)[78] 1130(7)[84] 1129(7)[60] 1112(8)[3] 1111(5)[11] 1108(1)[2] 1107(1)[1] 1106(3)[16] 1105(3)[26] 1103(1)[9] 1102(1)[13]	1120(2) 1117(<1) 1105(<1)	1104(6)	1131(7)[56] 1129(7)[66] 1122(21)[12] 1113(9)[5] 1110(<1)[1] 1101(<1)[6]	ν(PC)

Table 3.13. continued…

exptl	calcd		exptl		calcd	
$XeO_{3(aq)}$[a]	XeO_3 *B3LYP*[b]	$[(C_6H_5)_3PO]_2XeO_3$ *B3LYP*[b]	$[(C_6H_5)_3PO]_2XeO_3$[c]	$[(C_6H_5)_2POCH_2]_2XeO_3{\cdot}NCCH_3$	$(C_6H_5)_3PO$ *B3LYP*[b]	**vibrational assignments**[d]
		1052(5)[1] 1052(5)[2] 1051(4)[2] 1050(79)[1] 1050(5)[8] 1020(113)[1] 1020(79)[2] 1019(6)[5] 1019(24)[1] 1018(62)[1] 1018(14)[4] 1008(1)[1] 1008(3)[<1] 1007(7)[2] 999(1)[1] 998(1)[<1] 997(1)[<1] 985(<1)[<1] 984(<1)[<1] 982(<1)[<1] 981(<1)[<1] 980(<1)[<1] 978(<1)[<1]	1088(5) 1071(2) 1028(31) 998(100)	1073(2) 1028(32) 997(100)	1062(<1)[<1] 1057(2)[<1] 1051(4)[<1] 1050(3)[1] 1049(39)[<1] 1044(<1)[<1] 1038(2)[<1] 1034(<1)[<1] 1029(<1)[<1] 1017(69)[2] 1012(67)[2] 1011(19)[2] 1009(21)[<1] 1002(6)[<1] 996(<1)[1]	$\nu(C_6H_5)_{ip}$
		953(<1)[<1] 953(1)[1] 950(1)[<1] 948(1)[<1] 948(1)[<1] 947(1)[<1] 875(<1)[<1] 875(<1)[1] 870(1)[<1] 869(<1)[<1] 868(<1)[<1] 868(<1)[<1]	929(2) 860(1)	926(2) 882(2)	941(<1)[<1] 934(<1)[<1] 929(<1)[<1] 836(<1)[53]	$\delta(CH)_{oop}$–$\delta(CH)_{oop}$
857(8) 819(26) 809(63)	855(92)[11]	835(23)[198] 828(20)[130]	831(19)	826(20) 788(11)		$\nu_{as}(XeO_3)$

Table 3.13. continued…

exptl	calcd		exptl		calcd	
$XeO_{3(aq)}$[a]	**XeO_3** *B3LYP*[b]	**$[(C_6H_5)_3PO]_2XeO_3$** *B3LYP*[b]	**$[(C_6H_5)_3PO]_2XeO_3$** [c]	**$[(C_6H_5)_2POCH_2]_2XeO_3{\cdot}NCCH_3$**	**$(C_6H_5)_3PO$** *B3LYP*[b]	**vibrational assignments**[d]
764(100) 754, sh	788(4)[53]	785(113)[15]	776(100)	772(63)		$\nu_{sym}(XeO_3)$
		774(<1)[3] 774(<1)[4] 773(<1)[7] 772(<1)[8] 764(<1)[12] 764(<1)[24] 733(3)[90] 732(2)[60] 731(3)[107] 731(1)[27] 715(<1)[25] 714(<1)[31] 712(<1)[38] 711(<1)[19] 711(<1)[50] 710(<1)[25] 699(23)[1] 697(19)[1] 634(5)[<1] 634(4)[<1] 633(4)[1] 633(6)[1] 632(4)[<1] 632(6)[<1] 557(1)[166] 556(<1)[212] 554(<1)[47] 554(1)[42] 511(1)[9] 509(1)[8]	727(<1) 697(1) 684(28) 616(20) 545(1) 509(2) 401(<1)	691(31) 616(27) 554(2) 499(2)	831(<1)[26] 829(<1)[48] 746(2)[91] 744(2)[53] 730(1)[<1] 728(<1)[10]7 23(1)[8] 706(7)[8] 640(6)[1] 637(4)[<1] 635(4)[<1] 569(1)[116] 560(<1)[98] 553(19)[81]	$\delta(CH)_{oop} + \delta(CH)_{oop}$ $\delta(CH)_{ip} + \delta(CH)_{oop}$ $\delta_{umb}(PC_3)$

Table 3.13. continued…

exptl	calcd		exptl		calcd	
$XeO_{3(aq)}$[a]	XeO_3 *B3LYP*[b]	$[(CH_3)_2PO]_2XeO_3$ *B3LYP*[b]	$[(CH_3)_2PO]_2XeO_3$ [c]	$[(C_6H_5)_2POCH_2]_2XeO_3{\cdot}NCCH_3$	$(C_6H_5)_3PO$ *B3LYP*[b]	vibrational assignments[d]
		468(<1)[19] 467(<1)[11] 457(<1)[18] 456(<1)[14] 414(2)[3] 410(1)[2] 410(<1)[2] 409(<1)[<1] 408(<1)[<1] 407(<1)[<1] 407(<1)[<1] 405(<1)[<1]	395(4) 352(<1)	378(4)	499(10)[14] 484(2)[4] 465(1)[13] 436(<1)[<1] 426(<1)[<1] 424(<1)[<1] 379(7)[4]	$\delta(CC)_{oop} + \delta(CH)_{oop}$
351(1) 323(3)	308(33)[3]	341(3)[39]	345(3)	303(20)		$\delta_{umb}(XeO_3)$
			322(<1)		308(2)[2]	
311(42) 297(11)	271(9)[5]	312(1)[11] 308(1)[7] 301(2)[3] 296(3)[2] 295(4)[18] 290(7)[27]	307(11) 289(5)	269(10)		$\delta_{as}(XeO_3)$

Table 3.13. continued…

exptl	calcd		exptl		calcd	
$XeO_{3(aq)}$[a]	XeO_3 *B3LYP*[b]	$[(CH_3)_3PO]_2XeO_3$ *B3LYP*[b]	$[(CH_3)_3PO]_2XeO_3$ [c]	$[(C_6H_5)_2POCH_3]_2XeO_3$□$NCCH_3$	$(C_6H_5)_3PO$ *B3LYP*[b]	vibrational assignments[d]
146(5) 110(10) 99(16)		256(1)[2] 252(1)[2] 250(5)[2] 249(5)[2] 246(6)[1] 244(4)[1] 196(2)[7] 187(2)[4] 180(1)[<1] 179(1)[<1] 175(2)[7] 168(2)[5] 136(1)[22] 108(2)[5] 87(5)[2] 84(4)[1] 71(1)[1] 66(2)[<1] 62(1)[2] 57(4)[1] 56(4)[<1] 54(3)[<1] 53(3)[<1] 46(8)[<1] 44(4)[1] 40(5)[<1] 38(7)[1] 37(4)[<1] 33(2)[<1] 28(5)[<1] 27(1)[<1] 23(4)[<1] 15(2)[<1] 13(<1)[1] 8(<1)[<1] 3(<1)[<1]	270(2) 253(23) 201(7) 193(1) 168(3) 115(18) 84(168)	246(14) 225(9) 101(73)	296(1)[5] 273(1)[1] 258(5)[<1] 246(8)[<1] 222(1)[2] 208(2)[<1] 196(2)[<1] 120(5)[<1] 92(6)[<1] 82(6)[<1] 81(4)[<1] 70(5)[<1] 64(8)[<1]	deformation modes / lattice modes

[a] The spectrum was recorded in a ¼-in. diameter FEP sample tube at −140 °C. Values in parentheses are relative Raman intensities. Abbreviations denote shoulder (sh) and broad (br). [b] The B3LYP/Def2–TZVP level of theory was used. Values in parentheses and square brackets are calculated Raman intensities (Å amu^{-1}) and infrared intensities (km mol^{-1}), respectively. [c] The spectrum was recorded in an aluminum sample holder at 22 °C. Values in parentheses are relative Raman intensities. [d] Symbols denote stretch (ν), bend (δ), rock (ρ_r), twist (ρ_t), wag (ρ_ω), umbrella (umb), symmetric (s), and asymmetric (as).

Table 3.14. Natural population analysis (NPA) charges, Wiberg valencies, and Wiberg bond indices for XeO_3, $(CH_3)_2CO$, and $[(CH_3)_2CO)_3]XeO_3$.

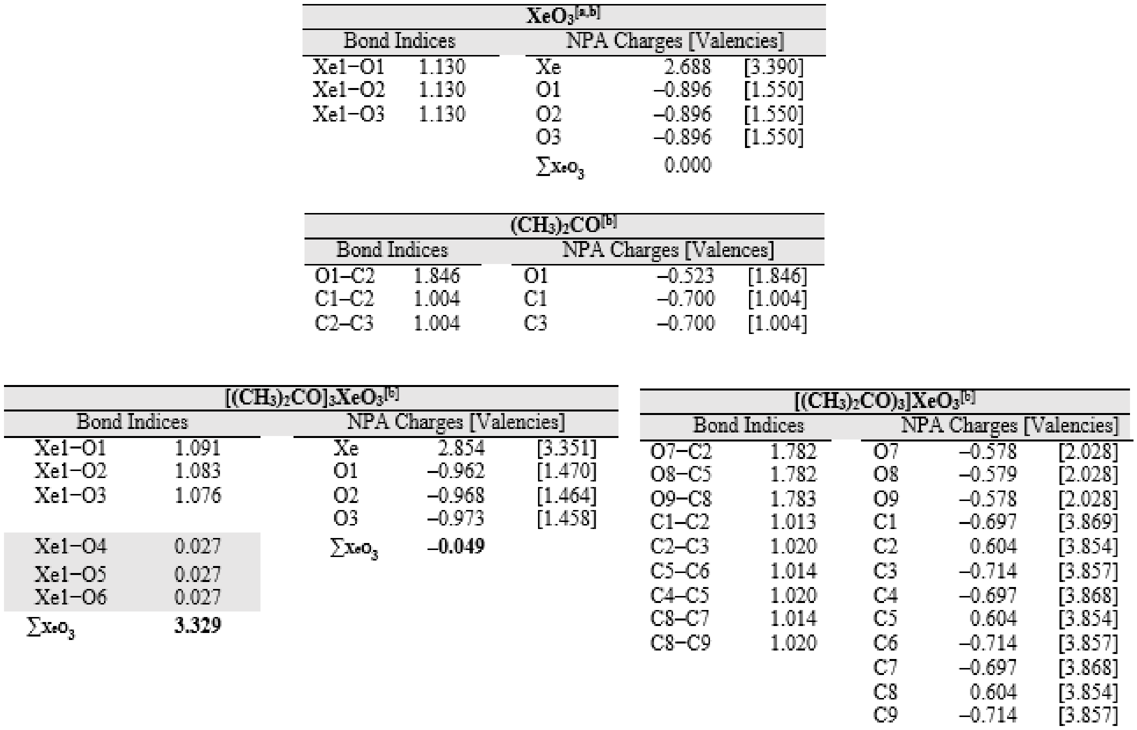

XeO_3[a,b]

Bond Indices		NPA Charges [Valencies]		
Xe1−O1	1.130	Xe	2.688	[3.390]
Xe1−O2	1.130	O1	−0.896	[1.550]
Xe1−O3	1.130	O2	−0.896	[1.550]
		O3	−0.896	[1.550]
		$\sum_{XeO_3}$	0.000	

$(CH_3)_2CO$[b]

Bond Indices		NPA Charges [Valences]		
O1–C2	1.846	O1	−0.523	[1.846]
C1–C2	1.004	C1	−0.700	[1.004]
C2–C3	1.004	C3	−0.700	[1.004]

$[(CH_3)_2CO]_3XeO_3$[b]

Bond Indices		NPA Charges [Valencies]		
Xe1−O1	1.091	Xe	2.854	[3.351]
Xe1−O2	1.083	O1	−0.962	[1.470]
Xe1−O3	1.076	O2	−0.968	[1.464]
		O3	−0.973	[1.458]
Xe1−O4	0.027	$\sum_{XeO_3}$	**−0.049**	
Xe1−O5	0.027			
Xe1−O6	0.027			
$\sum_{XeO_3}$	**3.329**			

$[(CH_3)_2CO)_3]XeO_3$[b]

Bond Indices		NPA Charges [Valencies]		
O7−C2	1.782	O7	−0.578	[2.028]
O8−C5	1.782	O8	−0.579	[2.028]
O9−C8	1.783	O9	−0.578	[2.028]
C1−C2	1.013	C1	−0.697	[3.869]
C2−C3	1.020	C2	0.604	[3.854]
C5−C6	1.014	C3	−0.714	[3.857]
C4−C5	1.020	C4	−0.697	[3.868]
C8−C7	1.014	C5	0.604	[3.854]
C8−C9	1.020	C6	−0.714	[3.857]
		C7	−0.697	[3.868]
		C8	0.604	[3.854]
		C9	−0.714	[3.857]

[a] The calculated geometric parameters for XeO_3: Xe−O, 1.779 Å; ∠O−Xe−O, 106.80°.
[b] The B3LYP/Def2–TZVP level of theory was used.

Table 3.15. Natural population analysis (NPA) charges, Wiberg valencies, and Wiberg bond indices for XeO_3, $(CH_3)_2SO$, and $[(CH_3)_2SO)_3]_3(XeO_3)_2$.

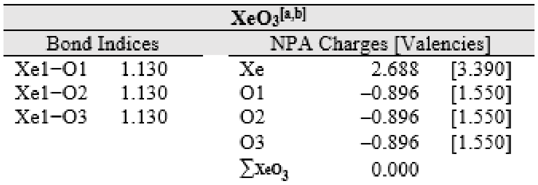

XeO_3[a,b]

Bond Indices		NPA Charges [Valencies]		
Xe1−O1	1.130	Xe	2.688	[3.390]
Xe1−O2	1.130	O1	−0.896	[1.550]
Xe1−O3	1.130	O2	−0.896	[1.550]
		O3	−0.896	[1.550]
		$\sum_{XeO_3}$	0.000	

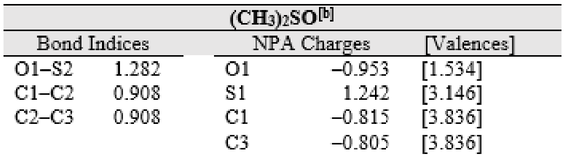

$(CH_3)_2SO$[b]

Bond Indices		NPA Charges		[Valences]
O1–S2	1.282	O1	–0.953	[1.534]
C1–C2	0.908	S1	1.242	[3.146]
C2–C3	0.908	C1	–0.815	[3.836]
		C3	–0.805	[3.836]

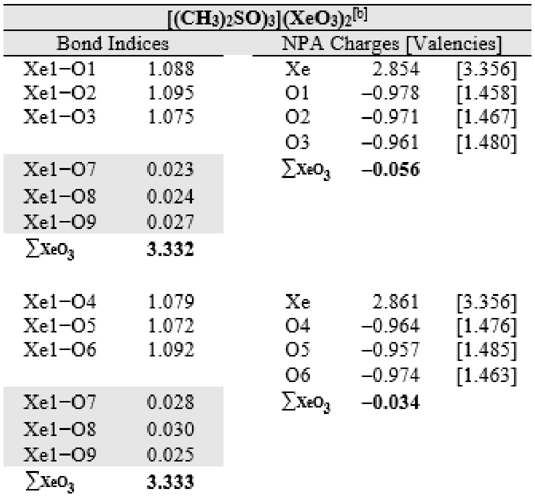

$[(CH_3)_2SO)_3](XeO_3)_2$[b]

Bond Indices		NPA Charges [Valencies]		
Xe1−O1	1.088	Xe	2.854	[3.356]
Xe1−O2	1.095	O1	−0.978	[1.458]
Xe1−O3	1.075	O2	−0.971	[1.467]
		O3	−0.961	[1.480]
Xe1−O7	0.023	$\sum_{XeO_3}$	**−0.056**	
Xe1−O8	0.024			
Xe1−O9	0.027			
$\sum_{XeO_3}$	**3.332**			
Xe1−O4	1.079	Xe	2.861	[3.356]
Xe1−O5	1.072	O4	−0.964	[1.476]
Xe1−O6	1.092	O5	−0.957	[1.485]
		O6	−0.974	[1.463]
Xe1−O7	0.028	$\sum_{XeO_3}$	**−0.034**	
Xe1−O8	0.030			
Xe1−O9	0.025			
$\sum_{XeO_3}$	**3.333**			

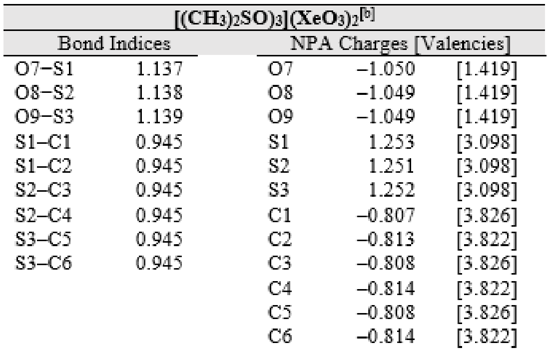

$[(CH_3)_2SO)_3](XeO_3)_2$[b]

Bond Indices		NPA Charges [Valencies]		
O7−S1	1.137	O7	−1.050	[1.419]
O8−S2	1.138	O8	−1.049	[1.419]
O9−S3	1.139	O9	−1.049	[1.419]
S1−C1	0.945	S1	1.253	[3.098]
S1−C2	0.945	S2	1.251	[3.098]
S2−C3	0.945	S3	1.252	[3.098]
S2−C4	0.945	C1	−0.807	[3.826]
S3−C5	0.945	C2	−0.813	[3.822]
S3−C6	0.945	C3	−0.808	[3.826]
		C4	−0.814	[3.822]
		C5	−0.808	[3.826]
		C6	−0.814	[3.822]

[a] The calculated geometric parameters for XeO_3: Xe−O, 1.779 Å; ∠O−Xe−O, 106.80°.
[b] The B3LYP/Def2–TZVP level of theory was used.

Table 3.16. Natural population analysis (NPA) charges, Wiberg valencies, and Wiberg bond indices for XeO_3, $(CH_3)_2SO$, and $[(CH_3)_2SO)_3]_3(XeO_3)_2$.

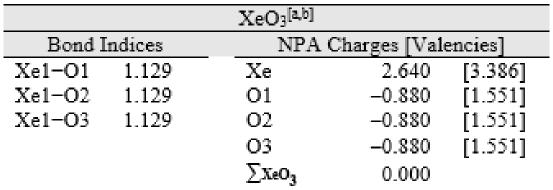

XeO_3[a,b]				
Bond Indices		NPA Charges [Valencies]		
Xe1−O1	1.129	Xe	2.640	[3.386]
Xe1−O2	1.129	O1	−0.880	[1.551]
Xe1−O3	1.129	O2	−0.880	[1.551]
		O3	−0.880	[1.551]
		$\sum_{XeO_3}$	0.000	

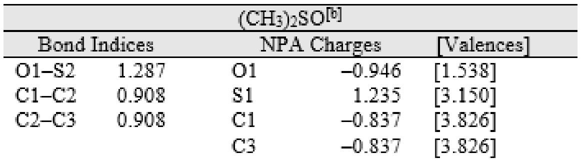

$(CH_3)_2SO$[b]				
Bond Indices		NPA Charges		[Valences]
O1–S2	1.287	O1	−0.946	[1.538]
C1–C2	0.908	S1	1.235	[3.150]
C2–C3	0.908	C1	−0.837	[3.826]
		C3	−0.837	[3.826]

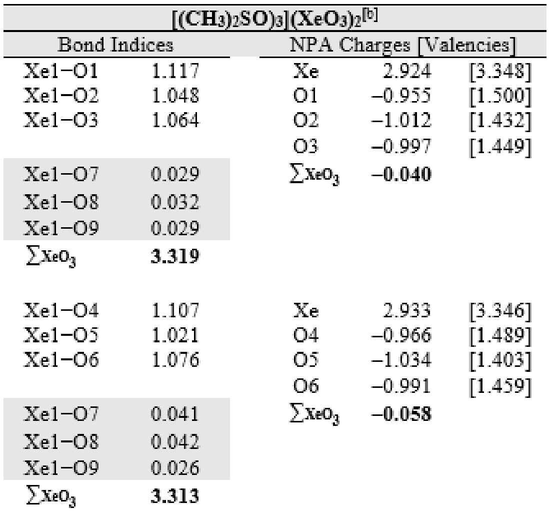

$[(CH_3)_2SO)_3](XeO_3)_2$[b]				
Bond Indices		NPA Charges [Valencies]		
Xe1−O1	1.117	Xe	2.924	[3.348]
Xe1−O2	1.048	O1	−0.955	[1.500]
Xe1−O3	1.064	O2	−1.012	[1.432]
		O3	−0.997	[1.449]
Xe1−O7	0.029	$\sum_{XeO_3}$	**−0.040**	
Xe1−O8	0.032			
Xe1−O9	0.029			
$\sum_{XeO_3}$	**3.319**			
Xe1−O4	1.107	Xe	2.933	[3.346]
Xe1−O5	1.021	O4	−0.966	[1.489]
Xe1−O6	1.076	O5	−1.034	[1.403]
		O6	−0.991	[1.459]
Xe1−O7	0.041	$\sum_{XeO_3}$	**−0.058**	
Xe1−O8	0.042			
Xe1−O9	0.026			
$\sum_{XeO_3}$	**3.313**			

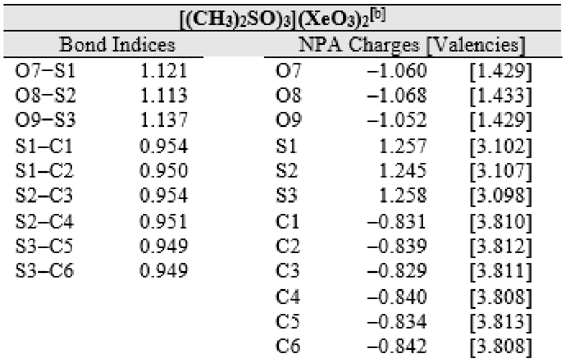

$[(CH_3)_2SO)_3](XeO_3)_2$[b]				
Bond Indices		NPA Charges [Valencies]		
O7−S1	1.121	O7	−1.060	[1.429]
O8−S2	1.113	O8	−1.068	[1.433]
O9−S3	1.137	O9	−1.052	[1.429]
S1−C1	0.954	S1	1.257	[3.102]
S1−C2	0.950	S2	1.245	[3.107]
S2−C3	0.954	S3	1.258	[3.098]
S2−C4	0.951	C1	−0.831	[3.810]
S3−C5	0.949	C2	−0.839	[3.812]
S3−C6	0.949	C3	−0.829	[3.811]
		C4	−0.840	[3.808]
		C5	−0.834	[3.813]
		C6	−0.842	[3.808]

[a] The calculated geometric parameters for XeO_3: Xe−O, 1.754 Å; ∠O−Xe−O, 107.18°.
[b] The APFD/Def2–TZVP level of theory was used.

Table 3.17. Natural population analysis (NPA) charges, Wiberg valencies, and Wiberg bond indices for XeO_3, C_5H_5NO, and $(C_5H_5NO)_3(XeO_3)_2$.

XeO_3[a,b]				
Bond Indices		NPA Charges [Valencies]		
Xe1−O1	1.129	Xe	2.640	[3.386]
Xe1−O2	1.129	O1	−0.880	[1.551]
Xe1−O3	1.129	O2	−0.880	[1.551]
		O3	−0.880	[1.551]
		$\sum_{XeO_3}$	0.000	

C_5H_5NO[b]				
Bond Indices		NPA Charges		[Valences]
O1–N1	1.299	O1	−0.500	[1.799]
N1–C1	1.201	N1	0.105	[3.809]
C1–C2	1.484	C1	−0.044	[3.923]
C2–C3	1.416	C2	−0.218	[3.961]
C3–C4	1.416	C3	−0.231	[3.963]
C4–C5	1.484	C4	−0.218	[3.961]
C5–N1	1.201	C5	−0.044	[3.923]

$(C_5H_5NO)_3(XeO_3)_2$[b]				
Bond Indices		NPA Charges [Valencies]		
Xe1−O1	1.050	Xe1	2.844	[3.402]
Xe1−O2	1.109	O1	−0.989	[1.439]
Xe1−O3	1.078	O2	−0.955	[1.507]
		O3	−0.979	[1.473]
Xe1−O4	0.076	$\sum_{XeO_3}$	**−0.056**	
Xe1−O5	0.049			
$\sum_{XeO_3}$	**3.332**			

$(C_5H_5NO)_3(XeO_3)_2$[b]				
Bond Indices		NPA Charges [Valencies]		
O4−N1	1.188	O4	−0.603	[1.685]
O5−N2	1.159	O5	−0.645	[1.651]
N1−C1	1.232	N1	0.075	[3.782]
C1–C2	1.464	C1	0.020	[3.909]
C2–C3	1.427	C2	−0.222	[3.956]
C3–C4	1.424	C3	−0.185	[3.960]
C4–C5	1.467	C4	−0.226	[3.957]
C5–N1	1.230	C5	0.015	[3.914]
N2–C6	1.234	N2	0.066	[3.771]
C6–C7	1.458	C6	0.051	[3.900]
C7–C8	1.426	C7	−0.253	[3.771

[a] The calculated geometric parameters for XeO_3: Xe−O, 1.754 Å; ∠O−Xe−O, 107.18°.
[b] The APFD/Def2–TZVP level of theory was used.

Table 3.18. Natural population analysis (NPA) charges, Wiberg valencies, and Wiberg bond indices for XeO_3, $(C_6H_5)_3PO$, and $[(C_6H_5)_3PO]_2XeO_3$.

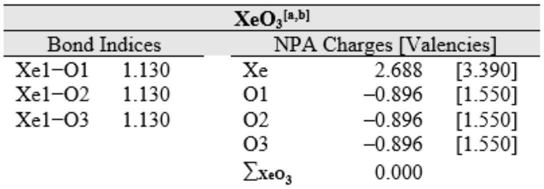

XeO_3[a,b]				
Bond Indices		NPA Charges [Valencies]		
Xe1−O1	1.130	Xe	2.688	[3.390]
Xe1−O2	1.130	O1	−0.896	[1.550]
Xe1−O3	1.130	O2	−0.896	[1.550]
		O3	−0.896	[1.550]
		$\sum_{XeO_3}$	0.000	

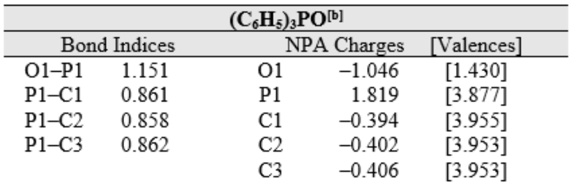

$(C_6H_5)_3PO$[b]				
Bond Indices		NPA Charges		[Valences]
O1–P1	1.151	O1	−1.046	[1.430]
P1–C1	0.861	P1	1.819	[3.877]
P1–C2	0.858	C1	−0.394	[3.955]
P1–C3	0.862	C2	−0.402	[3.953]
		C3	−0.406	[3.953]

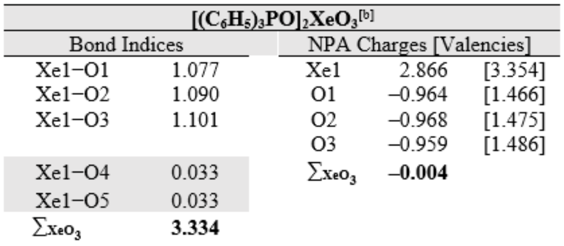

$[(C_6H_5)_3PO]_2XeO_3$[b]				
Bond Indices		NPA Charges [Valencies]		
Xe1−O1	1.077	Xe1	2.866	[3.354]
Xe1−O2	1.090	O1	−0.964	[1.466]
Xe1−O3	1.101	O2	−0.968	[1.475]
		O3	−0.959	[1.486]
Xe1−O4	0.033	$\sum_{XeO_3}$	**−0.004**	
Xe1−O5	0.033			
$\sum_{XeO_3}$	**3.334**			

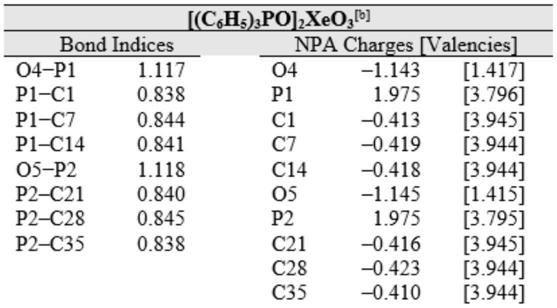

$[(C_6H_5)_3PO]_2XeO_3$[b]				
Bond Indices		NPA Charges [Valencies]		
O4−P1	1.117	O4	−1.143	[1.417]
P1−C1	0.838	P1	1.975	[3.796]
P1−C7	0.844	C1	−0.413	[3.945]
P1−C14	0.841	C7	−0.419	[3.944]
O5−P2	1.118	C14	−0.418	[3.944]
P2−C21	0.840	O5	−1.145	[1.415]
P2−C28	0.845	P2	1.975	[3.795]
P2−C35	0.838	C21	−0.416	[3.945]
		C28	−0.423	[3.944]
		C35	−0.410	[3.944]

[a] The calculated geometric parameters for XeO_3: Xe−O, 1.779 Å; ∠O−Xe−O, 106.80°.
[b] The B3LYP/Def2–TZVP level of theory was used.

CHAPTER 4

A Stable Crown Ether Complex with a Noble-Gas Compound

K. M. Marczenko, H. P. A. Mercier, G. J. Schrobilgen, *Angew. Chem. Int. Ed. Eng.* **2018**, *57*, 12448–12452.

Abstract: *Crown ethers have been known for over 50 years, but no example of a complex between a noble-gas compound and a crown ether or another polydentate ligand had previously been reported. Xenon trioxide is shown to react with 15-crown-5 to form the kinetically stable* $(CH_2CH_2O)_5XeO_3$ *adduct, which, in marked contrast with solid* XeO_3*, does not detonate when mechanically shocked. The crystal structure shows that the five oxygen atoms of the crown ether are coordinated to the xenon atom of* XeO_3*. The gas-phase Wiberg bond valences and indices and the empirical bond valences indicate that the* $Xe{---}O_{crown}$ *bonds are predominantly electrostatic and are consistent with σ-hole bonding. Mappings of the electrostatic potential (EP) onto the Hirshfeld surfaces of* XeO_3 *and 15-crown-5 in* $(CH_2CH_2O)_5XeO_3$ *and a detailed examination of the molecular electrostatic potential surface (MEPS) of* XeO_3 *and* $(CH_2CH_2O)_5$ *reveal regions of negative EP on the oxygen atoms of* $(CH_2CH_2O)_5$ *and regions of high positive EP on the xenon atom, which are also in accordance with σ-hole interactions.*

4.1 Manuscript

The strong oxidant properties of noble-gas fluorides, oxide fluorides, and oxides render the syntheses of isolable organic noble-gas compounds particularly challenging. The Xe–N bonded XeF_6 adducts of the oxidatively resistant acetonitrile ligand, $F_6XeNCCH_3$ and $F_6Xe(NCCH_3)_2$, have been synthesized and structurally characterized at low temperatures, however both compounds are highly energetic and shock-sensitive.[1] Xenon trioxide, a potent oxidizer that rapidly oxidizes primary and secondary alcohols to CO_2 and H_2O in aqueous media,[2,3,4] has marginal kinetic stability in the solid state and readily detonates when subjected to slight thermal or mechanical shock, liberating Xe and O_2 gases and 402 ±8 kJ mol^{-1} of energy.[5] Unlike XeF_6, adduct formation between XeO_3 and a Lewis base can dramatically reduce the shock sensitivity of XeO_3, as illustrated by $O_3Xe(NCCH_3)_2$[6] and $(C_5H_5N)_3XeO_3$,[7] which are stable at room temperature and are shock insensitive. The XeO_3 molecules in the three known phases of solid XeO_3 are extensively cross-linked through intermolecular Xe---O contacts that have been ascribed to σ-hole bonding.[6,8] The Xe---O---Xe bridge networks contribute significantly to the kinetic instability of XeO_3 by providing an efficient means to propagate the detonation shock wave throughout the crystal lattice. The crystal structures of XeO_3 and the limited number of XeO_3 adducts that have been synthesized thus far display three secondary Xe---L (L = O, N, F) bonding interactions that are approximately trans to the polar-covalent Xe–O double bonds of XeO_3.[6,7,8] Prior to this work, no examples of xenon coordinated to polydentate ligands, such as crown ethers, had been reported.

Crown ethers, cyclic oligomers of ethylene oxide, have cavities whose sizes, shapes, and donor properties can accommodate a wide variety of guest species.[9,10] Applications of crown ethers and their complexes are extensive and have progressed beyond their initial use as metal cation complexing agents.[11] Although structural studies of crown ether complexes with main-group species are much less prevalent, main-group Lewis acids of the type PnX_3 (Pn = As, Sb, Bi and X = F, Cl, Br, I) have been shown to form complexes with crown ethers.[12,13,14] The X-ray crystal structures of the SbF_3 adducts of 18-crown-6[12] and 15-crown-5[13] have Sb---O secondary bonding interactions (2.824(3)−3.344(2) Å) that are significantly shorter than the sum of the antimony and oxygen van der Waals radii (3.97 Å).[15] The trajectories of these short contacts are approximately trans to the Sb–F covalent bonds and may also be understood in terms of the noncovalent, σ-hole bonding model.[16] Interactions between elemental xenon and crown ethers have been studied by solution ^{129}Xe NMR spectroscopy. 129-Xenon complexation shifts were observed in the presence of 12-crown-4 and 15-crown-5 that were indicative of very weak Xe-crown ether interactions,[17] however no isolable crown ether complexes of elemental xenon have been reported thus far.

Crown ethers are not oxidized by $KMnO_4$ and CrO_3,[18] indicating that these macrocycles are relatively robust in strongly oxidizing environments and may therefore be candidates for complex formation with XeO_3. The 15-crown-5 adduct of XeO_3 was synthesized at room temperature by reaction of 15-crown-5 with an HF-acidified aqueous solution of XeO_3. The adduct was also synthesized by addition of liquid 15-crown-5 to a solution of XeO_3 in acetone at room temperature. Remarkably, solid XeO_3 quiescently dissolves in acetone without detonation. In both instances, slow evaporation of the solvent in air gave colorless, block-shaped crystals of $(CH_2CH_2O)_5XeO_3$ that were suitable for a single-crystal X-ray structure determination. Crystalline $(CH_2CH_2O)_5XeO_3$ failed to detonate when mechanically shocked, but underwent rapid deflagration when ignited in a flame.

Raman spectra of $(CH_2CH_2O)_5XeO_3$ were recorded at intervals in air at 20 ^{o}C, over a period of several days, confirming the solid adduct is stable at room temperature and is insensitive to atmospheric moisture. Vibrational frequencies and assignments for $(CH_2CH_2O)_5XeO_3$ are listed in Table 4.2 and the Raman spectrum is depicted in Figure 4.3. The Raman assignments were aided by comparison with the calculated vibrational frequencies and intensities of the energy-minimized gas-phase geometry (Figure 4.1) and with previous assignments for aqueous XeO_3[8] and its adducts.[6,7,8] Complex formation is indicated by a shift of the most intense band to lower frequency (A_1, ν_{sym} exptl 772, calcd 832 cm^{-1}) relative to that of $XeO_{3(aq)}$. The remaining XeO_3 bands of the adduct (E, ν_{as} (853, 825, 811); A_1, δ_{umb} (356, 346); E, δ_{as} (317, 302) cm^{-1}) are similar to those observed for $XeO_{3(aq)}$.[8]

The X-ray crystal structure of $(CH_2CH_2O)_5XeO_3$ was determined at –173 ^{o}C (Figure 4.1). Details of the crystal data and refinement results are provided in Table 4.3. A summary of important geometrical parameters is given in Table 4.1 and a more complete list is provided in Table 4.4. The crystal structure of $(CH_2CH_2O)_5XeO_3$ ($P2_1/m$, $Z = 4$, $T = –173$ ^{o}C, $R_1 = 0.0196$), consists of well-isolated $(CH_2CH_2O)_5XeO_3$ structural units in which the XeO_3 molecule is coordinated to the five oxygen atoms of the 15-crown-5 molecule (Figure

4.1). The XeO_3 moieties of neighboring adduct molecules do not interact through Xe---O---Xe bridges (Figure 4.2), thereby substantially reducing the shock-sensitivity of coordinated XeO_3.[6,7,8] The primary Xe–O bond lengths and O–Xe–O bond angles lie within the bond length and bond angle ranges of the three solid phases of XeO_3 (1.7558(11)–1.7801(11) Å and 100.51(5)−105.09(6)°).[8] The $(CH_2CH_2O)_5XeO_3$ structural unit has three short Xe---O_{crown} contacts (2.895(1), 2.932(1), 2.970(1) Å) and two long Xe---O_{crown} contacts (3.114(1), 3.124(1) Å). The shorter Xe---O contacts are approximately trans to the primary polar-covalent Xe–O bonds, with O–Xe---O angles of 155.00(4), 159.86(4), and 176.63(4)°, whereas the longer Xe---O contacts have significantly smaller O–Xe---O angles (129.93(4), 134.79(4)°). The XeO_3 molecule (Figure 4.1a) is centered on and positioned 1.917 Å below the plane defined by the oxygen ligand atoms. The ring conformation of the 15-crown-5 ligand belongs to a global minimum and is similar to that observed in the 15-crown-5 adducts of PnX_3.[13,14]

The empirical bond valence method of I. D. Brown[19] was used to determine which Xe---O contacts are significant contributors to the total bond valence of Xe^{VI} in $(CH_2CH_2O_5)XeO_3$ (Table 4.1). Inclusion of the three shortest Xe---O contacts resulted in a Xe bond valence of 5.91 v.u. whereas inclusion of all five contacts gave a Xe bond valence of 6.01 v.u., in accordance with the ideal total bond valence of 6 for Xe^{VI}. Overall, the small Xe---O bond valences (0.048−0.089 v.u.) are consistent with very weak covalent bonding between O and Xe.

Table 4.1. Summary of important experimental bond lengths (Å) and bond angles (°) in $(CH_2CH_2O)_5XeO_3$ and their calculated bond valences, *S*, and Wiberg bond indices.

Xe−O			Xe---O		
Bond Lengths	*S* (v.u.)[a]	Wiberg Indices[b]	Bond Lengths	*S* (v.u.)[a]	Wiberg Indices[b]
			2.895(1)	0.089	0.019
1.763(1)	1.898	1.101	2.932(1)	0.081	0.015
1.763(1)	1.898	1.092	2.970(1)	0.073	0.013
1.767(1)	1.877	1.074	3.114(1)	0.049	0.009
			3.124(1)	0.048	0.006

O---Xe---O	*trans*- O---Xe–O	*cis*- O---Xe−O	O–Xe–O
54.03(2)	155.00(4)	70.93(4)	
54.19(3)	159.86(4)	72.37(4)	99.80(5)
54.22(2)	176.63(4)	75.91(4)	100.96(5)
56.40(2)	134.79(4)	78.98(4)	102.53(5)
58.23(3)	129.93(4)	79.11(4)	

[a] I. D. Brown, reference [19]. [b] APFD/Def2-TZVPD.

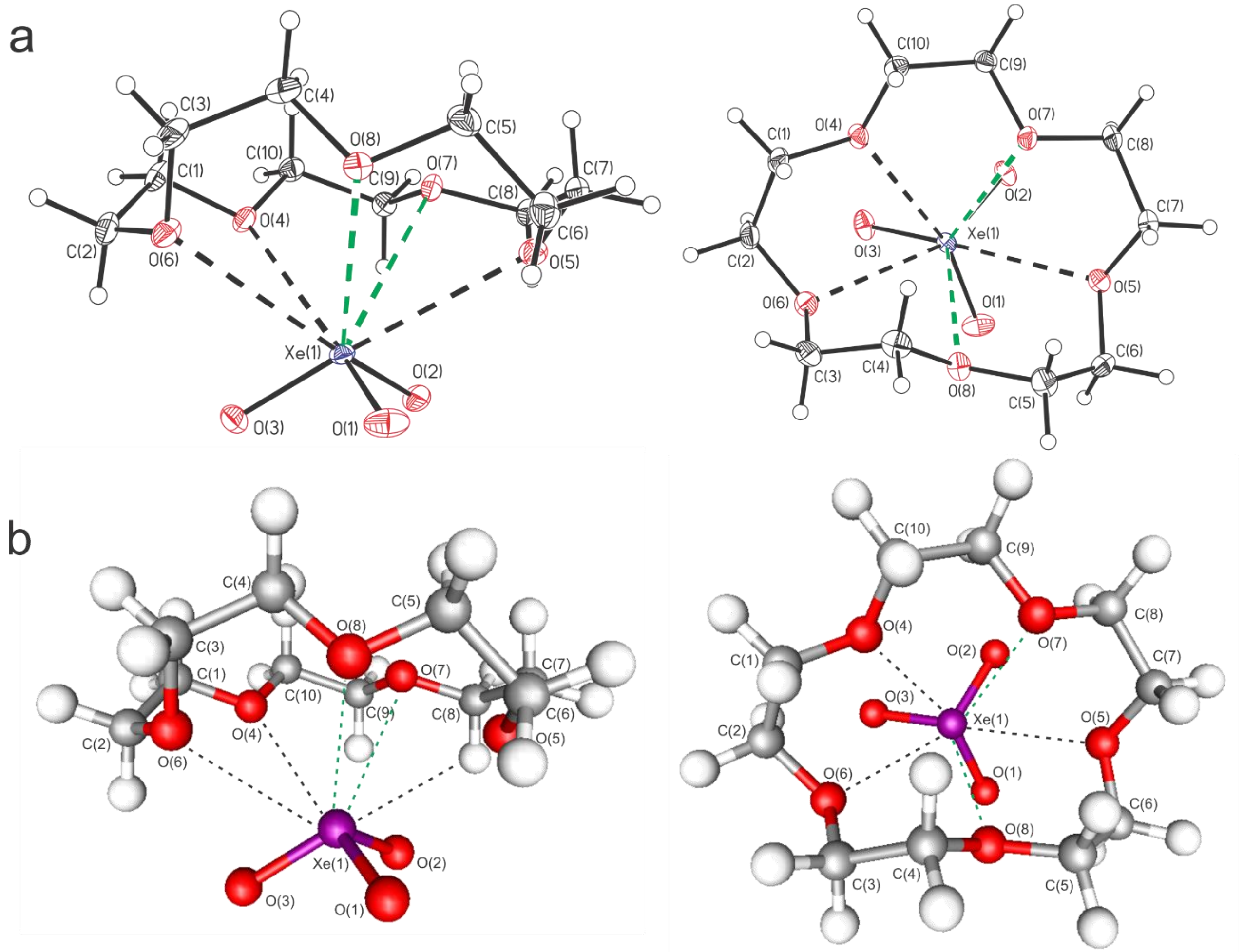

Figure 4.1. Side-on (left) and top-on (right) views of (**a**) the structural unit in the crystal structure of $(CH_2CH_2O)_5XeO_3$ and (**b**) the calculated gas-phase structure of $(CH_2CH_2O)_5XeO_3$. Thermal ellipsoids (**a**) are drawn at the 50% probability level. Gas-phase structure optimizations (**b**) were carried out at the APFD/Def2-TZVP level. The two longest Xe---O contacts are shown in green

Contributions from five Xe---O bonding interactions are also supported by analyses of the Hirshfeld surfaces of XeO_3 and 15-crown-5 in the crystal structure of $(CH_2CH_2O)_5XeO_3$, which provide clear visualizations of the Xe---O interactions. When the Hirshfeld surfaces of the 15-crown-5 ligand (Figure 4.2, left) and XeO_3 (Figure 4.5a) are mapped with the d_{norm} function,[20] five circular regions (denoted in red) are visible which correspond to contacts that are shorter than the sum of the Xe and O van der Waals radii (3.68 Å).[21] Regions of very low intensity also occur on the surfaces which arise from O---C(H) hydrogen bonding between neighboring $(CH_2CH_2O)_5XeO_3$ molecules in the crystal lattice. When the electrostatic potential (EP) is mapped onto the Hirshfeld surface of XeO_3 (Figure 4.2, right), corresponding regions of positive EP (blue) are visible on the surface of the electrophilic Xe atom. These regions are mirrored by regions of negative EP (red) on the Hirshfeld surface of the ligand (Figure 4.5b).

The energy-minimized geometry (Figure 4.1), with all frequencies real, was calculated for $(CH_2CH_2O)_5XeO_3$ (C_1 symmetry) using several basis sets and DFT functionals: APFD, APF, M062X, M052X, B3LYP, wB97XD (Table 4.5). Experimental Xe–O and Xe---O bond distances were compared with the calculated distances by use of least squares regression analyses (Table 4.6). Within the scope of this study, the APFD method provided the gas-phase structure that best agreed with the X-ray crystal structure (Xe–O: calcd, 1.762, 1.763, 1.767 Å; exptl, 1.767(1), 1.763(1), 1.763(1) Å). Three Xe---O bond distances (calcd, 2.909, 2.963, 3.074 Å; exptl, 2.932(1), 2.970(1), 3.124(1) Å) are slightly underestimated whereas the remaining two Xe---O bond distances (calcd, 2.962, 3.253 Å; exptl, 2.895(1), 3.114(1) Å) are slightly overestimated.

The molecular electrostatic potential surfaces (MEPS) of XeO_3 (Figure 4.2b) and $(CH_2CH_2O)_5XeO_3$ (Figure 4.6) were also examined. Upon adduct formation, the most negative EP regions of XeO_3, the oxygen atoms of the primary Xe–O bonds, become more negative, and the most positive EP regions of the ligand, the hydrophobic exterior, become more positive, in accordance with enhanced polarization of the primary Xe–O bonds (*vide infra*). Although regions of positive EP on the XeO_3 moiety of $(CH_2CH_2O)_5XeO_3$ are obscured within its MEPS (Figure 4.6a), the MEPS of XeO_3 shows three discrete regions of maximum positive EP (Figure 4.2b; 241 kJ mol^{-1}) that align with regions of high EP on the Hirshfeld surface of the xenon atom in XeO_3 (Figure 4.2a, right). These regions were visualized by examination of the top 20% of the MEPS and are located trans to the highly electronegative oxygen atoms of the primary Xe–O bonds, a characteristic of σ-hole bonding.[7,8,15] The center of the xenon atom is only ~17 kJ mol^{-1} lower in energy than the maximum EP of the σ-hole regions. The overall high positive EP of the xenon atom surface and constraints imposed by the ligand likely account for the greater number of secondary bonds observed in $(CH_2CH_2O)_5XeO_3$ than in the crystal structures of monodentate ligand adducts of XeO_3[6,8] and solid XeO_3.[8] Similar distinct regions of maximum EP are also observed for SbF_3 (Figure 4.6c) which forms Sb---O bonded adducts with 15-crown-5 and 18-crown-6.[12,13]

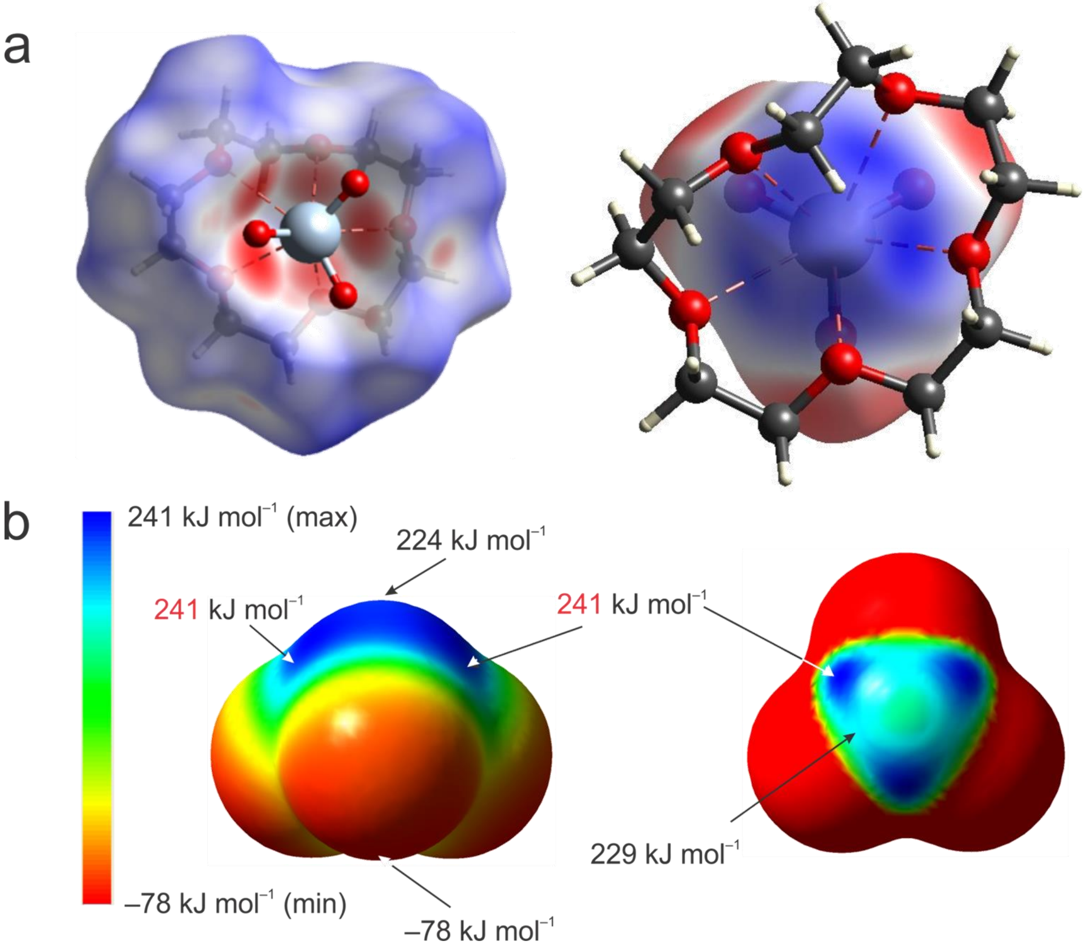

Figure 4.2. The **(a)** Hirshfeld surfaces in $(CH_2CH_2O)_5XeO_3$ mapped with the d_{norm} function[20] of 15-crown-5 (left) and the electrostatic potential surface (B88LYP/321-G) of XeO_3 (right).[22] The **(b)** molecular electrostatic potential surface (MEPS) of XeO_3 at the 0.001 e bohr^{-3} isosurface (right; APFD/Def2-TZVPD) and the top 20% of the positive electrostatic potential range (left; 193–241 kJ mol^{-1}).

The Xe–O and Xe---O Wiberg bond indices (Tables 4.1 and 4.7) are in accordance with the bond valences calculated by the empirical method of I. D. Brown.[19] The Wiberg bond indices of the primary Xe–O bonds decrease somewhat upon coordination of XeO_3 to 15-crown-5. The small Wiberg bond indices (0.006–0.019) of the Xe---O adduct bonds are consistent with very weak covalent bonding. The Wiberg valences of Xe (gas-phase, 3.379;

adduct, 3.350) and O_{XeO3} (gas-phase, av. 1.537; adduct, av. 1.476) also decrease somewhat upon coordination. The NPA charges of the Xe atom and O_{XeO3} atoms in $(CH_2CH_2O)_5XeO_3$ are significantly more positive and are somewhat more negative, respectively, than those of XeO_3 (Xe: gas-phase, 2.758, adduct, 2.898; O_{XeO3}: gas-phase, −0.920, adduct, av. −0.973). The changes in atomic charges (Table 4.7) and bond indices that accompany coordination are consistent with enhanced polar-covalent character of the primary Xe–O bonds of XeO_3 in the crown ether adduct, as also observed for the *N*-base adducts of XeO_3.[7,8] The experimental and gas-phase studies concur, showing that five weakly covalent (essentially electrostatic) Xe---O and three polar-covalent primary Xe–O bonding interactions occur in $(CH_2CH_2O)_5XeO_3$, which result in a total Xe coordination number of 8 and a Xe(VI) bond valence that is very close to 6.

An example of a stable crown ether complex of a group 18 compound, $(CH_2CH_2O)_5XeO_3$, has been synthesized and structurally characterized by Raman spectroscopy and single-crystal X-ray diffraction. Empirical bond valence calculations were used to determine the degree to which the Xe---O secondary bonding interactions contribute to the total bond valence of xenon. Hirshfeld surface analyses confirmed five secondary Xe---O bonding interactions. The complex exhibits the highest xenon coordination number observed thus far for XeO_3 and is presently the only example of XeO_3 coordinated to a polydentate ligand. The Xe---O_{crown} bonding interactions may be described as primarily electrostatic interactions between the nucleophilic O atoms of the crown ether and the electrophilic σ-holes of the xenon atoms. MEPS analyses of XeO_3 and $(CH_2CH_2O)_5XeO_3$ corroborated the positions of regions of high EP on the Xe atom of XeO_3

and the trajectories of the O−Xe---O contacts corresponding to σ-hole interactions in the adduct. Further studies of the coordination chemistry of XeO_3 with other macrocyclic and chelating ligands are in progress.

Experimental Section

Caution! *Solid* XeO_3 *detonates when subjected to mild thermal or mechanical shock. Consequently, great care must be exercised during the syntheses and handling of* XeO_3 *and* $(CH_2CH_2O)_5XeO_3$*. For these reasons, the quantity of* XeO_3 *used in a typical synthetic procedure has been limited to 5–15 mg. Reaction vessels fabricated from materials which produce sharp shards when shattered must be avoided and appropriate protective equipment must be used (see Supporting Information).*

Xenon trioxide was synthesized by hydrolysis of XeF_6 as previously described.[8] An aliquot (ca. 10 mg, 0.056 mmol XeO_3) of the resulting aqueous solution, $XeO_3{\cdot}6HF_{(aq)}$, was transferred into a 3 × 3 cm FEP (hexafluoropropylene, tetrafluoroethylene copolymer) fluoroplastic tray by use of a pipette fabricated from FEP tubing. Water and HF were removed from XeO_3 by evaporation overnight in a fume hood to give solid XeO_3. The sample was transferred to a plastic (HDPE) desiccator and dried over 4 Å molecular sieves for 2−3 h to ensure that all surface water had been removed from $XeO_{3(s)}$. Careful dissolution of $XeO_{3(s)}$ in dry acetone (1 mL)[17] gave a clear, colorless solution. Liquid 15-crown-5 (11.0 μL, 0.056 mmol) was pipetted onto the XeO_3 solution surface. Evaporation of the solvent in a fume hood (ca. 1 h) yielded colorless, block-shaped crystals of $(CH_2CH_2O)_5XeO_3$ that were used in the X-ray crystal structure determination.

The following alternative synthetic route is preferred because it avoids the isolation of solid XeO_3 and is therefore significantly less hazardous. After transferring an aliquot of $XeO_3{\cdot}6HF_{(aq)}$ (ca. 10 mg, 0.056 mmol XeO_3) to an FEP tray, one equivalent of liquid 15-crown-5 (11.0 μL, 0.056 mmol) was added. Evaporation of $HF_{(aq)}$ (ca. 36 h) in a fume hood followed by further drying in a desiccator (2-3 h) to remove residual moisture afforded

$(CH_2CH_2O)_5XeO_3$ crystals that were also suitable for a single crystal X-ray structure determination.

Details which relate to the synthetic work, Raman spectroscopy, and X-ray crystallography are provided in the Supporting Information. CCDC 1846353 contains the supplementary crystallographic data for this paper, whcih can be obtained free of charge from The Cambridge Crystallographic Data Centre.

Acknowledgements

We thank the Natural Sciences and Engineering Research Council of Canada (NSERC) for support in the form of a Discovery Grant (G. J. S.) and Prof. Michael Denk (University of Guelph, Guelph, Ontario) for advice on the use of the APFD functional. We are also grateful for the computational resources provided by SHARCNet (Shared Hierarchical Academic Research Computing Network, www.sharcnet.ca).

Keywords: crown ether • xenon trioxide • xenon chemistry • noncovalent bonding • single-crystal X-ray diffraction • Raman spectroscopy • quantum-chemical calculations

References

[1] K. Matsumoto, J. Haner, H. P. A. Mercier, G. J. Schrobilgen, *Angew. Chem. Int. Ed.* **2015**, *54*, 14169.

[2] B. Jaselskis, J. P. Warriner, *Anal. Chem.* **1966**, *38*, 563.

[3] S. A. Shackelford, G. U. Yuen, *Inorg. Nucl. Chem. Lett.* **1973**, *9,* 605.

[4] L. A. Khamidullina, S. V. Lotnik, V. P. Kazakov, *Kinet. Catal.* **2008**, *49*, 27.

[5] S. R. Gunn in *Noble-Gas Compounds* (Ed.: H. H. Hyman), University of Chicago Press, Chicago, **1963**, pp. 149–151.

[6] J. T. Goettel, K. Matsumoto, H. P. A. Mercier, G. J. Schrobilgen, *Angew. Chem. Int. Ed. Engl.* **2016**, *55*, 13780.

[7] J. T. Goettel, H. P. A. Mercier, G. J. Schrobilgen, *J. Fluorine Chem.* **2018**, *211*, 60.

[8] J. T. Goettel, G. J. Schrobilgen, *Inorg. Chem.* **2016**, *55*, 12975.

[9] G. W. Gokel, W. M. Leevy, M. E. Weber. *Chem. Rev.* **2004**, *104*, 2723.

[10] J. W. Steed, J. L. Atwood, *Supramolecular Chemistry, 2nd ed.*, Wiley, Chichester, **2009**.

[11] C. J. Pedersen, *Angew. Chem. Int. Ed. Engl.* **1988**, *27*, 1021.

[12] J. Lipkowski, M. S. Fonari, V. Ch. Kravtsov, Y. A. Simonov, E. V. Ganin, V. O. Gelmboldt, *J. Chem. Crystallogr.* **1996**, *26*, 823.

[13] M. Scharfer, J. Pebler, B. Borgsen, F. Weller, K. Dehnicke, *Z. Naturforsch.* **1990**, *45b*, 1243.

[14] N. W. Alcock, M. Ravindran, G. R. Willey, *Acta. Cryst.* **1993**, *B49*, 507.

[15] S. Alvarez, *Dalton Trans.* **2013**, *42,* 8617.

[16] P. Scilabra, G. Terraneo, G. Resnati, *J. Fluorine Chem.* **2017**, *203*, 62, and references therein.

[17] M. Claessens, O. Fabre, D. Zimmermann, J. Reisse, *Bull. Soc. Chim. Belg.* **1984**, *93*, 983.

[18] M. Hronec in *Handbook of Phase Transfer Catalysis* (Eds.: Y. Sasson, R. Neuman), Chapman & Hall, London, **1997**, pp. 317–332.

[19] I. D. Brown, *The Chemical Bond in Inorganic Chemistry*, IUCr Monographs in Crystallography, 12, Oxford University Press, **2002**.

[20] a) S. K. Wolff, D. J. Grimwood, J. J. McKinnon, M. J. Turner, D. Jayatilaka, M. A. Spackman, *CrystalExplorer* (Version 3.1), University of Western Australia, **2012**; b) M. A. Spackman, J. J. McKinnon, D. Jayatilaka, *CrystEngComm*. **2008**, *10*, 377; c) J. J. McKinnon, D. Jayatilaka, M. A. Spackman, *Chem. Commun.* **2007**, 3814. d) M. A. Spackman, D. Jayatilaka, *CrystEngComm.* **2009**, *11*, 19.

[21] A. Bondi, *J. Phys. Chem.* **1964**, *68*, 441.

[22] Tonto: A Fortran Based Object-Oriented System for Quantum Chemistry and Crystallography, D. Jayatilaka and D. J. Grimwood, Computational Science - ICCS **2003**, *4*, 142.

4.2 Supporting Information

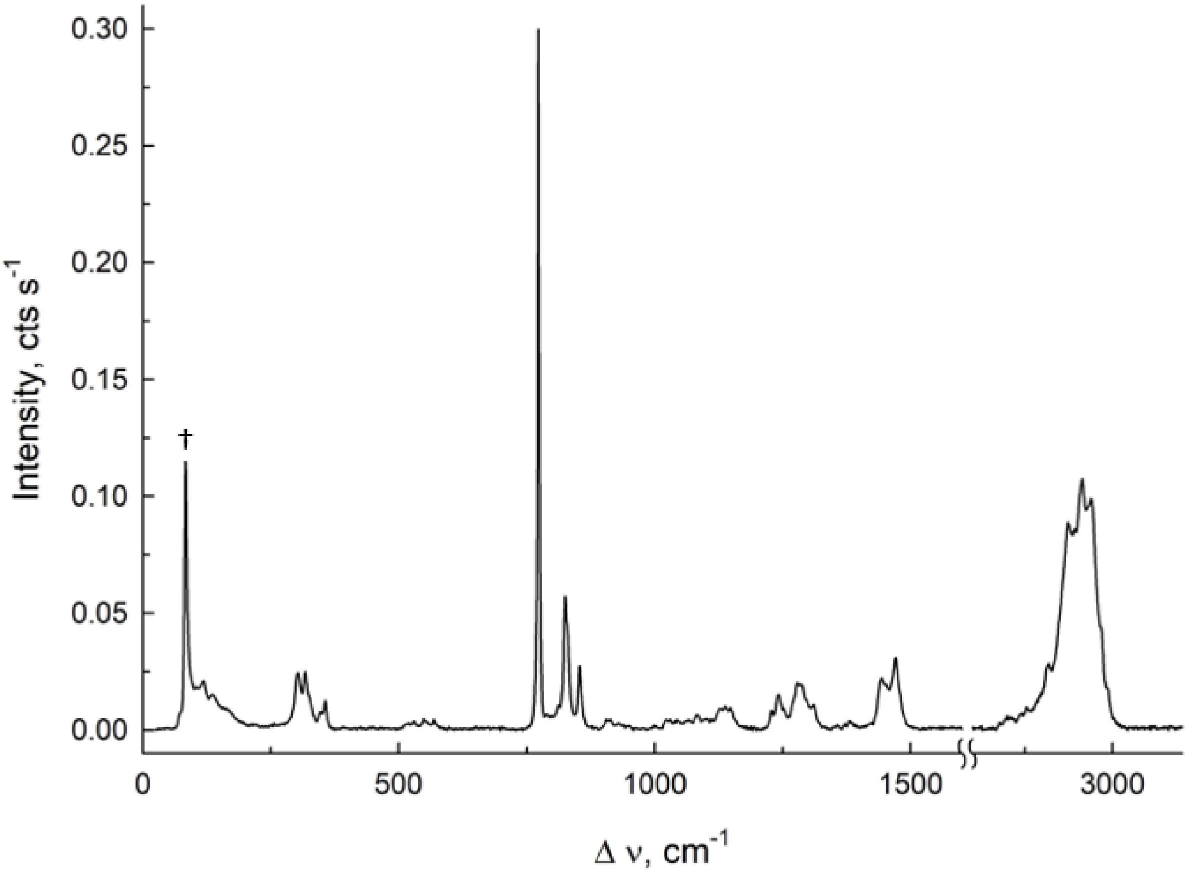

Figure 4.3. Raman spectrum of $(CH_2CH_2)_5XeO_3$ recorded at room temperature in an aluminum sample holder using 1064-nm excitation. The symbol (†) denotes an instrumental artifact.

Table 4.2. Experimental Raman frequencies, calculated vibrational frequencies, and assignments for $(CH_2CH_2O)_5XeO_3$, $XeO_{3(aq)}$, and $(CH_2CH_2O)_5$.

exptl	calcd				exptl	calcd		Vibrational
$XeO_{3(aq)}$[a,b]	**XeO_3 (C_{3v})**		**$(CH_2CH_2O)_5XeO_3$**		**$(CH_2CH_2O)_5XeO_3$**[a,c]	**$(CH_2CH_2O)_5$**		**Assignments**[f]
	B3LYP[a,d]	*APFD*[a,e]	*B3LYP*[a,d]	*APFD*[a,e]		*B3LYP*[a,d]	*APFD*[a,e]	
			3108(41)[7]	3143(38)[4]		3084(80)[27]	3101(78)[24]	ν(CH), combination bands, and overtones
			3099(40)[9]	3126(37)[5]		3080(88)[32]	3099(86)[27]	
			3064(61)[32]	3081(63)[32]		3058(67)[49]	3079(52)[48]	
			3054(16)[18]	3080(25)[13]		3033(52)[51]	3045(119)[15]	
			3036(19)[29]	3049(22)[25]		3014(30)[55]	3041(44)[51]	
			3027(77)[21]	3043(71)[23]		3013(91)[20]	3024(28)[35]	
			3016(255)[86]	3031(46)[3]		3006(92)[17]	3022(55)[25]	
			3013(193)[55]	3027(65)[69]	2937(36)	3002(46)[31]	3017(91)[51]	
			3012(67)[35]	3023(79)[29]	2913(39)	2993(80)[26]	2999(371)[74]	
			3008(180)[82]	3016(647)[91]	2890(32)	2987(513)[95]	2998(104)[65]	
			3006(121)[64]	3014(82)[158]	2873(33)	2956(53)[146]	2990(163)[125]	
			3003(59)[20]	3010(118)[87]	2816(14)	2978(74)[31]	2988(57)[49]	
			2992(203)[87]	3004(64)[10]		2977(134)[100]	2986(79)[54]	
			2988(77)[48]	3003(62)[44]		2970(280)[178]	2978(291)[116]	
			2985(248)[109]	2992(245)[104]		2967(73)[80]	2971(135)[114]	
			2974(154)[66]	2989(120)[41]		2954(77)[21]	2963(67)[18]	
			2973(134)[41]	2983(105)[40]		2951(16)[6]	2960(40)[22]	
			2969(17)[9]	2979(25)[11]		2944(142)[80]	2952(122)[73]	
			2962(92)[53]	2978(38)[18]		2940(62)[27]	2951(36)[7]	
			2961(24)[4]	2972(28)[15]		2932(50)[35]	2943(35)[25]	

Table 4.2. continued…

Exptl	calcd				exptl	calcd		Vibrational Assignments[f]
$XeO_{3(aq)}$[a,b]	XeO_3 (C_{3v})		$(CH_2CH_2O)_5XeO_3$		$(CH_2CH_2O)_5XeO_3$[a,c]	$(CH_2CH_2O)_5$		
	B3LYP[a,d]	*APFD*[a,e]	*B3LYP*[a,d]	*APFD*[a,e]		*B3LYP*[a,d]	*APFD*[a,e]	
			1515(12)[9]	1512(7)[5]		1518(10)[6]	1512(7)[7]	δ(CH_2)
			1514(4)[8]	1507(13)[14]		1513(10)[4]	1507(11)[7]	
			1510(5)[2]	1504(5)[3]		1509(5)[2]	1500(5)[2]	
			1502(3)[5]	1495(3)[4]	1470(12)	1500(7)[5]	1489(2)[6]	
			1496(2)[3]	1490(3)[3]	1452(8)	1497(2)[9]	1486(7)[4]	
			1495(2)[5]	1486(1)[1]	1449(8)	1491(2)[8]	1482(1)[6]	
			1490(3)[11]	1481(3)[13]	1443(9)	1488(4)[14]	1479(7)[22]	
			1488(4)[12]	1480(4)[16]		1484(4)[6]	1478(4)[5]	
			1486(7)[5]	1478(7)[11]		1483(8)[3]	1475(4)[1]	
			1480(7)[4]	1473(9)[6]		1475(10)[1]	1468(9)[2]	
			1460(1)[2]	1468(2)[3]		1455(2)[2]	1460(2)[4]	ρ_ω(CH_2)
			1446(2)[4]	1452(2)[4]		1449(2)[5]	1455(2)[9]	
			1440(2)[2]	1443(3)[5]		1435(2)[2]	1434(3)[5]	
			1422(1)[<1]	1420(<1)[<1]	1379(3)	1420(3)[1]	1412(3)[1]	
			1419(2)[1]	1416(3)[5]	1310(5)	1420(3)[<1]	1412(2)[3]	
			1411(<1)[<1]	1409(1)[1]	1302(5)	1409(<1)[<1]	1404(1)[<1]	
			1405(1)[3]	1399(3)[2]		1403(1)[8]	1398(1)[5]	
			1390(<1)[30]	1383(1)[21]		1389(<1)[49]	1383(1)[48]	
			1383(1)[50]	1376(1)[46]		1385(2)[87]	1379(1)[78]	
			1374(<1)[1]	1366(1)[1]		1375(<1)[6]	1367(<1)[9]	
			1337(7)[4]	1328(8)[5]		1344(9)[5]	1341(8)[5]	ρ_t(CH_2)
			1321(5)[20]	1318(7)[29]		1323(6)[18]	1325(9)[4]	
			1309(5)[3]	1311(7)[2]		1312(7)[10]	1320(7)[43]	
			1301(9)[18]	1300(9)[43]	1295(6)	1309(13)[18]	1310(7)[16]	
			1296(8)[3]	1295(8)[43]	1286(8)	1300(11)[7]	1300(9)[16]	
			1277(2)[43]	1281(6)[7]	1278(8)	1282(3)[52]	1293(3)[51]	
			1273(1)[19]	1277(2)[36]		1274(6)[29]	1280(9)[25]	
			1269(8)[4]	1272(13)[17]		1268(6)[5]	1271(1)[21]	
			1264(6)[<1]	1267(7)[9]		1266(9)[5]	1266(11)[6]	
				1261(3)[3]				

Table 4.2. continued…

exptl	calcd				exptl	calcd		Vibrational Assignments[f]
$XeO_{3(aq)}$[a,b]	XeO_3 (C_{3v})		$(CH_2CH_2O)_5XeO_3$		$(CH_2CH_2O)_5XeO_3$[a,c]	$(CH_2CH_2O)_5$		
	B3LYP[a,d]	*APFD*[a,e]	*B3LYP*[a,d]	*APFD*[a,e]		*B3LYP*[a,d]	*APFD*[a,e]	
			1257(2)[2] 1179(1)[7] 1175(6)[42] 1167(2)[20] 1156(1)[9] 1149(1)[155] 1144(2)[310] 1126(<1)[25] 1121(1)[5] 1108(2)[142] 1093(3)[26] 1090(2)[21] 1074(2)[22] 1067(1)[18] 1051(1)[36] 1042(2)[25] 956(1)[45] 950(1)[57] 941(1)[1] 927(3)[6] 915(2)[8] 861(8)[33] 844(3)[9]	1230(9)[9] 1209(1)[19] 1199(2)[33] 1188(4)[148] 1175(1)[259] 1168(1)[70] 1167(2)[40] 1143(1)[25] 1133(2)[21] 1119(3)[46] 1109(1)[27] 1104(2)[26] 1096(1)[23] 1094(1)[13] 1069(2)[29] 1056(2)[12] 969(1)[30] 963(2)[48] 951(2)[2] 942(2)[9] 933(2)[6] 885(8)[36]	1251(5) 1240(6) 1228(4) 1148(4) 1142(4) 1137(5) 1132(4) 1126(5) 1123(4) 1084(4) 1029(3) 906(3)	1256(3)[3] 1185(2)[17] 1178(5)[82] 1171(2)[12] 1164(2)[49] 1158(1)[242] 1158(2)[249] 1131(1)[10] 1122(1)[27] 1113(3)[86] 1093(4)[27] 1090(2)[18] 1081(2)[23] 1070(1)[28] 1050(2)[21] 1044(2)[10] 954(2)[61] 950(1)[39] 945(1)[16] 926(3)[8] 904(2)[5] 857(6)[34] 843(8)[4]	1258(3)[11] 1213(3)[31] 1202(2)[102] 1193(5)[113] 1182(2)[270] 1176(3)[51] 1174(2)[49] 1147(2)[9] 1130(3)[28] 1118(2)[41] 1110(2)[10] 1105(2)[21] 1098(1)[40] 1091(1)[19] 1063(3)[17] 1056(3)[<1] 957(1)[49] 943(1)[42] 940(2)[12] 929(2)[7] 896(2)[11] 870(6)[28]	ν(CO)-(CO) ν(CO)-(CC) $\rho_r(CH_2)$
833(14)	855(92)[11]	901(11)[98]	840(12)[55] 837(4)[46] 833(12)[87]	882(11)[85] 872(11)[107]	853(10) 825(20) 811(5)			$\nu_{as}(XeO_3)$
			823(3)[13] 799(3)[9]	859(2)[11] 854(1)[13] 846(2)[3] 823(4)[6]		836(2)[4] 825(5)[3] 807(5)[4]	854(3)[2] 845(4)[2] 837(5)[4]	$\rho_r(CH_2)$

Table 4.2. continued…

exptl	calcd				exptl	calcd		Vibrational Assignments[f]
$XeO_{3(aq)}$[a,b]	**XeO_3 (C_{3v})**		**$(CH_2CH_2O)_5XeO_3$**		**$(CH_2CH_2O)_5XeO_3$[a,c]**	**$(CH_2CH_2O)_5$**		
	B3LYP[a,d]	*APFD*[a,e]	*B3LYP*[a,d]	*APFD*[a,e]		*B3LYP*[a,d]	*APFD*[a,e]	
780(100)	788(4)[53]	836(51)[4]	785(65)[14]	832(56)[19]	772(100)			$\nu_s(XeO_3)$
			571(1)[<1] 545(1)[2] 542(1)[7] 529(1)[2] 511(1)[7] 438(<1)[4] 389(<1)[2] 338(1)[1]	832(56)[19] 584(1)[<1] 570(1)[12] 559(1)[1] 540(<1)[1] 527(1)[9] 447(<1)[5] 406(<1)[2]	569(2) 554(2) 549(2) 537(2) 529(2) 519(2)	568(2)[2] 555(1)[13] 538(1)[1] 522(1)[3] 498(<1)[12] 438(<1)[2] 397(<1)[1] 339(1)[<1]	825(4)[4] 581(2)[12] 558(1)[3] 537(1)[1] 515(1)[7] 490(<1)[18] 435(<1)[2] 409(<1)[1]	δ(CCO) δ(COC)
344, sh	308(33)[3]	322(3)[34]	333(2)[59]	366(3)[63]	356(6) 346(4)			$\delta_{umb}(XeO_3)$
			322(1)[<1] 312(2)[1] 289(4)[4]	348(1)[3] 334(1)[2] 328(2)[<1] 304(1)[7]		312(<1)[2] 306(2)[1] 288(3)[1] 284(<1)[1]	333(1)[<1] 308(1)[1]	δ(CCO) δ(COC)
317(7), br	271(9)[5] 271(9)[5]	284(4)[10]	297(2)[7] 294(1)[6] 283(3)[10]	319(2)[10] 310(1)[5]	317(10) 302(10)			$\delta_{as}(XeO_3)$

Table 4.2. continued…

exptl	calcd				exptl	calcd		Vibrational Assignments[f]
$XeO_{3(aq)}$ [a,b]	XeO_3 (C_{3v})		$(CH_2CH_2O)_5XeO_3$		$(CH_2CH_2O)_5XeO_3$[a,c]	$(CH_2CH_2O)_5$		
	B3LYP[a,d]	*APFD*[a,e]	*B3LYP*[a,d]	*APFD*[a,e]		*B3LYP*[a,d]	*APFD*[a,e]	
			234(<1)[1]	300(3)[11]				deformation modes / lattice modes
			215(<1)[4]	263(<1)[3]				
			198(<1)[2]	241(<1)[4]			300(1)[<1]	
			180(<1)[6]	222(<1)[2]		230(<1)[2]	296(2)[<1]	
			172(<1)[4]	203(<1)[11]		200(<1)[<1]	288(<1)[<1]	
			170(<1)[11]	181(<1)[5]		178(<1)[3]	237(<1)[2]	
			158(<1)[4]	177(<1)[2]		172(<1)[6]	213(<1)[<1]	
			137(<1)[4]	164(1)[4]		166(<1)[3]	189(<1)[6]	
			121(1)[4]	160(1)[5]	137(5)	162(<1)[10]	173(<1)[7]	
			98(1)[4]	142(<1)[11]	119(7)	147(<1)[5]	163(<1)[3]	
			90(<1)[1]	131(1)[1]		112(<1)[3]	152(<1)[1]	
			81(<1)[3]	113(<1)[1]		63(<1)[2]	141(<1)[8]	
			67(<1)[1]	107(<1)[2]		58(<1)[<1]	131(<1)[4]	
			63(<1)[<1]	95(<1)[1]		47(<1)[2]	75(<1)[1]	
			57(<1)[<1]	91(<1)[2]		37(<1)[1]	66(<1)[1]	
			54(<1)[2]	85(<1)[2]			56(<1)[1]	
			48(<1)[<1]	68(<1)[1]			45(<1)[1]	
			42(<1)[<1]	58(1)[<1]				
				45(1)[1]				

[a] Frequencies are given in cm^{-1}. Abbreviations denote shoulder (sh) and broad (br). [b] The spectrum was recorded in a ¼-in. FEP diameter sample tube at −140 °C. Values in parentheses are relative Raman intensities. [c] The spectrum was recorded in an aluminum sample holder at 22 °C. Values in parentheses are relative Raman intensities. [d] The B3LYP/Def2–TZVP level was used. [e] The APFD/Def2–TZVP level was used. Values in parentheses and square brackets are calculated Raman intensities (Å amu^{-1}) and infrared intensities (km mol^{-1}), respectively. [f] Symbols denote stretch (ν), bend (δ), rock (ρ_r), twist (ρ_t), wag (ρ_ω), umbrella (umb), symmetric (s), and asymmetric (as).

Table 4.3 Summary of X-ray crystal data and refinement results for $(CH_2CH_2O)_5XeO_3$.

	$(CH_2CH_2O)_5XeO_3$
Crystal system	monoclinic
space group	$P2_1/n$
a (Å)	8.6728(3)
b (Å)	12.9457(4)
c (Å)	12.4511(4)
α (deg)	90
β (deg)	96.557(2)
γ (deg)	90
V (Å^3)	1338.81(8)
Z (molecules/unit cell)	4
mol. wt. (g mol^{-1})	399.55
ρ_{calc} (g cm^{-3})	1.911
T (°C)	−173
μ (mm^{-1})	2.51
F(000)	792.0
Reflections collected	35053
GOF	1.0140
R_1[a]	0.0198
wR_2[b]	0.0486

[a] $R_1 = \Sigma||F_o|-|F_c||/\Sigma|F_o|$. [b] $wR_2 = [\Sigma(w(F_o^2-F_c^2)^2)/\Sigma(w(F_o^2)^2)]^{½}$.

Table 4.4. Experimental and calculated (C_1 symmetry) primary and secondary bond lengths and angles for $(CH_2CH_2)_5XeO_3$.

	Bond Lengths (Å)			**Bond Angles (°)**	
	exptl	calcd[a]		exptl	calcd[a]
Xe1–O1	1.763(1)	1.767	O1−Xe1−O3	100.96(5)	101.23
Xe1–O2	1.767(1)	1.762	O3−Xe1−O2	99.80(5)	103.21
Xe1–O3	1.763(1)	1.763	O2−Xe1−O1	102.53(5)	105.1
Xe1–O4	2.895(1)	2.962	O1−Xe1−O5	75.91(4)	77.68
Xe1–O5	2.932(1)	2.909	O1−Xe1−O4	159.86(4)	152.42
Xe1–O6	2.970(1)	2.963	O1−Xe1−O7	129.93(4)	132.34
Xe1–O7	3.114(1)	3.253	O2−Xe1−O7	70.93(4)	79.22
Xe1–O8	3.124(1)	3.074	O2−Xe1−O8	134.79(4)	128.07
O4−C1	1.428(2)	1.404	O2−Xe1−O6	155.00(4)	156.78
O4−C10	1.433(2)	1.406	O3−Xe1−O4	78.98(4)	71.09
O5−C6	1.437(2)	1.412	O3−Xe1−O5	176.63(4)	177.79
O5−C7	1.438(1)	1.409	O3−Xe1−O6	72.37(4)	80.41
O6−C2	1.439(2)	1.411	C7−O5−C6	113.0(1)	114.5
O6−C3	1.431(2)	1.410	C8−O7−C9	113.3(1)	113.2
O7−C8	1.425(2)	1.409	C10−O4−C1	111.6(1)	113.6
O7−C9	1.424(1)	1.405	C4−O8−C5	112.4(1)	113.8
O8−C4	1.424(2)	1.405	C2−O6−C3	114.4(1)	116.6
O8−C5	1.431(2)	1.407	O5−C7−C8	108.1(1)	109.0
C1−C2	1.508(2)	1.514	O4−C10−C9	108.0(1)	108.6
C3−C4	1.505(2)	1.512	O6−C2−C1	113.0(1)	113.5
C5−C6	1.506(2)	1.513	O7−C9−C10	106.7(1)	107.8
C7−C8	1.504(2)	1.504	O5−C6−C5	111.5(1)	111.6
C9−C10	1.503(2)	1.503	O8−C5−C6	106.7(1)	108.0
C1−H1A	0.96(2)	1.100	O8−C4−C3	108.4(1)	107.6
C1−H1B	0.98(2)	1.101	O4−C1−C2	109.4(1)	108.6
C2−H2A	0.96(2)	1.090	O6−C3−C4	111.2(1)	112.2
C2−H2B	1.02(2)	1.099			
C3−H3A	0.95(2)	1.097			
C3−H3B	0.93(2)	1.095			
C4−H4A	0.98(2)	1.099			
C4−H4B	0.91(2)	1.101			
C5−H5A	0.94(2)	1.099			
C5−H5B	0.91(2)	1.100			
C6−H6A	1.03(2)	1.098			
C6−H6B	1.02(2)	1.091			
C7−H7A	0.98(2)	1.097			
C7−H7B	1.03(2)	1.098			
C8−H8A	1.00(2)	1.100			
C8−H8B	1.00(2)	1.095			
C9−H9A	0.96(2)	1.100			
C9−H9B	0.96(2)	1.098			
C10−H10A	0.95(2)	1.100			
C10−H10B	0.95(2)	1.100			

[a] APFD/Def2-TZVP.

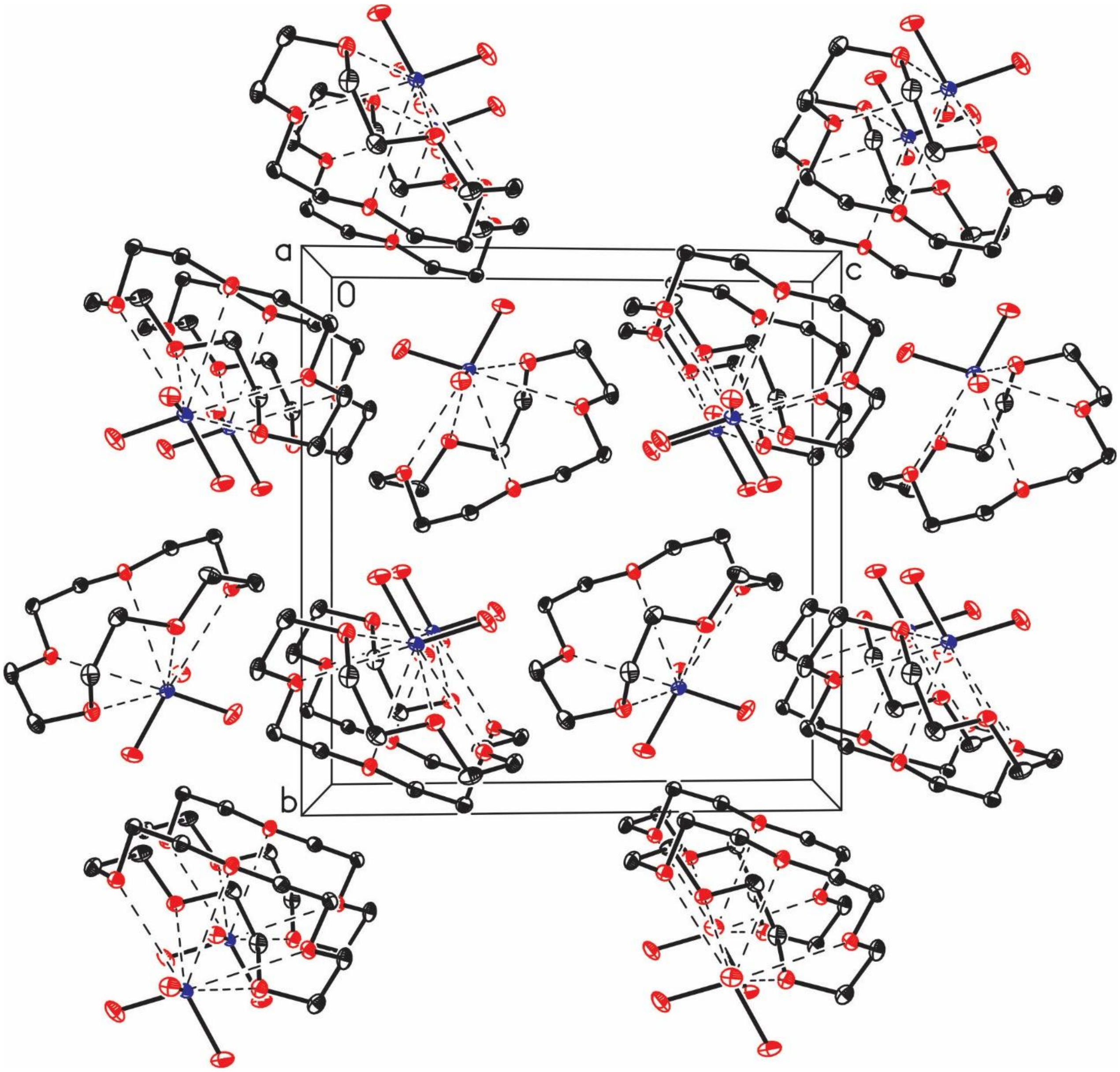

Figure 4.4. The packing diagram for $(CH_2CH_2)_5XeO_3$; thermal ellipsoids are shown at their 50% probability levels and the hydrogen atoms have been removed for clarity.

Hirshfeld Surface Analysis

The Hirshfeld surface is based on "Hirshfeld's stockholder partitioning scheme" which partitions the electron density of a molecule into molecular fragments.[S1] The molecular weight function for a molecule in a crystal, $w_A(r)$, depends on the specific atomic electron density and the proximity and identities of neighboring atoms (eq 4.1). The Hirshfeld surface is the region where $w_A(r)$ is equal to 0.5. This partitions the crystal space such that the electron density inside the surface (the molecule) exceeds that of its surroundings (all neighboring molecules), guaranteeing a maximum proximity for the smooth, nonoverlapping, neighboring molecular volumes. The Hirshfeld surface of an individual molecule passes along, or close to, regions of lowest electron density between neighboring molecules, closely approximating Bader's QTAIM scheme.

$$w_A(r) = \frac{\sum_{i \in molecule\ A} \rho_i^{at}(r)}{\sum_{i \in crystal} \rho_i^{at}(r)} = \frac{\rho_{promolecule}(r)}{\rho_{procrystal}(r)} \qquad (4.1)^{[a,b]}$$

[a] $\rho_i^{at}(r)$ is a spherically-averaged atomic electron densities of the various atoms.
[b] The promolecule and procrystal are defined as a sum of the atoms belonging to a single molecule and a crystal, respectively.

The distance from a point on the Hirshfeld surface to the nearest nucleus of the molecule inside and outside of the surface is denoted by d_i and d_e, respectively. The d_{norm} function (eq 4.2) is a combination of d_e and d_i, each of which are normalized by the van der Waals radii (vdWr) of the particular atoms involved. Contacts shorter than the sum of the vdWr appear as circular red areas on a light blue-gray surface.

$$d_{norm} = \frac{d_i - r_i^{vdW}}{r_i^{vdW}} + \frac{d_e - r_e^{vdW}}{r_e^{vdW}} \qquad (4.2)$$

The Hirshfeld surface of a molecule is generated from the crystallographic information file (.cif) and can be mapped with other properties, such as the electrostatic potential, by means of *ab initio* calculations using Tonto (integrated with the CrystalExplorer 3.1 software). The result is the calculated electron density at points on the Hirshfeld surface, which are displayed as a color-coded electron density surface that shows areas of electron density excess (negative potential) and electron deficiency (positive potential).

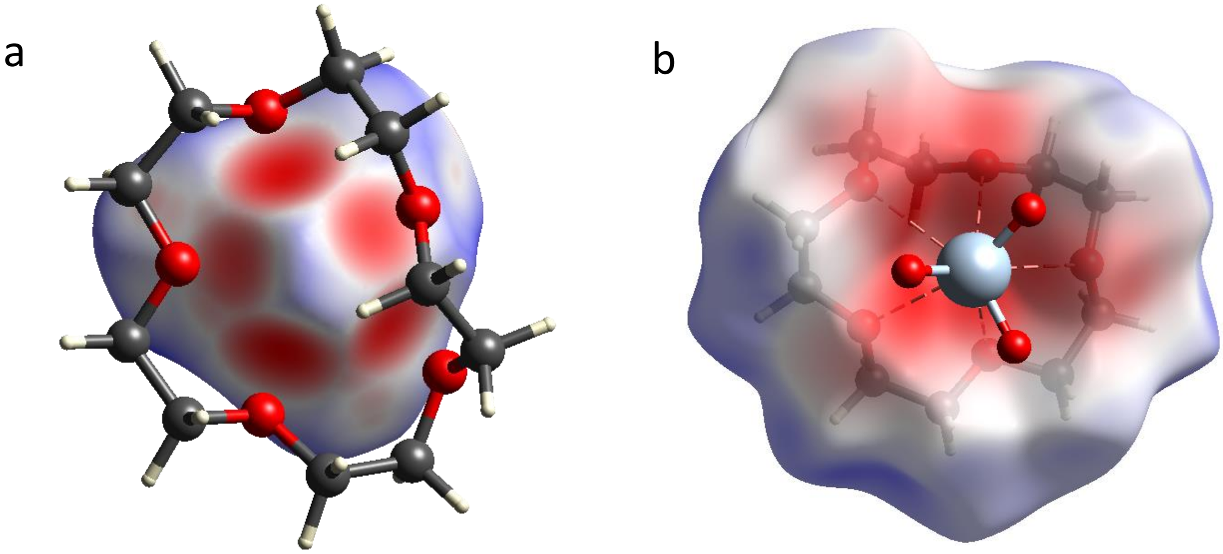

Figure 4.5. The Hirshfeld surfaces in $(CH_2CH_2O)_5XeO_3$ are mapped with (**a**) the d_{norm} function of XeO_3 and (**b**) the electrostatic potential surface (B88LYP/321-G) of 15-crown-5.

Computational Results

Quantum-chemical calculations were used to study the bonding in $(CH_2CH_2O)_5XeO_3$. Several DFT functionals (APFD, APF, M062X, M052X, B3LYP, WB97XD) were used to optimize the structure of $(CH_2CH_2O)_5XeO_3$ (Table S4). A statistical analysis was carried out to compare these methods and to determine which best reproduces the experimental geometry of $(CH_2CH_2O)_5XeO_3$. The calculated primary and secondary Xe−O bond lengths were compared with their experimental values. Linear correlations gave values of the intercept, slope, and correlation coefficients (R^2) which have also been considered (Table S5). The best methods should provide values close to zero, one, and one, respectively. In addition, two estimates of the error are given: the average absolute error (AAE, eq 4) and the mean absolute percentage error (MAPE, eq 5). A similar analysis was applied to $\nu_s(XeO_3)$ and $\nu_{as}(XeO_3)$ which showed that the B3LYP functional gives the best agreement with experiment.

$$\mathrm{AAE}_i = \frac{1}{n}\sum_{j=1}^{n}\left|E_j(i) - E_j[\mathrm{Expt}]\right| \tag{4.4}$$

$$\mathrm{MAPE}_i = 100 * \frac{1}{n}\sum_{j=1}^{n}\frac{\left|E_j(i)-E_j[\mathrm{Expt}]\right|}{\left|E_j[\mathrm{Expt}]\right|} \tag{4.5}$$

Scheme 4.1. Formulae used to calculate the AAE (eq 4) and the MAPE (eq 5), where *$E_j(i)$* is the bond distance calculated using method *i* for compound *j*.

Table 4.5. A comparison of experimental primary and secondary Xe−O bond lengths in $(CH_2CH_2O)_5XeO_3$ with those of the calculated geometry- optimized structure using a variety of methods and basis sets.

	exptl	**calcd**								
		APFD	**APFD**	**M062X**	**M052X**	**wB97XD**	**APF**	**B3LYP**	**B3LYP**	**B3LYP**
		Def2-TZVP	Def2-TZVPD	Def2-TZVP	Def2-TZVP	Def2-TZVP	Def2-TZVPD	Def2-TZVPD	aVDZ (Xe) Def2-TZVPD	aVDZ
Xe−O	1.763(1)	1.767	1.767	1.760	1.761	1.759	1.768	1.830	1.785	1.843
	1.767(1)	1.762	1.762	1.755	1.756	1.753	1.763	1.825	1.780	1.838
	1.763(1)	1.763	1.764	1.756	1.757	1.755	1.764	1.826	1.781	1.839
Xe---O	2.932(1)	2.909	2.909	2.908	2.895	3.010	3.024	3.050	3.075	3.066
	3.124(1)	3.074	3.074	3.141	3.142	3.219	3.324	3.380	3.387	3.368
	2.970(1)	2.962	2.961	2.975	2.962	3.048	3.025	3.069	3.052	3.199
	2.895(1)	2.963	2.963	2.975	2.997	3.089	3.153	3.198	3.210	3.081
	3.114(1)	3.253	3.258	3.280	3.331	3.469	3.572	3.651	3.686	3.681

Table 4.6. Statistical analyses of the experimental and calculated Xe−O primary and secondary bond lengths in $(CH_2CH_2O)_5XeO_3$, sorted from lowest to highest MAPE.

	APFD	**APFD**	**M062X**	**M052X**	**wB97XD**	**APF**	**B3LYP**	**B3LYP**	**B3LYP**
	Def2-TZVP	Def-2TZVPD	Def2-TZVP	Def2-TZVP	Def2-TZVP	Def2-TZVPD	Def2-TZVPD	aVDZ (Xe) Def2-TZVPD	aVDZ
***R*^{2}**	0.992	0.992	0.993	0.988	0.986	0.978	0.971	0.973	0.976
Slope	1.02	1.02	1.05	1.06	1.14	1.18	1.22	1.17	1.17
Intercept	–0.04	–0.04	–0.10	–0.11	–0.26	–0.32	–0.38	–0.25	–0.24
AAE	0.037	0.038	0.039	0.050	0.103	0.134	0.179	0.188	0.198
MAPE	1.247	1.277	1.356	1.709	3.485	4.443	6.040	6.743	7.197

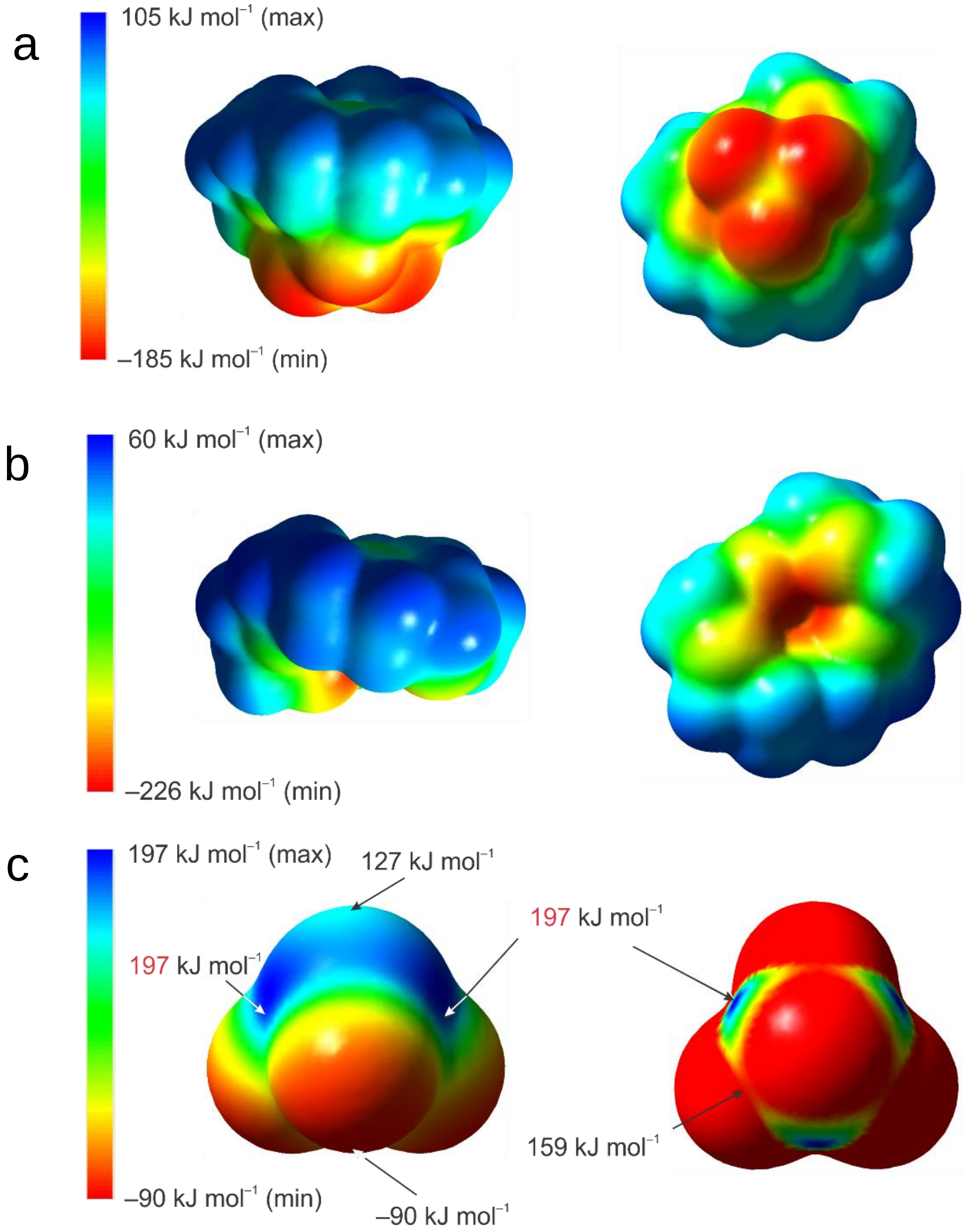

Figure 4.6. The molecular electrostatic potential surfaces (MEPS) of $(CH_2CH_2O)_5XeO_3$, $(CH_2CH_2O)_5$, and SbF_3 at the 0.001 e bohr^{-3} isosurface (APFD/Def2-TZVPD). In the case of SbF_3, the illustration on the right represents the top 20% of the positive electrostatic potential range (left; 158–197 kJ mol^{-1}).

Table 4.7. Natural population analysis (NPA) charges, bond valences, Wiberg valencies, and Wiberg bond indices for XeO_3, $(CH_2CH_2O)_5$, and $(CH_2CH_2O)_5XeO_3$.

XeO_3[a,b]				
Bond Indices		NPA Charges [Valencies]		
Xe1−O1	1.126	Xe	2.758	[3.379]
Xe1−O2	1.126	O1	–0.920	[1.537]
Xe1−O3	1.126	O2	–0.919	[1.537]
		O3	–0.919	[1.537]
		$\sum_{XeO_3}$	**0.000**	

$(CH_2CH_2O)_5$[b]									
Bond Indices		NPA Charges		[Valences]	Bond Indices		NPA Charges		[Valences]
O5–C3	0.946	O5	–0.515	[2.059]	H1A–C1	0.924	H1A	0.159	[0.977]
C3–C4	1.009	C3	–0.091	[3.863]	H1B–C1	0.919	H1B	0.174	[0.973]
C4–O7	0.936	C4	–0.089	[3.853]	H2A–C2	0.932	H2A	0.164	[0.976]
O7–C5	0.941	O7	–0.523	[2.055]	H2B–C2	0.919	H2B	0.198	[0.963]
C5–C6	1.012	C5	–0.085	[3.854]	H3A–C3	0.921	H3A	0.199	[0.962]
C6–O4	0.942	C6	–0.085	[3.856]	H3B–C3	0.926	H3B	0.162	[0.976]
O4–C7	0.943	O4	–0.518	[2.069]	H4A–C4	0.923	H4A	0.163	[0.977]
C7–C8	0.999	C7	–0.103	[3.855]	H4B–C4	0.921	H4B	0.171	[0.973]
C8–O6	0.958	C8	–0.084	[3.861]	H5A–C5	0.925	H5A	0.169	[0.973]
O6–C9	0.947	O6	–0.500	[2.082]	H5B–C5	0.920	H5B	0.172	[0.973]
C9–C10	1.002	C9	–0.093	[3.860]	H6A–C6	0.926	H6A	0.167	[0.974]
C10–O8	0.945	C10	–0.094	[3.860]	H6B–C6	0.920	H6B	0.181	[0.970]
O8–C1	0.943	O8	–0.518	[2.069]	H7A–C7	0.919	H7A	0.181	[0.970]
C1–C2	1.003	C1	–0.106	[3.854]	H7B–C7	0.926	H7B	0.164	[0.975]
C2–O5	0.943	C2	–0.084	[3.853]	H8A–C8	0.928	H8A	0.175	[0.973]
					H8B–C8	0.923	H8B	0.179	[0.970]
					H9A–C9	0.920	H9A	0.204	[0.961]
					H9B–C9	0.932	H9B	0.164	[0.975]
					H10A–C10	0.916	H10A	0.184	[0.969]
					H10B–C10	0.924	H10B	0.160	[0.976]
							$\sum_{C_{10}H_{20}O_5}$	**–0.007**	

Table 4.7. continued…

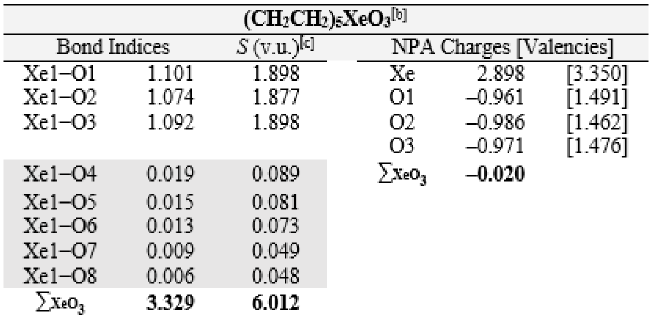

$(CH_2CH_2)_5XeO_3$[b]					
Bond Indices		S (v.u.)[c]	NPA Charges [Valencies]		
Xe1–O1	1.101	1.898	Xe	2.898	[3.350]
Xe1–O2	1.074	1.877	O1	–0.961	[1.491]
Xe1–O3	1.092	1.898	O2	–0.986	[1.462]
			O3	–0.971	[1.476]
Xe1–O4	0.019	0.089	$\sum_{XeO_3}$	**–0.020**	
Xe1–O5	0.015	0.081			
Xe1–O6	0.013	0.073			
Xe1–O7	0.009	0.049			
Xe1–O8	0.006	0.048			
$\sum_{XeO_3}$	**3.329**	**6.012**			

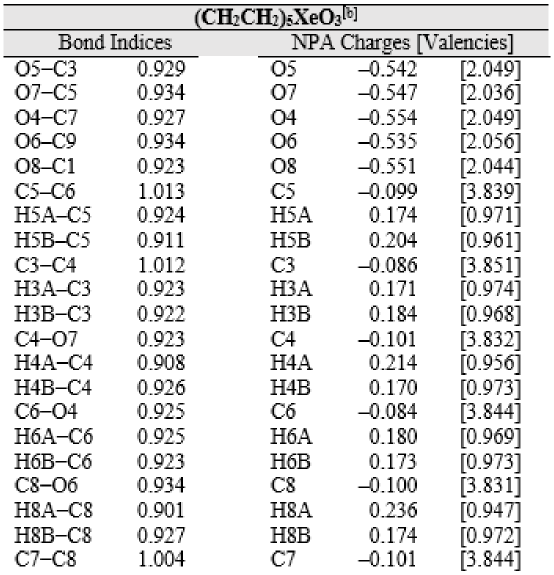

$(CH_2CH_2)_5XeO_3$[b]				
Bond Indices		NPA Charges [Valencies]		
O5–C3	0.929	O5	–0.542	[2.049]
O7–C5	0.934	O7	–0.547	[2.036]
O4–C7	0.927	O4	–0.554	[2.049]
O6–C9	0.934	O6	–0.535	[2.056]
O8–C1	0.923	O8	–0.551	[2.044]
C5–C6	1.013	C5	–0.099	[3.839]
H5A–C5	0.924	H5A	0.174	[0.971]
H5B–C5	0.911	H5B	0.204	[0.961]
C3–C4	1.012	C3	–0.086	[3.851]
H3A–C3	0.923	H3A	0.171	[0.974]
H3B–C3	0.922	H3B	0.184	[0.968]
C4–O7	0.923	C4	–0.101	[3.832]
H4A–C4	0.908	H4A	0.214	[0.956]
H4B–C4	0.926	H4B	0.170	[0.973]
C6–O4	0.925	C6	–0.084	[3.844]
H6A–C6	0.925	H6A	0.180	[0.969]
H6B–C6	0.923	H6B	0.173	[0.973]
C8–O6	0.934	C8	–0.100	[3.831]
H8A–C8	0.901	H8A	0.236	[0.947]
H8B–C8	0.927	H8B	0.174	[0.972]
C7–C8	1.004	C7	–0.101	[3.844]

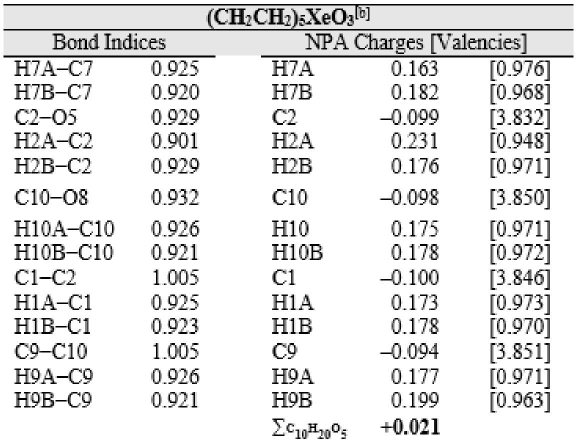

$(CH_2CH_2)_5XeO_3$[b]				
Bond Indices		NPA Charges [Valencies]		
H7A–C7	0.925	H7A	0.163	[0.976]
H7B–C7	0.920	H7B	0.182	[0.968]
C2–O5	0.929	C2	–0.099	[3.832]
H2A–C2	0.901	H2A	0.231	[0.948]
H2B–C2	0.929	H2B	0.176	[0.971]
C10–O8	0.932	C10	–0.098	[3.850]
H10A–C10	0.926	H10	0.175	[0.971]
H10B–C10	0.921	H10B	0.178	[0.972]
C1–C2	1.005	C1	–0.100	[3.846]
H1A–C1	0.925	H1A	0.173	[0.973]
H1B–C1	0.923	H1B	0.178	[0.970]
C9–C10	1.005	C9	–0.094	[3.851]
H9A–C9	0.926	H9A	0.177	[0.971]
H9B–C9	0.921	H9B	0.199	[0.963]
		$\sum_{C_{10}H_{20}O_5}$	**+0.021**	

[a] The calculated geometric parameters of XeO_3: Xe−O, 1.754 Å; ∠O−Xe−O, 107.18°. [b] The APFD/Def2–TZVPD level was used. [c] I. D. Brown, reference [S2].

Experimental Section

Caution! *Solid XeO_3 detonates when subjected to mild thermal or mechanical shock. Great care must be taken during the syntheses and handling of XeO_3 and $(CH_2CH_2O)_5XeO_3$. For these reasons, the quantity of XeO_3 used in each synthesis has been limited to 5–15 mg. Reaction vessels fabricated from FEP (hexafluoropropylene, tetrafluoroethylene copolymer) fluoroplastic, which is inert to attack by HF, strong oxidants, and fluorinating agents, generally does not shatter to produce sharp shards when a detonation occurs at the reagent scales described in this study. Appropriate protective equipment (face shield, leather gloves, ear protection) must be used.*

Apparatus and Materials *(a) General*. Anhydrous HF (Harshaw Chemicals Co.) was purified as previously described.[S3]

(b) Xenon hexafluoride. Xenon hexafluoride was prepared by the reaction of Xe (99.995%, Air Products and Chemicals, Inc.) and F_2 (98+%, Air Products and Chemicals, Inc.) similar to the method described by Malm and Chernick.[S4] Small amounts of XeF_4 impurity, identified by two strong peaks at 502 and 543 cm^{-1} in the Raman spectrum, also formed XeO_3 when hydrolyzed[S5] and therefore did not interfere with the synthesis of XeO_3.

X-ray Crystallography. *(a) Crystal Mounting.* Single-crystals of $(CH_2CH_2O)_5XeO_3$ were submerged in perfluoropolyether oil (Fomblin Z-25) in the open atmosphere and were selected at room temperature and mounted at the tip of a dual-thickness polymer loop (MiTeGen, Ithaca, NY; MicroMount;™ 100–500 μm) using Halocarbon 25-5S grease (Halocarbon Products Corporation, River Edge, NJ).

(b) Collection and Reduction of X-ray Data. Crystals were centered on a Bruker SMART APEX II diffractometer equipped with an APEX II 4K CCD (charge-coupled device) area detector and a triple-axis goniometer that was controlled by the APEX II Graphical User Interface (GUI) software.[S6] A Bruker Triumph curved crystal monochromator was used with a Mo Kα (λ = 0.71073 Å) radiation source for all compounds. Diffraction data collection at −173 °C consisted of ω- and ϕ-scans collected at 0.5° intervals. The crystal-

to-detector distance was 4.954 cm and data collection was carried out in a 512 x 512 pixel mode using 2 x 2 pixel binning. The raw data was processed by use of the APEX III GUI software.[S6] The SADABS[S7] program was used for scaling the diffraction data.

(c) Solution and Refinement of the Structure. The XPREP program[S8] was used to confirm unit cell dimensions and the crystal lattice. All calculations were carried out using the SHELXTL-plus[S8] and the Olex2[S9] packages for structure determination, solution refinement, and molecular graphics. The space group choice was confirmed using Platon.[S10] The final refinement was obtained by introducing anisotropic thermal parameters and the recommended weightings for all of the atoms except the hydrogen atoms. The H atoms were placed at locations derived from a difference map. The H atoms were included as riding contributions with isotropic displacement parameters that were 1.2 times those of the attached carbon atoms. The maximum electron density in the final difference Fourier map was located near the xenon atom.

Raman Spectroscopy. The Raman spectrum was recorded on a Bruker RFS 100 FT-Raman spectrometer using 1064-nm excitation, 300 mW laser power, and ±0.5 cm^{-1} resolution as previously described.[S11]

Computational Details. Density-functional theory (DFT) was employed to study the electronic structures of $(CH_2CH_2O)_5XeO_3$, XeO_3, and $(CH_2CH_2O)_5$. All basis sets were obtained online from the EMSL Basis Set Exchange (https://bse.pnl.gov/bse/portal).[S12] Quantum-chemical calculations were carried out using the program Gaussian 09[S13] for geometry optimizations and to create wavefunction files. The GaussView[S14] program was used to visualize the vibrational displacements that form the basis for the vibrational mode descriptions given in Table S1. Natural bond orbital analyses were performed using APFD densities with the NBO program (version 6.0).[S15] The CrystalExplorer 3.1[S1a] program was used for Hirshfeld surface analyses and the computational program Tonto,[S16] as implemented in CrystalExplorer, was used for wavefunction calculations and for mapping of the electrostatic potential surface (B88LYP/321-G) onto the Hirshfeld surface. The MEPS diagrams were drawn with Jmol.[S17]

References

[S1] a) S. K. Wolff, D. J. Grimwood, J. J. McKinnon, M. J. Turner, D. Jayatilaka, M. A. Spackman, University of Western Australia, **2012**; b) M. A. Spackman, J. J. McKinnon, D. Jayatilaka, *CrystEngComm*. **2008**, *10*, 377; c) J. J. McKinnon, D. Jayatilaka, M. A. Spackman, *Chem. Commun.* **2007**, 3814; d) M. A. Spackman, D. Jayatilaka, *CrystEngComm.* **2009**, *11*, 19.

[S2] I. D. Brown, *The Chemical Bond in Inorganic Chemistry*, IUCr Monographs in Crystallography, 12, Oxford University Press, **2002**.

[S3] A. A. A. Emara, G. J. Schrobilgen, *Inorg. Chem.* **1992**, *31*, 1323.

[S4] J. G. Malm, C. L. Chernick, *Inorg. Synth.* **1966**, *8*, 258.

[S5] J. L. Huston, *Inorg. Chem.* **1982**, *21*, 685.

[S6] APEX2, release v2014.9-0; Bruker AXS Inc.: Madison, WI, **1995**.

[S7] Sheldrick, G. M. SADABS (Siemens Area Detector Absorption Corrections), version 2.03; Siemens Analytical X-ray Instruments, Inc.: Madison, WI, **1999**.

[S8] Sheldrick, G. M. SHELXTL-Plus, release 5.1; Siemens Analytical X-ray Instruments, Inc.: Madison, WI, **1998**.

[S9] O. V. Dolomanov, L. J. Bourhis, R. J. Gildea, J. A. K. Howard, J. Puschmann, *J. Appl. Crystallogr*. **2009**, *42*, 339.

[S10] A. L. Spek, *J. Appl. Crystallogr*. **2003**, *36*, 7.

[S11] M. Gerken, D. A. Dixon, G. J. Schrobilgen, *Inorg. Chem*. **2000**, *39*, 4244.

[S12] Basis sets were obtained from the Extensible Computatuional Chemistry Environment Basis set Database, version 2/25/04, as developed and distributed by the Molecular Science Computing Facility, Environmental and Molecular Science Laboratory, which is part of the Pacific Northwest Laboratory, P.O. Box 999, Richland, WA, 99352.

[S13] M. J. Frisch, G. W. Trucks, H. B. Schlegel, G. E. Scuseria, M. A. Robb, J. R. Cheeseman, G. Scalmani, V. Barone, B. Mennucci, G. A. Petersson, H. Nakatsuji, M. Caricato, X. Li, H. P. Hratchian, A. F. Izmaylov, J. Bloino, G. Zheng, J. L.

Sonnenberg, M. Hada, M. Ehara, K. Toyota, R. Fukuda, J. Hasegawa, M. Ishida, T. Nakajima, Y. Honda, O. Kitao, H. Nakai, T. Vreven, J. A. Montgomery, J. E. Peralta, F. Ogliaro, M.. Bearpark, J. J. Heyd, E. Brothers, K. N. Kudin, V. N. Staroverov, R. Kobayashi, J. Normand, K. Raghavachari, A. Rendell, J. C. Burant, S. S. Iyengar, J. Tomasi, M. Cossi, N. Rega, N. J. Millam, M. Klene, J. E. Knox, J. B. Cross, V. Bakken, C. Adamo, J. Jaramillo, R. Gomperts, R. E. Stratmann, O. Yazyev, A. J. Austin, R. Cammi, C. Pomelli, J. W. Ochterski, R. L. Martin, K. Morokuma, V. G. Zakrzewski, G. A. Voth, P. Salvador, J. J. Dannenberg, S. Dapprich, A. Daniels, D. Farkas, J. Foresman, J. V. Ortiz, J. Cioslowski, D. J. Fox, Gaussian 09, Revision D.01; Gaussian, Inc: Wallingford, CT, **2009**.

[S14] GaussView, version 3.0; Gaussian Inc.: Pittsburgh, PA, **2003**.

[S15] NBO 6.0. Glendening, E. D.; Badenhoop, J. K.; Reed, A. E.; Carpenter, J. E.; Bohmann, J. A.; Morales, C. M.; Landis, C. R.; Weinhold, F. Theoretical Chemistry Institute, University of Wisconsin, Madison, **2013**.

[S16] Tonto: A Fortran Based Object-Oriented System for Quantum Chemistry and Crystallography, D. Jayatilaka and D. J. Grimwood, Computational Science - ICCS **2003**, *4*, 142.

[S17] Jmol, an open-source Java viewer for chemical structures in 3D (http://www.jmol.org/).

CHAPTER 5

Crown Ether and Cryptand Complexes with Xenon Trioxide

Abstract: *This work provides a series of crown ether complexes of* XeO_3 *following on the report of the first* XeO_3 *complex with a macrocyclic ligand, namely* $(CH_2CH_2O)_5XeO_3$ *discussed in Chapter 4. Reactions of crown ethers with HF acidified aqueous solutions of* XeO_3 *at room-temperature yielded adducts of 12-crown-4,* $(CH_2CH_2O)_4XeO_3$*, and 18-crown-6,* $[(CH_2CH_2O)_6XeO_3{\cdot}2H_2O]_2{\cdot}HF$*, whereas slow cooling of a solution of* XeO_3 *with 18-crown-6 in acetone yielded* $(CH_2CH_2O)_6XeO_3{\cdot}2H_2O$*. The adducts* $(CH_2CH_2O)_4XeO_3$ *and* $(CH_2CH_2O)_6XeO_3{\cdot}2H_2O$ *are shock-insensitive whereas the former adduct is air-stable at room temperature. The low-temperature, single-crystal X-ray structures show the Xe atom of* XeO_3 *coordinated to the oxygen atoms of the crown ether ring. Uncharacteristic xenon coordination numbers exceeding six (including the three primary bonds of* XeO_3*) were observed for all crown ether adducts. Raman spectroscopy frequency shifts are consistent with complex formation and provided evidence for the 2,2,1-cryptand adduct of* XeO_3*. Gas-phase Wiberg bond valences and indices and empirical solid-state bond valences confirmed the electrostatic nature of the Xe---O bonding interactions. Comparisons between the* XeO_3 *and* SbF_3 *18-crown-6, 15-crown-5, and 12-crown-4 complexes are made.*

5.1 Introduction

The 15-crown-5 adduct of XeO_3, $(CH_2CH_2O)_5XeO_3$, has recently been reported and provides the first example of a crown ether complex with a noble-gas compound.[1] The low-temperature, single-crystal X-ray structure revealed coordination of the Xe atom of XeO_3 to five oxygen atoms of the crown ether with bond distances that are significantly less than the sum of the xenon and oxygen van der Waals radii. The five Xe---O bonding interactions were shown to arise from electrostatic interactions between the highly electrophilic region of the Xe atom and the nucleophilic region of the ligand atom, and may be described in terms of σ-hole bonds. They provide the highest coordination number, eight, thus far encountered for the Xe atom of XeO_3.[1] In contrast, the large steric bulk of the $(C_6H_5)_3PO$ ligands in $[(C_6H_5)_3PO]_2XeO_3$ resulted in two Xe---O bonding interactions, providing the only example where the coordination number of the Xe atom is less than six.[2] A coordination number of six is observed in all nitrogen base adducts of XeO_3.[3] Coordination with adjacent XeO_3 molecules in $RCNXeO_3$ and $(RCN)_2XeO_3$ ($R = CH_3$, CH_2CH_3) occur to achieve this coordination number of six.[4]

The three known solid phases of XeO_3 are extensively cross-linked through intermolecular $O_3Xe{-}{-}{-}O_{(XeO3)}$ interactions.[5] These interactions provide a means to propagate the detonation shock wave front throughout the crystal lattice, yielding Xe and O_2 with the liberation of 402 ±8 kJ mol^{-1} of energy.[6] Xenon-ligand σ-bonding interactions Xe---LR (L = N, O, F) disrupt the extended $O_3Xe{-}{-}{-}O_{(XeO3)}$ networks and are partially responsible for the formation of kinetically stable adducts with XeO_3.[2] Unlike solid XeO_3, which readily detonates upon heating, mild friction, and, in some cases when left undisturbed,[7,8,9] solids that pack as discrete dimers or chains in which the XeO_3 molecules are well isolated do not detonate upon impact but undergo deflagration when exposed to a flame.[2] This dramatic range of kinetic stabilization reflects a significant difference among the crystal structure of XeO_3-containing compounds.

Crown ethers and cryptands are macrocyclic polyethers and macropolycyclic ligands, respectively, which preferentially coordinate to, or “trap”, spherical cations. The later ligand class possess three-dimensional cavities whereas crown ethers are two-dimensional.[10] Main-group Lewis acids of the type PnX_3 (Pn = As, Sb, Bi; X = F, Cl, Br, I) have been shown to form complexes with crown ethers.[11−14] Although complexes of cyrptands with main-group copmounds are much less prevalent, several cryptand complexes with group 13 and 14 compounds have been structurally characterized. Tin(II),[15] germanium(II),[16] gallium(I),[17] and gallium(III)[17] species all form stable complexes with 2,2,2-cryptand.

Herein, the synthesis and structural characterization of three novel crown ether XeO_3 adducts are reported, and spectroscopic evidence for a 2,2,1-crpytand adduct of XeO_3 is presented.

5.2 Results and Discussion

5.2.1 Synthesis

Reactions of crown ethers with acidified aqueous solutions of XeO_3 in HF at room-temperature yielded adducts of 18-crown-6, $[(CH_2CH_2O)_6XeO_3{\cdot}2H_2O]_2{\cdot}HF$ (**1**), and 12-crown-4, $(CH_2CH_2O)_4XeO_3$ (**3**). Slow evaporation of the solvent in a fume hood yielded crystals suitable for a single-crystal X-ray structure determination. Addition of a solution of XeO_3 in acetone to a solution of 18-crown-6 in acetone at –78 °C resulted in immediate (ca. 1 minute) precipitation of a white solid. Reduction of XeO_3 to Xe and O_2 gases was observed at temperatures between –60 and –30 °C under dynamic vacuum. Solvent removal at –78 °C afforded crystalline $(CH_2CH_2O)_6XeO_3{\cdot}2H_2O$ (**2**). Adduct (**3**) was also synthesized by addition of the corresponding liquid crown ether to a solution of XeO_3 in acetone at room temperature. Crystalline (**2**) and (**3**) did not detonate when mechanically shocked, but underwent deflagration when exposed to a flame. The shock sensitivity of $(CH_2CH_2O)_6XeO_3{\cdot}2H_2O$ (**2**) was not tested due to temperature sensitivity of the compound. Solid $[(CH_2CH_2O)_6XeO_3{\cdot}2H_2O]_2{\cdot}HF$ (**1**) was extremely shock-sensitive and samples of (**1**) frequently detonated before they were completely dried.

The addition of 2,2,2-cryptand or 2,2,1-cryptand to solid XeO_3, or XeO_3 in acetone, at room temperature resulted in violent detonations. The addition of 2,2,2-cryptand in acetone to a solution of XeO_3 in acetone at –78 °C immediatly resulted in precipitation of a white solid; however the sample detonated upon solvent removal under dynamic vacuum. The Raman spectrum of the white precipitate was recorded under a solvent layer but did not show vibrational bands corresponding to XeO_3.

The addition of a solution of 2,2,1-cryptand to a solution of XeO_3 in acetone at –78 °C gave a fine white precipitate. Decomposition of the solid was observed at –50 °C. The solvent was slowly removed under dynamic vacuum at –78 °C. The Raman spectrum of the white solid confirmed the formation of an adduct between XeO_3 and 2,2,1-crpytand; $[(CH_2CH_2O)_4(CH_2CH_2N)_2O]_nXeO_3$ (**4**). However, attempts to grow crystals suitable for an X-ray crystal structure determination were unsuccessful. Solid

$[(CH_2CH_2O)_4(CH_2CH_2N)_2O]_nXeO_3$ was extremely shock-sensitive and handling of the material frequently resulted in detonations.

5.2.2 X-ray Cyrstallography

The low-temperature single-crystal X-ray structures of $[(CH_2CH_2O)_6XeO_3{\cdot}2H_2O]_2{\cdot}HF$ (**1**), $(CH_2CH_2O)_6XeO_3{\cdot}2H_2O$ (**2**), and $(CH_2CH_2O)_4XeO_3$ (**3**) were determined and are depicted in Figure 5.1. A summary of crystal data and refinement results is provided in Table 5.1 and a summary of important geometrical parameters is given in Table 5.2 with more complete lists in Tables 5.6–5.8. The primary Xe–O bond lengths (1.754(7)–1.774(3) Å) and O–Xe–O bond angles (100.3(2)–102.4(1)°) in (**1**), (**2**), and (**3**) lie within the corresponding ranges of the three solid phases of XeO_3 (1.7558(11)–1.7801(11) Å and 100.51(5)−105.09(6)°).[5] The crystal structures of (**2**) and (**3**) contain isolated XeO_3 moieties that are well separated in the crystal lattice and do not form extended networks, therefore mitigating against the shock-sensitivity of coordinated XeO_3. Although (**1**) also contains well-isolated XeO_3 moieties, solvent evaporation form the crystal lattice is suspected to contribute to the instability of the solid. The adducts (**1**), (**2**) and (**3**) each have a total of four Xe---O secondary contacts resulting in total Xe coordination numbers of seven.

Table 5.1. Details of the data collection parameters and crystallographic information for $[(CH_2CH_2O)_6XeO_3{\cdot}2H_2O]_2{\cdot}HF$ **(1)**, $(CH_2CH_2O)_6XeO_3{\cdot}2H_2O$ **(2)**, and $(CH_2CH_2O)_4XeO_3$ **(3)**.

Compound	**(1)**	**(2)**	**(3)**
space group	$P2_12_12_1$	$P2_1/m$	$P2_1/c$
a (Å)	9.8195(3)	9.6019(16)	11.1329(15)
b (Å)	10.7022(2)	11.0079(18)	7.3575(10)
c (Å)	36.6649(9)	10.0140(17)	14.1421(18)
α (deg)	90	90	90
β (deg)	90	117.755(4)	89.981(2)
γ (deg)	90	90	90
V (Å^3)	3853.1(2)	936.7(3)	1158.4(3)
Z	8	2	1
mol. wt. (g mol^{-1})	355.50	399.55	978.37
calcd density (g cm^{-3})	2.038	1.911	1.687
T (K)	−173	−173	−173
μ (μμ^{-1})			1.85
$R_1{}^a$	0.0396	0.0436	0.0275
$wR_2{}^b$	0.0543	0.0486	0.0903

[a] $R_1 = \Sigma||F_o|-|F_c||/\Sigma|F_o|$. [b] $wR_2 = [\Sigma(w(F_o^2-F_c^2)^2)/\Sigma(w(F_o^2)^2)]^{½}$.

5.2.2.1 $[(CH_2CH_2O)_6XeO_3{\cdot}2H_2O]_2{\cdot}HF$ (1)

The crystal structure of $[(CH_2CH_2O)_6XeO_3{\cdot}2H_2O]_2{\cdot}HF$ (**1**) was solved in the orthorhombic space group $P2_12_12_1$ (Figure 5.1). The structural unit of (**1**) consists of two units of $(CH_2CH_2O)_6XeO_3{\cdot}H_2O$ that are hydrogen bridged by two additional water molecules and a HF molecule. Each XeO_3 molecule is coordinated to three oxygen atoms of the 18-crown-6 ring and one water molecule ($Xe_{(1)}$---OH_2 2.716(3); $Xe_{(2)}$---OH_2 2.704(3) Å). One $(CH_2CH_2O)_6XeO_3{\cdot}H_2O$ unit contains one short and two long $Xe_{(1)}$---O_{crown} contacts (2.844(4), 2.981(3), 2.982(3) Å). Twisting of the –CH_2–O(11)–CH_2– portion of the ring away from $Xe_{(1)}$ results in extension of the fourth secondary bond to give the other contributing structure, which has two short and one long $Xe_{(2)}$---O_{crown} secondary contacts (2.791(3), 2.806(3), 3.078(3) Å). The short $Xe_{(1)}$---O and $Xe_{(2)}$---O contacts have *trans*–O–Xe---O angles of 160.8(2), 168.9(2)° and 162.4(1), 164.9(1), 166.1(1)°, and the long $Xe_{(1)}$---O and $Xe_{(2)}$---O contacts have *trans*-O–Xe---O angles of 135.2(2), 148.1(2)°, and 130.2(1)°, respectively. The *cis*-O–Xe---O_{crown} angles ($Xe_{(1)}$ 75.4(1), 75.5(2), 78.6(2); $Xe_{(2)}$ 75.0(1), 76.0(1), 76.2(1)°) are much narrower than the *cis*-O–Xe---O_{water} angles ($Xe_{(1)}$ 81.3(2)°; $Xe_{(2)}$ 88.6(1)°). Both 18-crown-6 units contain H_2O molecules that are hydrogen bonded to oxygen atoms of the crown ether that are greater than the sum of the Xe and O van der Waals radii. The XeO_3 molecules of both contributors are slightly off center with respect to 18-crown-6 and the $Xe_{(1)}$ and $Xe_{(2)}$ atoms are positioned 2.225 and 2.091 Å below the plane defined by the oxygen atoms of 18-crown-6. The C−O−C−C torsion angles involving the oxygen atoms interacting with Xe are significantly different between the two units ($Xe_{(1)}$, C3–O8–C2–C1, –174.6(4); C1–O7–C12–C11, –178.3(3); C10–O12–C11–C12, 176.4(3), and $Xe_{(2)}$, C15–O15–C14–C13, –161.9(4); C13–O14–C24–C23, –178.32(4); C22–O19–C23–C24, –159.3(4)).

The empirical bond valence method of I. D. Brown[18] was used to asses which Xe---O contacts make significant contributions to the total bond valence of xenon (Table 5.9) in (**1**). Inclusion of the shortest Xe---O contacts resulted in Xe bond valences below the expected value of 6 ($Xe_{(1)}$ 5.97, $Xe_{(2)}$ 5.88 v. u.), whereas inclusion of all Xe---O contacts below the sum of the O and Xe van der Waals radii gave values that are very close to the ideal bond value of 6 for Xe^{VI} ($Xe_{(1)}$ 6.03, $Xe_{(2)}$ 6.02 v. u.). The Xe---O bond valences, which span 0.054−0.149 v. u., are consistent with very weak covalent bonding between O and Xe, in accordance with experimental bond lengths (2.701−3.078 Å). These results, in combination with the bond valence analysis of $(CH_2CH_2O)_5XeO_3$, were used to assign a coordination number of seven to the Xe atom of XeO_3 in (**1**), (**2**), and (**3**).

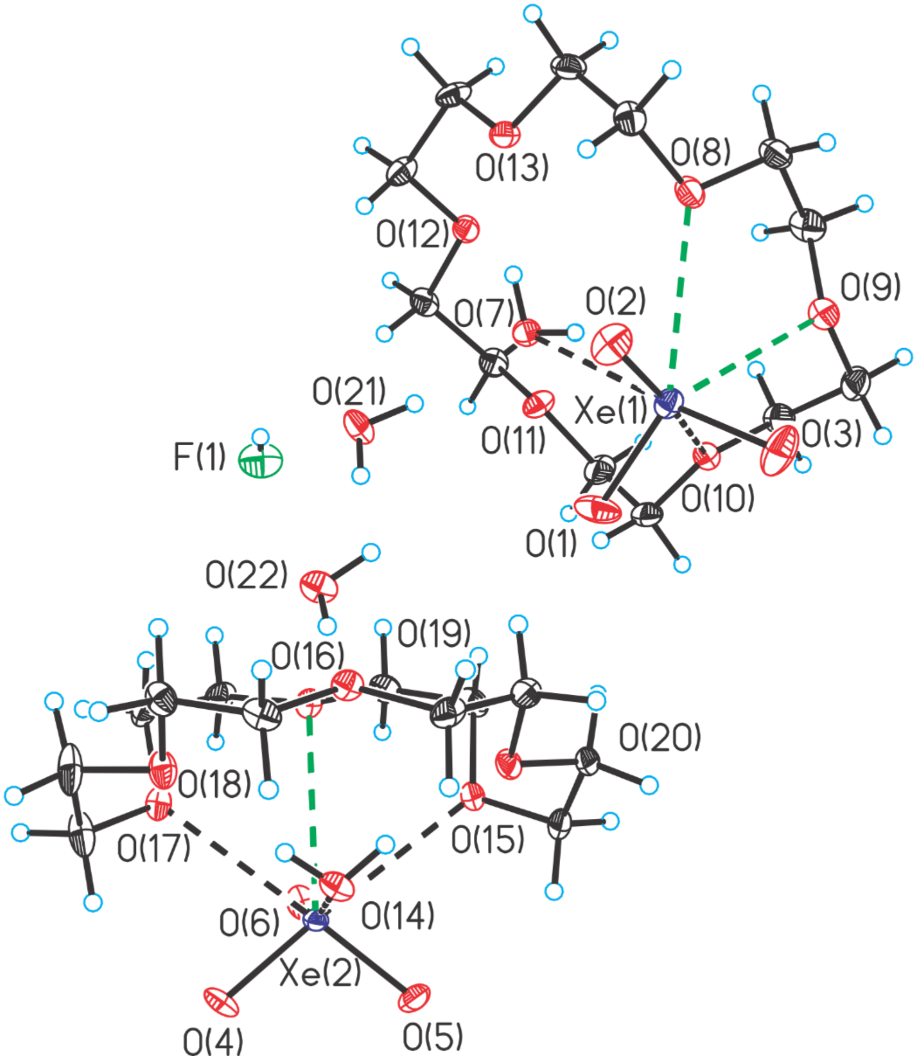

Figure 5.1. The low-temperature (asymmetric unit is shown) X-ray structure of $[(CH_2CH_2O)_6XeO_3{\cdot}2H_2O]_2{\cdot}HF$ (**1**); thermal ellipsoids are shown at their 50% probability levels and the longest Xe---O contacts are shown in green.

5.2.2.2 $(CH_2CH_2O)_6XeO_3{\cdot}2H_2O$ (2)

The crystal structure of $(CH_2CH_2O)_6XeO_3{\cdot}2H_2O$ (**2**) was solved in the monoclinic $P2_1/m$ space group (Figure 5.2). The coordination environment of XeO_3 in (**2**) is very similar to the environment of $Xe_{(2)}$ in (**1**); XeO_3 is coordinated to three oxygen atoms in 18-crown-6 and one molecule of water (Xe---OH_2, 2.702(1) Å; *trans*-O–Xe---O, 163.3(3); *cis*-O–Xe---O, 88.9(3)). The most notable difference between (**2**) and the $(CH_2CH_2O)_6XeO_3{\cdot}H_2O$ unit in (**1**) is the pseudo-mirror plane that bisects (**2**), resulting in two identical short Xe---O_{crown} bonds (2.839(7) Å; *trans*-O–Xe---O, 164.9(3); *cis*-O–Xe---O, 75.2(3)) and one long Xe----O_{crown} bonds (3.093(7) Å; *trans*-O–Xe---O, 129.3(3); *cis*-O–Xe---O, 78.8(3)). The XeO_3 molecule is slightly off center and positioned 2.110 Å below the plane defined by the oxygen atoms of 18-crown-6.

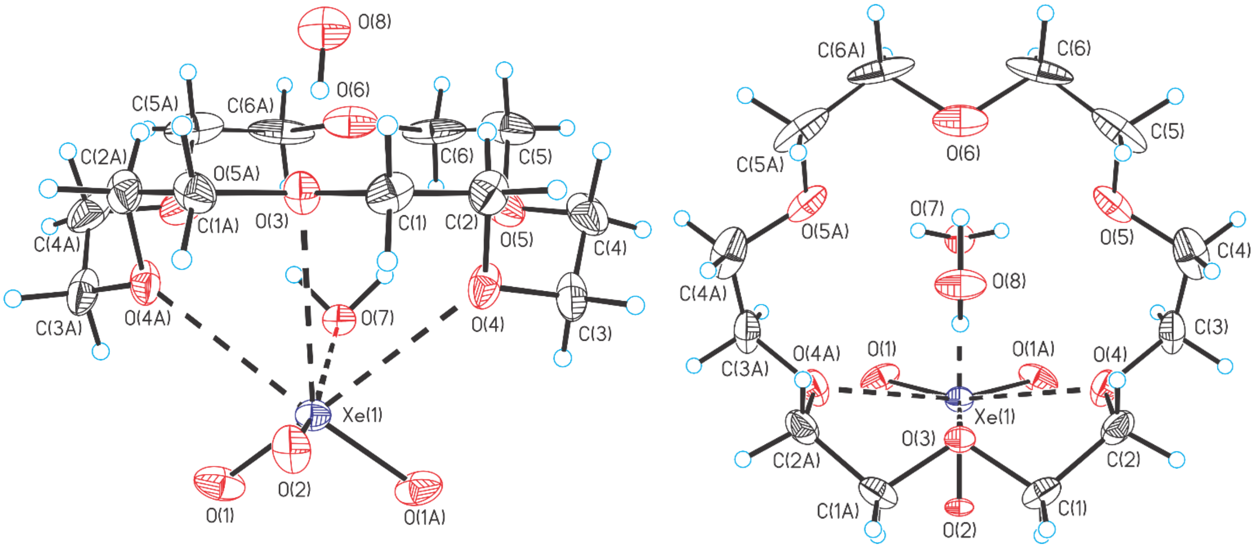

Figure 5.2. Views of the low-temperature, single-crystal X-ray structure of $(CH_2CH_2O)_6XeO_3{\cdot}2H_2O$ (**2**); thermal ellipsoids are shown at their 50% probability levels and the longest Xe---O contacts are shown in green.

Hirshfeld surfaces were shown to be a useful tool for the visualization of close contacts and electron density within $(CH_2CH_2O)_5XeO_3$.[1] Hirshfeld surfaces of XeO_3 and 18-crown-6 in $(CH_2CH_2O)_6XeO_32H_2O$ were generated using CrystalExplorer3.1.[19] Four areas on the Hirshfeld surface of XeO_3 mapped with the d_{norm} function (Figure 5.3, left) are denoted in red and indicate the location of a contact which is shorter than the sum of the Xe and ligand O van der Waals radii. The relative intensities of circular regions on the surfaces of $(CH_2CH_2O)_5XeO_3$ and (**2**) are consistent with similar Xe---O contact distances in both XeO_3 crown ether adducts. When the electrostatic potential (EP)[20] is mapped onto the Hirshfeld surface of 18-crown-6 (Figure 5.3, right), corresponding regions of negative EP (red) are visible on the surface of the nucleophilic oxygen atoms of the ligand. These regions are mirrored by regions of positive EP (blue) on the Hirshfeld surface of XeO_3. The $(CH_2CH_2O)_4XeO_3$ Hirshfeld surfaces were not mapped because the structure is disordered.

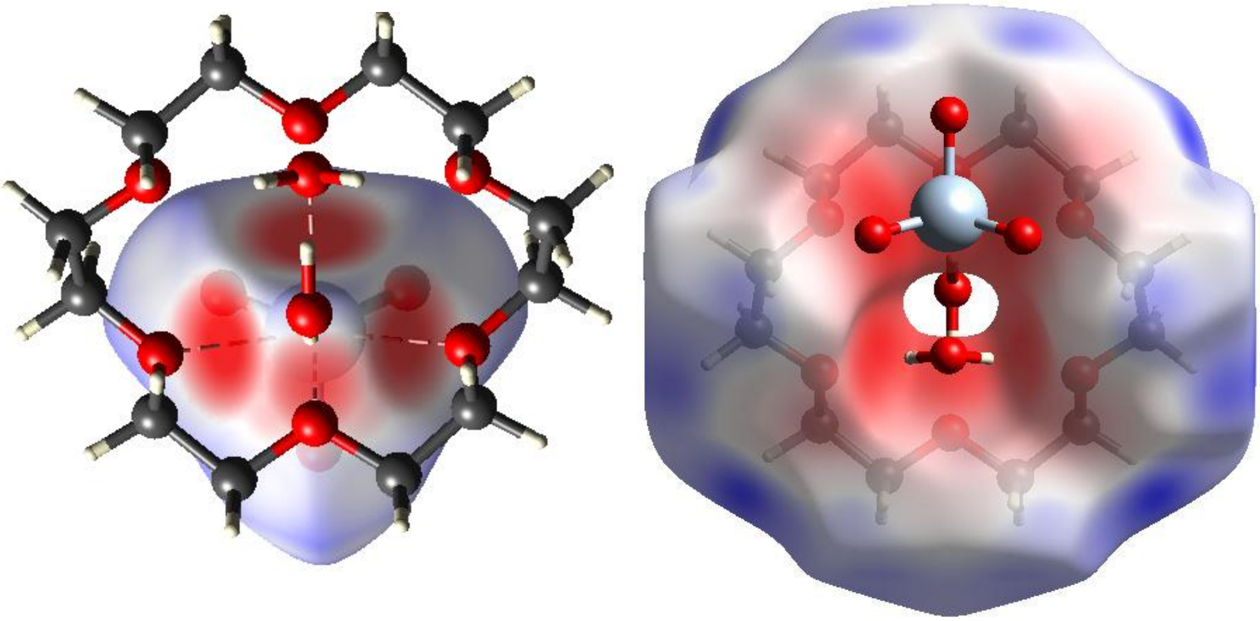

Figure 5.3. The Hirshfeld surfaces in $(CH_2CH_2O)_6XeO_32H_2O$ mapped with the d_{norm} function of XeO_3 (left) and electrostatic pontial surface (B88LYP/321-G) of 19-crown-6 (right).

The crystal structures of $(CH_2CH_2O)_4XeO_3$ (**3**) (Figure 5.4) and $(CH_2CH_2O)_5XeO_3$[1] contain isolated units of one molecule of XeO_3 coordinated to one molecule of the respective crown ether. Unlike adducts of XeO_3 with 18-crown-6, no water or solvent molecules are incorporated into the crystal lattice. The 12-crown-4 ring of (**3**) displays a 50:50 positional disorder. Similar to $(CH_2CH_2O)_5XeO_3$,[1] the structural unit of $(CH_2CH_2O)_4XeO_3$ (**3**) has two short Xe---O$_{\text{crown}}$ contacts (part 1: 2.761(6), 2.780(6) Å; part 2: 2.758(5), 2.779(6) Å). The two long Xe---O$_{\text{crown}}$ contacts (part 1: 2.945(5), 2.951(5) Å; part 2: 2.944(5), 2.955(5) Å) are comparable to the long Xe$_{(2)}$---O$_{\text{crown}}$ distances in (**1**). The *trans*-O–Xe---O and *cis*-O–Xe---O angles in part 1 and part 2 of (**3**) are identical (trans 131.7(1), 147.1(1), 152.5(1), 162.2(1)°; cis 74.1(1), 77.7(1), 78.7(1), 87.5(1)°). The XeO_3 molecule in (**3**) is slightly displaced away from O(9) and O(11) and toward O(5) and O(7) and is positioned 2.045 below the plane defined by the oxygen atoms of 12-crown-4.

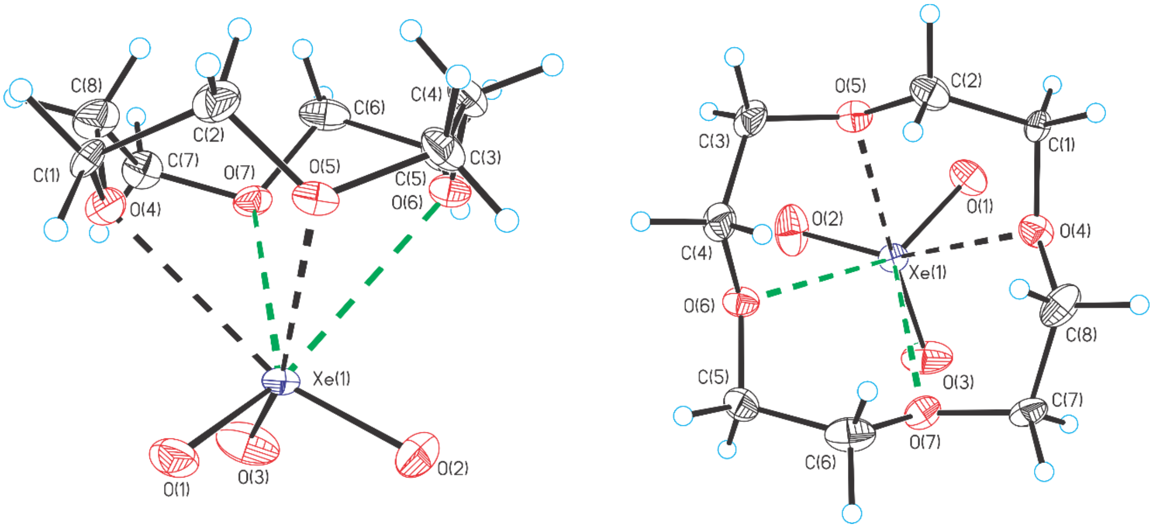

Figure 5.4. The low-temperature, single-crystal X-ray structures of $(CH_2CH_2O)_4XeO_3$ (**3**); thermal ellipsoids are shown at their 50% probability levels and the longest Xe---O contacts are shown in green.

Table 5.2. Selected bond lengths (Å), contact distances (Å), bond angles (deg), and contact angles (deg) for $[(CH_2CH_2O)_6XeO_3{\cdot}2H_2O]_2{\cdot}HF$ (**1**), $(CH_2CH_2O)_6XeO_3{\cdot}2H_2O$ (**2**), and $(CH_2CH_2O)_4XeO_3$ (**3**).

Compound	**(1)**		**(2)**	**(3)**	
	$Xe_{(1)}$	**$Xe_{(2)}$**		**Part 1**	**Part 2**
Xe---O	2.716(3)	2.704(3)	2.702(1)	2.780(6)	2.758(5)
	2.844(4)	2.791(3)	2.839(7)	2.761(6)	2.779(6)
	2.981(3)	2.806(3)	3.093(5)	2.951(5)	2.944(5)
	2.982(3)	3.078(3)		2.945(5)	2.955(5)
***trans*-O---Xe−O**	135.2(1)	130.3(1)	129.3(1)	131.7(1)	131.7(1)
	148.1(2)	162.4(1)	163.3(1)	147.1(1)	147.0(1)
	160.8(2)	164.9(1)	164.9(1)	152.5(1)	152.9(1)
	168.9(2)	166.1(1)		162.2(1)	161.8(1)
***cis*-O---Xe−O**	75.4(1)	74.9(1)	75.2(1)	74.1(1)	74.1(1)
	75.5(2)	76.1(1)	78.8(1)	77.7(1)	77.8(1)
	78.6(2)	76.3(1)	88.9(1)	78.7(1)	78.7(1)
	81.5(2)	88.6(1)		87.5(1)	87.4(1)
Xe−O	1.761(4)	1.762(4)	1.754(7)	1.759(2)	
	1.768(4)	1.769(3)	1.768(9)	1.760(2)	
	1.769(4)	1.774(3)		1.766(2)	
O–Xe–O	101.6(2)	102.0(2)	100.7(5)	100.9(1)	
	101.4(2)	100.3(2)	101.6(3)	100.9(1)	
	102.0(2)	102.1(2)		102.4(1)	

5.2.3 Raman Spectroscopy

A complete list of vibrational frequencies and assignments is provided for $(CH_2CH_2O)_6XeO_3{\cdot}2H_2O$ (**2**), $(CH_2CH_2O)_4XeO_3$ (**3**) and $[(CH_2CH_2O)_4(CH_2CH_2N)_2O]_n$-$XeO_3$ (**4**) in Tables 5.10–5.12 and their Raman spectra are depicted in Figures 5.5–5.7. The Raman spectrum of $(CH_2CH_2O)_4XeO_3$ was recorded in an aluminum sample holder in air at 20 °C, which also confirmed that the solid compounds are stable at room-temperature and insensitive to atmospheric moisture. The Raman spectra of $(CH_2CH_2O)XeO_3{\cdot}2H_2O$ and $[(CH_2CH_2O)_4(CH_2CH_2N)_2O]_nXeO_3$ were recorded in closed FEP reaction vessels at –78 °C because of the temperature sensitivities of the compounds. Raman spectral assignments were aided by comparison with the calculated vibrational frequencies and intensities of the energy-minimized gas-phase geometries of $(CH_2CH_2O)_6XeO_3{\cdot}2H_2O$ and $(CH_2CH_2O)_4XeO_3$, as well as with the previous assignments for aqueous XeO_3 and $(CH_2CH_2O)_5XeO_3$.[1] As previously shown for other adducts, complexation of XeO_3 by crown ethers and cryptands is indicated by a shift of the most intense band, $\nu_1(A_1)$, to lower frequency.[1–4] A summary of observed Raman frequencies for the vibrational modes of XeO_3 in (**2**), (**3**), and (**4**) is provided in Table 5.3. No obvious trends that correlate with the number of bonding interactions and Xe–O stretching frequencies were observed.

Table 5.3. Observed Raman frequencies[a] for the vibrational modes of XeO_3 in $(CH_2CH_2O)_6XeO_3{\cdot}2H_2O$ (**2**), $(CH_2CH_2O)_4XeO_3$ (**3**) and $[(CH_2CH_2O)_4(CH_2CH_2N)_2O]_n$-$XeO_3$ (**4**).

	(2)	**(3)**	**(4)**
E, $\nu_{as}(XeO_3)$	829 866	821 830 846	820 828
A_1, $\nu_{sym}(XeO_3)$	776	765	771
A_1, $\delta_{umb}(XeO_3)$	348	369 340	349
E, $\delta_{as}(XeO_3)$	317 310	311 304	319 306

[a] Frequencies are given in cm^{-1}.

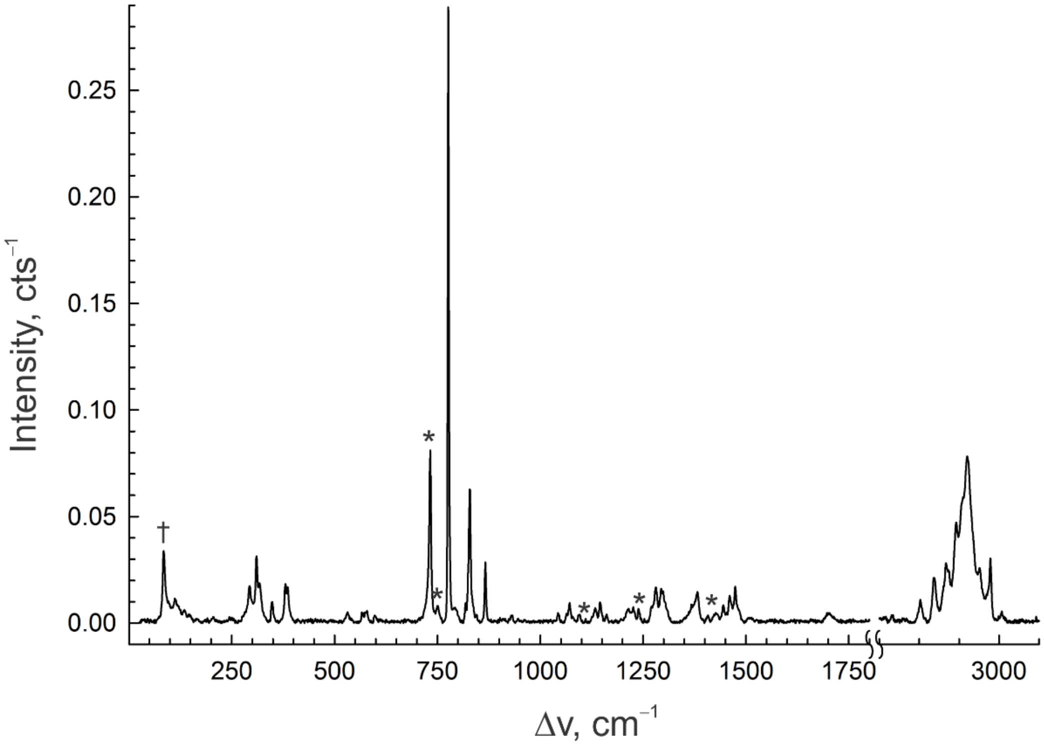

Figure 5.5. The Raman spectrum for $(CH_2CH_2)_6XeO_3{\cdot}2H_2O$ (**2**), recorded at −78 °C in a FEP sample tube using 1064-nm excitation. The symbol denotes an instrumental artifact (†).

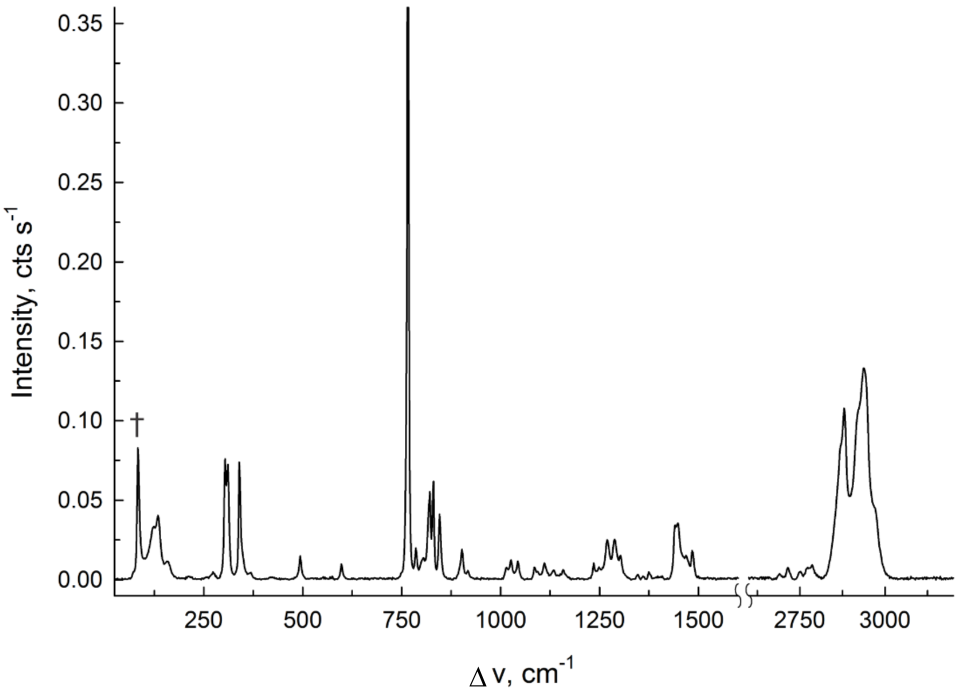

Figure 5.6. The Raman spectrum for $(CH_2CH_2)_4XeO_3$(**3**), recorded at room temperature in an aluminum sample holder using 1064-nm excitation. The symbol denotes an instrumental artifact (†).

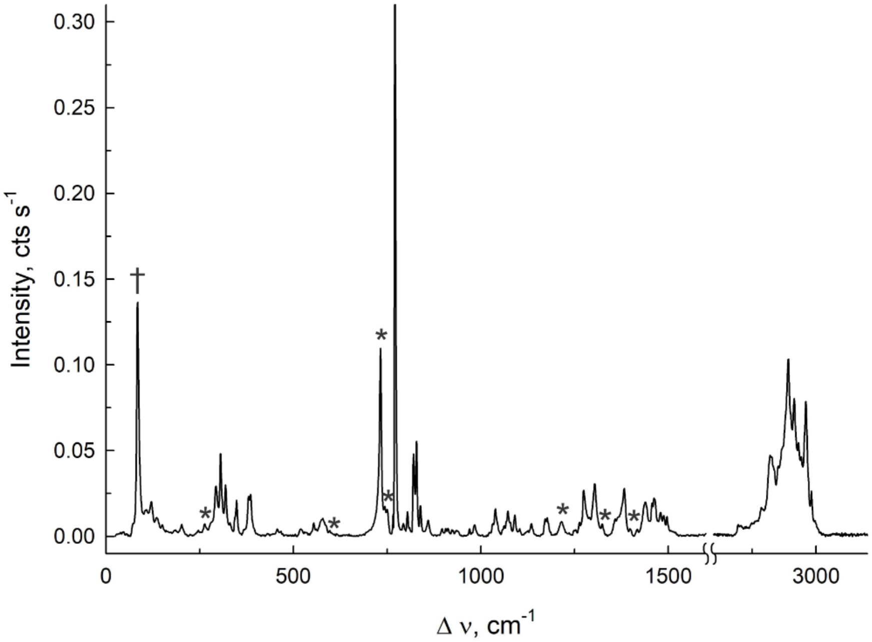

Figure 5.7. The Raman spectrum for $[(CH_2CH_2O)_4(CH_2CH_2N)_2O]_nXeO_3$ (**4**) recorded at −78 °C in a FEP sample vessel using 1064-nm excitation. The symbol denotes an instrumental artifact (†).

5.2.4 Quantum Chemical Calculations

As shown with $(CH_2CH_2O)_5XeO_3$,[1] gas-phase optimization of crown ether XeO_3 adducts are most accurate at the APFD/Def2-TZVPD level. The energy-minimized geometries, with all frequencies real, were calculated for $(CH_2CH_2O)_6XeO_3{\cdot}2H_2O$ (C_s symmetry; Figure 5.8), $(CH_2CH_2O)_4XeO_3$ (C_1 symmetry; Figure 5.9), $(CH_2CH_2O)_6SbF_3$ (C_s symmetry; Figure 5.8), $(CH_2CH_2O)_5SbF_3$ (Figure 5.13; C_1 symmetry), and $(CH_2CH_2O)_4SbF_3$ (Figure 5.9; C_1 symmetry). No attempts were made to optimize $[(CH_2CH_2O)_6XeO_3{\cdot}2H_2O]_2{\cdot}HF$. The gas-phase optimized structure of (**2**) slightly overestimates the Xe–O primary bond lengths (1.763 and 1.772 Å) and one of the Xe---O secondary bonds (2.873 Å) (Table 5.7). The other Xe---O bonding interaction (2.708 Å) is in very good agreement with the experimental bond length (2.701 Å).

The coordinates for part 1 of $(CH_2CH_2O)_4XeO_3$ were used for optimization. The XeO_3 molecule contains three equivalent Xe–O primary bonds that are overestimated compared to the experimental bond lengths. Unlike the experimental structure, which contains two shorter and two longer Xe---O contacts, the gas-phase optimized structure contains one short, one intermediate length, and two longer Xe---O contacts. The shortest Xe---O contact is trans to a Xe–O bond and has a *trans*-O–Xe---O angle of 163°. All other *trans*-O–Xe---O angles are less than 145°. The differences between the bonding environment of calculated and experimental structures may aris from the twofold disorder of 12-crown-4 ligand in the crystal structure.

The Xe–O and Xe---O Wiberg bond indices (Tables 5.13, 5.14) are consistent with the empirical bond valences calculated using the empirical method of I. D. Brown.[18] The Xe–

O Wiberg bond indices decrease upon coordination to a crown ether. The Xe---O Wiberg bond indices span 0.006−0.047 and are consistent with very weak covalent, essentially electrostatic, bonding between O and Xe, in accordance with experimental bond lengths (2.702−3.124 Å). The Wiberg valences of Xe (free, 3.379; adducted, 3.343 (**2**) and 3.355 (**3**)) and O_{XeO_3} (free, av. 1.537; adducted, av. 1.476 (**2**) and 1.486 (**3**)) significantly decrease upon coordination. The NPA charges are consistent with the enhanced polar covalent character of the Xe–O bonds that results from coordination. The Xe and O_{XeO_3} charges increase and decrease, respectively, upon coordination to a crown ether. The NPA charge of the Xe atom in $(CH_2CH_2O)_6XeO_3{\cdot}2H_2O$ and $(CH_2CH_2O)_4XeO_3$ is significantly more positive than that of free XeO_3 (free, 2.758; adducted, av. 2.913 (**2**) and 2.877 (**3**)) and is less than the average charges for the pure covalent (0) and ionic models (+6). The O_{XeO_3} atom charges are significantly more negative than those of XeO_3 (free, −0.920; adducted, av. –0.994 (**2**) and –0.967 (**3**)). The atomic charges and bond indices are consistent with essentially electrostatic, σ-hole bonding interactions between XeO_3 and the crown ether. Both experimental and gas-phase studies are consistent with the formation of four weakly covalent (essentially electrostatic) Xe---O interactions (**2**) and (**3**), in addition to the three polar-covalent Xe–O bonding interactions, resulting in a total Xe coordination numbers of sevevn and a Xe bond valence that is close to six.

5.2.5 Comparison of XeO_3 and SbF_3 Crown Ether Adducts

Unlike $[(CH_2CH_2O)_6XeO_3H_2O]_2{\cdot}HF$ and $(CH_2CH_2O)_6XeO_3{\cdot}2H_2O$, the crystal structure of $(CH_2CH_2O)_6SbF_3$ contains six Sb---O (2.975(2)–3.214(2) Å)[14] bonding interactions between the Sb atom of SbF_3 and the oxygen atoms of the crown ether ring.

The coordinates of 18-crown-6 and XeO_3 in $(CH_2CH_2O)_6XeO_3{\cdot}2H_2O$ were used for gas-phase optimizations of $(CH_2CH_2O)_6XeO_3$ and $(CH_2CH_2O)_6SbF_3$. The structure of $(CH_2CH_2O)_6XeO_3$ (Figure 5.13) contains three Xe---O bonding interactions (2.870–3.144 Å) and is not significantly distorted from the starting geometry despite the absence of the OH_2---XeO_3 contacts. However, the structure of $(CH_2CH_2O)_6SbF_3$ (Figure 5.8) is slightly distorted from the starting geometry and contains six Sb---O (2.865–3.625 Å) bonding interactions that are less than the sum of the Sb and O van der Waals radii (3.98 Å),[21] closely resembling the experimental structure.

The X-ray crystal structure of the 12-crown-4 adduct of SbF_3, $(CH_2CH_2O)_4Sb_2F_6$,[14] contains poisitional disorder of the crown ether ring that is similar to the crystal structure of (**3**). The SbF_3 molecule in the gas-phase structure of $(CH_2CH_2O)_4SbF_3$ (Figure 5.9) is significantly twisted away from the plane defined by the oxygen atoms of the crown ring, resembling the crystal structure of $(CH_2CH_2O)_4Sb_2F_6$, indicating an added tendency for a weak Sb---F_{SbF_3} bonding interaction in addition to its Sb---O (2.844–3.386 Å)[14] bonding interactions. The gas-phase geometry of $(CH_2CH_2O)_5SbF_3$ (Figure 5.13) is similar to that of $(CH_2CH_2O)_5XeO_3$ and contains five Sb---O bonding interactions (3.018–3.304 Å).

The calculated binding energies of the 18-crown-6, 15-crown-5, and 12-crown-4 adducts of XeO_3 and SbF_3 are provided in Tables 5.4 and 5.5 respectively. The binding energy of $(CH_2CH_2O)_4XeO_3$ is similar to $(CH_2CH_2O)_5XeO_3$ but slightly smaller, which is in accordance with fewer Xe---O bonding interactions. Although $(CH_2CH_2O)_6XeO_3{\cdot}2H_2O$ and $(CH_2CH_2O)_4XeO_3$ have the same number of Xe---O bonds, the binding energy of the hydrate is approximately twice that of $(CH_2CH_2O)_4XeO_3$ and reflects the energy required for hydrogen bonding with two H_2O molecules. The formation of all adducts is spontaneous and exothermic at room temperature. Although the binding energies, enthalpies, and Gibbs free energies of formation of the crown ether SbF_3 adducts are less, similar trends are ed.

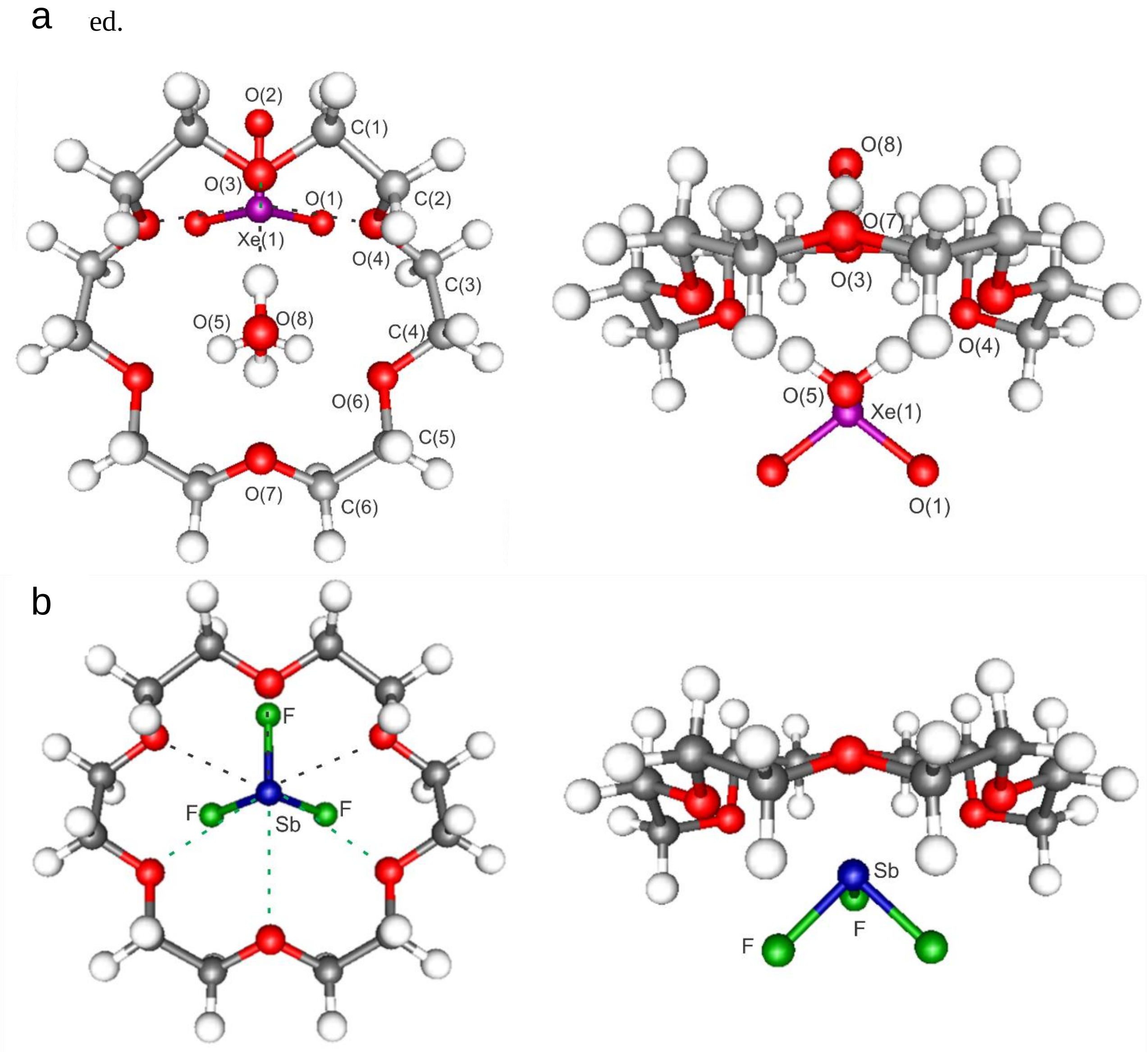

Figure 5.8. The top-on (left) and side-on (right) views of the calculated (APFD/Def2/TZVP) gas-phase structures of (**a**) $(CH_2CH_2O)_6XeO_3 \cdot 2H_2O$, and (**b**) $(CH_2CH_2O)_6SbF_3$. The longest Xe---O and Sb---O contacts are shown in green.

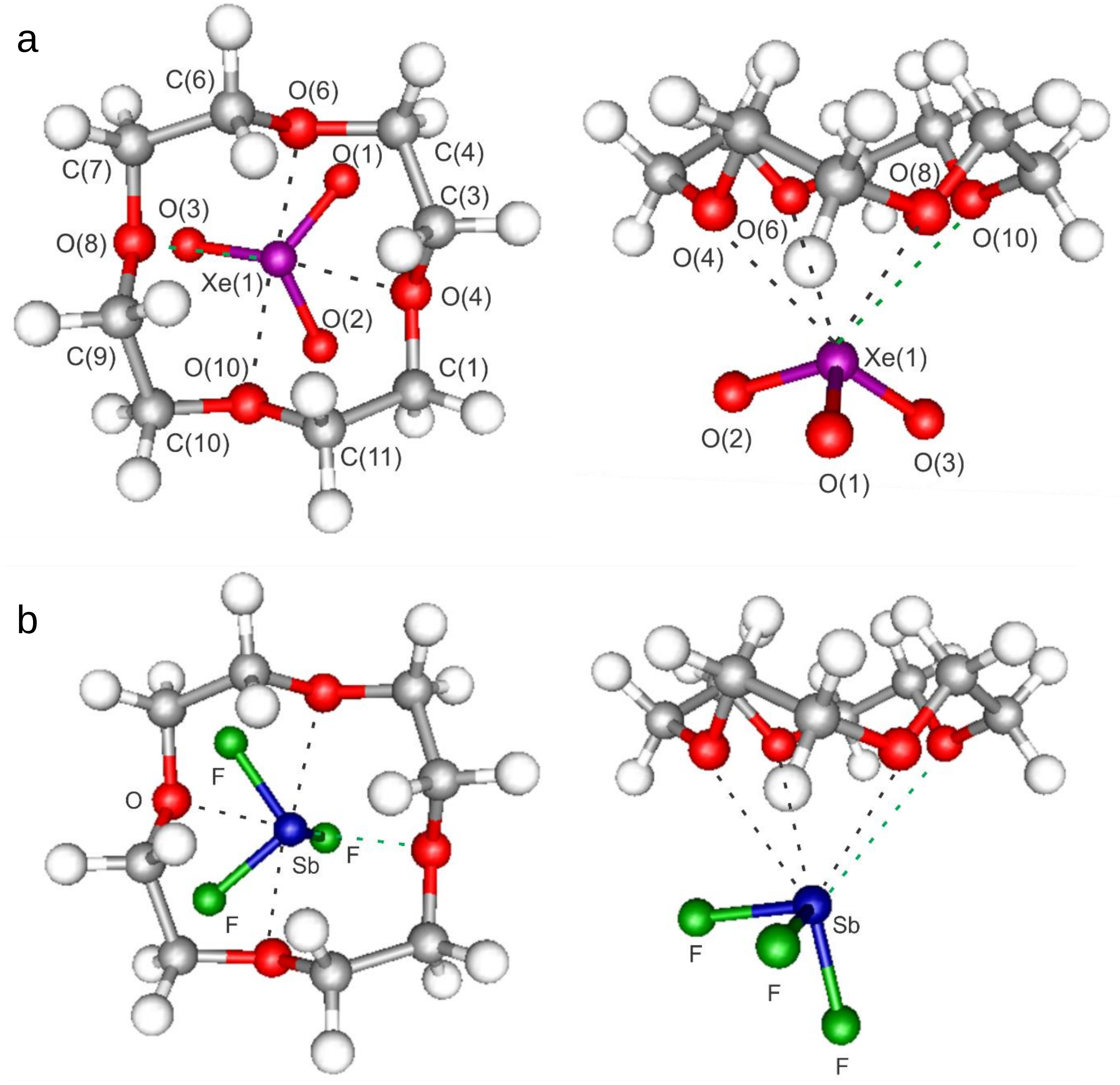

Figure 5.9. The top-on (left) and side-on (right) views of the calculated (APFD/Def2-TZVP) gas-phase structures of (**a**) $(CH_2CH_2O)_4XeO_3$ and (**b**) $(CH_2CH_2O)_4XeO_3$. The longest Xe---O and Sb---O contacts are shown in green.

Table 5.4. Calculated binding energies, ΔH_f^o and ΔG_f^o for $(CH_2CH_2O)_5XeO_3$, $(CH_2CH_2O)_6XeO_3{\cdot}2H_2O$, and $(CH_2CH_2O)_4XeO_3$.

	$(CH_2CH_2O)_6XeO_3{\cdot}2H_2O$	**$(CH_2CH_2O)_5XeO_3$**	**$(CH_2CH_2O)_4XeO_3$**
Binding energy (kJ mol^{-1})	–259.37	–150.00	–127.12
ΔH_f^o	–152.66	–143.01	–121.23
ΔG_f^o	–88.45	–85.95	–69.54

Table 5.5. Calculated binding energies, ΔH_f^o and ΔG_f^o for $(CH_2CH_2O)_5SbF_3$, $(CH_2CH_2O)_6SbF_3$, and $(CH_2CH_2O)_4SbF_3$.

	$(CH_2CH_2O)_6SbF_3$	**$(CH_2CH_2O)_5SbF_3$**	**$(CH_2CH_2O)_4SbF_3$**
Binding energy (kJ mol^{-1})	–132.35	–107.46	–92.75
ΔH_f^o	–128.68	–102.75	–85.29
ΔG_f^o	–72.47	–53.95	–35.68

5.3 Conclusion

This work completes a series of the first crown ether complexes of XeO_3 and of a noble-gas compound. Adducts of XeO_3 with 18-crown-6, 12-crown-4, and 2,2,1-cryptand were synthesized and characterized by Raman spectroscopy and/or low-temperature single-crystal X-ray diffraction. The adducts $(CH_2CH_2O)_4XeO_3$ and $(CH_2CH_2O)_6XeO_3{\cdot}2H_2O$ are shock-insensitive and $(CH_2CH_2O)_4XeO_3$ and $[(CH_2CH_2O)_6XeO_3H_2O]_2{\cdot}HF$ are stable in air at room-temperature. Uncharacteristic xenon coordination numbers exceeding six (with inclusion of the three primary bonds of XeO_3) were observed for all crown ether adducts.

Shifts in the XeO_3 vibrational frequencies of adducted XeO_3 are consistent with complex formation and provided evidence for the 2,2,1-cryptand adduct of XeO_3. Gas-phase Wiberg bond valences and indices and the empirical solid-state bond valences of I. D. Brown confirmed the electrostatic nature of the Xe---O bonding interactions. The crown ether adducts of XeO_3 are similar to those of SbF_3 with the formation of the adduct series occuring spontaneously and exothermically and room temperature.

Experimental Section

Caution! *Solid XeO_3 detonates when subjected to mild thermal or mechanical shock. Great care must be taken during the syntheses and handling of XeO_3 and the compounds described herein. For these reasons, the quantity of XeO_3 used in each synthesis has been restricted to 10–20 mg. Reaction vessels fabricated from FEP (hexafluoropropylene-tetrafluoroethylenecopolymer) fluoroplastic, which is inert to attack by HF, strong oxidants and fluorinating agents, and generally does not shatter to produce sharp shards when a detonation occurs at the reagent scales described in this study. Appropriate protective equipment (face shield, leather gloves, ear protection) must be used.*

Apparatus and Materials.

Anhydrous HF (Harshaw Chemicals Co.) was purified as previously described.[22] Xenon hexafluoride was prepared by the reaction of Xe (99.995%, Air Products and Chemicals, Inc.) and F_2 (98+%, Air Products and Chemicals, Inc.) similar to the method described by Malm and Chernick.[23] Small amounts of XeF_4 impurity, identified by two strong peaks at 502 and 543 cm^{-1} in the Raman spectrum, also formed XeO_3 when hydrolyzed[24] and therefore did not interfere with the synthesis of XeO_3.

An aqueous solution of XeO_3 was synthesized by hydrolysis of XeF_6 as previously described.[5]

(a) $[(CH_2CH_2O)_6XeO_3{\cdot}H_2O]_2{\cdot}H_2O{\cdot}HF$ (**1**): An aliquot (containing ca. 10 mg, 0.056 mmol XeO_3) of the resulting aqueous solution, $XeO_3{\cdot}6HF_{(aq)}$, was transferred into a 3 × 3 cm FEP (hexafluoropropylene, tetrafluoroethylene copolymer) fluoroplastic tray by use of a pipette fabricated from FEP tubing. One equivalent of 18-crown-6 (14.80 mg, 0.056 mmol) in 0.5 μL of H_2O was added. Evaporation of $HF_{(aq)}$ and water (ca. 36 h.) in a fume hood afforded crystals of $[(CH_2CH_2O)_6XeO_3{\cdot}2H_2O]_2{\cdot}HF$. Unlike the crystal growths of (**2**) and (**3**), additional drying in a plastic desiccator to remove residual moisture always resulted in detonation of the solid. A crystal was however obtained from a sample that contained low levels of residual moisture. The bulk sample detonated within 30 min. after removal of a suitable crystal.

(b) $(CH_2CH_2O)_6XeO_3{\cdot}2H_2O$ (**2**): An aliquot (ca. 7.3 mg, 0.041 mmol XeO_3) of the resulting aqueous solution, $XeO_3{\cdot}6HF_{(aq)}$, was pipetted into a FEP tray by use of an FEP pipette. Water and HF were removed from XeO_3 by evaporation overnight in a fume hood to give solid XeO_3. The sample was transferred to a plastic (HDPE) desiccator and dried over 4 Å molecular sieves for 2−3 h to ensure that all surface water had been removed from $XeO_{3(s)}$. Careful dissolution of $XeO_{3(s)}$ in dry acetone (1 mL) gave a clear, colorless solution. The solution was transferred to a reactor constructed from FEP and slowly cooled to –78 ^{o}C to avoid detonation that thermal shock may result from. Half a molar equivalent of 18-crown-6 (0.051 mg, 0.020 mmol) in 0.5 μL of acetone was carefully layered on top of the XeO_3 solution at –78 ^{o}C, which immediately yielded a precipitate of

$(CH_2CH_2O)_6XeO_3{\cdot}2H_2O$. Solvent removal under dynamic vacuum at –78 °C gave crystalline $(CH_2CH_2O)_6XeO_3{\cdot}2H_2O$.

(c) $(CH_2CH_2O)_4XeO_3$ (3): An aliquot (ca. 10 mg, 0.056 mmol XeO_3) of the resulting aqueous solution, $XeO_3{\cdot}6HF_{(aq)}$, was pipetted into a FEP tray by use of a FEP pipette. Water and HF were removed from XeO_3 by evaporation overnight in a fume hood to give solid XeO_3. The sample was transferred to a plastic (HDPE) desiccator and dried over 4 Å molecular sieves for 2−3 h to ensure that all surface water had been removed from $XeO_{3(s)}$. Careful dissolution of $XeO_{3(s)}$ in dry acetone (1 mL) gave a clear, colorless solution. Liquid 12-crown-4 (11.1 μL, 0.056 mmol) was pipetted onto the surface of the XeO_3 solution. Evaporation of the solvent in a fume hood (ca. 1 h) yielded colorless, block-shaped crystals of $(CH_2CH_2O)_4XeO_3$ that were used for an X-ray crystal structure determination.

The following alternative synthetic route is preferred because it avoids the isolation of solid XeO_3 and is therefore significantly less hazardous. After transferring an aliquot of $XeO_3{\cdot}6HF_{(aq)}$ (ca. 10 mg, 0.056 mmol XeO_3) to an FEP tray, one equivalent of liquid 12-crown-4 (11.0 μL, 0.056 mmol) was added. Evaporation of $HF_{(aq)}$ (ca. 36 h) in a fume hood followed by further drying in a desiccator (2-3 h) to remove residual moisture afforded $(CH_2CH_2O)_4XeO_3$ crystals that were suitable for a single crystal X-ray structure determination. The shock sensitivity of $(CH_2CH_2O)_4XeO_3$ was tested at room temperature by striking several crystals with a steel hammer which did not result in detonations.

(d) $[(CH_2CH_2O)_4(CH_2CH_2N)_2O]_nXeO_3$ (4): An aliquot (ca. 10 mg, 0.056 mmol XeO_3) of $XeO_3{\cdot}6HF_{(aq)}$ was transferred into a FEP tray by use of a FEP pipette. Water and HF were removed from XeO_3 by evaporation overnight in a fume hood to give solid XeO_3. The sample was transferred to a plastic (HDPE) desiccator and dried over 4 Å molecular sieves for 2−3 h to ensure that all surface water had been removed from $XeO_{3(s)}$. Careful dissolution of $XeO_{3(s)}$ in dry acetone (1 mL) gave a clear, colorless solution. The solution was transferred to a reactor constructed from FEP and slowly cooled to –78 °C to avoid detonation that may result from thermal shock. One equivalent of 2,2,1-cryptand (18.91 mg, 0.057 mmol) in 0.5 μL of acetone was carefully layered on top of the XeO_3 solution at –78 °C immediately giving a precipitate of $[(CH_2CH_2O)_4(CH_2CH_2N)_2O]_nXeO_3$. Solvent removal under dynamic vacuum at –78 °C gave powder $[(CH_2CH_2O)_4(CH_2CH_2N)_2O]_nXeO_3$. All attempts to crystallize $[(CH_2CH_2O)_4$-$(CH_2CH_2N)_2O]_nXeO_3$ were unsuccessful and handling of the solid frequently resulted in detonations.

X-ray Crystallography. *(a) Crystal Mounting.* Single-crystals of (**2**) were mounted on an X-ray diffractometer at low-temperatures using a previously described procedure.[25] Samples which contained isolated dry crystals were mounted by carefully pouring the crystals into a ¾-in. FEP cold trough held at −80 ±5 °C. While still inside the cold trough, the crystal was affixed to a nylon cryoloop (MiTeGen, Ithaca, NY; MicroMount;™ 100–500 μm) that had been dipped in an inert perfluorinated polyether. Single crystals of (**1**) and (**3**) were submerged in perfluoropolyether oil (Fomblin Z-25) in the open atmosphere and were selected at room temperature and mounted at the tip of a dual-thickness polymer loop using Halocarbon 25-5S grease (Halocarbon Products Corporation, River Edge, NJ).

(b) Collection and Reduction of X-ray data. Crystals were centered on a Bruker SMART APEX II diffractometer equipped with an APEX II 4K CCD area detector and a triple-axis

goniometer that was controlled by the APEX II Graphical User Interface (GUI) software.[26] A Bruker Triumph curved crystal monochromator was used with a Mo Kα ($\lambda = 0.71073$ Å) radiation source for all compounds. Diffraction data collection at −173 °C consisted of ω- and ϕ-scans collected at 0.5° intervals. The crystal-to-detector distance was 4.954 cm and data collection was carried out in a 512 x 512 pixel mode using 2 x 2 pixel binning. The raw data was processed by use of the APEX III GUI software.[26] The SADABS[27] program was used for scaling the diffraction data.

(c) Solution and Refinement of the Structures. The XPREP program[28] was used to confirm unit cell dimensions and the crystal lattice. All calculations were carried out using the SHELXTL-plus[28] and the Olex2[29] packages for structure determination, solution refinement, and molecular graphics. The $[(CH_2CH_2O)_6XeO_3H_2O]_2\cdot HF$ **(1b)** adduct was solved in the orthorhombic space group $P2_12_12_1$ whereas $(CH_2CH_2O)_6XeO_3\cdot 2H_2O$ was solved in the monoclinic space group $P2_1/m$. The positional disorder in $(CH_2CH_2O)_4XeO_3$ imposes a structure solution with a higher symmetry orthorhombic $P2_12_12_1$ space group. The disorder was properly modeled in the monoclinic $P2_1/c$ space group. The PLATON[30] program did not find additional symmetries. The final refinement was obtained by introducing anisotropic thermal parameters and the recommended weightings for all of the atoms except the hydrogen atoms. The H atoms were placed at locations derived from a difference map. The H atoms were included as riding contributions with isotropic displacement parameters that were 1.2 times those of the attached carbon atoms. The maximum electron density in the final difference Fourier map was located near the xenon atom.

Raman Spectroscopy. The Raman spectrum was recorded on a Bruker RFS 100 FT-Raman spectrometer using 1000 scans, 1064-nm excitation, 300 mW laser power, and ±0.5 cm^{-1} resolution as previously described.[25]

Computational Details. Density-functional theory (DFT) was employed to study the electronic structures of $(CH_2CH_2O)_6XeO_3{\cdot}2H_2O$ **(2)**, and $(CH_2CH_2O)_4XeO_3$ **(3)**, XeO_3, $(CH_2CH_2O)_6$, and $(CH_2CH_2O)_4$. All basis sets were obtained online from the EMSL Basis Set Exchange (https://bse.pnl.gov/bse/portal).[31] Quantum-chemical calculations were carried out using the program Gaussian 09[32] for geometry optimizations and to create wavefunction files. The GaussView[33] program was used to visualize the vibrational displacements that form the basis for the vibrational mode descriptions given in Tables 5.10–5.12. Natural bond orbital analyses were performed using APFD densities with the NBO program (version 6.0).[34] The CrystalExplorer 3.1[35] program was used for Hirshfeld surface analyses and the computational program Tonto,[36] as implemented in CrystalExplorer, was used for wavefunction calculations and for mapping of the electrostatic potential surface (B88LYP/321-G) onto the Hirshfeld surface.

References

[1] K. M. Marczenko, H. P. A. Mercier, G. J. Schrobilgen, *Angew. Chem. Int. Ed. Eng.*, **2018**, *57*, 12448–12452.

[2] K. M. Marczenko, J. T. Goettel, G. J. Schrobilgen, *Chem. Eur. J.*, Submitted Sept. **2018**.

[3] J. T. Goettel, H. P. A. Mercier, G. J. Schrobilgen, *J. Fluor. Chem.*, **2018**, *211*, 60.

[4] J. T. Goettel, K. Matsumoto, H. P. A. Mercier, G. J. Schrobilgen, *Angew. Chem. Int. Ed. Engl.* **2016**, *55*, 13780.

[5] J. T. Goettel, G. J. Schrobilgen, *Inorg. Chem.*, **2016**, 55, 12975.

[6] S. R. Gunn in Noble-Gas Compounds (Ed.: H. H. Hyman), University of Chicago Press, Chicago, IL, 1963, pp. 149–151.

[7] B. Jaselskis, J. P. Warriner, *Anal. Chem.* **1966**, *38*, 563.

[8] S. A. Shackelford, G. U. Yuen, *Inorg. Nucl. Chem. Lett.* **1973**, *9*, 605.

[9] L. A. Khamidullina, S. V. Lotnik, V. P. Kazakov, *Kinet. Catal.* **2008**, *49*, 27.

[10] A. Swidan, C. L. B. Macdonald, *Chem. Soc. Rev.*, **2016**, *45*, 3883.

[11] J. Lipkowski, M. S. Fonari, V. Ch. Kravtsov, Y. A. Simonov, E. V. Ganin, V. O. Gelmboldt, *J. Chem. Crystallogr.* **1996**, *26*, 823.

[12] M. Scharfer, J. Pebler, B. Borgsen, F. Weller, K. Dehnicke, *Z. Naturforsch.* **1990**, *45b*, 1243.

[13] N. W. Alcock, M. Ravindran, G. R. Willey, *Acta. Cryst.* **1993**, *B49*, 507.

[14] I. Becker, M. Windhaus, R. Mattes, *Z. Naturforsch*, **1994**, *49b*, 870.

[15] J. C. Avery, M. A. Hanson, R. H. Herber, K. J. Bladek, P. A. Rupar, I. Nowik, Y. Huang, K. M. Baines, *Inorganic Chemistry*, **2012**, *51*, 7306.

[16] P. A. Rupar, V. N. Staroverov, K. M. Baines, *Science*, **2008**, *322*, 1360.

[17] J. L. Bourque, P. D. Boyle, K. M. Baines, *Chem. Eur. J.*, **2015**, *21*, 9790.

[18] I.D. Brown, "The Chemical Bond in Inorganic Chemistry", IUCr Monographs in Crystallography **12,** 2002: Oxford University Press.

[19] [a]Crystal Explorer (Version 3.1), S. K. Wolff, D. J. Grimwood, J. J. McKinnon, M. J. Turner, D. Jayatilaka, M. A. Spackman, University of Western Australia, **2012**. [b]M. A. Spackman, J. J. McKinnon, D. Jayatilaka, *Cryst. Eng. Comm*. **2008**, *10*, 377. [c]J. J. McKinnon, D. Jayatilaka, M. A. Spackman, *Chem Commun.* **2007**, 3814.

[20] Tonto: A Fortran Based Object-Oriented System for Quantum Chemistry and Crystallography, D. Jayatilaka and D. J. Grimwood, Computational Science - ICCS 2003, *4*, 142.

[21] S. Alvarez, *Dalton Trans.* **2013**, *42*, 8617.

[22] A. A. A. Emara, G. J. Schrobilgen, *Inorg. Chem.* **1992**, *31*, 1323.

[23] J. G. Malm, C. L. Chernick, *Inorg. Synth.* **1966**, *8*, 258.

[24] J. L. Huston, *Inorg. Chem.* **1982**, *21*, 685.

[25] M. Gerken, D. A. Dixon, G. J. Schrobilgen, *Inorg. Chem*. **2000**, *39*, 4244.

[26] APEX2, release v2014.9-0; Bruker AXS Inc.: Madison, WI, **1995**.

[27] Sheldrick, G. M. SADABS (Siemens Area Detector Absorption Corrections), version 2.03; Siemens Analytical X-ray Instruments, Inc.: Madison, WI, **1999**.

[28] Sheldrick, G. M. SHELXTL-Plus, release 5.1; Siemens Analytical X-ray Instruments, Inc.: Madison, WI, **1998**.

[29] O. V. Dolomanov, L. J. Bourhis, R. J. Gildea, J. A. K. Howard, J. Puschmann, *J. Appl. Crystallogr*. **2009**, *42*, 339.

[30] A. L. Spek, *J. Appl. Crystallogr*. **2003**, *36*, 7.

[311] Basis sets were obtained from the Extensible Computatuional Chemistry Environment Basis set Database, version 2/25/04, as developed and distributed by the Molecular Science Computing Facility, Environmental and Molecular Science Laboratory, which is part of the Pacific Northwest Laboratory, P.O. Box 999, Richland, WA, 99352.

[32] M. J. Frisch, G. W. Trucks, H. B. Schlegel, G. E. Scuseria, M. A. Robb, J. R. Cheeseman, G. Scalmani, V. Barone, B. Mennucci, G. A. Petersson, H. Nakatsuji, M. Caricato, X. Li, H. P. Hratchian, A. F. Izmaylov, J. Bloino, G. Zheng, J. L. Sonnenberg, M. Hada, M. Ehara, K. Toyota, R. Fukuda, J. Hasegawa, M. Ishida, T. Nakajima, Y. Honda, O. Kitao, H. Nakai, T. Vreven, J. A. Montgomery, J. E. Peralta, F. Ogliaro, M.. Bearpark, J. J. Heyd, E. Brothers, K. N. Kudin, V. N. Staroverov, R. Kobayashi, J. Normand, K. Raghavachari, A. Rendell, J. C. Burant, S. S. Iyengar, J. Tomasi, M. Cossi, N. Rega, N. J. Millam, M. Klene, J. E. Knox, J. B. Cross, V. Bakken, C. Adamo, J. Jaramillo, R. Gomperts, R. E. Stratmann, O. Yazyev, A. J. Austin, R. Cammi, C. Pomelli, J. W. Ochterski, R. L. Martin, K. Morokuma, V. G. Zakrzewski, G. A. Voth, P. Salvador, J. J. Dannenberg, S. Dapprich, A. Daniels, D. Farkas, J. Foresman, J. V. Ortiz, J. Cioslowski, D. J. Fox, Gaussian 09, Revision D.01; Gaussian, Inc: Wallingford, CT, **2009**.

[33] GaussView, version 3.0; Gaussian Inc.: Pittsburgh, PA, **2003**.

[34] NBO 6.0. Glendening, E. D.; Badenhoop, J. K.; Reed, A. E.; Carpenter, J. E.; Bohmann, J. A.; Morales, C. M.; Landis, C. R.; Weinhold, F. Theoretical Chemistry Institute, University of Wisconsin, Madison, **2013**.

[35] Crystal Explorer (Version 3.1) S. K. Wolff, D. J. Grimwood, J. J. McKinnon, M. J. Turner, D. Jayatilaka, M. A. Spackman, University of Western Australia, **2012**.

[36] Tonto: A Fortran Based Object-Oriented System for Quantum Chemistry and Crystallography, D. Jayatilaka and D. J. Grimwood, Computational Science - ICCS **2003**, *4*, 142.

5.4 Supporting Information

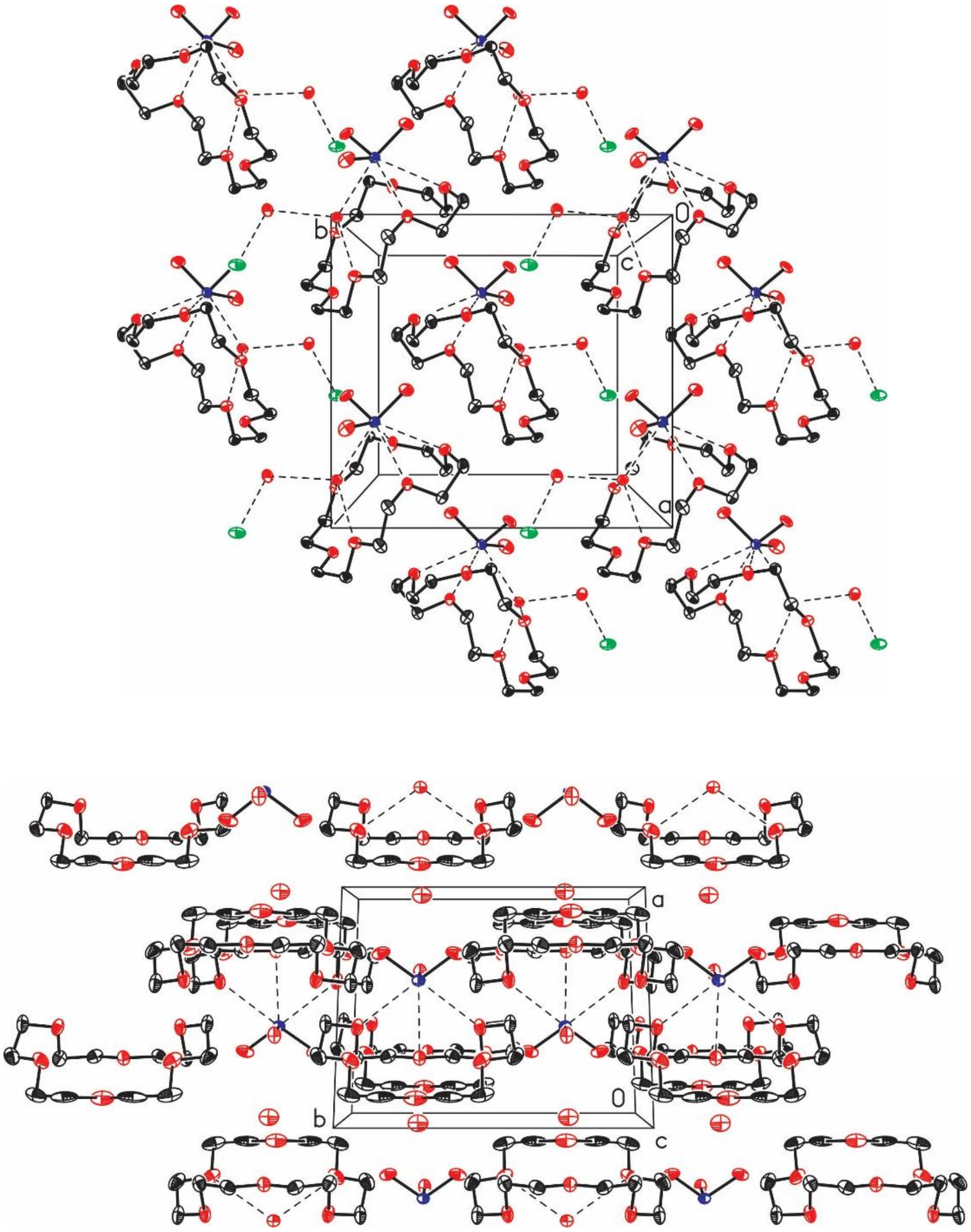

Figure 5.10. Packing diagram of $[(CH_2CH_2O)_6XeO_3{\cdot}2H_2O]_2HF$ **(1)** and $(CH_2CH_2O)_6XeO_3{\cdot}2H_2O$ (**2**); thermal ellipsoids are shown at their 50% probability levels and hydrogen atoms are omitted for clarity.

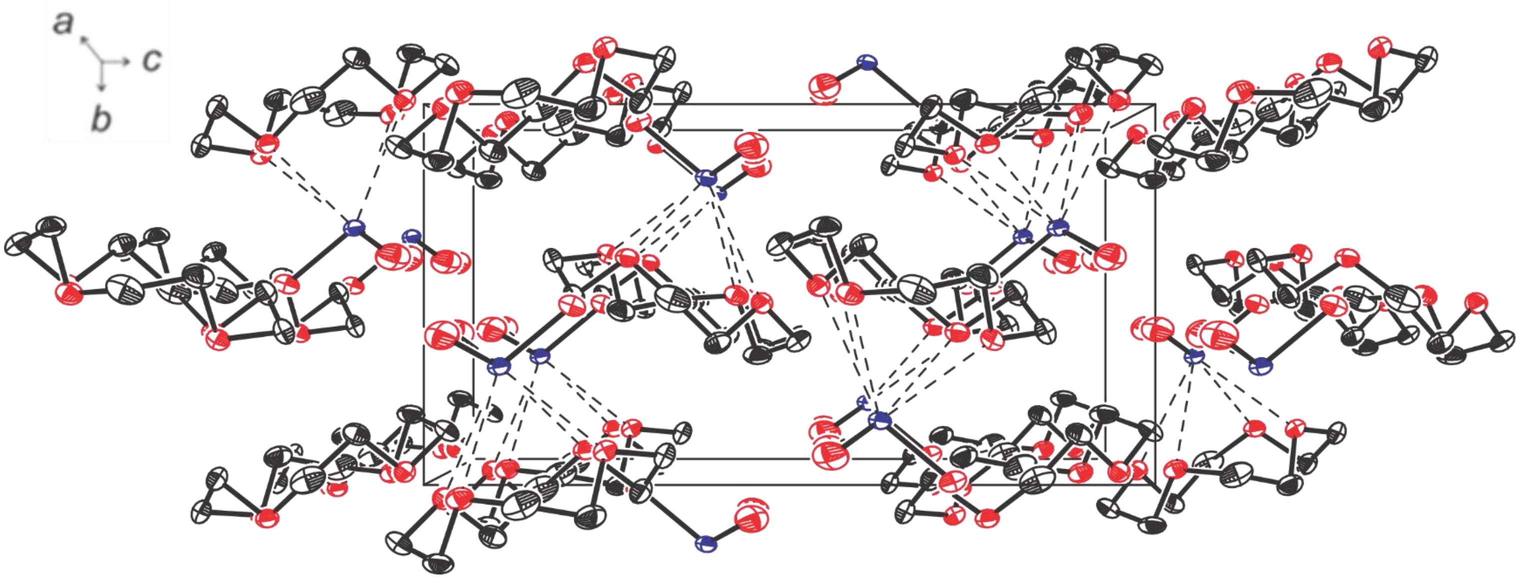

Figure 5.11. The crystal structure of $(CH_2CH_2)_4XeO_3$ (**3**); thermal ellipsoids are shown at their 50% probability levels and hydrogen atoms are omitted for clarity.

Table 5.6. Selected bond lengths (Å) and angles (deg) for $[(CH_2CH_2O)_6XeO_3{\cdot}2H_2O]_2HF$ **(1)**.

Bond Lengths (Å)				Bond Angles (deg)			
Xe1–O1	1.764(4)	Xe1–O13	2.704(3)	O1–Xe1–O3	100.3(2)	O4–Xe2–O20	168.9(2)
Xe1–O2	1.775(3)	Xe1–O8	2.791(3)	O2–Xe1–O3	102.1(2)	O5–Xe2–O19	148.1(2)
Xe1–O3	1.770(3)	Xe1–O12	2.806(3)	O4–Xe2–O5	101.6(2)	O6–Xe2–O15	160.8(2)
Xe2–O4	1.768(4)	Xe2–O20	2.716(3)	O5–Xe2–O6	101.4(2)	O5–Xe2–O14	135.2(2)
Xe2–O5	1.762(4)	Xe2–O14	2.981(3)	O4–Xe2–O6	102.0(2)	O6–Xe2–O14	123.1(1)
Xe2–O6	1.770(4)	Xe2–O15	2.844(4)	O1–Xe1–O8	164.9(1)	O4–Xe2–O14	75.5(4)
Xe1–O7	3.078(3)	Xe2–O19	2.982(3)	O3–Xe1–O12	166.1(1)	O2–Xe1–O13	162.4(1)
O8–C3	1.428(5)	O19–C22	1.428(5)	O1–Xe1–O2	102.0(2)	O10–C7–C8–O11	68.4(4)
09–C5	1.428(6)	O19–C23	1.436(5)	O7–C1–C2–O8	56.9(4)	O11–C9–C10–O12	58.3(4)
O9–C4	1.412(6)	O18–C20	1.434(6)	O8–C3–C4–O9	58.2(5)	O12–C11–C12–O7	58.4(4)
08–C2	1.436(6)	O18–C21	1.425(6)	O9–C5–C6–O10	65.4(4)	C15–O15–C14	114.1(4)
O7–C1	1.428(5)	O17–C19	1.422(5)	C4–O9–C5	111.8(4)	C17–O16–C16	112.2(3)
O7–C12	1.434(5)	O16–C17	1.429(6)	C6–O10–C7	112.9(3)	C19–O17–C18	112.1(3)
O14–C13	1.428(6)	O16–C16	1.427(6)	C8–O11–C9	111.1(3)	C21–O18–C20	112.3(3)
O14–C24	1.414(6)	O15–C14	1.427(6)	C2–O8–C3	113.8(3)	C22–O19–C23	113.6(3)
O12–C10	1.436(5)	O15–C15	1.430(6)	C10–O12–C11	114.0(3)	C24–O14–C13	114.2(4)
O12–C11	1.434(6)	O10–C6	1.428(5)	C12–O7–C1	114.0(3)		
O11–C9	1.431(5)	O10–C7	1.421(5)				
O11–C8	1.427(6)	C8–C7	1.507(6)				
C6–C5	1.508(6)	C3–C4	1.517(8)				
C24–C23	1.510(7)	C21–C22	1.507(6)				
C1–C2	1.501(6)	C20–C19	1.505(6)				
C17–C18	1.486(6)	C16–C15	1.521(7)				
C14–C13	1.521(7)	C11–C12	1.496(6)				
C10–C9	1.507(6)						

Table 5.7. Selected bond lengths (Å) and angles (deg) for $(CH_2CH_2)_6XeO_3{\cdot}2H_2O$ **(2)**.

Bond Lengths (Å)			**Bond Angles (deg)**		
	exptl	cacld[a]		exptl	cacld[a]
Xe1–O1	1.754(7)	1.764	O1–Xe1–O2	101.6(3)	103.5
Xe1–O2	1.768(9)	1.772	O1–Xe1–O1A	100.7(5)	103.4
Xe1–O7	2.702(1)	2.705	O1–Xe1–O7	88.9(3)	87.0
Xe1–O4	2.839(7)	2.869	O1A–Xe1–O4	164.9(3)	164.0
Xe1–O3	3.093(7)	3.190	O2–Xe1–O7	163.3(3)	162.7
O4–C2	1.430(12)	1.408	O2–Xe1–O3	78.8(3)	73.9
O4–C3	1.439(21)	1.409	O2–Xe1–O4	93.5(3)	92.0
O5–C5	1.428(13)	1.409	O6–C6–C5	107.3(8)	108.8
O6–C6	1.435(13)	1.408	C6–O6–C6’	110.9(12)	113.5
C2–C1	1.496(14)	1.504	C1–O3–C1’	113.3(10)	114.4
O3–C1	1.445(11)	3.266	C2–O4–C3	112.9(8)	115.5
O5–C4	1.413(14)	1.409	O4–C2–C1	106.9(9)	107.6
C5–C6	1.494(18)	1.504	O3–C1–C2	106.1(8)	107.0
C3–C4	1.519(16)	1.514	O4–C3–C4	115.9(9)	114.0
			O5–C4–C3	107.9(9)	109.9
			O5–C5–C6	110.5(10)	108.8
			C4–O5–C5	111.2(9)	113.1

[a] APFD/Def2-TZVP.

Table 5.8. Selected bond lengths (Å) and angles (deg) of $(CH_2CH_2)_4XeO_3$ (**3**).

Bond Lengths (Å)					**Bond Angles**				
	exptl			cacld[a]		exptl			cacld[a]
Xe1–O1	1.766(2)			1.764	O1–Xe1–O2	100.9(1)			103.6
Xe1–O2	1.759(2)			1.764	O2–Xe1–O3	102.4(1)			104.4
Xe1–O3	1.760(2)			1.764	O1–Xe1–O3	100.9(1)			104.3
Xe1–O4	2.780(6)	Xe1–O4A	2.758(5)	2.804	O2–Xe1–O4	152.5(1)	O2–Xe1–O4A	161.8(1)	163.5
Xe1–O5	2.761(6)	Xe1–O5A	2.779(6)	2.941	O1–Xe1–O6	147.1(1)	O1–Xe1–O6A	131.7(1)	146.0
Xe1–O6	2.951(5)	Xe1–O6A	2.944(5)	3.111	O3–Xe1–O5	162.2(1)	O3–Xe1–O5A	152.9(1)	142.6
Xe1–O7	2.945(5)	Xe1–O7A	2.955(5)	2.980	O1–Xe1–O7	131.7(1)	O1–Xe1–O7A	147.0(1)	125.4
C1−C2	1.54(2)	C1A−C2A	1.54(1)	1.515	O1–Xe1–O5	87.5(1)	O1–Xe1–O5A	77.8(1)	87.5
C3−C4	1.52(2)	C3A−C4A	1.52(2)	1.516	O1–Xe1–O4	77.7(1)	O1–Xe1–O4A	87.4(1)	77.0
C5−C6	1.54(2)	C5A−C6A	1.53(2)	1.515	O2–Xe1–O6	78.7(1)	O2–Xe1–O6A	74.1(1)	78.7
C7−C8	1.52(2)	C7A−C8A	1.53(2)	1.514	O3–Xe1–O7	74.1(1)	O3–Xe1–O7A	78.7(1)	74.9
O4–C1	1.42(2)	O4A–C1A	1.42(1)	1.414	C1–O4–C8	112.9(8)	C1A–O4A–C8A	113.7(9)	116.1
O5–C2	1.42(1)	O5A–C2A	1.40(1)	1.409	C2–O5–C3	114.5(9)	C2A–O5A–C3A	114.9(7)	116.0
O5–C3	1.41(2)	O5A–C3A	1.42(1)	1.412	C4–O6–C5	114.1(9)	C4A–O6A–C5A	113.1(9)	115.1
O6–C4	1.43(1)	O6A–C4A	1.43(2)	1.404	C7–O7–C8	113.5(9)	C7A–O7A–C8A	113.3(9)	115.5
O6–C5	1.40(2)	O6A–C5A	1.41(1)	1.404	C1–C2–O5	110.4(8)	C1A–C2A–O5A	112(1)	112.3
O7–C6	1.41(1)	O7A–C6A	1.41(2)	1.410	C3–C4–O6	108.4(9)	C3A–C4A–O6A	112(1)	112.3
O7–C7	1.42(2)	O7A–C7A	1.42(1)	1.411	C5–C6–O7	110.1(9)	C5A–C6A–O7A	111(1)	112.5
O4–C8	1.43(1)	O4A–C8A	1.42(2)	1.416	C7–C8–O4	107.9(8)	C7A–C8A–O4A	113(1)	112.6

[a] APFD/Def2-TZVP

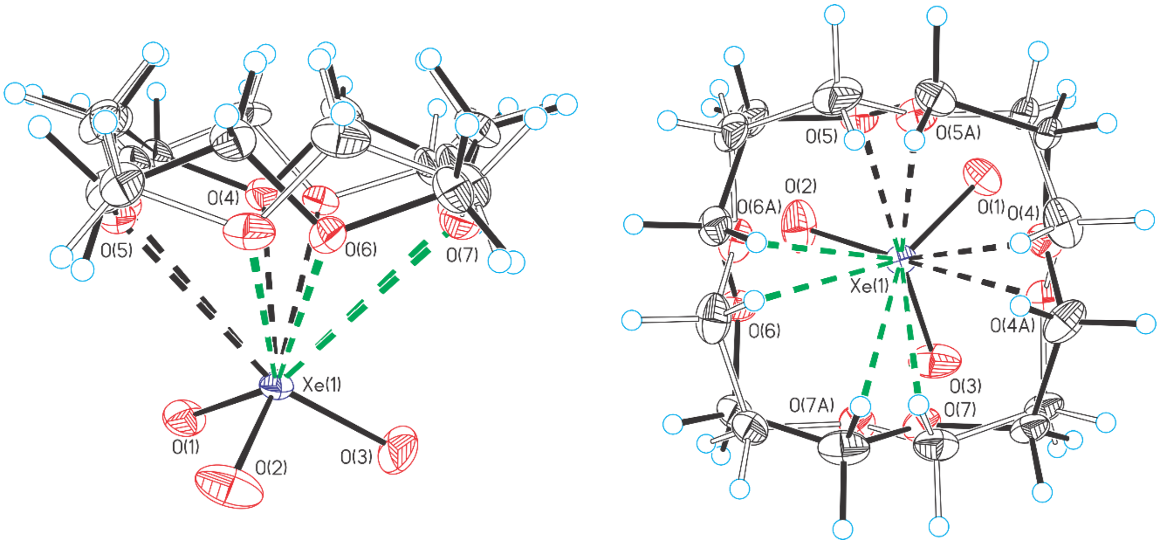

Figure 5.12. The X-ray crystal structure of $(CH_2CH_2O)_4XeO_3$; thermal elipsoids are shown at the 50% probability level and the longest contacts are highlighted in green. Both contributions to the disorder model are shown.

Bond Valence Calculations

Table 5.9. Bond valences[a] for $[(CH_2CH_2O)_6XeO_32H_2O]_2{\cdot}HF$, $(CH_2CH_2O)_6XeO_32H_2O$, and $(CH_2CH_2O)_4XeO_3$.

	$[(CH_2CH_2O)_6XeO_32H_2O]_2{\cdot}HF$		$(CH_2CH_2O)_6XeO_32H_2O$	$(CH_2CH_2O)_4XeO_3$	
Xe–O	1.862	1.837	1.872	1.882	1.882
	1.872	1.862	1.944	1.913	1.913
	1.903	1.892	1.944	1.918	1.918
Xe---O	0.070	0.054	0.052	0.077	0.076
	0.071	0.113	0.104	0.078	0.078
	0.102	0.118	0.104	0.121	0.122
	0.144	0.149	0.150	0.128	0.129
Total	6.024	6.025	6.170	6.117	6.118

[a] Values are in valence units (v.u.) as defined in reference [S1].

Table 5.10. Experimental Raman frequencies, calculated Raman, and infrared frequencies, and assignments for $(CH_2CH_2O)_4XeO_3$.

exptl	calcd				exptl	calcd		vibrational
$XeO_{3(aq)}$[a,b]	XeO_3		$(CH_2CH_2O)_4XeO_3$		$(CH_2CH_2O)_4XeO_3$[a,c]	$(CH_2CH_2O)_4$		assignments[f]
	B3LYP[a,d]	*APFD*[a,e]	*B3LYP*[a,d]	*APFD*[a,e]		*B3LYP*[a,d]	*APFD*[a,e]	
			3108(43)[7]	3127(40)[4]		3087(144)[60]	3102(150)[51]	ν(CH), combination bands, and overtones
			3105(43)[8]	3124(41)[5]		3087(87)[29]	3102(86)[29]	
			3096(57)[16]	3110(63)[18]		3087(82)[27]	3101(86)[29]	
			3094(57)[16]	3110(46)[6]		3087(37)[3]	3101(34)[<1]	
			3031(106)[64]	3038(47)[36]		3026(173)[72]	3027(139)[62]	
			3020(47)[36]	3029(64)[45]	2937(31)	3011(34)[27]	3015(41)[41]	
			3016(37)[35]	3026(67)[76]	2880(27)	3011(34)[27]	3015(41)[41]	
			3011(236)[63]	3021(82)[31]	2786(6)	2999(2)[<1]	3004(8)[<1]	
			3011(173)[24]	3018(473)[83]	2752(5)	2977(592)[79]	2982(688)[102]	
			3005(134)[131]	3012(163)[90]	2716(5)	2973(73)[222]	2977(70)[221]	
			3004(218)[88]	3010(191)[97]	2689(4)	2973(73)[222]	2977(70)[221]	
			2998(113)[62]	3003(115)[51]		2971(76)[<1]	2973(71)[<1]	
			2986(72)[24]	2996(32)[17]		2951(72)[20]	2960(146)[<1]	
			2980(68)[24]	2989(28)[10]		2950(62)[24]	2960(11)[3]	
			2977(66)[25]	2988(32)[13]		2950(80)[19]	2960(11)[3]	
			2975(95)[12]	2984(38)[3]		2950(69)[22]	2960(21)[13]	

Table 5.10. continued…

exptl	calcd				exptl	calcd		vibrational assignments^{f}
$XeO_{3(aq)}$^{a,b}	XeO_3		$(CH_2CH_2O)_4XeO_3$		$(CH_2CH_2O)_4XeO_3$^{a,c}	$(CH_2CH_2O)_4$		
	B3LYP^{a,d}	*APFD*^{a,e}	*B3LYP*^{a,d}	*APFD*^{a,e}		*B3LYP*^{a,d}	*APFD*^{a,e}	
			1523(10)[4]	1497(2)[10]		1524(12)[5]	1514(12)[6]	$\delta(CH_2)$
			1507(2)[10]	1495(2)[9]		1506(2)[11]	1494(2)[12]	
			1507(2)[9]	1484(2)[<1]	1484(6)	1506(3)[11]	1494(2)[12]	
			1497(2)[0]	1481(7)[5]	1468(5)	1495(3)[<1]	1481(3)[0]	
			1490(8)[2]	1479(8)[7]	1448(9)	1485(9)[1]	1476(9)[1]	
			1488(6)[8]	1475(5)[13]	1440(9)	1483(1)[6]	1474(1)[7]	
			1487(4)[11]	1474(12)[10]		1483(1)[6]	1474(1)[7]	
			1486(15)[5]	1430(<1)[1]		1481(23)[<1]	1473(22)[0]	
			1430(<1)[<1]	1426(<1)[5]		1430(1)[<1]	1428(1)[<1]	$\rho_r(CH_2)$
			1426(1)[4]	1424(<1)[6]		1425(<1)[2]	1424(1)[5]	
			1425(1)[4]	1418(1)[6]	1375(3)	1425(<1)[2]	1424(1)[5]	
			1419(1)[3]	1405(2)[<1]	1360(2)	1416(2)[1]	1416(2)[2]	
			1414(3)[<1]	1389(1)[8]	1346(2)	1415(3)[<1]	1406(2)[0]	
			1399(1)[16]	1387(1)[11]		1399(1)[34]	1388(<1)[29]	
			1399(1)[17]	1377(3)[3]		1399(1)[34]	1388(<1)[29]	
			1385(2)[1]	1320(4)[14]		1384(2)[<1]	1374(3)[2]	
			1331(4)[12]	1312(6)[56]		1333(4)[11]	1323(4)[12]	$\rho_t(CH_2)$
			1317(7)[28]	1311(6)[51]	1302(5)	1318(7)[37]	1313(5)[69]	
			1290(27)[<1]	1290(20)[<1]	1288(7)	1318(7)[37]	1313(5)[69]	
			1283(2)[<1]	1280(7)[1]	1270(7)	1296(31)[]	1293(27)[0]	
			1270(1)[23]	1266(2)[29]	1249(3)	1284(1)[<1]	1281(5)[0]	
			1269(1)[22]	1263(2)[30]	1235(3)	1273(2)[31]	1268(3)[35]	
			1256(4)[4]	1246(4)[4]		1273(2)[31]	1268(3)[35]	
						1257(4)[3]	1249(4)[3]	

Table 5.10. continued…

exptl	calcd				exptl	calcd		vibrational
$XeO_{3(aq)}$[a,b]	XeO_3		$(CH_2CH_2O)_4XeO_3$		$(CH_2CH_2O)_4XeO_3$[a,c]	$(CH_2CH_2O)_4$		assignments[f]
	B3LYP[a,d]	*APFD*[a,c]	*B3LYP*[a,d]	*APFD*[a,c]		*B3LYP*[a,d]	*APFD*[a,c]	
			1180(2)[<1] 1160(1)[107] 1158(1)[101] 1148(2)[3] 1138(5)[6] 1119(1)[137] 1118(1)[128] 1075(1)[2] 1061(5)[<1] 1045(2)[21] 1043(2)[19] 1035(1)[90] 926(<1)[37] 924(<1)[38] 922(1)[1] 909(7)[<1] 854(10)[44]	1179(2)[83] 1178(2)[100] 1175(2)[51] 1174(3)[55] 1157(4)[9] 1124(1)[58] 1124(1)[55] 1083(2)[<1] 1072(4)[<1] 1060(1)[20] 1060(1)[32] 1056(2)[83] 948(<1)[28] 947(<1)[26] 935(3)[1] 932(3)[2] 882(9)[33]	1228(4) 1148(4) 1142(4) 1137(5) 1132(4) 1126(5) 1123(4) 1084(4) 1029(3) 906(3)	1181(2)[<1] 1166(1)[163] 1166(1)[163] 1162(5)[<1] 1147(4)[10] 1124(1)[101] 1124(1)[101] 1079(2)[<1] 1060(7)[<1] 1047(3)[14] 1047(3)[13] 1041(<1)[66] 922(1)[1] 921(<1)[43] 921(<1)[43] 903(9)[<1] 846(12)[28]	1190(4)[<1] 1186(2)[171] 1186(2)[171] 1178(4)[0] 1166(3)[9] 1127(1)[46] 1127(1)[46] 1084(2)[1] 1070(7)[0] 1064(1)[66] 1063(2)[12] 163(2)[12] 931(<1)[36] 931(<1)[36] 923(1)[<1] 316(8)[0] 867(12)[24]	ν(CO)-(CO) ν(CO)-(CC) $\rho_r(CH_2)$
857(8) 819(26) 809(63)	855(92)[11]	901(11)[98]	844(14)[90] 840(11)[86]	885(14)[106] 879(11)[96]	853(10) 825(20) 811(5)			$\nu_{as}(XeO_3)$
			817(<1)[4] 817(<1)[4] 800(8)[<1]	839(<1)[2] 838(<1)[2] 819(6)[<1]		819(<1)[1] 818(<1)[1] 807(11)[<1]	834(<1)[<1] 835(<1)[<1] 824(9)[0]	ν(CO)-(CO) ν(CO)-(CC) $\rho_r(CH_2)$

Table 5.10. continued…

exptl $XeO_{3(aq)}$[a,b]	calcd XeO$_3$ B3LYP[a,d]	calcd XeO$_3$ APFD[a,e]	calcd $(CH_2CH_2O)_4XeO_3$ B3LYP[a,d]	calcd $(CH_2CH_2O)_4XeO_3$ APFD[a,e]	exptl $(CH_2CH_2O)_4XeO_3$[a,c]	calcd $(CH_2CH_2O)_4$ B3LYP[a,d]	calcd $(CH_2CH_2O)_4$ APFD[a,e]	vibrational assignments[f]
764(100) 754, sh	788(4)[53]	836(51)[4]	787(51)[17]	833(52)[25]	772(100)			$\nu_1(XeO_3)$
			598(3)[<1] 554(<1)[9] 551(<1)[9] 489(2)[<1] 411(<1)[<1] 359(<1)[5] 356(<1)[4] 340(1)[10]	612(2)[<1] 568(<1)[9] 565(<1)[9] 502(2)[<1] 428(<1)[<1] 374(<1)[7] 372(<1)[5] 351(2)[44]	569(2) 554(2) 549(2) 537(2) 529(2) 519(2)	596(3)[1] 551(<1)[12] 551(<1)[12] 483(2)[0] 407(<1)[0] 349(<1)[5] 348(<1)[5]	601(3)[1] 555(<1)[13] 555(<1)[13] 486(2)[0] 411(<1)[0] 354(<1)[5] 354(<1)[5]	δ(CCO) δ(COC)
351(1) 323(3)	308(33)[3]	322(3)[34]	326(4)[66]	345(3)[39]	356(6) 346(4)			$\delta_{umb}(XeO_3)$
			290(4)[1]	309(3)[1]		327(1)[6] 292(3)[<1]	332(1)[5] 302(3)[<1]	δ(CCO) δ(COC)
311(42) 297(11)	271(9)[5]	284(4)[10]	287(4)[9] 284(4)[9]	304(3)[10] 299(3)[9]	317(10) 302(10)			$\delta_{as}(XeO_3)$

Table 5.10. continued…

exptl $XeO_{3(aq)}$ [a,b]	**XeO_3** *B3LYP* [a,d]	**XeO_3** *APFD* [a,e]	**calcd** $(CH_2CH_2O)_4XeO_3$ *B3LYP* [a,d]	**calcd** $(CH_2CH_2O)_4XeO_3$ *APFD* [a,e]	**exptl** $(CH_2CH_2O)_4XeO_3$ [a,c]	**calcd** $(CH_2CH_2O)_4$ *B3LYP* [a,d]	**calcd** $(CH_2CH_2O)_4$ *APFD* [a,e]	**vibrational assignments** [f]
			264(<1)[2]	275(<1)[2]				ν(Xe---O) ν(XeO) ρ_r(XeO) ρ_t(XeO) lattice modes
			260(<1)[2]	275(<1)[2]				
			241(<1)[<1]	251(<1)[<1]				
			197(<1)[12]	209(<1)[5]		253(<1)[<1]	259(<1)[<1]	
			195(<1)[1]	204(<1)[10]		253(<1)[<1]	259(<1)[<1]	
			190(<1)[13]	200(<1)[12]		237(<1)[1]	238(<1)[1]	
146(5)			140(<1)[<1]	148(<1)[<1]	137(5)	191(<1)[13]	193(<1)[12]	
110(10)			102(<1)[1]	125(<1)[1]	119(7)	191(<1)[13]	193(<1)[12]	
99(16)			94(1)[4]	118(1)[3]		188(<1)[<1]	190(<1)[<1]	
			81(1)[3]	107(<1)[1]		119(<1)[0]	122(<1)[0]	
			77(<1)[1]	102(1)[2]		79(1)[0]	74(1)[0]	
			71(<1)[<1]	95(<1)[<1]		38(<1)[0]	16(<1)[0]	
			56(<1)[<1]	72(<1)[<1]				
			48(<1)[<1]	47(1)[<1]				
			20(<1)[<1]	23(<1)[<1]				

[a] Frequencies are given in cm^{-1}. Abbreviations denote shoulder (sh) and broad (br). [b] The spectrum was recorded in a ¼-in. o.d. FEP diameter sample tube at −140 °C. Values in parentheses are relative Raman intensities. [c] The spectrum was recorded in an aluminum sample holder at 22 °C. Values in parentheses are relative Raman intensities. [d] The B3LYP/Def2–TZVP level was used. [e] The APFD/Def2–TZVP level was used. Values in parentheses and square brackets are calculated Raman intensities (Å amu^{-1}) and infrared intensities (km mol^{-1}), respectively. [f] Symbols and abbreviations denote stretch (ν), bend (δ), rock (ρ_r), twist (ρ_t), umbrella (umb), symmetric (s), and asymmetric (as).

Table 5.11. Experimental Raman frequencies, calculated Raman, and infrared frequencies, and assignments for $(CH_2CH_2O)_6XeO_3{\cdot}2H_2O$, $(CH_2CH_2O)_6$, and $XeO_{3(aq)}$.

exptl	calcd				exptl		calcd		vibrational
$XeO_{3(aq)}$^{a,b}	XeO_3		$(CH_2CH_2O)_6XeO_3{\cdot}2H_2O$		$(CH_2CH_2O)_6XeO_3{\cdot}2H_2O$^{a,c}	$(CH_2CH_2O)_6$	$(CH_2CH_2O)_6{\cdot}2H_2O$		assignments^{f}
	B3LYP^{a,d}	*APFD*^{a,c}	*B3LYP*^{a,d}	*APFD*^{a,c}			*B3LYP*^{a,d}	*APFD*^{a,c}	
			3776(35)[313]	3810(28)[406]	3399(1)		3782(33)[341]	3857(30)[233]	$\nu_{as}(OH_2)$
			3701(45)[431]	3710(40)[556]			3724(41)[373]	3801(21)[471]	
			3689(97)[98]	3722(95)[99]			3701(107)[66]	3776(84)[55]	$\nu_{s}(OH_2)$
			3638(131)[215]	3648(123)[252]			3652(108)[89]	3723(124)[49]	
			3102(62)[13]	3122(51)[11]			3095(112)[38]	3099(98)[45]	$\nu(CH)$, combination bands, and overtones
			3102(8)[<1]	3122(10)[1]			3095(3)[<1]	3099(24)[2]	
			3052(2)[1]	3070(3)[3]			3037(6)[3]	3051(1)[3]	
			3051(21)[55]	3069(33)[36]			3037(28)[128]	3049(42)[51]	
			3033(5)[2]	3048(5)[2]			3028(3)[2]	3036(3)[7]	
			3032(19)[70]	3046(17)[52]			3026(31)[80]	3035(36)[102]	
			3031(140)[20]	3043(14)[5]	3007(3)	2988(6)	3018(4)[1]	3026(13)[3]	
			3031(11)[2]	3043(117)[23]	2999(2)	2949(60)	3018(212)[3]	3026(43)[6]	
			3018(12)[7]	3035(15)[8]	2978(12)	2895(100)	3011(9)[8]	3023(16)[21]	
			3017(35)[38]	3033(53)[43]	2951(11)	2874(69)	3011(23)[25]	3023(192)[44]	
			3015(54)[5]	3030(69)[11]	2920(29)	2842(56)	3008(58)[8]	3016(26)[<1]	
			3015(165)[61]	3021(158)[74]	2893(18)	2823(24)	3008(177)[79]	3015(123)[48]	
			2998(989)[25]	3012(849)[18]	2867(12)	2810(39)	2991(1109)[3]	2997(750)[130]	
			2997(26)[286]	3011(26)[252]	2838(8)	2766(8)	2989(32)[365]	2992(31)[156]	
			2993(51)[159]	3005(159)[114]	2803(4)	2737(4)	2987(72)[224]	2990(578)[195]	
			2992(300)[103]	3003(337)[128]	2735(1)	2703(7)	2983(121)[103]	2957(32)[221]	
			2990(47)[6]	3002(28)[20]	2716(1)	2663(3)	2983(87)[12]	2985(123)[21]	
			2988(69)[44]	2999(70)[47]	2696(2)		2980(22)[24]	2981(20)[1]	
			2981(65)[7]	2992(70)[4]			2974(64)[8]	2978(22)[10]	
			2980(65)[5]	2992(54)[9]			2972(35)[5]	2977(29)[<1]	
			2979(2)[<1]	2992(2)[3]			2969(64)[16]	2969(37)[8]	
			2977(35)[6]	2990(39)[5]			2967(20)[<1]	2968(4)[4]	
			2975(20)[<1]	2988(12)[<1]			2967(27)[12]	2968(38)[6]	
			2974(19)[14]	2987(6)[6]			2966(5)[4]	2968(31)[1]	

Table 5.11. continued…

exptl $XeO_{3(aq)}$^{a,b}	XeO_3		calcd $(CH_2CH_2O)_6XeO_3{\cdot}2H_2O$		exptl $(CH_2CH_2O)_6XeO_3{\cdot}2H_2O$^{a,c}	$(CH_2CH_2O)_6$	calcd $(CH_2CH_2O)_6{\cdot}2H_2O$		vibrational assignments^{f}
	B3LYP^{a,d}	*APFD*^{a,c}	*B3LYP*^{a,d}	*APFD*^{a,c}			*B3LYP*^{a,d}	*APFD*^{a,c}	
			1652(1)[22]	1651(1)[19]	1701(2)		1665(1)[35]	1669(2)[9]	δ(H_2O)
			1626(1)[55]	1611(1)[43]	1509(1)		1624(2)[48]	1609(2)[44]	
			1520(10)[8]	1509(5)[8]					
			1516(7)[7]	1509(8)[13]			1514(4)[6]	1509(4)[5]	δ(CH_2)
			1516(12)[5]	1508(16)[8]			1513(14)[4]	1508(14)[7]	
			1515(14)[5]	1508(11)[6]			1213(12)[3]	1507(14)[11]	
			1507(1)[4]	1499(1)[6]	1474(6)	1493(24)	1510(11)[2]	1502(8)[10]	
			1507(1)[4]	1499(2)[2]	1460(5)	1476(18)	1502(3)[5]	1495(2)[7]	
			1501(2)[3]	1492(1)[2]	1445(3)	1462(6)	1502(4)[2]	1495(2)[1]	
			1497(2)[13]	1488(1)[11]		1454(6)	1495(2)[14]	1487(1)[14]	
			1496(<1)[2]	1488(1)[1]		1445(14)	1495(1)[4]	1487(1)[10]	
			1496(1)[8]	1487(1)[8]			1493(1)[7]	1485(2)[6]	
			1489(17)[3]	1481(2)[15]			1491(2)[7]	1482(1)[2]	
			1489(1)[10]	1481(17)[4]					
							1477(14)[2]	1477(1)[7]	ρ_r(CH_2)
			1467(<1)[3]	1474(<1)[7]			1477(4)[8]	1475(5)[8]	
			1464(2)[2]	1467(1)[2]			1466(1)[3]	1473(15)[1]	
			1453(1)[1]	1456(2)[4]			1454(2)[1]	1464(1)[<1]	
			1437(3)[1]	1435(3)[1]			1451(1)[3]	1457(1)[8]	
			1435(1)[1]	1432(<1)[3]	1426(2)	1413(2)	1435(3)[1]	1436(4)[<1]	
			1424(2)[2]	1417(1)[<1]	1408(1)	1373(3)	1430(<1)[<1]	1435(<1)[2]	
			1416(<1)[<1]	1413(<1)[<1]	1382(5)	1354(1)	1420(1)[<1]	1418(1)[1]	
			1409(2)[3]	1402(2)[4]	1367(3)	1336(1)	1409(<1)[2]	1414(1)[2]	
			1400(3)[<1]	1396(3)[1]			1403(3)[5]	1401(3)[1]	
			1388(<1)[58]	1380(2)[44]			1397(4)[2]	1396(4)[<1]	
			1388(2)[50]	1378(<1)[53]			1384(1)[67]	1379(<1)[100]	
			1378(<1)[8]	1368(<1)[5]			1382(1)[96]	1379(1)[65]	
							1373(<1)[1]	1368(<1)[1]	

Table 5.11. continued…

exptl			calcd		exptl		calcd		vibrational
$XeO_{3(aq)}$[a,b]	XeO_3		$(CH_2CH_2O)_6XeO_3{\cdot}2H_2O$		$(CH_2CH_2O)_6XeO_3{\cdot}2H_2O$[a,c]	$(CH_2CH_2O)_6$	$(CH_2CH_2O)_6{\cdot}2H_2O$		assignments[f]
	B3LYP[a,d]	*APFD*[a,c]	*B3LYP*[a,d]	*APFD*[a,c]			*B3LYP*[a,d]	*APFD*[a,c]	
			1331(15)[21]	1334(16)[23]			1321(12)[17]	1335(5)[44]	$\rho_t(CH_2)$
			1329(2)[2]	1331(7)[1]			1318(7)[5]	1332(10)[2]	
			1314(12)[12]	1319(2)[22]			1310(1)[18]	1325(1)[36]	
			1305(3)[3]	1307(4)[8]			1299(4)[2]	1314(6)[4]	
			1304(3)[3]	1304(22)[2]	1294(6)	1296(11)	1298(29)[1]	1312(26)[2]	
			1295(1)[1]	1293(17)[<1]	1281(6)	1275(12)	1290(20)[<1]	1302(11)[1]	
			1280(41)[41]	1287(1)[49]	1239(2)	1258(14)	1276(1)[49]	1284(2)[40]	
			1277(8)[8]	1279(2)[15]	1226(3)	1237(7)	1270(2)[14]	1278(3)[21]	
			1277(13)[13]	1275(3)[3]	1215(2)	1217(1)	1267(4)[4]	1273(9)[14]	
			1270(7)[7]	1273(7)[15]			1264(4)[14]	1265(4)[14]	
			1261(6)[6]	1259(2)[2]			1256(1)[<1]	1259(2)[2]	
			1258(<1)[<1]	1257(2)[21]			1251(3)[5]	1249(2)[22]	
			1173(4)[4]	1203(2)[9]			1171(5)[6]	1208(4)[2]	ν(CO)-(CO) ν(CO)-(CC) $\rho_t(CH_2)$
			1164(1)[1]	1197(7)[10]			1161(1)[2]	1206(4)[21]	
			1162(1)[1]	1192(2)[50]			1159(9)[19]	1199(5)[17]	
			1162(8)[8]	1177(6)[51]			1157(4)[4]	1186(<1)[499]	
			1156(11)[11]	1172(<1)[448]			1152(1)[18]	1176(2)[51]	
			1152(61)[61]	1167(1)[291]			1149(4)[65]	1173(5)[333]	
			1144(20)[20]	1165(2)[22]			1142(2)[30]	1161(2)[16]	
			1135(369)[369]	1159(2)[65]			1133(<1)[409]	1155(4)[19]	
			1131(404)[404]	1154(2)[9]		1158(5)	1127(<1)[414]	1153(1)[1]	
			1124(113)[113]	1142(2)[1]		1133(15)	1119(1)[80]	1151(2)[47]	
			1110(12)[12]	1129(1)[4]	1162(2)	1110(3)	1108(<1)[17]	1132(3)[20]	
			1106(18)[18]	1124(3)[18]	1145(3)	1091(4)	1103(2)[15]	1125(1)[8]	
			1104(3)[3]	1114(<1)[4]	1134(3)	1063(3)	1099(2)[1]	1110(1)[1]	
			1084(2)[2]	1100(1)[25]	1095(1)	1046(6)	1079(2)[35]	1107(1)[21]	
			1081(29)[29]	1100(1)[36]	1071(3)	987(7)	1078(5)[2]	1106(1)[4]	
			1073(21)[21]	1097(2)[5]	1043(2)	939(1)	1069(1)[12]	1105(1)[26]	
			1059(16)[16]	10080(3)[22]	930(1)	932(1)	1054(2)[10]	1088(4)[16]	
			1050(38)[38]	1066(<1)[31]		892(14)	1044(<1)[23]	1074(1)[10]	
			968(62)[62]	981(<1)[42]			965(<1)[74]	982(1)[57]	
			957(79)[79]	974(2)[<1]			955(1)[85]	973(<1)[62]	
			956(<1)[<1]	964(1)[54]			955(1)[<1]	972(1)[1]	
			942(1)[1]	942(1)[1]			938(1)[<1]	952(1)[1]	
			932(29)[29]	939(2)[45]			930(2)[27]	950(2)[21]	
			917(1)[1]	920(1)[3]			915(1)[2]	927(<1)[2]	
			869(8)[8]	893(10)[7]			866(16)[3]	890(12)[7]	
			854(31)[31]	871(<1)[20]			851(<1)[29]		

Table 5.11. continued…

exptl $XeO_{3(aq)}$[a,b]	XeO_3		calcd $(CH_2CH_2O)_6XeO_3{\cdot}2H_2O$		exptl $(CH_2CH_2O)_6XeO_3{\cdot}2H_2O$[a,c]	$(CH_2CH_2O)_6$	calcd $(CH_2CH_2O)_6{\cdot}2H_2O$		vibrational assignments[f]
	B3LYP[a,d]	*APFD*[a,c]	*B3LYP*[a,d]	*APFD*[a,c]			*B3LYP*[a,d]	*APFD*[a,c]	
857(8) 819(26) 809(63)	855(92)[11]	901(11)[98]	838(118)[118] 829(98)[98]	877(11)[115] 868(13)[113]	845(1) 829(22) 818(3)				$\nu_{as}(XeO_3)$
			833(5)[5] 826(6)[6]	850(4)[<1] 843(4)[<1]	866(10)	866(10) 823(13)	825(4)[2] 819(7)[1]	823(1)[3] 843(8)[<1]	$\nu(CO)$-(CO) $\nu(CO)$-(CC) $\rho_r(CH_2)$
764(100) 754, sh	788(4)[53]	836(51)[4]	783(19)[19]	829(59)[27]	776(100)				$\nu_s(XeO_3)$
			683(11)[11] 611(54)[54]	743(<1)[6] 647(<1)[33]			609(<1)[108] 592(<1)[5]	625(<1)[9] 412(<1)[13]	$\rho_t(OH_2)$
			648(148)[148] 557(69)[69]	682(3)[153] 596(<1)[32]	597(2)		551(<1)[133]	597(<1)[130]	$\rho_r(OH_2)$
			590(6)[6] 566(1)[1]	597(1)[7] 573(2)[1]	579(2)	580(6) 523(2)	589(2)[5] 572(<1)[14]	601(1)[7] 580(1)[1]	$\delta(CCO)$ $\delta(COC)$
			573(3)[3] 526(18)[18] 520(6)[6] 516(1)[1] 404(<1)[<1] 351(<1)[<1]	570(<1)[55] 532(<1)[5] 509(1)[2] 506(<1)[13] 405(<1)[8] 377(1)[3]	566(2) 532(2)		570(2)[36] 561(<1)[62] 528(<1)[14] 515(1)[8] 513(<1)[1] 395(<1)[1]	566(<1)[32] 529(1)[8] 526(1)[29] 513(<1)[5] 406(1)[1] 379(1)[28]	$\rho_r(OH_2)$ $\rho_t(OH_2)$ $\rho_r(COC)$ $\rho_r(CCO)$ $\delta(CCO)$ $\delta(COC)$

Table 5.11. continued…

exptl $XeO_{3(aq)}$ ^{a,b}	XeO_3		calcd $(CH_2CH_2O)_6XeO_3{\cdot}2H_2O$		exptl $(CH_2CH_2O)_6XeO_3{\cdot}2H_2O$ ^{a,c}	$(CH_2CH_2O)_6$	calcd $(CH_2CH_2O)_6{\cdot}2H_2O$		vibrational assignments ^{f}
	B3LYP ^{a,d}	*APFD* ^{a,c}	*B3LYP* ^{a,d}	*APFD* ^{a,c}			*B3LYP* ^{a,d}	*APFD* ^{a,c}	
			385(50)[50] 345(85)[85]	439(<1)[71] 372(<1)[101]			449(<1)[55] 332(<1)[94]	439(1)[104] 375(<1)[83]	$\rho_w(OH_2)$
			381(1)[1] 330(10)[10] 314(1)[1] 311(6)[6]	357(<1)[1] 344(1)[<1] 324(1)[1] 320(<1)[9]		451(1) 431(1) 416(14) 320(3)	375(1)[<1] 351(<1)[<1] 314(1)[3] 310(1)[3] 298(<1)[4]	387(<1)[163] 365(<1)[3] 322(1)[4] 311(<1)[7] 311(<1)[3]	$\rho_r(CCO)$ $\rho_r(COC)$
351(1) 323(3)	308(33)[3]	322(3)[34]	332(59)[59]	357(2)[76]	348(4)				$\delta_{umb}(XeO_3)$
311(42) 297(11)	271(9)[5]	284(4)[10]	295(12)[12] 293(11)[11]	319(3)[14] 305(3)[11]	317(7) 310(11)				$\delta_{as}(XeO_3)$

Table 5.11. continued…

exptl $XeO_{3(aq)}$^{a,b}	XeO_3		calcd $(CH_2CH_2O)_6XeO_3·2H_2O$		exptl $(CH_2CH_2O)_4XeO_3·2H_2O$^{a,c}	$(CH_2CH_2O)_6$	calcd $(CH_2CH_2O)_6·2H_2O$		Vibrational Assignments^f
	B3LYP^{a,d}	*APFD*^{a,e}	*B3LYP*^{a,d}	*APFD*^{a,e}			*B3LYP*^{a,d}	*APFD*^{a,e}	
			288(3)[3]	295(<1)[2]					
			270(3)[3]	286(2)[4]					
			229(4)[4]	248(2)[5]					
			226(7)[7]	239(<1)[6]			290(<1)[2]	290(<1)[4]	
			222(1)[1]	237(<1)[7]			265(3)[4]	259(3)[4]	
			219(1)[1]	228(<1)[2]			230(<1)[5]	239(<1)[4]	
			197(16)[16]	214(1)[11]			221(<1)[3]	233(<1)[4]	
			184(8)[8]	196(<1)[16]			218(<1)[2]	221(<1)[7]	
			181(1)[1]	186(1)[<1]			207(<1)[5]	213(<1)[20]	
			169(20)[20]	176(<1)[4]			175(<1)[4]	181(<1)[7]	
			161(1)[1]	176(<1)[10]			172(<1)[4]	171(<1)[2]	
			159(3)[3]	158(<1)[<1]			166(<1)[4]	168(1)[1]	
			147(1)[1]	155(<1)[2]			156(<1)[11]	156(<1)[16]	ν(Xe---O)
			137(1)[1]	146(<1)[1]			142(<1)[<1]	141(<1)[3]	ν(XeO)
146(5)			123(2)[2]	143(1)[4]	148(2)	217(1)	138(<1)[2]	139(<1)[1]	ρ_r(XeO)
110(10)			120(<1)[<1]	136(<1)[<1]	135(3)	186(1)	133(<1)[2]	125(<1)[7]	ρ_t(XeO)
99(16)			111(2)[2]	130(1)[6]	112(5)	120(6)	132(<1)[4]	124(<1)[8]	lattice modes
			98(4)[4]	122(<1)[1]			115(<1)[1]	110(<1)[2]	
			98(5)[5]	117(<1)[5]			110(<1)[3]	98(<1)[3]	
			88(1)[1]	109(1)[1]			90(<1)[4]	91(<1)[<1]	
			87(<1)[<1]	107(<1)[1]			77(<1)[<1]	73(<1)[3]	
			78(<1)[<1]	92(<1)[<1]			69(<1)[3]	73(<1)[1]	
			68(2)[2]	91(<1)[4]			61(<1)[1]	48(<1)[1]	
			66(1)[1]	84(<1)[1]			47(1)[1]	40(1)[<1]	
			62(1)[1]	70(<1)[3]			44(<1)[1]	40(<1)[8]	
			53(<1)[<1]	58(<1)[1]			41(<1)[9]	28(<1)[<1]	
			53(<1)[<1]	58(<1)[4]			33(<1)[1]	23(<1)[2]	
			43(8)[8]	41(1)[1]					
			41(1)[1]	41(<1)[4]					
			40(1)[1]	33(<1)[6]					

[a] Frequencies are given in cm^{-1}. Abbreviations denote shoulder (sh) and broad (br). [b] The spectrum was recorded in a ¼-in. o.d. FEP diameter sample tube at −140 °C. Values in parentheses are relative Raman intensities. [c] The spectrum was recorded in a ¼-in. FEP diameter sample tube at −78 °C. Values in parentheses are relative Raman intensities. [d] The B3LYP/Def2–TZVP level was used. [e] The APFD/Def2–TZVP level was used. Values in parentheses and square brackets are calculated Raman intensities (Å amu^{-1}) and infrared intensities (km mol^{-1}), respectively. [f] Symbols and abbreviations denote stretch (ν), bend (δ), rock (ρ_r), twist (ρ_t), wag (ρ_ω), umbrella (umb), symmetric (s), and asymmetric (as).

Table 5.12. Experimental Raman frequencies and assignments for $(CH_2CH_2O)_4(CH_2CH_2N)_2O]_n$-$XeO_3$ (**4**).[a]

$XeO_{3(aq)}$	(4)	2,2,1-crytpand
	2994(<1) 2982(3) 2960(11) 2942(1) 2914(5) 2892(30) 2852(1) 2821(5) 2787(1) 2763(<1) 2698(<1)	2943(16) 2855(100) 2801(15) 2729(1)
	1497(1) 1488(1) 1480(1) 1462(7) 1457(1) 1439(4) 1417(1) 1398(1) 1358(1) 1358(1) 1324(1)	1470(1) 1456(19)
	1290(<1) 1274(5) 1264(1) 1252(1)	1288(10) 1251(1)
	1177(3) 1172(1) 1135(2) 1103(1) 1090(3) 1072(4)	1186(4) 1125(5) 1081(8)
	1062(1) 1039(5) 1033(<1)	1065(1) 1028(2)
	982(2) 970(1)	986(4)

Table 5.12. continued…

XeO$_{3(aq)}$	**(4)**	**2,2,1-crytpand**	**Vibrational Assignments**
	935(1) 927(<1) 912(1) 906(1)	936(3)	
	896(1) 859(2) 839(4)	872(1) 859(3) 830(9) 811(2)	
857(8) 819(26) 809(63)	828(16) 820(10) 804(3)		$\nu_{as}(XeO_3)$
764(100) 754, sh	771(100)		$\nu_s(XeO_3)$
	744(1)	772(1) 765(2) 746(3)	
	587(<1) 561(<1) 554(1) 530(<1) 520(1)	575(3) 543(<1) 539(1)	
351(1) 323(3)	349(5) 331(1)		$\delta_{umb}(XeO_3)$
311(42) 297(11)	319(5) 306(14)		$\delta_{as}(XeO_3)$
146(5) 110(10)	264(1) 247(1) 225(<1) 202(2) 186(1) 150(1) 135(1) 121(3) 107(1)	107(1)	Deformation modes / lattice vibrations

[a] Frequencies are given in cm^{-1}. Values in parentheses denote relative Raman intensities. Abbreviations denote broad (br) and shoulder (sh). Abbreviations denote stretch (ν), bend (δ), rock (ρ_r), twist (ρ_t), umbrella (umb), symmetric (s), asymmetric (as), in–plane (ip), out–of–plane (oop).

Table 5.13. Natural Population Analysis (NPA) charges, Wiberg valencies, and Wiberg bond indices for XeO_3, $(CH_2CH_2O)_4$, and $(CH_2CH_2O)_4XeO_3$.

XeO_3[a,b]				
Bond Indices		NPA Charges		[Valencies]
Xe1−O1	1.126	Xe	2.758	[3.379]
Xe1−O2	1.126	O1	–0.920	[1.537]
Xe1−O3	1.126	O2	–0.919	[1.537]
		O3	–0.919	[1.537]
		$\sum_{XeO_3}$	**0.000**	

$(CH_2CH_2O)_4$[b]									
Bond Indices		NPA Charges		[Valences]	Bond Indices		NPA Charges		[Valences]
C1-O4	0.947	O4	–0.510	[2.073]	H1A–C1	0.930	H1A	0.164	0.975
O4-C3	0.949	C3	–0.101	[3.864]	H1B–C1	0.920	H1B	0.203	0.961
C3-C4	1.001	C4	–0.085	[3.855]	H3A–C3	0.925	H3A	0.160	0.977
C4-O6	0.947	O6	–0.510	[2.073]	H3B–C3	0.921	H3B	0.170	0.973
O6-C6	0.949	C6	–0.101	[3.864]	H4A–C4	0.930	H4A	0.164	0.975
C6-C7	1.001	C7	–0.085	[3.855]	H4B–C4	0.920	H4B	0.203	0.961
C7-O8	0.947	O8	–0.510	[2.073]	H6A–C6	0.925	H6A	0.160	0.977
O8-C9	0.949	C9	–0.101	[3.864]	H6B–C6	0.921	H6B	0.170	0.973
C9-C10	1.001	C10	–0.085	[3.855]	H7A–C7	0.930	H7A	0.164	0.975
C10-O10	0.947	O10	–0.510	[2.073]	H7B–C7	0.920	H7B	0.203	0.961
O10-C11	0.949	C11	–0.101	[3.864]	H9A–C9	0.925	H9A	0.160	0.977
C11-C1	1.001	C1	–0.085	[3.855]	H9B–C9	0.921	H9B	0.170	0.973
					H10A–C10	0.930	H10A	0.164	0.975
					H10B–C10	0.920	H10B	0.203	0.961
					H11A–C11	0.925	H11A	0.160	0.977
					H11B–C11	0.921	H11B	0.170	0.973

Table 5.13. continued …

$(CH_2CH_2)_4XeO_3$[b]				
Bond Indices		NPA Charges		[Valencies]
Xe1−O1	1.089	Xe	2.877	[3.355]
Xe1−O2	1.089	O1	–0.968	[1.481]
Xe1−O3	1.101	O2	–0.968	[1.482]
		O3	–0.963	[1.496]
Xe1−O4	0.024	$\sum_{XeO_3}$	**–0.022**	
Xe1−O6	0.014			
Xe1−O8	0.008			
Xe1−O10	0.012			
$\sum_{XeO_3}$	**3.337**			

$(CH_2CH_2)_4XeO_3$[b]				
Bond Indices		NPA Charges [Valencies]		
C1–O4	0.923	O4	–0.553	[2.049]
C1–H1A	0.929	H1A	0.180	[0.969]
C1–H1B	0.901	H1B	0.233	[0.945]
O4–C3	0.923	C3	–0.103	[3.848]
C3–H3A	0.928	H3A	0.165	[0.975]
C3–H3B	0.920	H3B	0.186	[0.967]
C3–C4	1.004	C4	–0.102	[3.831]
C4–H4A	0.928	H4A	0.179	[0.97]
C4–H4B	0.909	H4B	0.232	[0.948]
C4–O6	0.923	O6	–0.545	[2.050]
O6–C6	0.934	C6	–0.103	[3.853]
C6–H6A	0.927	H6A	0.164	[0.946]
C6–H6B	0.920	H6B	0.184	[0.968]
C6–C7	1.003	C7	–0.094	[3.841]

$(CH_2CH_2)_4XeO_3$[b]				
Bond Indices		NPA Charges [Valencies]		
C7–H7A	0.916	H7A	0.214	[0.957]
C7–H7B	0.928	H7B	0.177	[0.970]
C7–O8	0.934	O8	–0.535	[2.055]
O8–C9	0.938	C9	–0.104	[3.855]
C9–H9A	0.920	H9A	0.182	[0.969]
C9–H9B	0.927	H9B	0.163	[0.976]
C9–C10	1.004	C10	–0.093	[3.841]
C10–H10A	0.916	H10A	0.213	[0.957]
C10–H10B	0.929	H10B	0.179	[0.970]
C10–O10	0.932	O10	–0.542	[2.051]
O10–C11	0.934	C11	–0.104	[3.852]
C11–H11A	0.927	H11A	0.164	[0.976]
C11–H11B	0.919	H11B	0.185	[0.967]
C11–C1	1.005	C1	–0.100	[3.827]

[a] The calculated geometric parameters for XeO_3: Xe−O, 1.754 Å; ∠O−Xe−O, 107.18°.

[b] The APFD/Def2–TZVPD level was used.

Table 5.14. Natural Population Analysis (NPA) charges, Wiberg valencies, and Wiberg bond indices for XeO_3, $(CH_2CH_2O)_6$, and $(CH_2CH_2O)_6XeO_3{\cdot}2H_2O$.

XeO_3[a,b]				
Bond Indices		NPA Charges [Valencies]		
Xe1−O1	1.126	Xe	2.758	[3.379]
Xe1−O2	1.126	O1	–0.920	[1.537]
Xe1−O3	1.126	O2	–0.919	[1.537]
		O3	–0.919	[1.537]
		$\sum_{XeO_3}$	**0.000**	

$(CH_2CH_2O)_6$[b]									
Bond Indices		NPA Charges		[Valences]	Bond Indices		NPA Charges		[Valences]
O3–C1	0.944	O3	–0.511	[2.046]	H1A–C1	0.934	H1A	0.173	[0.973]
C1–C2	1.004	C1	–0.082	[3.864]	H1B–C1	0.923	H1B	0.164	[0.975]
C2–O4	0.943	C2	–0.081	[3.864]	H2A–C2	0.934	H2A	0.170	[0.975]
O4–C3	0.942	O4	–0.509	[2.043]	H2B–C2	0.930	H2B	0.166	[0.974]
C3–C4	0.997	C3	–0.100	[3.863]	H3A–C3	0.927	H3A	0.167	[0.976]
C4–O6	0.948	C4	–0.085	[3.860]	H3B–C3	0.932	H3B	0.162	[0.975]
O6–C5	0.946	O6	–0.499	[2.051]	H4A–C4	0.928	H4A	0.164	[0.976]
C5–C6	1.003	C5	–0.088	[3.869]	H4B–C4	0.934	H4B	0.199	[0.962]
C6–O7	0.946	C6	–0.079	[3.866]	H5A–C5	0.923	H5A	0.172	[0.974]
O7–C6A	0.946	O7	–0.508	[2.052]	H5B–C5	0.934	H5B	0.163	[0.975]
					H6A–C6	0.929	H6A	0.171	[0.973]
					H6B–C6	0.934	H6B	0.163	[0.975]

Table 5.14. continued …

$(CH_2CH_2O)_6XeO_3{\cdot}2H_2O$[b]

Bond Indices		NPA Charges [Valencies]		
Xe1−O1	1.088	Xe	2.913	[3.343]
Xe1−O1A	1.088	O1	-0.975	[1.459]
Xe1−O2	1.061	O2	-1.004	[1.450]
Xe1−O3	0.006	O2A	-1.004	[1.450]
Xe1−O4	0.018	$\sum_{XeO_3}$	**–0.070**	
Xe1−O4A	0.018			
Xe1−O5	0.047			
$\sum Xe^{VI}O_3$	**3.326**			

$(CH_2CH_2O)_6XeO_3{\cdot}2H_2O$ [b]

Bond Indices		NPA Charges [Valencies]		
C1-O3	0.920	O3	-0.566	[2.043]
C1-H1A	0.911	H1A	0.210	[0.958]
C1-H1B	0.926	H1B	0.177	[0.970]
O4-C2	0.926	C2	-0.096	[3.843]
C2-H2A	0.918	H2A	0.187	[0.967]
C2-H2B	0.926	H2B	0.180	[0.969]
C3-C4	1.006	C4	-0.099	[3.838]
C4-H4A	0.923	H4A	0.177	[0.971]
C4-H4B	0.923	H4B	0.179	[0.970]
C4-O6	0.921	O6	-0.55	[2.049]
O6-C5	0.927	C5	-0.089	[3.838]
C5-H5A	0.924	H5A	0.180	[0.969]
C5-H5B	0.917	H5B	0.192	[0.966]
C5-C6	1.014	C6	-0.091	[3.838]
C6-H6A	0.924	H6A	0.180	[0.969]
C6-H6B	0.918	H6B	0.191	[0.966]
C6-O7	0.926	O7	-0.551	[2.043]
C1-C2	1.011	C2	-0.096	[3.843]
O4-C3	0.928	C3	-0.099	[3.828]
C3-H3A	0.905	H3A	0.236	[0.947]
C3-H3B	0.925	H3B	0.177	[0.971]

[a] The calculated geometric parameters for XeO_3: Xe−O, 1.754 Å; ∠O−Xe−O, 107.18°.
[b] The APFD/Def2–TZVPD level was used.

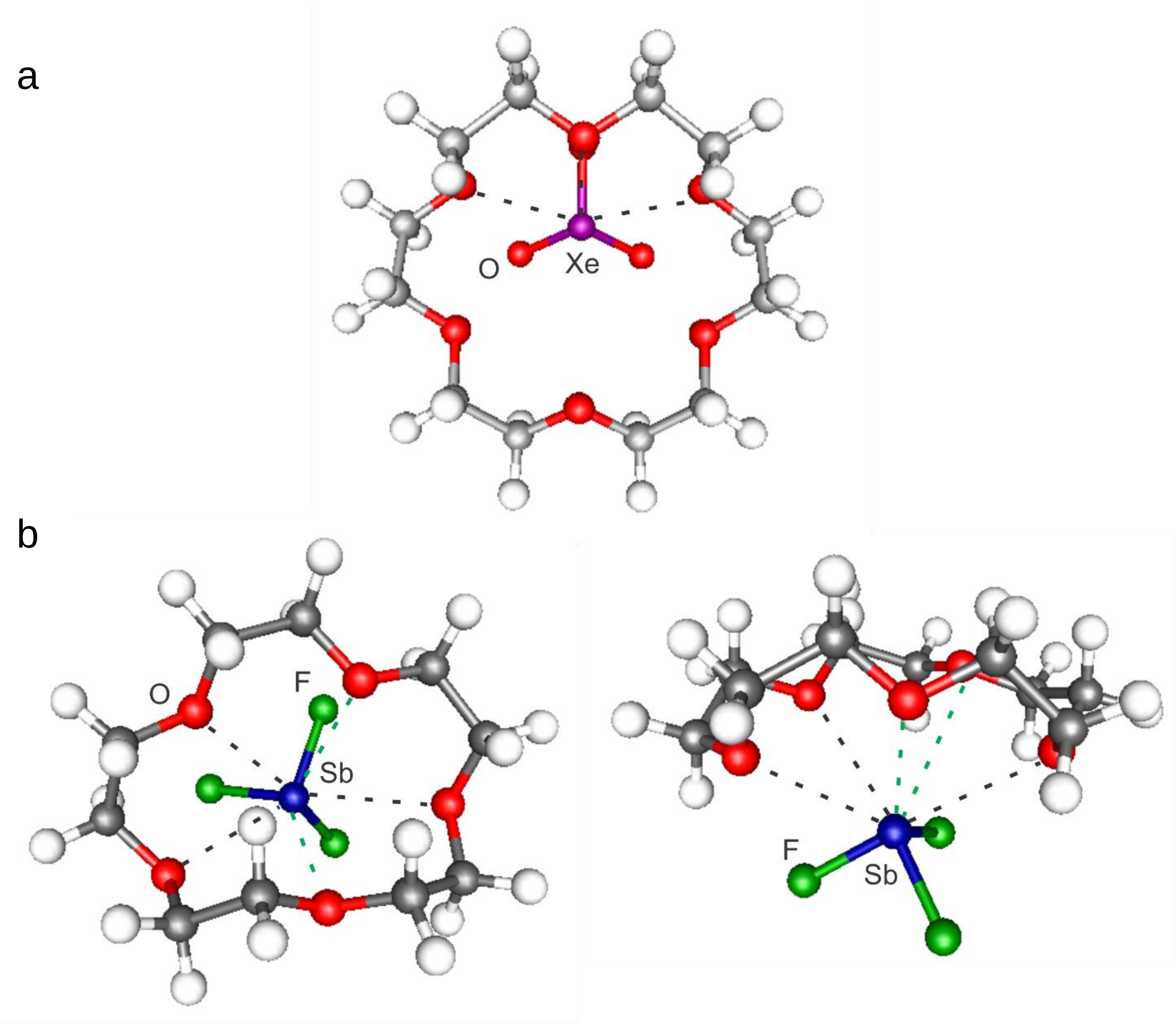

Figure 5.13. The (**a**) top-on view of the calculated (APFD/Def2-TZVP) gas-phase structure of $(CH_2CH_2O)_6XeO_3$ and (**b**) the top-on (left) and side-on views (right) of the calculated (APFD/Def2-TZVP) gas-phase structure of $(CH_2CH_2O)_5SbF_3$.

CHAPTER 6

Oxo-Anion Adducts of Xenon Trioxide

Abstract. *Incorporation of xenon trioxide,* XeO_3*, into inorganic polyatomic salts under ambient conditions has been observed in several mixed xenate salts;* $K[XeO_3XO_3]$ *(X = Cl, Br),* $K_2[XeO_3SeO_4]\cdot HF$*,* $K[(XeO_3)_xZO_3]$ *(Z = I, N), and* $M_2[(XeO_3)_nCO_3]\cdot xH_2O$ *(M = Na, K, Rb, Ba). Raman spectroscopy was used to identify the aforementioned compounds and* $K[XeO_3ClO_3]$*,* $K[XeO_3BrO_3]$*,* $K_2[XeO_3SeO_4]\cdot HF$*, and* $Rb_2[(XeO_3)_2CO_3]\cdot 2H_2O$ *were also characterized by low-temperature, single-crystal X-ray diffraction. The xenon atom of* XeO_3 *is seven coordinate in* $K[XeO_3ClO_3]$ *and six coordinate in all other compounds with Xe---O distances that are significantly less than the sum of the Xe and O van der Waals radii. These salts provide examples of* XeO_3 *coordinated to inorganic compounds and may provide insights into the inclusion of xenon oxides in minerals.*

6.1 Introduction

The expansion of XeO_3 chemistry in the recent years[1–6] accounts for the vast majority of xenon oxide chemistry. Xenon tetroxide[7] and xenon dioxide[8] are the only other binary xenon oxides that have been synthesized in macroscopic quantities. The UV photolysis of XeO_4 in noble-gas matrices at low-temperature afforded the Xe(VIII) peroxo-species $(\eta^2{-}O_2)(Xe^{VIII}O_3)$ and XeO_3.[9] Although the xenon(II) oxide, $Xe^{II}O$, has been postulated as an intermediate in some oxidation reactions of XeO_3,[10] it has not been synthesized in macroscopic amounts and has only been obtained in an argon matrix by Hg-arc photolysis of $Ar/O_3/Xe$.[11] UV spectroscopy suggested the ground state of XeO is essentially a van der Waals molecule with a bond length that is considerably longer than that of the excited state value.[12,13] Two novel xenon oxides, Xe_2O_5 and Xe_3O_2, were synthesized under oxygen-rich and oxygen-poor conditions, respectively, by means of a direct reaction between xenon and oxygen at pressures around 75 GPa.[14] Both compounds were characterized at high pressures using powder X-ray diffraction, X-ray absorption spectroscopy, and Raman spectroscopy. The syntheses of novel xenon oxides under high-pressure conditions suggest that xenon is more reactive under pressure than previously thought, and that other xenon oxides are also anticipated to be stable at high pressures.[15]

Earth's atmosphere contains less than 10% of the aticpiated amount of xenon gas. It was hypothesized that xenon displaces silicon from quartz at high pressures and temperature, with the implication that xenon may be retained within silicate minerals deep in the Earth's core, providing a plausible explanation for the Earth's missing xenon.

Only one oxo-anion of xenon has been synthesied and structurally characterized.[16,17] Alkali metal xenates were synthesized by the reaction of stoichiometric amounts of MOH (M = Na, K, Rb, Cs) and XeO_3 in aqueous solutions and initially characterized by mass balance measurements, infrared spectroscopy, and powder X-ray diffraction.[18–22] The xenate salts were reported to be stable at room-temperature, but rapidly underwent disproportionation in the presence of water to perxenate, Xe, and O_2. Sodium perxenate, the first example of a Xe(VIII) compound, was synthesized by the reaction of XeO_3 with hydroxide in aqueous solutions.[23,24] The crystal structures of $Na_4XeO_6{\cdot}8H_2O$,[25,26] $Na_4XeO_6{\cdot}6H_2O$,[27,28] $K_4XeO_6{\cdot}9H_2O$,[29] $K_2Na_2XeO_6{\cdot}8H_2O$,[30] and $K_4XeO_6{\cdot}2XeO_3$[31] were reported shortly thereafter. Carbonates are well known contaminants of most perxenate samples due to absorption of carbon dioxide by the alkali metal hydroxide from the air.[32] Despite the previously characterized fluoro-,[33] chloro-,[34] and bromoxenates,[4] and the interaction of the perxenate anion with XeO_3, no studies of the interactions of polyatomic anions such as carbonates, with XeO_3 have been reported.

Although xenon trioxide is highly unstable to thermal and mechanical shock,[35–38] coordination of a *N*- or *O*-base to the Xe atom through σ-hole bonding interactions often results in significant kinetic stabilization.[5,6] Compounds containing a five (Chapter 3), six (Chapter 3), seven (Chapter 5) and eight (Chapter 4) coordinate Xe atom in XeO_3 have been synthesized and structurally characterized in adducts of XeO_3 with organic bases.[2–6] Prior to this study, the only example of XeO_3 coordinated to an inorganic compound was the mixed xenate salt, $K_4XeO_6{\cdot}2XeO_3$[31].

The oxygen atoms of KNO_3 and K_2SeO_4 interact with the antimony atom of SbF_3 to form the complexes $KSbF_3NO_3$,[39] $K_2SeO_4(SbF_3)_2{\cdot}H_2O$,[40] and $K_2SeO_4SbF_3{\cdot}0.5H_2O$.[41] The Sb---O interactions are significantly less than the sum of the van der Waals radii of Sb and O and are likely similar to the Sb---O_{crown} interactions in the crown ether adducts of SbF_3.[42,43]

The present work shows that XeO_3 can be incorporated into nitrate, carbonate, selenate, and oxohalide salts under ambient conditions to provide examples of XeO_3 coordinated to inorganic oxo-anions.

6.2 Results and Discussion

6.2.1 Synthesis

6.2.1.1 Synthesis of K[XO_3XeO_3] (X = Cl (1), Br (2)), K[$(XeO_3)_nXO_3$] (Z = I (3), N (4)) and K_2[XeO_3SeO_4]·HF (5)

Aqueous potassium chlorate, bromate, iodate, nitrate, and selenate solutions were mixed with aqueous solutions of XeO_3 in dilute HF (molar ratios XeO_3:HF = 1:6, see Experimental) at room temperature. Evaporation of water and HF from the resulting solutions yielded colorless crystals of potassium xenon trioxide chlorate, bromate, iodate, nitrate (K[XeO_3XO_3] (X = Cl (**1**), Br (**2**)), K[$(XeO_3)_nXO_3$) (X = I (**3**), N (**4**)) and dipotassium xenon trioxide selenate, K_2[XeO_3SeO_4]·HF (**5**). All solids were significantly less shock sensitive than solid XeO_3 but did detonate when struck extremely hard with a steel hammer. The solids (**1**), (**2**), (**3**) and (**4**) were stable at room temperature but rapidly decomposed with the liberation of a gas when dissolved in water. Crystalline

$K[(XeO_3)_nXO_3]$ (X = I (**3**), N (**4**)) did not diffract at low- or room-temperatures whereas crystalline (**5**) slowly decomposed over a period of several days.

6.2.1.2 Synthesis of $M_2[(XeO_3)_nCO_3]\cdot xH_2O$ (M = Na, K, Rb, Ba) (6)

Aqueous alkali metal carbonate solutions were mixed with neutralized aqueous solutions of XeO_3 at room temperature. Evaporation of water from the resulting solutions at room temperature yielded fine, colorless powders of the alkali metal xenon trioxide carbonate hydrates. The dry powders were stable under atmospheric conditions but slowly decomposed in water over several months. Very slow evaporation of the solutions resulted in the formation of crystals which were too small for structure determination by single-crystal X-ray diffraction. Needle-shaped crystals of the rubidium salt were however grown by mixing dilute solutions of aqueous RbOH and XeO_3 and allowing the solution to slowly absorb CO_2 from the air.

6.2.2 X-ray Crystallography

The low-temperature, single-crystal X-ray structures of $K[XeO_3ClO_3]$ (**1**), $K[XeO_3BrO_3]$ (**2**), $K_2[XeO_3SeO_4]\cdot HF$ (**5**) and $Rb_2[(XeO_3)_2CO_3]\cdot 2H_2O$ (**6**) were determined and are shown in Figures 6.1–6.4. A summary of crystal data and refinement results are provided in Tables 6.1 and 6.2 and a summary of geometrical parameters is given in Tables 6.3 and 6.4. More complete lists are provided in Tables 6.3–6.6. The primary Xe–O bonds and O–Xe–O angles of (**1**), (**2**), and (**5**) fall within ranges of all three phases of solid XeO_3 (1.7624(16)–1.7772(18) Å; α-XeO_3 (100.51(5)–105.09(6)°), β-XeO_3 (102.9(2)°), and γ–XeO_3 (101.72(10)–102.52(11)°).[1] The Xe atom of XeO_3 is six coordinate in (**2**), (**5**) and (**6**) and seven coordinate in (**1**) with *trans*–O---Xe−O angles

Table 6.1. Summary of X-ray Crystal Data and Refinement Results for K[XeO_3ClO_3] (**1**), K[XeO_3BrO_3] (**2**), K_2[XeO_3SeO_4] (**5**) and Rb_2[$(XeO_3)_2CO_3$]·$2H_2O$ (**6**).

Compound	**(1)**	**(2)**	**(5)**	**(6)**
Chemical formula	KO_6ClXe	KO_6BrXe	$K_2O_7SeXeHF$	$CH_4O_{11}Rb_2Xe_2$
space group	*C*2/*c*	*P*2/*c*	$P2_1/n$	*C*2/*c*
a (Å)	14.2450(13)	8.3456(2)	9.2182(4)	8.8135(6)
b (Å)	5.5199(6)	6.6192(2)	5.7597(3)	21.1307(14)
c (Å)	15.4120(14)	11.0651(3)	15.5966(7)	12.6101(9)
α (deg)	90	90	90	90
β (deg)	98.052(2)	92.875(1)	100.484(2)	91.844(3)
γ (deg)	90	90	90	90
V (Å^3)	1199.9(2)	610.48(3)	814.26(7)	2347.2(3)
Z (molecules/unit cell)	8	4	4	8
mol. wt. (g mol^{-1})	301.84	346.29	420.46	625.58
calcd density (g cm^{-3})	3.342	3.768	3.430	3.541
T (K)	−173	−173	−173	−173
μ (μμ^{-1})	6.843	12.833	9.741	14.060
$R_1{}^a$	0.0195	0.0212	0.0270	0.0347
$wR_2{}^b$	0.0511	0.0481	0.0690	0.0861

[a] $R_1 = \Sigma||F_o|-|F_c||/\Sigma|F_o|$. [b] $wR_2 = [\Sigma(w(F_o^2-F_c^2)^2)/\Sigma(w(F_o^2)^2)]^{½}$.

Table 6.2. Summary of important Bond Lengths (Å) and Angles (deg) of K[XeO_3ClO_3] (**1**), K[XeO_3BrO_3] (**2**), K_2[XeO_3SeO_4]·HF (**5**), and Rb_2[$(XeO_3)_2CO_3$]·$2H_2O$ (**6**).

Compound	**1**	**2**
Xe−O	1.7597(8)–1.7683(8)	1.765(1)–1.775(1)
Xe---O	2.7002(8)–2.9268(9)	2.625(1)–2.684(1)
O–Xe–O	101.15(4)–103.84(4)	100.80(5)–101.44(5)
***trans*–O---Xe−O**	151.65(3)–165.86(4)	157.94(4)–168.15(4)
cis−O---Xe−O	76.96(3)–86.96(3)	87.90(4)–96.07(4)

Compound	**5**	**6**
Xe−O	1.769(1)–1.778(1)	1.762(2)–1.791(2)
Xe---O	2.609(5)–2.705(6)	2.376(2)–2.9712(4)
O–Xe–O	99.14(6)–102.55(6)	97.80(8)–103.90(9)
***trans*–O---Xe−O**	160.84(5)–170.82(6)	157.24(8)–169.73(7)
cis−O---Xe−O	81.50(5)–90.65(4)	79.48(7)–94.49(7)

(151.65(3)–170.82(6)°) angles that are consistent with predominantly electrostatic σ-hole bonding.[5,6]

K[XeO_3ClO_3] (1). The crystal structure of K[XeO_3ClO_3] belongs to the monoclinic *C*2/*c* space group (Figure 6.1). Molecules of XeO_3 are oxygen bridged by ClO_3^- molecules forming forming chains comprised of $_{(ClO3)}$O---XeO_3----$O_{(ClO3)}$ interactions. The resulting chains run parallel to the *b*-axis and are separated by layers of the cation, K^+, that are aligned along the *a*-axis. The structural unit of (**1**) contains one K^+ cation and one molecule of XeO_3 coordinated to one molecule of the anion ClO_3^-. The Xe atom of XeO_3 is coordinated to the oxygen atoms of three different ClO_3^- anions (2.7002(8), 2.9168(8), 2.9268(9), 3.3776(9) Å) giving Xe a total coordination number of seven. The *trans*-O–Xe---O angle with the fourth contact (141.78(3)°) is slightly contracted compared to the other *trans*-O–Xe---O angles (151.65(3), 161.03(3), 165.86(4)°) but comparable to the trans angles observed in other XeO_3 adducts[5] where the coordination number of the Xe atom exceeds six.

The potassium cation interacts with the oxygen atoms of both ClO_3^- and XeO_3 through five K---O_{ClO3} (2.764–2.989 Å) and five K---O_{XeO3} (2.790(1)–3.194(1) Å) bonding interactions. No contacts exist between the Cl atom of ClO_3^- and K^+. The bond lengths of ClO_3^- (1.4832(8), 1.4997(9), 1.5017(8) Å) are not significantly distorted from those observed in the crystal structure of $KClO_3$ (1.488, 1.487 Å) but one of the bond angles (105.29(5), 106.43(5), 106.60(5)°) is less from those of solid $KClO_3$ (106.4, 106.5°).[44]

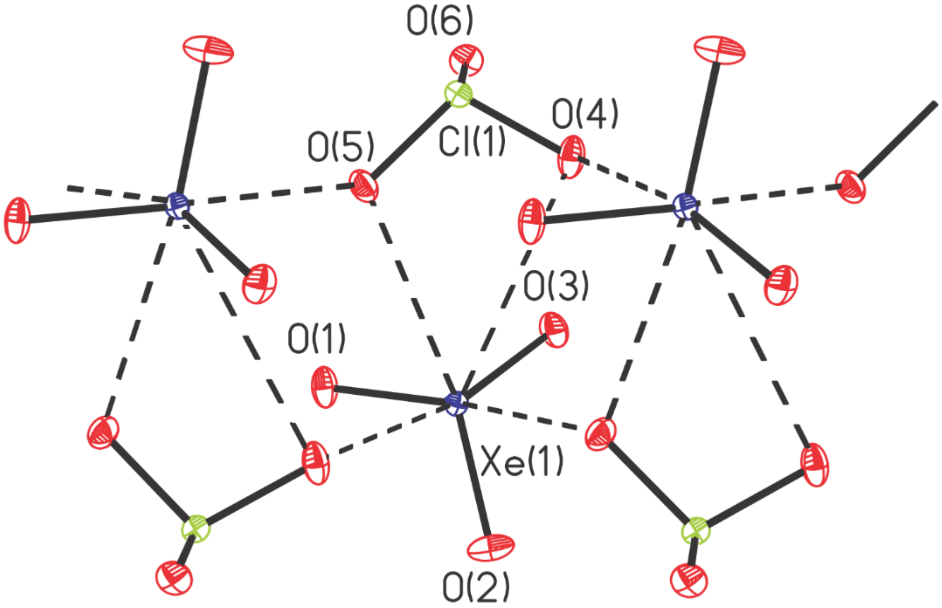

Figure 6.1. A view of the coordination environment of the Xe atom in the crystal structure of K[XeO_3ClO_3] (**1**); K^+ ions have been deleted for clarity. Thermal ellipsoids are shown at the 50% probability level.

K[XeO_3BrO_3] (2). The crystal structure of K[XeO_3BrO_3] belongs to the monoclinic *P*2/*c* space group (Figure 6.2). Similar to (**1**), the structural unit of (**2**) contains one molecule of XeO_3 that is coordinated to one molecule of the BrO_3^- anion. Two crystallographically unique K^+ cations lie on special positions in the asymmetric unit. Layers of the XeO_3BrO_3 unit in the *bc*-plane are arranged around atoms of K^+ and are connected through O_3Xe---$O_{(BrO3)}$ bonding interactions. Unlike (**1**), which contains one shorter and two longer Xe---O contacts, all three Xe---O bonding interactions in (**2**) are short and are within 0.06 Å of one another (2.625(1), 2.642(1), 2.684(1) Å). All three Xe---O contacts are with O atoms of different neighboring BrO_3^- molecules. The K^+ cations interact with the oxygen atoms of both BrO_3^- (2.861, 2.885, 2.912, 3.107 Å) and XeO_3 (2.767, 2.804, 2.857, 3.019, 3.358 Å). The K^+ to O atom distances are slightly elongated but are comparable to the distances in $Ba(BrO_3)_2{\cdot}H_2O$ (2.728–3.062 Å).[45] Overall, the Br–O bonds (1.651(1), 1.659(1), 1.669(1) Å) are slightly elongated when compared with those of solid $KBrO_3$ (1.651(2) Å)[46] and are similar to those of $Ba(BrO_3)_2{\cdot}H_2O$ (1.655(5), 1.657(4), 1.658(4) Å).[45]

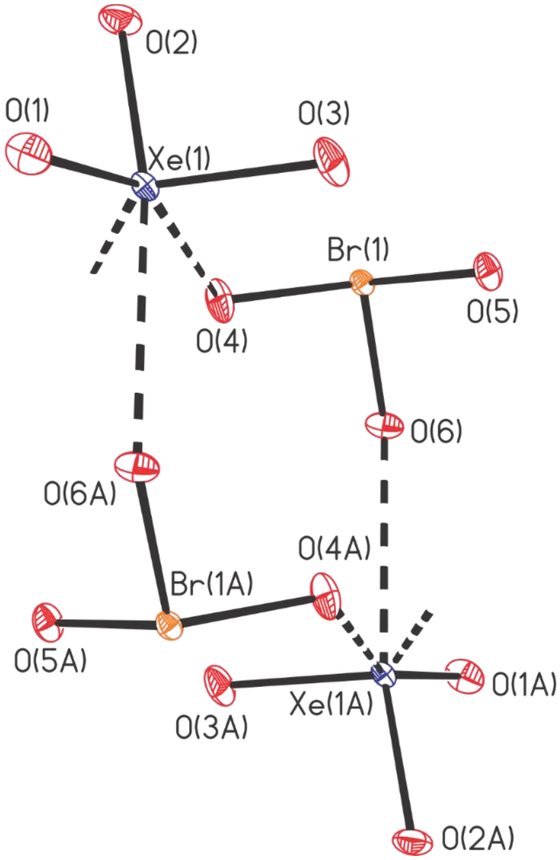

Figure 6.2. A view of the coordination environment of the Xe atom in the crystal structure of $K[XeO_3BrO_3]$ (**2**); K^+ cations have been deleted for clarity. Thermal ellipsoids are shown at the 50% probability level.

$K_2[XeO_3SeO_4]{\cdot}HF$ (3). The crystal structure of $K_2[XeO_3SeO_4]{\cdot}HF$ (**3**) belongs to the monoclinic spacegroup $P2_1/n$ (Figure 6.3). Similar to (**1**) and (**2**), the structural unit of (**3**) contains one XeO_3 molecule coordinated to one SeO_4^{2-} anion. The structural unit also contains a HF molecule that is approximately equidistant (2.649(1), 2.736(1) Å) between two K^+ cations and hydrogen bonded to an $O_{(SeO4)}$ atom (1.654 Å). The HF molecule primarily interacts with K^+, as observed in $K_2SeO_4(SbF_3)_2{\cdot}H_2O$,[40] and $K_2SeO_4SbF_3{\cdot}0.5H_2O$.[41] Infinite chains of the XeO_3SeO_4-unit extend along the *b*–axis with molecules of HF and K^+ cations situated between the chains. The Xe atom of XeO_3 has three Xe---O contacts (2.617(1), 2.645(1), 2.718(1) Å) with oxygen atoms of SeO_4^{2-}. The shortest contact between the K^+ cations and the Se atom of SeO_4^{2-} (3.586 Å) is slightly elongated compared to that of solid K_2SeO_4 (3.552 Å)[47] and is somewhat greater than the sum of the ionic radii for Se^{2-} and K^+ (3.36 Å).[ref]

The Se–O bonds (1.635(1)–1.655(1) Å) are slightly elongated compared with those of solid K_2SeO_4 (1.63(1) Å)[47] but fall within the ranges for theose of $K_2SeO_4SbF_3{\cdot}0.5H_2O$ (1.61(1)–1.67(1) Å)[41] and $K_2SeO_4(SbF_3)_2{\cdot}H_2O$ (1.63(1)–1.65(1) Å).[40] The SeO_4^{2-} anion has tetrahedral geometry and the O–Se–O angles (108.16(7), 108.97(7), 110.14(6), 110.51(6)°) are similar to those of K_2SeO_4 (108.4–110.5°).[47] The primary and O–Xe–O angles (99.50(6), 99.14(6), 102.55(6)°) are slightly contracted compared to those of the three solid phases of XeO_3 (α-XeO_3 (100.51(5)–105.09(6)°), β-XeO_3 (102.9(2)°), and γ-XeO_3 (101.72(10)–102.52(11)°).[1]

$Rb_2[(XeO_3)_2CO_3]{\cdot}2H_2O$ (4). The salt crystallizes in the *C*2/*c* space group (Figure 6.4). The structure consists of chains formed between bridged carbonate anions and XeO_3 molecules running parallel to the *a*-axis of the unit cell. Water molecules are aligned along the *c*-axis and separate the chains. The bridging carbonate anions have two short Xe---O interactions ($Xe_{(1)}$ 2.376(2), $Xe_{(2)}$ 2.378(2) Å) which are significantly shorter than other Xe---O inter-

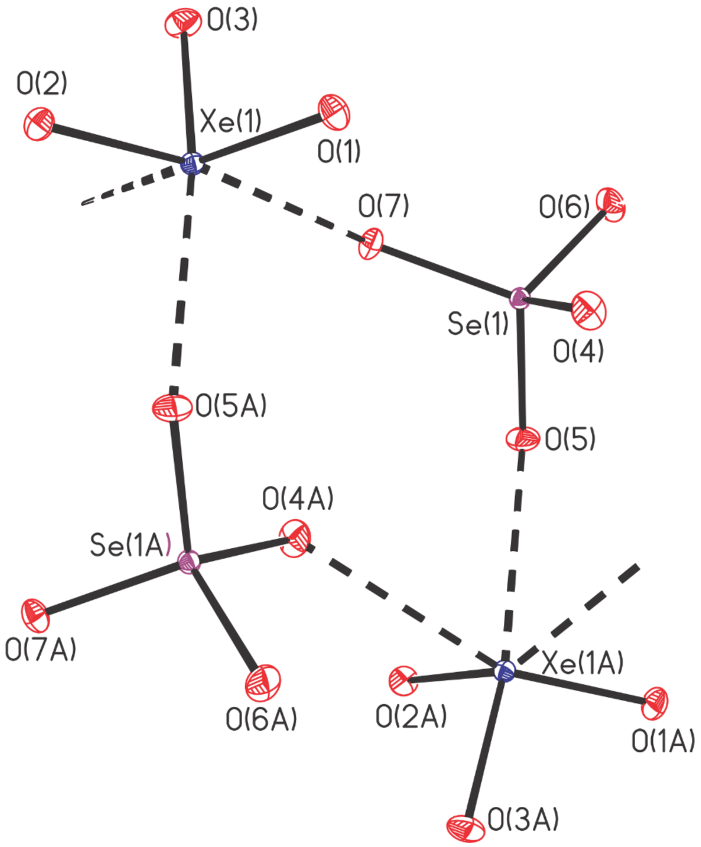

Figure 6.3. A view of the coordination environment of the Xe atom in the crystal structure of $K_2[XeO_3SeO_4]\cdot HF$ (**3**); K^+ cations and HF molecules have been removed for clarity. Thermal ellipsoids are draw at the 50% probability level.

actions ($Xe_{(1)}$ 2.9651(4), $Xe_{(2)}$ 2.9712(4) Å). In addition to Xe---O_{CO3}–XeO_3 bonding interactions, each XeO_3 molecule has a shorter Xe---O bond (2.714(2), 2.715(2) Å) between adjacent XeO_3 molecules within the chain and a longer Xe---O bond (2.888(2), 2.898(2) Å) with XeO_3 molecules belonging to adjacent chains. The O(H)---O_{CO3} bond lengths (2.792(3), 2.801(3) Å) are similar to those of $Cs_2CO_3\cdot 3H_2O$ (2.730(4)–2.835(4) Å)[49] but are longer than those of $K_2CO_3\cdot 1.5H_2O$ (2.698–2.717 Å)[50] and $Rb_2CO_3\cdot 1.5H_2O$ (2.664(4)–2.720(4) Å)[49]. The O atoms of CO_3^{2-} have *trans*–O---Xe–O bond angles

(174.45(7), 174.76(7)°) that are closer to 180° than those of the central O atoms (134.06(7), 134.19(7)°) or the *trans*–O---Xe–O angles formed between the XeO_3 molecules within the chain (157.24(8), 157.46(8)°) and with an adjacent chain (166.02(7), 169.73(7)°).

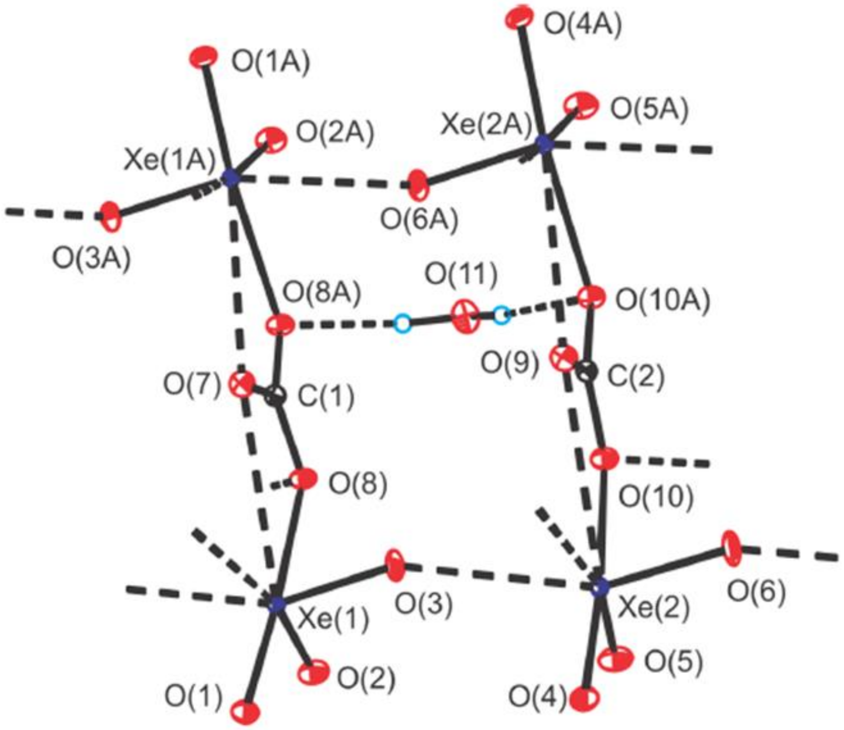

Figure 6.4. A view of the coordination environment of the Xe atom in the crystal structure of $Rb_2[(XeO_3)_2CO_3]\cdot 2H_2O$ (**4**); Rb^{2+} cations have been deleted for clarity. Thermal ellipsoids are shown at the 50% probability level.

The primary Xe–O bonds (1.7891(16), 1.7913(16) Å) that are trans to the Xe---O bonds with CO_3^{2-} are significantly longer than the other primary Xe–O bonds (1.7624(16)–1.7772(18) Å). The primary O–Xe–O bond angles (97.80(8)– 103.9(1)°) fall within the same range as those of α-XeO_3 (100.51(5)–105.09(6)°), β-XeO_3 (102.9(2)°), and γ-XeO_3 (101.72(10)–102.52(11)°),[1] but some of the angles are significantly more closed than those of the three phases of XeO_3. The primary O–C–O bond angles (117.2(2)–121.38(12)° are somewhat more distorted when compared with those of $Rb_2CO_3{\cdot}1.5H_2O$ (119.2(3)–120.6(3)°) and $Cs_2CO_3{\cdot}3H_2O$ (119.2(4)–120.4(2)°).[49]

6.2.3 Raman Spectroscopy

A complete list of vibrational frequencies and assignments is provided for $K[XeO_3XO_3]$ (X = Cl, Br), $K[(XeO_3)_nZO_3]$ (Z = I, N), $K_2[XeO_3SeO_4]$, and $M_2[(XeO_3)_nCO_3]{\cdot}xH_2O$ (M = Na, K, Rb, Ba), in Tables 6.7–6.12 and the Raman spectra are depicted in Figures 6.5–6.9. Raman spectral assignments of the XeO_3 bands were aided by comparison with the previously reported Raman spectra of $[X_3(XeO_3)_3]^{3-}$ and $[X_4(XeO_3)_4]^{4-}$ (X = Cl or Br) anions[4] which were assigned based on the calculated vibrational frequencies and intensities of their energy-minimized gas-phase geometries. Vibrational assignments for the anions were made by comparison with their previously published assignments.[51–56]

6.2.3.1 Raman Spectra of K[XeO$_3$ClO$_3$] (1), K[XeO$_3$BrO$_3$] (2), and K[(IO$_3$)$_n$XeO$_3$] (3)

The Raman spectra of these compounds were analyzed based on crystal structures of $K[XeO_3ClO_3]$ (**1**) and $K[XeO_3BrO_3]$ (**2**) and were used as the basis for the Raman assignment of $K[(IO_3)_nXeO_3]$ (**3**) for which single crystals suitable for X-ray crystallography could not be grown. The most intense bands (A_1; 764, 787 (**1**), 766 (**2**) and 776 (**3**) cm^{-1}) are assigned to the XeO_3 symmetric stretching mode, $\nu_{sym}(XeO_3)$. The bands assigned to the $\nu_{asym}(XeO_3)$ asymmetric stretching mode (E; 807, 828, 848 (**1**), 809, 820, 830 (**2**) and 830, 840, 859 (**3**) cm^{-1}), the $\delta_{asym}(XeO_3)$ asymmetric bending mode (E; 301, 309, 318 **(1)** and 305, 317 **(2)** cm^{-1}) and the δ_{umb}(XeO_3) symmetric bending mode (A_1; 334, 348, 362 **(1)** and 329 **(2)** cm^{-1}) could be unambiguously assigned. The region in the Raman spectrum of (**3**) corresponding to the δ_{as}(XeO_3)/(IO_3) bending modes could not be assigned with certainty due to overlapping vibrational bands.

The Raman spectrum of (**3**) displays a band at 471 cm^{-1} that could not be assigned to IO_3^- or XeO_3 stretching or bending bands. A band attributable to the ν_4(E, IO_3)$^-$ bending mode of solid KIO_3 (371 cm^{-1}) was not present in the Raman spectrum of (**3**). The ν_3(E, IO_3) stretching bands of (**3**) (806, 819 cm^{-1}) are shifted to a significantly higher frequency than those of KIO_3 (783, 791, 813 cm^{-1}).

The asymmetric and symmetric ClO_3^- bends in (**1**) (ν_4(E), 465, 480, 491; ν_2(A_1) 590, 592, 605, 611(sh), 618 cm^{-1}) occur in the same ranges as observed for solid $KClO_3$ (δ_{asym} 487; δsym 619 cm^{-1}). The asymmetric and symmetric ClO_3^- stretching bands (ν_3(E), 978, 993; ν_1(A_1) 905, 927, 938 cm^{-1}) are significantly less intense in (**1**) than in solid $KClO_3$ (ν_3(E), 977; ν_1(A_1), 938 cm^{-1}).

The shoulder observed at 758 cm^{-1} and the band observed at 783 cm^{-1} in **(2)** are most likely assigned to symmetric [BrO_3]$^-$ stretching modes. The ν_4(E) mode (353(sh), 360, 366, 378 cm^{-1}) is shifted to a significantly higher frequency than that observed in solid $KBrO_3$ (358 cm^{-1}).

6.2.3.2 Raman Spectra of K[(XeO_3)$_n$$NO_3$] (4) and K_2[XeO_3SeO_4]·HF (5)

All four Raman active XeO_3 vibrational bands of K_2[XeO_3SeO_4]·HF (**4**) (A_1, ν_{sym} (765, 757); E, ν_{as} (825, 819, 811, 805); A_1, δ_{umb} (334); E, δ_{as} (320, 303) cm^{-1}) and K[XeO_3NO_3) (**5**) (A_1, ν_{sym} (789); E, ν_{as} (837, 830, 821); A_1, δ_{umb} (376, 363, 347); E, δ_{as}

(329, 318) cm^{-1}) were assigned without ambiguity and are shifter slightly with respect to those of $XeO_{3(aq)}$. The stretching mode of HF could not be detected in (**4**). The vibrational bands of ν_4(E, SeO_4) bending modes (378, 349 cm^{-1}) are shifted to higher frequency than those of K_2SeO_4 (342, 335 cm^{-1}). The $\nu_2(NO_3)$ bending modes were not detected in the Raman spectrum of (**5**).

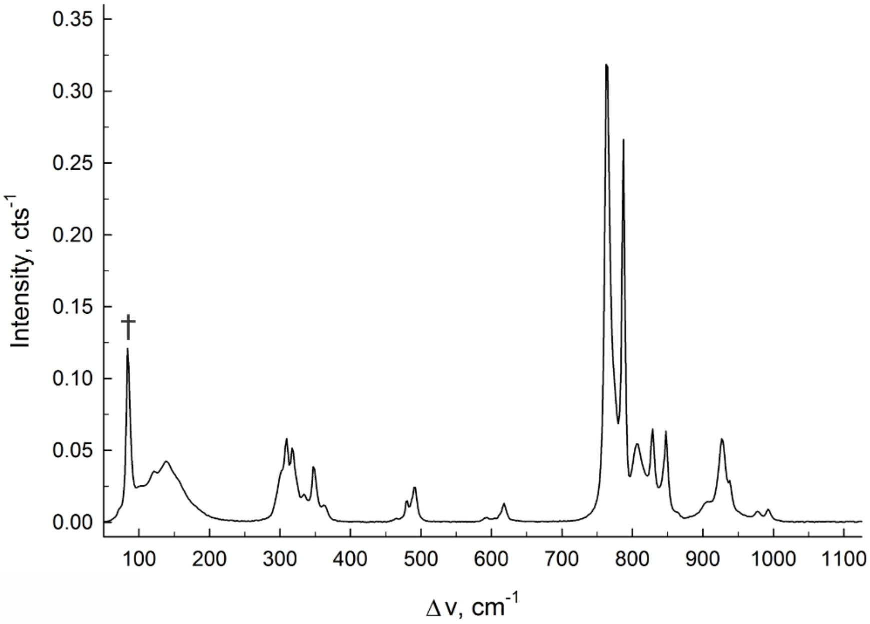

Figure 6.5. Raman spectrum of $K[XeO_3ClO_3]$ (**1**) recorded at room temperature in an aluminum sample holder using 1064–nm excitation. The symbol (†) denotes an instrumental artifact.

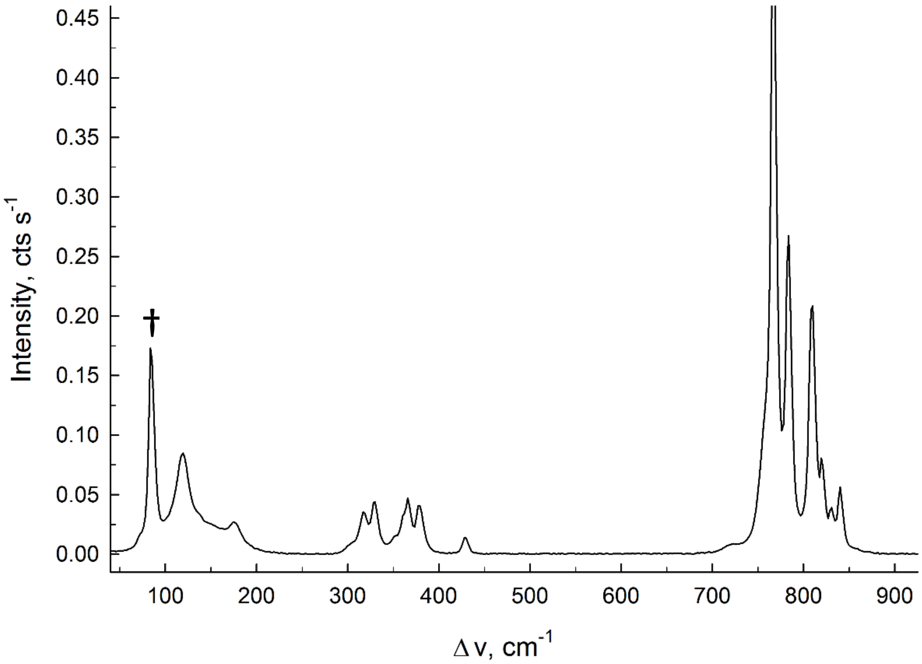

Figure 6.6. Raman spectrum of K[XeO_3BrO_3] (**2**) recorded at room temperature in an aluminum sample holder using 1064–nm excitation. The symbol (†) denotes an instrumental artifact.

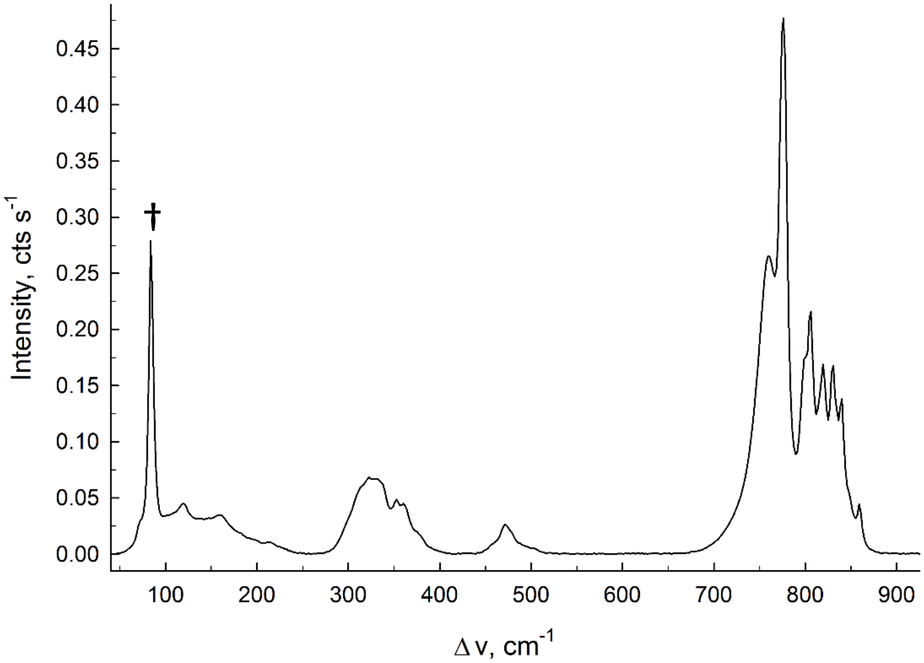

Figure 6.7. Raman spectrum of K[$(XeO_3)_nIO_3$] (**3**) recorded at room temperature in an aluminum sample holder using 1064–nm excitation. The symbol (†) denotes an instrumental artifact.

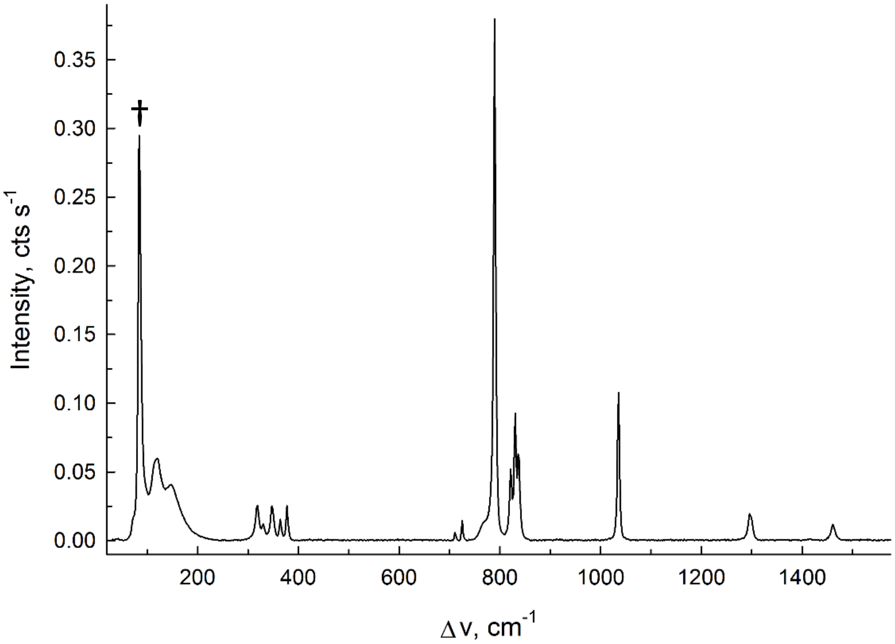

Figure 6.8. Raman spectrum of K[$(XeO_3)_nNO_3$] (**4**) recorded at room temperature in an aluminum sample holder using 1064−nm excitation. The symbol (†) denotes an instrumental artifact.

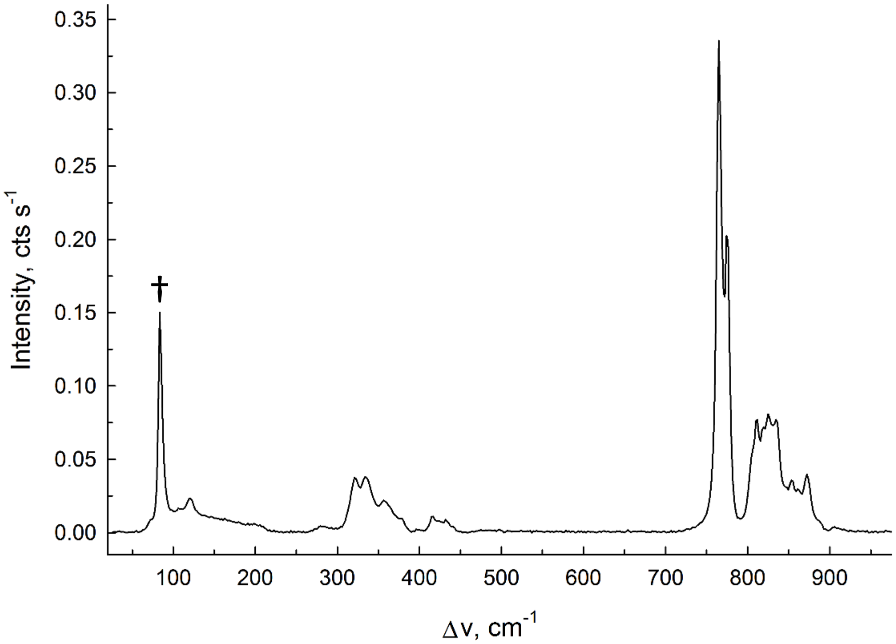

Figure 6.9. Raman spectrum of $K_2[XeO_3SeO_4]\cdot HF$ (**5**) recorded at room temperature in an aluminum sample holder using 1064−nm excitation. The symbol (†) denotes an instrumental artifact.

6.2.3.3 Raman Spectra of $Rb_2[CO_3(XeO_3)_2]\cdot2H_2O$ (4), $Na_2[CO_3(XeO_3)_n]\cdot xH_2O$ [4b], $K_2[CO_3(XeO_3)_n]\cdot xH_2O$ [4c] and $Ba[CO_3(XeO_3)_n]\cdot xH_2O$ [4d]

Because the crystal structure of $Rb_2[(XeO_3)_2CO_3]\cdot2H_2O$ was obtained, the Raman spectrum of this compound was analyzed and used as the basis for the Raman assignments of other $[(XeO_3)_nCO_3]$ salts for which single crystals suitable for X-ray crystallography could not be grown. The highest frequency band (1503 cm^{-1}) was assigned to the asymmetric (E′, $\nu_3(CO_3)$ stretching mode of the carbonate anion.[56] The band at 1056 cm^{-1} was assigned to the symmetric CO_3 stretching mode (A_1, $\nu_1(CO_3)$). Bands assigned to the XeO_3 stretching modes are shifted to lower frequencies ($\nu_{as}(XeO_3)$, 777, 822 cm^{-1}; $\nu_s(XeO_3)$,749 cm^{-1}) relative to those of aqueous and solid XeO_3. No bands occur in the region where the ν_4(E’) band of $[CO_3]^{2-}$ is generally found (ca. 680–710 cm^{-1}). Bands attributable to the XeO_3 bending modes are shifted to higher frequencies ($\delta_{umb}(XeO_3)$ 383 cm^{-1}; $\delta_{as}(XeO_3)$, 322, 336 cm^{-1}) relative to those of α-XeO_3 ($\delta_{umb}(XeO_3)$, 323, 351 cm^{-1}; δas(XeO_3), 297, 311 cm^{-1}). The band at 225 cm^{-1} is likely attributable to ν(Xe---O) of the Xe---O−C bridge between CO_3^{2-} and XeO_3, but as previously observed for chloro– and bromoxenate anion clusters, may be coupled with other deformation modes such as $\rho_r(XeO_2)$ and $\rho_t(XeO_2)$. The other Na^+, K^+, and Ba^{2+} salts exhibit bands that are similar to those of $Rb[CO_3XeO_3]\cdot2H_2O$. Bands attributable to the ν_4(E’) mode of $[CO_3]^{2-}$ were observed at 696 and 696 cm^{-1} (**4b**), 677 and 703 cm^{-1} (**4c**), and 679 cm^{-1} (**4d**). The large number of bands assigned to the ν_3(E’) modes in the Raman spectra of **4b** (1306−1519 cm^{-1}) and **4c** (1352−1437 cm^{-1}) may be the result of factor-group splittings or may arise from a mixture, although only single bands assigned to the $\nu_1(A_1')$ mode of $[CO_3]^{2-}$ were observed at 1062 cm^{-1} (**4b**) and 1052 cm^{-1} (**4c**), providing support for a single compound.

A general trend of decreasing frequencies of the XeO_3 bending modes with increasing cation mass was observed. For example, bands assigned to the $\delta_{as}(XeO_3)$ mode occur at 351, 348, and 336 cm^{-1} for the Na$^+$, K$^+$, and Rb$^+$ salts, respectively. A band at 3052 cm^{-1} in the Raman spectrum of the Ba^{2+} salt is assignable to H_2O and suggests that the Ba^{2+} cation is coordinated to H_2O.

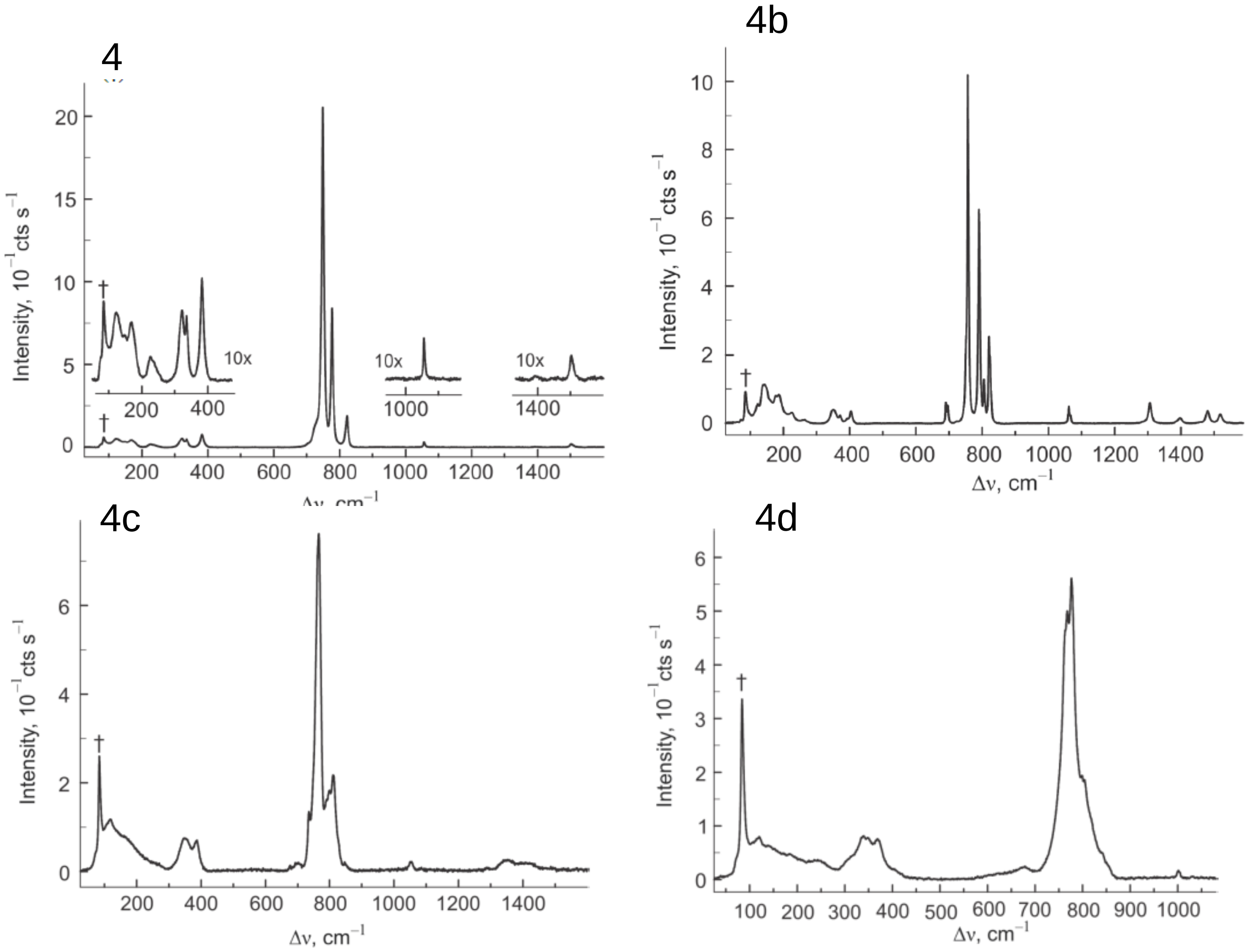

Figure 6.10. Raman spectra of $Rb_2[CO_3(XeO_3)_2]\cdot 2H_2O$ **(4)**, $Na_2[CO_3(XeO_3)_n]\cdot xH_2O$ **(4b)**, $K_2[CO_3(XeO_3)n]\cdot xH_2O$ **(4c)** and $Ba[CO_3(XeO_3)n]\cdot xH_2O$ **(4d)**, recorded at room temperature in an aluminum sample holder using 1064-nm excitation; the symbol (†) denotes an instrumental artifact.

6.3 Conclusion

Incorporation of xenon trioxide, XeO_3, into inorganic polyatomic salts under ambient conditions by adduct formation with oxoanions is observed in several mixed xenate salts; $K[XeO_3XO_3]$ (X = Cl, Br), $K_2[XeO_3SeO_4]\cdot HF$, $K[(XeO_3)_xZO_3]$ (Z = I, N), and $M_2[(XeO_3)_nCO_3]\cdot xH_2O$ (M = Na, K, Rb, Ba). Raman spectroscopy was used to identify the aforementioned compounds and $K[XeO_3ClO_3]$, $K[XeO_3BrO_3]$, $K_2[XeO_3SeO_4]\cdot HF$, and $Rb_2[(XeO_3)_2CO_3]\cdot 2H_2O$ were also characterized by low-temperature, single-crystal X-ray diffraction. These salts display intense bands assigned to XeO_3 stretching and bending modes and considerably weaker bands assigned to the vibrational modes of the anions. The xenon atom of XeO_3 is seven coordinate in $K[XeO_3ClO_3]$ and six coordinate in all other compounds with Xe---O distances that are significantly less than the sum of the Xe and O van der Waals radii.

Experimental Section

Caution! *Solid XeO_3 detonates when subjected to mild thermal or mechanical shock. Great care must be taken during the syntheses and handling of XeO_3 and its compounds. For these reasons, the quantity of XeO_3 used in each synthesis has been limited to 5–15 mg. Reaction vessels fabricated from FEP (hexafluoropropylene, tetrafluoroethylene copolymer) fluoroplastic, which is inert to attack by HF, strong oxidants, and fluorinating agents, generally does not shatter to produce sharp shards when detonation occurs at the reagent scales described in this study. Appropriate protective equipment (face shield, leather gloves, ear protection) must be used.*

$K[XeO_3XO_3]$ (X = Cl (1), Br (2)). In a typical reaction, an aliquot of $XeO_3\cdot 6HF_{(aq)}$ (ca. 6 mg, 33 μmol, XeO_3) was transferred into a 3×3 cm FEP (hexafluoropropylene, tetrafluoroethylene copolymer) fluoroplastic tray by use of a FEP pipette. A saturated aqueous solution containing potassium chlorate or bromate ($KClO_3$, 4.10 mg, 33.5 μmol, ca. 0.2 mL H_2O; $KBrO_3$ 5.59 mg, 33.5 μmol, ca. 0.2 mL H_2O) was prepared in deionized water. This solution was added dropwise on top of the aliquot of $XeO_3{\cdot}6HF_{(aq)}$. Evaporation of $HF_{(aq)}$ (ca. 36 h) in a fume hood followed by further drying in a desiccator (2–3 h) to remove residual moisture afforded crystals that were suitable for a single crystal X-ray structure determination.

$K[(XeO_3)_nZO_3]$ (Z = I (3), N (4)). In a typical reaction, an aliquot of $XeO_3{\cdot}6HF_{(aq)}$ (ca. 6 mg, 33 μmol mmol XeO_3) was transferred into FEP tray by use of a FEP pipette. A saturated aqueous solution containing potassium iodate or nitrate (KIO_3, 7.17 mg, 33.5 μmol, ca. 0.2 mL H_2O; KNO_3 3.38 mg, 33.5 μmol, ca. 0.3 mL H_2O) was prepared in deionized water. This solution was added dropwise on top of the aliquot of $XeO_3{\cdot}6HF_{(aq)}$. Evaporation of $HF_{(aq)}$ (ca. 24 h) in a fume hood afforded crystals of (**3**) that did not diffract and crystals of (**4**) that were severely disordered.

$K_2[XeO_3SeO_4]{\cdot}HF$ (5). In a typical reaction, an aliquot of $XeO_3{\cdot}6HF_{(aq)}$ (ca. 6 mg, 33 μmol XeO_3) was transferred into a FEP tray by use of a FEP pipette. A saturated aqueous solution containing potassium selenate (7.10 mg, 33.5 μmol, ca. 0.2 mL H_2O) was prepared using deionized water. This solution was added dropwise on top of the aliquot of $XeO_3{\cdot}6HF_{(aq)}$. Evaporation of $HF_{(aq)}$ (ca. 36 h) in a fume hood followed by further drying in a desiccator (2–3 h) to remove residual moisture afforded crystals that were suitable for a single crystal X-ray structure determination.

$M_2[CO_3(XeO_3)_n]{\cdot}xH2O$ (M = Na, K, Rb, Ba) (6). In a typical reaction, an aqueous solution of an alkali-metal carbonate salt (ca. 20 mg, 0.18 mmol) was layered onto an aqueous solution of XeO3 (ca. 10 mg, 0.056 mmol) at 0 °C. After several days, no precipitate formed and the solution was poured into a polystyrene Petri dish. Evaporation of the water from the resulting solution at room temperature resulted in the formation of a fine, colorless powder which was stable in the atmosphere but slowly decomposed in water over a month. Very slow evaporation of the solution over five days resulted in the formation of very small crystals, which were unsuitable for a structure determination by single-crystal X-ray diffraction. Large, needle-shaped crystals of $Rb_2[CO_3(XeO_3)_2]\cdot 2H_2O$ were grown by mixing dilute solutions of aqueous RbOH and XeO_3 and allowing the solution to slowly absorb CO_2 from the air.

References

[1] J. T. Goettel, G. J. Schrobilgen *Inorg. Chem.* **2016**, *55*, 12975.

[2] J. T. Goettel, K. Matsumoto, H. P. A. Mercier, G. J. Schrobilgen, *Angew. Chem. Int. Ed. Engl.* **2016**, *55*, 13780.

[3] J. T. Goettel, H. P. A. Mercier, G. J. Schrobilgen, *J. Fluorine Chem.* **2018**, *211*, 60.

[4] J. T. Goettel, V. G. Haensch, G. J. Schrobilgen, *J. Am. Chem. Soc.*, **2017**, *139*, 8725.

[5] K. M. Marczenko, H. P. A. Mercier, G. J. Schrobilgen, *Angew. Chem. Int. Ed. Eng.*, **2018**, *57*, 12448–12452.

[6] K. M. Marczenko, J. T. Goettel, G. J. Schrobilgen, *Chem. Eur. J.*, Submitted Sept. **2018**.

[7] J. T. Goettel, Ph. D. Thesis, McMaster University, Hamilton, ON, Canada, 2017.

[8] D. S. Brock, G. J. Schrobilgen, *J. Am. Chem. Soc.* **2011**, 133, 6265.

[9] T. Vent- Schmidt, J. T. Goettel, G. J. Schrobilgen, S. Riedel, *Chem. Eur. J.* **2015**, *21*, 11244.

[10] E. H. Appelman, J. G. Malm, *J. Am. Chem. Soc.* **1964**, *86*, 2141.

[11] B. S. Ault, L. Andrews, *Chem. Phys. Lett.* **1976**, *43*, 350.

[12] T. H. Dunning, P. J. Hay, *J. Chem. Phys.* **1977**, *66*, 3767.

[13] M. Yamanishi, K. Hirao, K. Yamashita, *J. Chem. Phys.* **1998**, *108*, 1514.

[14] A. Dewaele, N. Worth, C. J. Pickard, R. J. Needs, S. Pascarelli, O. Mathon, M. Mezouar, T. Irifune, *Nature Chem.*, **2016**, *8*, 784.

[15] C. Hou, X. Wang, J. Botana, M. Miao, *Phys Chem Chem Phys*, **2017**, *19*, 27463.

[16] M. V. Ivanova, H. P. A. Mercier, G. J. Schrobilgen, *J. Am. Soc. Chem.* **2015**, 137, 13398.

[17] J. R. DeBackere, M. B. Bortolus, G. J. Schrobilgen, *Angew. Chem. Int. Ed.* **2016**, 55, 11917.

[18] N. N. Aleinikov, V. K. Isupov, I. S. Kirin, B. L. Korsunskii, F. I. Dubovitskii, *Chem. Russ. Bull.* **1974**, *23*, 250.

[19] V. K. Isupov, I. S. Kirin, N. N. Alejnikov, B. L. Korsunskij, *Zh. Neorg. Khim.* **1977**, *22*, 1297.

[20] E. H. Appelman, J. G. Malm, *J. Am. Chem. Soc.* **1964**, *86*, 2141.

[21] L. D. Shustov, N. S. Tolmacheva, S. Nabiev, E. K. Il'in, V. D. Klimov, V. P. Ushakov, *Zh. Neorg. Khim.* **1989**, *34*, 1673.

[22] Y. Marcus, D. Cohen, *Inorg. Chem.* **1966**, *5*, 1740.

[23] J. G. Malm, B. D. Holt, R. W. Bane, In *Noble Gas Compounds*; Hyman, H. H., Ed.; University of Chicago Press: Chicago, IL, 1963; p 167.

[24] E. H. Appelman, S. M. Williamson, *Inorg. Synth.* **1968**, *11*, 210.

[25] E. H. Appelman, G. D. Downey, H. H. Claassen, *Inorg. Chem.* **1971**, *10*, 1817.

[26] J. A. Ibers, W. C. Hamilton, D. R. MacKenzie, *Inorg. Chem.* **1964**, *3*, 1412.

[27] A. Zalkin, J. D. Forrester, D. H. Templeton, S. M. Williamson, C. W. Koch, *Science* **1963**, *142*, 501.

[28] A. Zalkin, J. D. Forrester, D. H. Templeton, *Inorg. Chem.* **1964**, *3*, 1417.

[29] A. Zalkin, J. D. Forrester, D. H. Templeton, S. M. Williamson, C. W. Koch, *J. Am. Chem. Soc.* **1964**, *86*, 3569.

[30] S. N. Britvin, S. A. Kashtanov, M. G. Krzhizhanovskaya, A. A. Gurinov, O. V. Glumov, S. Strekopytov, Y. L. Kretser, A. N. Zaitsev, N. V. Chukanov, S. V. Krivovichev, *Angew. Chem. Int. Ed.* **2015**, *54*, 14340.

[31] S. N. Britvin, S. A. Kashtanov, S. V. Krivovichev, N. V. Chukanov, *J. Am. Chem. Soc.* **2016**, *138*, 13838.

[32] H. Selig, H. H. Claassen, C. L. Chernick, J. G. Malm, J. L. Huston, *Science* **1964**, *143*, 1322.

[33] D. Hodgson, J. A. Ibers, *Inorg. Chem.* **1969**, *8*, 326.

[34] R. D. Willett, S. W. Peterson, B. A. Coyle, *J. Am. Chem. Soc.* **1977**, *99*, 8202.

[35] B. Jaselskis, J. P. Warriner, *Anal. Chem.* **1966**, *38*, 563.

[36] S. A. Shackelford, G. U. Yuen, *Inorg. Nucl. Chem. Lett.* **1973**, *9*, 605.

[37] L. A. Khamidullina, S. V. Lotnik, V. P. Kazakov, *Kinet. Catal.* **2008**, *49*, 27.

[38] S. R. Gunn in *Noble-Gas Compounds* (Ed.: H. H. Hyman), University of Chicago Press, Chicago, **1963**, pp. 149–151.

[39] M. Bourgault, M. B. Ducourant, D. Mascherpa-Corral, R. Fourcade, *J. Fluorine Chem.*, **1981**, *17*, 215.

[40] D. Mascherpa-Corral, M. B. Ducourant, R. Fourcade, G. Mashcerpa, S. Alberola, *J. Solid State Chem.* **1986**, *63*, 52.

[41] D. Mascherpa-Corral, M. B. Ducourant, S. Alberola, *J. Solid State Chem.*, **1988**, *76*, 276.

[42] J. Lipkowski, M. S. Fonari, V. Ch. Kravtsov, Y. A. Simonov, E. V. Ganin, V. O. Gelmboldt, *J. Chem. Crystallogr.* **1996**, *26*, 823.

[43] M. Scharfer, J. Pebler, B. Borgsen, F. Weller, K. Dehnicke, K. *Z. Naturforsch.* **1990**, *45b*, 1243.

[44] J. Danielsen, A. Hazell, F. K. Larsen, *Acta Cryst. B.*, **1981**, *37*, 913.

[45] L. K. Templeton, D. H. Templeton, *Acta Cryst. C.*, **1989**, *25*, 672.

[46] M. Szafranski, K. Stahl, *Zeitschrift fuer Kristallographie*, **1994**, *209*, 491.

[47] A. Kalmar, J. S. Stephens, D. W. J. Cruickshank, *Acta Cryst. B.*, **1970**, *26*, 1451.

[48] L. Pauling, *The Nature of the Chemical Bond* (3rd e.d.), Cornell University Press, Ithica, **1960**.

[49] V. Cirpus, J. Wittrock, A. Z. Adam, *Anorg. Allg. Chem.* **2001**, *627*, 533.

[50] F. D. Hunter, G. A. Jeffrey, *J. Chem. Phys.* **1967**, *47*, 3297.

[51] D. W. James, W. H. Leong, *Aus. J. Chem.*, **1970**, *23*, 1087.

[52] G. Davidson in *Spectroscopic Properties of Inorganic and Organometallic Compounds* (Ed.: G. Davidson), Royal Scoeitry of Chemistry, Cambridge, **1993**, pp. 253.

[53] N. E. Massa, F. G. Ullman, J. R. Hardy, *Ferroelectrics*, **1980**, *25*, 601.

[54] M. H. Brooker, *Can. J. Chem.*, **1976**, *55*, 1242.

[55] J. R. Durig, O.D. Bonner, W. H. Breazeale, *J. Phys. Chem.*, **1965**, *69*, 3886.

[56] M. L. Saboungi, *J. Mol. Structure.*, **1996**, *382*, 163.

6.4 Supporting Information

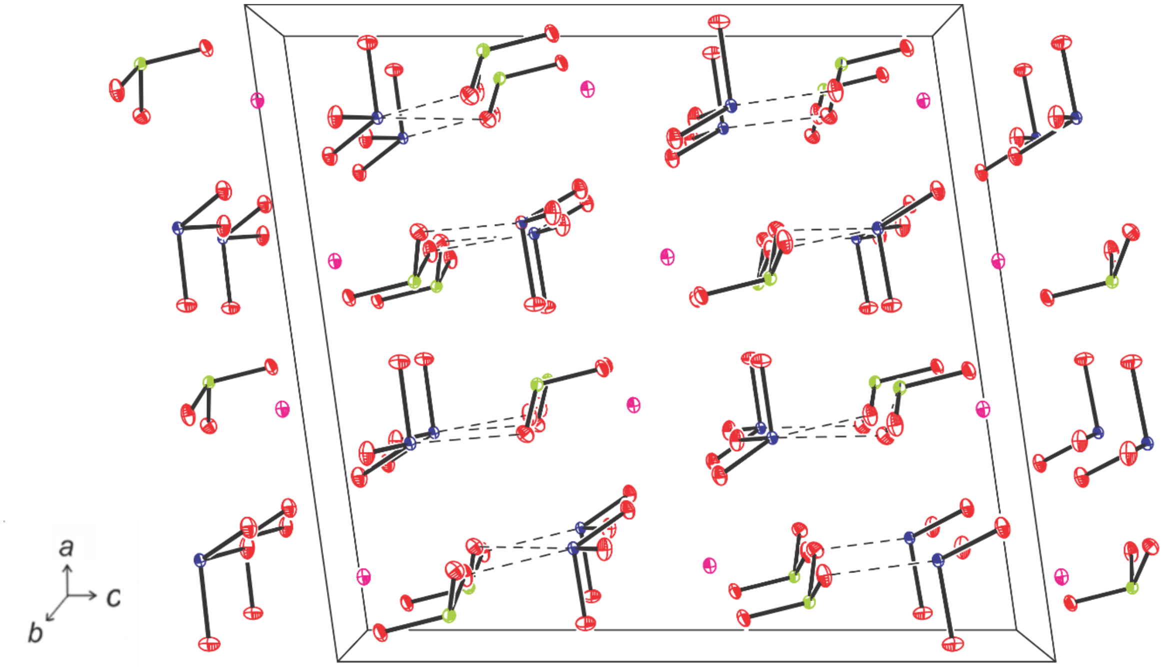

Figure 6.11. Packing diagram of K[XeO_3ClO_3] **(1)**; thermal ellipsoids are shown at the 50% probability level.

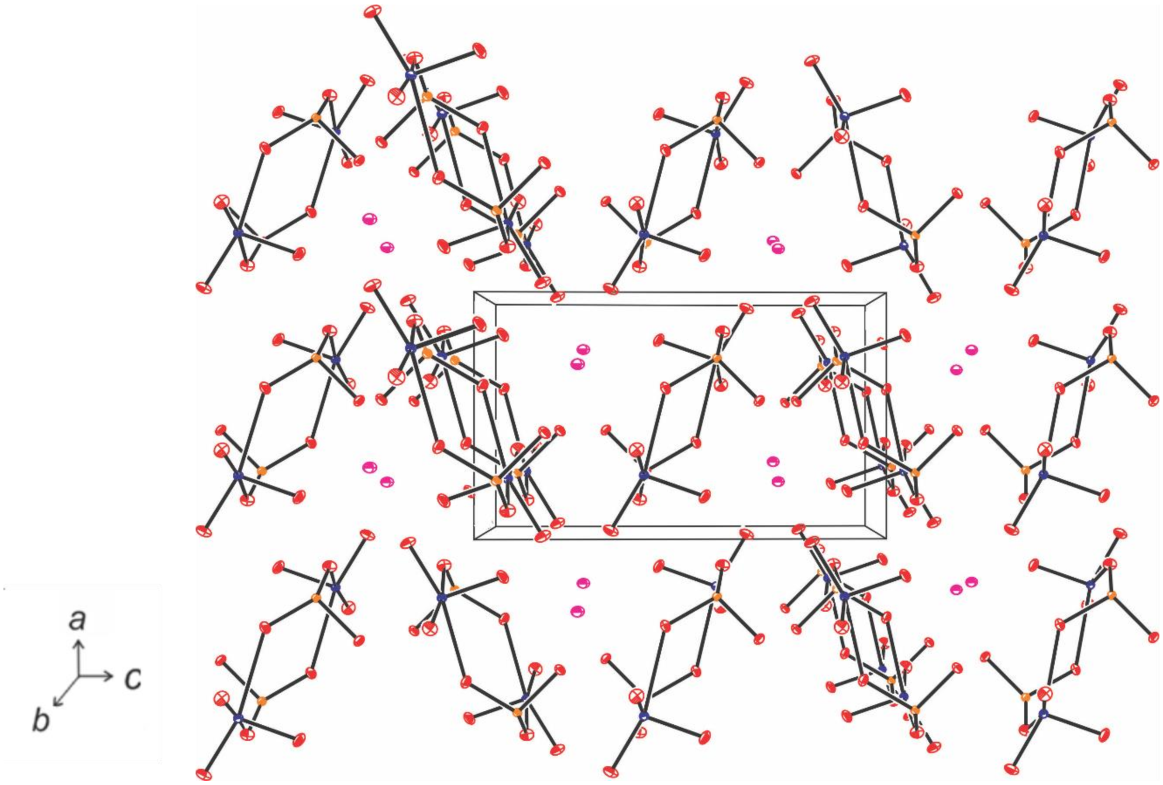

Figure 6.12. Packing diagram of K[XeO_3BrO_3] **(2)**; thermal ellipsoids are shown at the 50% probability level.

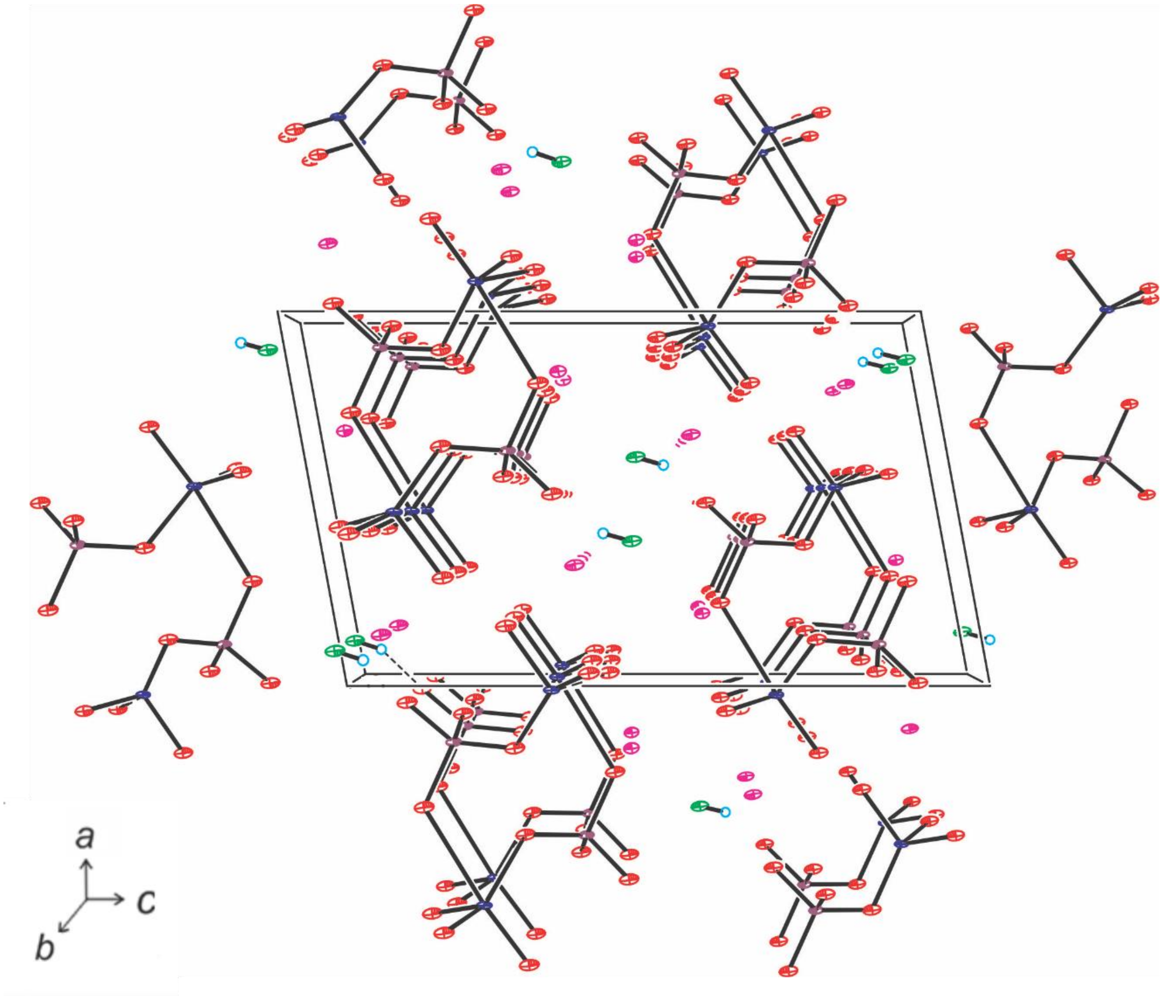

Figure 6.13. Packing diagram of $K_2[XeO_3SeO_4]\cdot HF$ (**5**); thermal ellipsoids are shown at the 50% probability level.

Table 6.3. Selected bond lengths (Å) and angles (deg) of K[XeO_3ClO_3] **(1)**.

Bond Lengths (Å)		**Bond Angles (deg)**	
Xe1–O1	1.7683(8)	O1–Xe1–O2	101.74(4)
Xe1–O2	1.7597(8)	O2–Xe1–O3	101.15(4)
Xe1–O3	1.7646(8)	O3–Xe1–O1	103.84(4)
Xe1–O5	2.9268(9)	O3–Xe1–O4	161.03(3)
Xe1–O5'	2.9196(8)	O1–Xe1–O5	151.65(3)
Xe1–O4	2.7002(8)	O2–Xe1–O5'	165.86(4)
Cl1–O4	1.4997(9)	O3–Xe1–O4	161.03(3)
Cl1–O5	1.5017(8)	O1–Xe1–O5	76.96(3)
Cl1–O6	1.4832(8)	O2–Xe1–O5'	86.96(3)
K1–O1	3.1941(9) 2.7897(9)	O3–Xe1–O4	76.65(3)
K1–O2	3.0770(9)	O4–Xe1–O5	68.59(2)
K1–O3	2.9155(9) 2.8280(9)		71.78(2) 88.07(2)
K1–O4	2.7636(9)		
K1–O5	2.9312(9)		
	2.9666(9)		
K1–O6	2.8532(8)		
	2.9894(9)		

Table 6.4. Selected bond lengths (Å) and angles (deg) of K[XeO_3BrO_3] **(2)**.

Bond Lengths (Å)		**Bond Angles (deg)**	
Xe1–O1	1.775(1)	O1–Xe1–O2	101.44(5)
Xe1–O2	1.765(1)	O2–Xe1–O3	100.80(5)
Xe1–O3	1.769(1)	O3–Xe1–O1	101.37(5)
Xe1–O5	2.684(1)	O1–Xe1–O4	157.59(4)
Xe1–O6	2.625(1)	O2–Xe1–O6	168.15(4)
Xe1–O4	2.642(1)	O3–Xe1–O5	167.86(4)
Br1–O4	1.659(1)	O3–Xe1–O4	161.03(3)
Br1–O5	1.669 (1)	O1–Xe1–O5	87.90(4)
Br1–O6	1.765(1)	O3–Xe1–O4	96.07(4)
Xe1–K1	3.985(1)	O4–Xe1–O5	73.13(3)
Xe1–K2	4.509(1)	O5–Xe1–O6	83.48(3)
Br1–K1	4.242(1)	O6–Xe1–O4	86.04(3)
Br1–K2	4.254(1)	Xe1–O1–K1	147.07
K1–O1	2.857(1)	O2–Xe1–O6	
K1–O2	2.804		
K1–O3	2.767		
K1–O5	3.107		

Table 6.5. Selected bond lengths (Å) and angles (deg) of $K_2[XeO_3SeO_4]\cdot HF$ **(5)**.

Bond Lengths (Å)		**Bond Angles (deg)**	
Xe1–O1	1.778(1)	O2–Xe1–O1	99.50(6)
Xe1–O2	1.771(1)	O2–Xe1–O3	99.14(6)
Xe1–O3	1.769(1)	O1–Xe1–O3	102.55(6)
Xe1–O4	2.617(1)	O2–Xe1–O7	169.39(5)
Xe1–O5	2.645(1)	O4–Xe1–O1	160.84(5)
Xe1–O7	2.718(1)	O3–Xe1–O5	170.82(6)
Se1–O4	1.636(1)	O2–Xe1–O4	80.49(5)
Se1–O5	1.647(1)	O2–Xe1–O5	78.87(5)
Se1–O6	1.655(1)	O4–Xe1–O3	96.33(6)
Se1–O7	1.635(1)	O4–Xe1–O7	88.91(4)
K1–O2	2.888(1)	O4–Xe1–O5	74.51(4)
K1–O6	2.760(1)	O1–Xe1–O7	90.65(5)
K1–O1	2.845(1)	O1–Xe1–O5	86.64(5)
F1–H1	0.74(5)	O3–Xe1–O7	81.50(5)
K1–F1	2.736(1)	O7–Xe1–O5	98.81(4)
K1–O7	2.825(1)	O7–Se1–O6	110.51(6)
K1–F1	2.915(1)	O7–Se1–O5	110.14(6)
K1–O3	2.796(1)	O7–Se1–O4	112.31(6)
K2–O7	3.035(1)	O6–Se1–O5	106.56(6)
K2–O2	2.833(1)	O6–Se1–O4	108.16(7)
K2–O5	2.936(1)	O5–Se1–O4	108.97(7)
K2–O4	2.809(1)	O7–K1–O2	123.12(4)
K2–F1	2.649(1)	O7–K1–O6	79.60(4)

Table 6.6. Selected bond lengths (Å) and angles (deg) of $Rb_2[(XeO_3)_2CO_3]\cdot 2H_2O$ **(6)**.

Bond Lengths (Å)		Bond Angles (deg)	
Xe1–O1	1.789(2)	O2–Xe1–O3	102.67(9)
Xe1–O2	1.764(2)	O3–Xe1–O1	99.16(8)
Xe1–O3	1.777(2)	O3–Xe1–O8	85.91(8)
Xe2–O4	1.791(2)	O2–Xe1–O6	94.09(8)
Xe2–O5	1.762(2)	O1–Xe1–O6	93.63(7)
Xe2–O6	1.777(2)	O 2–Xe1–O4	169.73(7)
Xe1–O7	2.9651(4)	O1–Xe1–O4	72.35(6)
Xe1–O8	2.376(2)	O2–Xe1–O1	97.80(8)
Xe2–O1	2.898(2)	O2–Xe1–O8	79.67(7)
Xe2–O3	2.714(2)	O1–Xe1–O8	174.76(7)
Xe2–O9	2.9712(4)	O3–Xe1–O6	157.24(8)
Xe2–O10	2.378(2)	O3–Xe1–O4	82.19(7)
C1–O7	1.259(3)	O8–Xe1–O4	109.90(5)
C1–O8	1.301(2)	O5–Xe2–O6	103.90(10)
C2–O9	1.259(3)	O6–Xe2–O4	99.14(8)
C2–O10	1.300(2)	O6–Xe2–O10	86.24(8)
Rb1–O1	2.981(2)	O5–Xe2–O3	91.84(8)
Rb2–O2	3.042(2)	O4–Xe2–O3	94.49(7)
Rb1–O4	2.977(2)	O5–Xe2–O1	166.02(7)
Rb1–O4	2.990(2)	O4–Xe2–O1	72.27(6)
Rb1–O7	2.850(1)	O8–C1–O8	117.2(2)
Rb2–O8	2.960(2)	O7–C1–O8	121.38(12)
Rb2–O10	2.947(2)	O9–C2–O10	121.24(12)

Table 6.7. Raman frequencies[a] and assignments for K[XeO_3ClO_3], $XeO_{3(aq)}$ (2.0 M) and $KClO_3$.

$XeO_{3(aq)}$[b]	**$KClO_3$**	**K[XeO_3ClO_3)[c]**	**vibrational assignments[d]**
	977(29)	993(2) 978(1)	$\nu_{as}(ClO_3)$
	938(100) 931, sh	938(1) 927(17) 905(1)	$\nu_{sym}(ClO_3)$
833		848(12) 828(11) 807(7)	$\nu_{as}(XeO_3)$
780		787(62) 772, sh 764(100)	$\nu_s(XeO_3)$
	619(11)	618(4) 611, sh 605(<1) 592(1) 590(<1)	$\delta_{sym}(ClO_3)$
	487(52)	491(8) 480(2) 465(<1)	$\delta_{as}(ClO_3)$
344, sh		362(1) 348(8) 334(1)	$\delta_{umb}(XeO_3)$
317, br		318(5) 309(17) 301, sh	$\delta_{as}(XeO_3)$
	132(7) 100(13)	138(8) 122(1) 103(<1)	deformation modes latticee modes

[a] Frequencies are given in cm^{-1}. Abbreviations denote shoulder (sh) and broad (br). [b] The spectrum was recorded in a ¼-in. o.d. FEP diameter sample tube at −140 °C. Values in parentheses are relative Raman intensities. [c] The spectrum was recorded in an aluminum sample holder at 22 °C. Values in parentheses are relative Raman intensities. [d] Symbols and abbreviations denote stretch (ν), bend (δ), rock (ρ_r), twist (ρ_t), umbrella (umb), symmetric (s), and asymmetric (as).

Table 6.8. Raman frequencies[a] and assignments for K[XeO_3BrO_3], $XeO_{3(aq)}$ (2.0 M) and $KBrO_3$.

$XeO_{3(aq)}$[a,b]	**$KBrO_{3(s)}$**	**K[XeO_3BrO_3)[c]**	**vibrational assignment[d]**
	836(2)	840(5)	$\nu_{as}(BrO_3)$
833		830(2) 820(3) 809(31)	$\nu_{as}(XeO_3)$
	803(6) 791(100) 778(22) 757(<1)	783(29) 758, sh	$\nu_{sym}(BrO_3)$
780		766(100)	$\nu_s(XeO_3)$
	440(<1) 432(<1) 421(1) 418(<1)	429(2)	$\delta_{sym}(BrO_3)$
	367(<1) 358(12)	378(3) 366(8) 360(2) 353, sh	$\delta_{as}(BrO_3)$
344, sh		329(6)	$\delta_{umb}(XeO_3)$
317, br		317(2) 305, sh	$\delta_{as}(XeO_3)$
	155(5) 131(<1) 118(1)	200(<1) 175(2) 162(<1) 119(10) 84(31)	ν(Xe---O) ν(XeO) ρ_r(XeO) ρ_t(XeO) lattice modes

[a] Abbreviations denote shoulder (sh) and broad (br). [b] The spectrum was recorded in a ¼-in. o.d. FEP diameter sample tube at −140 °C. Values in parentheses are relative Raman intensities. [c] The spectrum was recorded in an aluminum sample holder at 22 °C. Values in parentheses are relative Raman intensities. [d] Symbols and abbreviations denote stretch (ν), bend (δ), rock (ρ_r), twist (ρ_t), umbrella (umb), symmetric (s), and asymmetric (as).

Table 6.9. Raman frequencies[a] and assignments for $K[XeO_3IO_3]$, $XeO_{3(aq)}$ (2.0 M) and KIO_3.

$XeO_{3(aq)}$[a,b]	**$KIO_{3(s)}$**	**$K[XeO_3IO_3]$[c]**	**vibrational assignment[d]**
833		859(2) 840(4) 830(11)	$\nu_{as}(XeO_3)$
	813(3) 791(<1) 783(11)	819(10) 806(28) 800, sh	$\nu_{as}(IO_3)$
780		776(100)	$\nu_s(XeO_3)$
	768(2) 761, br 752(100) 734(43)	760(5) 753, sh 734, sh	$\nu_{sym}(IO_3)$
	371(2)		$\delta_{sym}(IO_3)$
	359(<1) 353(<1)	360(<1) 352(1)	$\delta_{asym}(IO_3)$
344, sh		323(14), br	$\delta_{umb}(XeO_3)$
317, br		311, sh	$\delta_{as}(XeO_3)$
	329(1)		$\delta_{asym}(IO_3)$
	302(3) 235(<1) 183(<1) 169(1) 137(<1) 117(<1) 113(<1) 97(<1)	212(<1) 160(1) 157(<1) 147(<1) 119(3)	$\nu(Xe{-}{-}{-}O)$ $\nu(XeO)$ $\rho_r(XeO)$ $\rho_t(XeO)$ lattice modes

[a] Abbreviations denote shoulder (sh) and broad (br). [b] The spectrum was recorded in a ¼-in. o.d. FEP diameter sample tube at −140 °C. Values in parentheses are relative Raman intensities. [c] The spectrum was recorded in an aluminum sample holder at 22 °C. Values in parentheses are relative Raman intensities. A weak band at 471 cm^{-1} could not be assigned. [d] Symbols and abbreviations denote stretch (ν), bend (δ), rock (ρ_r), twist (ρ_t), umbrella (umb), symmetric (s), and asymmetric (as).

Table 6.10. Raman frequencies[a] and assignments for $K_2[XeO_3SeO_4]\cdot HF$, $XeO_{3(aq)}$ (2.0 M) and K_2SeO_4.

$XeO_{3(aq)}$[a,b]	**$K_2SeO_{4(s)}$**	**$K_2(XeO_3SeO_4)\cdot HF$[c]**	**vibrational assignment[d]**
	900(11) 874(11) 863(7)	906(<1) 887 872(4) 861(<1)	$\nu_{as}(SeO_4)$
	841(100)	854(2) 835(1)	$\nu_{sym}(SeO_4)$
833		825(31) 819(1) 811(8) 805, sh	$\nu_{as}(XeO_3)$
780		775(17) 765(100)	$\nu_s(XeO_3)$
	429(6) 418(12) 414(<1)	440(<1) 432(<1) 428(<1) 424(<1) 416(3) 400(<1) 396(<1)	$\delta_{as}(SeO_4)$
	342(16) 335(<1)	378(<1) 349(<1)	$\delta_{sym}(SeO_4)$
344, sh		334(11)	$\delta_{umb}(XeO_3)$
317, br		320(2) 303(<1)	$\delta_{as}(XeO_3)$
	131(<1) 119(2) 108(<1) 102(<1)	287(<1) 282(<1) 279(<1) 121(3) 110(<1) 106(<1)	$\nu(Xe{-}{-}{-}O)$ $\nu(XeO)$ $\rho_r(XeO)$ $\rho_t(XeO)$ lattice modes

[a] Abbreviations denote shoulder (sh) and broad (br). [b] The spectrum was recorded in a ¼-in. o.d. FEP diameter sample tube at −140 °C. Values in parentheses are relative Raman intensities. [c] The spectrum was recorded in an aluminum sample holder at 22 °C. Values in parentheses are relative Raman intensities. [d] Symbols and abbreviations denote stretch (ν), bend (δ), rock (ρ_r), twist (ρ_t), umbrella (umb), symmetric (s), and asymmetric (as).

Table 6.11. Raman frequencies[a] and assignments for K[XeO_3NO_3], $XeO_{3(aq)}$ (2.0 M) and KNO_3.

$XeO_{3(aq)}$[a,b]	**$KNO_{3\,(s)}$**	**K[XeO_3NO_3][c]**	**vibrational assignment[d]**
	1358(2) 1343(1)	1461(3) 1295(5)	$\nu_{as}(NO_3)$
	1049(100)	1035(31)	$\nu_{sym}(NO_3)$
833		837(6) 830(24) 821(7)	$\nu_{as}(XeO_3)$
780		789(100)	$\nu_s(XeO_3)$
	714(12)	724(4) 710(1)	$\delta_{as}(NO_3)$
344, sh		376(6) 363(3) 347(5)	$\delta_{umb}(XeO_3)$
317, br		329(1) 318(6)	$\delta_{as}(XeO_3)$
	123(2)	148(1) 119(7)	ν(Xe---O) ν(XeO) ρ_r(XeO) ρ_t(XeO) lattice modes

[a] Abbreviations denote shoulder (sh) and broad (br). [b] The spectrum was recorded in a ¼-in. o.d. FEP diameter sample tube at −140 °C. Values in parentheses are relative Raman intensities. [c] The spectrum was recorded in an aluminum sample holder at 22 °C. Values in parentheses are relative Raman intensities. [d] Symbols abd abbreviations denote stretch (ν), bend (δ), rock (ρ_r), twist (ρ_t), umbrella (umb), symmetric (s), and asymmetric (as).

Table 6.12. Raman frequencies[a] and assignments for $Rb[CO_3(XeO_3)_2]\cdot 2H_2O$ (**4**), $Na_2[CO_3(XeO_3)_n]\cdot xH_2O$ (**4b**), $K_2[CO_3(XeO_3)_n]\cdot xH_2O$ (**4c**), $Ba[CO_3(XeO_3)_n]\cdot xH_2O$ (**4d**), $XeO_{3(aq)}$ (2.0 M) and $K_2[CO_3]$.

$XeO_{3(aq)}$[a,b]	K_2CO_3	$Rb[CO_3(XeO_3)_2]\cdot 2H_2O$[c]	$Na_2[CO_3(XeO_3)n]\cdot xH_2O$[c]	$K_2[CO_3(XeO_3)n]\cdot xH_2O$[c]	$Ba[CO_3(XeO_3)n]\cdot xH_2O$[c]	vibrational assignment[d]
	1426 1374	1503(1)	1519(3) 1481(4) 1397(1) 1306(6)	1437(2) 1393(3) 1352(4)	1601(2)	$\nu_3(E')(CO_3)$
	1063 1026	1056(2)	1062(5)	1053(3)	1001(3)	$\nu_1(A_1)(CO_3)$
833		822(9) 771(41)	821(25) 805(13) 790(61)	847(3) 811(29) 800(24)		$\nu_2(A_2'')(CO_3)$ $\nu_{as}(XeO_3)$
780		749(100)	757(100)	767(100)	776(100) 768(89)	$\nu_s(XeO_3)$
	702 677		696(5)	703(3) 677(2)	679(4)	$\nu_4(E')(CO_3)$
344, sh		383(4)	371(2)	371(2)	369(14)	$\delta_{umb}(XeO_3)$
317, br		336(2) 322(3)	351(4)	348(10)	340(14)	$\delta_{as}(XeO_3)$
	484 288 237	225(1) 169(2) 123(2)	265(1) 225(3) 186(8) 177(8) 143(11) 122(5)	118(15)	120(14)	$\nu(Xe{-}{-}{-}O)$ $\nu(XeO)$ $\rho_r(XeO)$ $\rho_t(XeO)$ Lattice modes

[a] Abbreviations denote shoulder (sh) and broad (br). [b] The spectrum was recorded in a ¼-in. o.d. FEP diameter sample tube at −140 °C. Values in parentheses are relative Raman intensities. [c] The spectrum was recorded in an aluminum sample holder at 22 °C. Values in parentheses are relative Raman intensities. Weak bands at 404 and 394 cm^{-1} in (**4b**) could not be assigned. [d] Symbols denote stretch (ν), bend (δ), rock (ρ_r), twist (ρ_t), umbrella (umb), symmetric (s), and asymmetric (as).

Experimental Section

Caution! *Solid XeO_3 detonates when subjected to mild thermal or mechanical shock. Great care must be taken during the syntheses and handling of XeO_3 and $(CH_2CH_2O)_5XeO_3$. For these reasons, the quantity of XeO_3 used in each synthesis has been limited to 5–15 mg. Reaction vessels fabricated from FEP (hexafluoropropylene, tetrafluoroethylene copolymer) fluoroplastic, which is inert to attack by HF, strong oxidants, and fluorinating agents, generally does not shatter to produce sharp shards when a detonation occurs at the reagent scales described in this study. Appropriate protective equipment (face shield, leather gloves, ear protection) must be used.*

Apparatus and Materials *(a) General*. Anhydrous HF (Harshaw Chemicals Co.) was purified as previously described.[S1]

(b) Xenon hexafluoride. Xenon hexafluoride was prepared by the reaction of Xe (99.995%, Air Products and Chemicals, Inc.) and F_2 (98+%, Air Products and Chemicals, Inc.) similar to the method described by Malm and Chernick.[S2] Small amounts of XeF_4 impurity, identified by two strong peaks at 502 and 543 cm^{-1} in the Raman spectrum, also formed XeO_3 when hydrolyzed.[S3]

X-ray Crystallography. *(a) Crystal Mounting.* Single crystals were submerged in perfluoropolyether oil (Fomblin Z-25) in the open atmosphere and were selected at room temperature and mounted at the tip of a dual-thickness polymer loop (MiTeGen, Ithaca, NY; MicroMount;™ 100–500 μm) using Halocarbon 25-5S grease (Halocarbon Products Corporation, River Edge, NJ).

(b) Collection and Reduction of X-ray Data. Crystals were centered on a Bruker SMART APEX II diffractometer equipped with an APEX II 4K CCD (charge-coupled device) area detector and a triple-axis goniometer that was controlled by the APEX II Graphical User Interface (GUI) software.[S5] A Bruker Triumph curved crystal monochromator was used with a Mo Kα (λ = 0.71073 Å) radiation source for all compounds. Diffraction data collection at −173 °C consisted of ω- and ϕ-scans collected at 0.5° intervals. Data collection

was carried out in a 512 x 512 pixel mode using 2 x 2 pixel binning. The raw data was processed by use of the APEX II GUI software.[S4] The SADABS[S5] program was used for scaling the diffraction data.

(c) Solution and Refinement of the Structure. The XPREP program[S5] was used to confirm unit cell dimensions and the crystal lattice. All calculations were carried out using the SHELXTL-plus[S6] and the Olex2[S7] packages for structure determination, solution refinement, and molecular graphics. The space group choice was confirmed using Platon.[S6] The final refinement was obtained by introducing anisotropic thermal parameters and the recommended weightings for all of the atoms except the hydrogen atoms. The H atoms were placed at locations derived from a difference map. The maximum electron density in the final difference Fourier map was located near the xenon atom.

Raman Spectroscopy. The Raman spectra were recorded on a Bruker RFS 100 FT-Raman spectrometer using 1064-nm excitation, 300 mW laser power, and ±0.5 cm^{-1} resolution as previously described.[S8]

References

[S1] A. A. A. Emara, G. J. Schrobilgen, *Inorg. Chem.* **1992**, *31*, 1323.

[S2] J. G. Malm, C. L. Chernick, *Inorg. Synth.* **1966**, *8*, 258.

[S3] J. L. Huston, *Inorg. Chem.* **1982**, *21*, 685.

[S4] APEX2, release v2014.9-0; Bruker AXS Inc.: Madison, WI, **1995**.

[S5] G. M. Sheldrick, SADABS (Siemens Area Detector Absorption Corrections), version 2.03; Siemens Analytical X-ray Instruments, Inc.: Madison, WI, **1999**.

[S6] G. M. Sheldrick, SHELXTL-Plus, release 5.1; Siemens Analytical X-ray Instruments, Inc.: Madison, WI, **1998**.

[S7] O. V. Dolomanov, L. J. Bourhis, R. J. Gildea, J. A. K. Howard, J. Puschmann, *J. Appl. Crystallogr.* **2009**, *42*, 339.

[S8] A. L. Spek, *J. Appl. Crystallogr*. **2003**, *36*, 7.

CHAPTER 7

CONCLUSIONS AND DIRECTIONS FOR FUTURE WORK

7.1 Conclusions

Stable crown ether complexes of XeO_3, $[(CH_2CH_2O)_6XeO_3H_2O]_2 \cdot HF$, $(CH_2CH_2O)_6XeO_3 \cdot 2H_2O$, $(CH_2CH_2O)_5XeO_3$, and $(CH_2CH_2O)_4XeO_3$, have been synthesized and structurally characterized by Raman spectroscopy and/or single-crystal X-ray diffraction. Frequency shifts of the XeO_3 vibrational bands were consistent with complex formation and provided evidence for the 2,2,1-cryptand adduct with XeO_3. The adducts $(CH_2CH_2O)_5XeO_3$, and $(CH_2CH_2O)_4XeO_3$ were insenstivie to mechanical shock and air-stable at room temperature. Empirical bond valence calculations were used to determine the degree to which the Xe---O secondary bonding interactions contribute to the total bond valence of xenon. Xenon coordination numbers exceeding six (with inclusion of the three primary bonds of XeO_3) were observed for all crown ether adducts. Hirshfeld surface analyses of $(CH_2CH_2O)_6XeO_3 \cdot 2H_2O$ and $(CH_2CH_2O)_5XeO_3$ confirmed four and five secondary Xe---O bonding interactions, respectively. The $(CH_2CH_2O)_5XeO_3$ complex exhibits the highest xenon coordination number observed thus far for XeO_3. The Xe---O_{crown} bonding interactions may be described as primarily electrostatic interactions between the nucleophilic O atoms of the crown ether and the electrophilic σ-holes of the xenon atoms. MEPS analyses of XeO_3 and $(CH_2CH_2O)_5XeO_3$ corroborated the positions of regions of high EP on the Xe atom of XeO_3 and the trajectories of the O–Xe---O contacts corresponding to σ-hole interactions in the adduct.

Examples of XeO_3 oxygen-base adducts were synthesized and structurally characterized. The $[(C_6H_5)_3PO]_2XeO_3$ adduct contains well-isolated, distorted square pyramidal XeO_3 units and provides the only example presently known of a XeO_3 adduct which has only two secondary bonding interactions. The $[(CH_3)_2CO]_3XeO_3$, $[(CH_3)_2SO]_3(XeO_3)_2$, and $(C_5H_5NO)_3(XeO_3)_2$ adducts each display different packing motifs which are well-isolated structural units consisting of dimers, and chains, respectively. The triphenylphosphine oxide and pyridine-*N*-oxide adducts are air-stable at room temperature and are insensitive to mechanical shock. The complexation shifts for the ν(PO) vibrational modes of $[(C_6H_5)_3PO]_2XeO_3$ indicates that XeO_3 is a weaker Lewis acid than $SbCl_3$ but is comparable to the Lewis acid strengths of $BiCl_3$ and $BiBr_3$. Calculations show enhancement of the Xe–O primary bond polarities upon coordination and predominantly electrostatic Xe---O bonding interactions between the nucleophilic O atoms of the oxygen bases and the electrophilic σ-holes of the xenon atoms.

Incorporation of xenon trioxide, XeO_3, into inorganic polyatomic salts under ambient conditions by adduct formation with oxoanions is observed in several mixed xenate salts; $K[XeO_3XO_3]$ (X = Cl, Br), $K_2[XeO_3SeO_4]\cdot HF$, $K[(XeO_3)_xZO_3]$ (Z = I, N), and $M_2[(XeO_3)_nCO_3]\cdot xH_2O$ (M = Na, K, Rb, Ba). Raman spectroscopy was used to identify the aforementioned compounds and $K[XeO_3ClO_3]$, $K[XeO_3BrO_3]$, $K_2[XeO_3SeO_4]\cdot HF$, and $Rb_2[(XeO_3)_2CO_3]\cdot 2H_2O$ were also characterized by low-temperature, single-crystal X-ray diffraction. These salts display intense bands assigned to XeO_3 stretching and bending modes and considerably weaker bands assigned to the vibrational modes of the anions. The xenon atom of XeO_3 is seven coordinate in $K[XeO_3ClO_3]$ and six coordinate in all other compounds with Xe---O distances that are significantly less than the sum of the Xe and O van der Waals radii.

7.2 Directions for Future Work

Further studies on the coordination chemistry of XeO_3 with other macrocyclic and chelating ligands should be completed. Although preliminary results indicate oxidation of sulfur Lewis base centers, it may be possible to isolate a thio-crown ether complex of XeO_3 at low temperatures in acetone. For example, aza-crown ethers and porphyrins are other macrocycles of interest.

Formation of an azido-derivative of xenon would represent a significant achievement in the isolation and stabilization of highly energetic compounds. Xenon trioxide was shown to coordinate to anions of inorganic polyatomic salts. The reaction of KN_3 and $XeO_3{\cdot}6HF$ could give $K[XeO_3N_3]$ (eq 1). The use of a bulky cation, such as $[N(CH_3)_4]^+$ (eq 2), a cation complexing agent such as 12-crown-4 (eq 3), and/or carrying out these reactions at low temperatures in acetone are possible reaction pathways.

$$KN_3 + XeO_3 \longrightarrow K(XeO_3N_3) \qquad (1)$$

$$[N(CH_3)_4]N_3 + XeO_3 \longrightarrow [N(CH_3)_4][XeO_3N_3] \qquad (2)$$

$$C_8H_{16}O_4 + XeO_3 + NaN_3 \longrightarrow (C_8H_{16}O_4Na)(XeO_3N_3) \qquad (3)$$

Shock-insensitive adducts of XeO_3 are potential clean oxidizers for organic transformations, such as epoxidations. Evaluation of the oxidizing strength of XeO_3 and oxidation reaction pathways with organic compounds should be completed. The products of these reactions could easily be studied by ^1H and ^{13}C NMR spectroscopy. Oxidation of an organic substrate should be accompanied with reduction of XeO_3 to Xe and O_2 gases, providing a simple reaction work-up and a non-toxic solution to chromium-based oxidatants.